Nonlinear viscoelastic response of a thermodynamically metastable polymer melt

by

Anurag V. Pandey

Doctoral Thesis
Submitted in partial fulfilment of the requirements
for the award of Doctor of Philosophy

Department of Materials
Loughborough University,
Loughborough LE11 3TU, Leicestershire
England, United Kingdom

The work submitted is original research conducted by the candidate and the proper credit has been given while referring to the work of others

This Research is part of the Research Programme of the Dutch Polymer Institute, DPI, Eindhoven, The Netherlands, project nr. #637.

To my beloved parents, teachers and the almighty…

Table of contents

List of Figures

List of Tables

Summary

The modern materials era is dominated by polymers as a material of enormous opportunity. The vast acceptance of these materials comes from the fact of their easy processability into complicated shapes and designs. Polymers are long molecules composed of repeating structural subunits viz. Ethylene (C_2H_4). By controlled synthesis, it is possible to tailor the molecular architecture to achieve the desired physical and mechanical properties, making these materials of great interest. Properties of synthetic polymers in the solid-state depend on the molecular weight, e.g. toughness and strength increases with increasing molecular weight. However, viscosity (resistance to flow) of polymers also increases with increasing molecular weight which makes it difficult to process. The viscosity (zero-shear) scales with $Mw^{\sim 3.4}$, where Mw is the weight-average molecular weight. This implies that if the molecular weight increases by two fold, the melt-viscosity increases by more than a factor of 10. Thus, the choice of molecular weight is a compromise between the ease of processability (low molecular weight) and better mechanical properties (high molecular weight).

The power law scaling of ~3.4 in viscosity to molecular weight is realised beyond a critical molecular weight (M_C), intrinsic to a given polymer. Polymer chains longer than the critical molecular weight overlap each other in melt, putting constraints on chain dynamics leading to the increase in viscosity (resistance to flow). The overlap points between the chains are termed as physical entanglements, which can be visualised as physical cross-linking similar to chemical cross-linking in rubbers. However, entanglements form physical networks are not fixed. Considering their relevance in polymer physics and processing, entanglements are considered to be the folklore of rheological concepts in polymer science. Thus, considerable in-depth studies are performed to correlate molecular configuration and conformation with entanglement and associated chain dynamics in a fully entangled thermodynamically stable polymer melt where molecular weight between entanglements is considered to be fixed. However, in reality, during processing applied deformation forces are extremely strong and the polymer melt goes from an equilibrium to a non-equilibrium state with the destruction of the physical network. Further, the establishment of the

entanglement process is also an unexplored area in polymer science because of the non-availability of such samples. In this thesis, some of the outstanding issues on chain dynamics of a melt state that transforms with entanglement formation from a metastable to a thermodynamically stable state have been studied. The response of a metastable melt in the non-linear viscoelastic regime and the role of amorphous phase in melting process of linear polyethylene are also addressed by using a combination of chemistry, physics and rheology. In view of experimental requirements, to capture the addressed challenges in the given experimental time scales, linear polyethylenes having a molecular weight greater than a million g/mol were used.

To tailor entanglement and molecular weight, with controlled synthesis using the same homogeneous catalytic system, linear polyethylene(s) with molecular weights ranging between 0.3 to 6.0 million g/mol have been synthesised. For syntheses, polymerisation conditions such as the catalytic system, concentration, temperature, solvent used (as polymerisation medium) have been kept the same, while the polymerisation time was varied to achieve the desired molecular weights. Polymerisation temperature was chosen such that the polymers with a lesser number of entanglements can be obtained. These polymers in this thesis are termed as disentangled (fewer overlapping chains). These disentangled polymers give a unique opportunity to get a further insight into the effect of entanglement on flow behaviour and polymer melt dynamics. Entanglements residing in the amorphous regions between crystals also influence the solid-state processing of the semi-crystalline polymers. Disentangled polymer presents many opportunities and has been studied in this thesis to explore and understand some of the several interesting and unresolved questions in polymer physics that has been summarised below.

This thesis is divided in three main chapters studying (a) entanglement formation during polymerisation, (b) non-linear behaviour of Ultra-high Molecular weight Polyethylene (UHMw-PE) melt and (c) effect of entanglement on melting-crystallisation aspects. Each chapter makes use of the same set of selected UHMw-PE samples.

Chapter 2, using melt rheology in the linear viscoelastic region, explores the effect of polymerisation conditions on entanglement formation and the resultant

morphology. It conclusively shows that the linear melt rheology can be effectively used to assess qualitatively the entanglement formation in a disentangled melt. From the rheological studies on disentangled UHMw-PE samples, it is shown that the entanglement formation and its distribution along the polymer chain length depends on polymerisation conditions. Entanglement formation is higher in the initial stages of polymerisation and tends to decrease with increasing polymerisation time (or increasing chain length). Difference in entanglement formation rate during the polymerisation leads to a heterogeneous distribution of entanglements over the entire chain length, where the maximum number of entanglements are in the vicinity of the part of chain produced during the initial stages of polymerisation. The heterogeneous distribution along the chain is explained with the help of crystallisation and polymerisation rate that the polymer experiences during synthesis. These polymers have been used to follow the rate of entanglement formation as a function of molecular weight, with homogenisation and formation of entanglement in the process of melt transformation from a metastable to a stable state. These studies have been further extended to investigate influence of entanglement on crystallisation.

In **chapter 3**, non-linear rheological behaviour of UHMw-PE has been studied. Large amplitude oscillatory shear (LAOS) experiments have been used to study the effect of entanglement under large deformation. The chapter addresses relaxation aspects of chains in the non-equilibrium melt state, and shows a method to follow the influence of molecular weight and molecular weight distribution on the annihilation of the physical network during large deformation in the non-linear viscoelastic region. One of the striking features from the study is that the polymer melt (UHMw-PE) shows G" peak in LAOS experiment which is a signature of glassy (metastable) systems. The finding suggests that the G" peak in LAOS experiments could be a universal and generic feature of soft materials; in the case of a polymer melt the peak may arise due to convective constraint release (CCR). However, this can be only observed in the frequency regime where G' shows a plateau and G" shows minima (in oscillatory frequency sweep). Such a frequency regime is accessible for high molecular weight polymer melts, hence, G" peak can be observed. G" peak intensity increases with increasing frequency (in G' plateau and G" minima regime). Whereas, in disentangled

UHMw-PE having a narrow polydispersity, G" peak intensity decreases with increasing entanglement and finally diminishes. The G" peak in commercial entangled UHMw-PE melt, having a broader polydispersity, remains strong.

Chapter 4 extends the understanding of crystal morphology. To get an insight on the melting and crystallisation aspects of entanglement, DSC and TM-DSC have been used. Heating rate dependence on melting between nascent (powders directly from the reactor) entangled, nascent disentangled and melt-crystallised UHMw-PE samples have been studied. All the samples show non-linear heating rate dependence in melting and are different due to topological differences in the amorphous region of the crystals. During a slow heating rate (or annealing under isothermal conditions), melting in nascent disentangled crystals is shown to proceed from the crystal surface, by the reeling out of chain stems and their diffusion in the polymer melt. Whereas, such a possibility even at low heating rates, does not arise in nascent entangled and melt-crystallised samples due to topological difference in the amorphous region. Thus, unlike entangled samples (nascent entangled and melt crystallised), the nascent disentangled crystals show two different non-linear heating rate dependences on melting, suggesting the presence of two melting mechanisms; (a) melting from the crystal surface by successive detachment of chain stems and their reeling in the melt, and (b) melting in a cluster of chain stems at higher heating rates.

Although, most of the studies performed in this thesis are on UHMw-PE samples; many of the results and understanding from this work can be extended and applied to flexible polymers in general. UHMw-PE, due to its very large chain length, provides an opportunity to follow entanglement formation due to the large number of entanglements and slower dynamics making experiments viable in laboratory conditions.

The studies on the nonlinear viscoelastic region have been applied for processing of intractable polyethylene where the Multi Pass Rheometer, available at Eindhoven University of Technology, has been used. The studies demonstrate the ease of flow of disentangled polymer compared to its entangled state through capillary geometry. This is presented as a part of Appendices.

Keywords*: entangled melt, disentangled melt, LAOS, melt rheology, melting kinetics, crystallisation, UHMw-PE, DSC, TM-DSC.*

Acknowledgements

I would like to express my gratitude to my supervisor Prof. Sanjay Rastogi, for his invaluable discussions, appreciation and support throughout the PhD. He has played an important role by believing in the work and supporting it against many odds. It has been a great journey while working on such a wonderful and challenging topic; and I have learnt a great deal from him through our untiring and regular discussions, critical inputs and most importantly learnt the importance of being a devil's advocate and a believer simultaneously. I am deeply thankful to the Dutch Polymer Institute (DPI) for the financial support for the work and the platform to meet and learn from some of the best from the area.

I am also deeply indebted to Dr. Ashish Lele from the National Chemical Laboratory (NCL), India without whom probably I would have not ever ventured for PhD study to work on this exciting topic. He has been always a source of inspiration. He always believed in me and has always been there to guide and motivate. Without critical discussion with him, some of the exciting work in this thesis would not possible. I owe a great deal to him and many at NCL for introducing me to the exciting world of polymer science and engineering.

I am greatly thankful to the Department of Materials at Loughborough University and its people who throughout have helped in managing and administrating my PhD. I am also very thankful to people from the Department who have supported me in many ways, specially, Mrs. Pat Storer, Ms. June Lennie, Mr. Ray Owens, Mr. Andy Woolley, Mr. Mac Callender and Mr. David Insley for always being there to help.

Furthermore I would like to thank the following,

- Dr. Jan Stamhuis at DPI for his support during DPI meetings and administrative help to carry out this work without any hassle.
- Prof. Akihiko Toda (Hiroshima University, Japan) for his guidance on measurements using TM-DSC.
- Dr. Bing Wang (Avantium Technologies B.V., Amsterdam) for synthesising important materials for early experiments on UHMw-PE.

- Prof. Doug Hourston (Loughborough University) for examining and correcting my report during the first year and his encouragement throughout.
- Prof. Dr. Manfred Wilhelm (Karlsruhe Institute of Technology, Germany) for giving me the opportunity to work in his lab; work and learn Fourier-Transform rheology.
- Mr. Deepak Arihwal for helping out with non-linear rheology experiments at Karlsruhe Institute of Technology.
- Dr. Yohan Champouret (Chemical Engineering Research Center, Toulouse, France) for actively participating and synthesising large amount of UHMw-PE samples used during this PhD.
- Dr. Iakovos Vittorias (LyondellBasell, Germany) for his encouraging discussion on rheology and introducing to Prof. Dr. Wilhelm for FT rheology.
- Dr. Sara Ronca and Mr. Giuseppe Forte from Loughborough University for their on SEM and DSC measurements.
- Prof. Gerrit Peters and Ramandeep Singh from Eindhoven University of Technology, The Netherlands, for providing Multi Pass rheometer data.
- Teijin Aramid, The Netherlands, for the hospitality during my visits to work with Sanjay on publications and the thesis.

I would also like to appreciate my colleagues in the lab at Loughborough University for all their help and creating a great working environment, specially Carmine, Nilesh Patil, Maurizio, Maria, Han Xu, Dario and Dr. Efren.

I would also like to take this opportunity and thank a few important people in my life who stood by and supported me during tough times, specially my friends: Jigna, Hetal, Samruddhi, Shailesh, Balaji, Ankeet, Shivakumar, my housemates Abhijeet and Krishna for tolerating me with my frustration during the writing up period. Sainath, Yogesh, Satyan for their hospitality and help during my several visits to The Netherlands. I wish to thank my mentors and colleagues at NCL: Dr. Guruswamy, Dr. Premnath, Sangeeta, Neelima, Anuya, Harsh and many others.

Finally, deepest of my gratitude to my family, for their untiring patience, love, unconditional support and belief, without whom this day would have not been possible. I am also grateful to the almighty to give me patience and strength to complete this exciting journey.

Chapter 1

Background and Introduction

A synthetic polymer is large molecule made up of simple repeating unit such as (C_2H_4), and plays an essential and ubiquitous role in everyday life because of its extraordinary range and tailor made properties. One of the interesting properties in polymers is their dependence on the molecular weights (size). Many fundamental properties of the polymer depend on molecular weight of the polymer chain viz. viscosity (flow-ability), melting, crystallisation, mechanical properties etc. For example, low molecular weight polymer (oligomers) can flow like viscous oil where as higher molecular weight of the same polymer could be practically intractable. Most of these fundamental properties are essentially affected due to physical constraints imposed by polymer chains on each-other after they grow beyond a certain chain length known as the 'entanglement molecular weight', where such constraints are known as entanglements.

This chapter introduces to some basic aspects of polymer physics in polymer chain dynamics, crystallisation, melting and mechanical properties while giving special consideration to effect of entanglement. For example, entanglement in a polymer melt gives rise to the famous power scaling ~3.4 of zero-shear viscosity on molecular weight, while same entanglement can play an important role in morphology of the crystals by influencing crystallisation which in turn controls the melting of the polymer. By controlling the entanglement, it is possible to achieve mechanical properties better than steel and approaching the theoretical value of the polymer chain [1].

1.1 Polymer chain dynamics:

Chain dynamics of flexible polymer chains is one of the intriguing areas in the field of polymer science and is of great relevance to polymer processing. In equilibrium, the polymer chains take a wide variety of conformations to behave as random coils because of a huge freedom in the spatial arrangements of the repeating units. The very local, rapid motion at the length scales of chemical bonds (e.g., the bond vibration) is not significantly different from that in low molecular weight (Mw) materials and is essentially determined by the chemical structure of the chains *[2,3]*. However, at larger scales, due to the entanglement (constraint) formation, the polymer chains exhibit dynamic features that are absent in the low molecular weight materials where the entanglement are absent.

These features, corresponding to the motion in length scales well above the repeating unit size and strongly influenced by the chain connectivity, are very similar for the polymer chains of various chemical structures. The universality (the independence from the chemical structure) allows scientists to coarse-grain the chains in both spatial and time scales to extract essential physics of the large scale dynamics of polymer chains. The presence of physical entanglement that changes continuously due to motion of polymer chains gives rise to the viscoelastic behaviour pertinent to polymer melts. The viscoelastic properties have been extensively studied over several decades now. A comprehensive summary of results of the early studies is given by Ferry *[4]* and Graessley *[5,6]*. To understand the underlying fundamental concepts, a brief summary of the involved polymer physics is described below.

1.1.1 Ideal chain

The concept of an ‘ideal chain’ or an ‘unperturbed chain’, where the restrictions arising due to bond angle and chain conformation prevails and is dominated by the intra-molecular interactions only, is the basic starting point to understand the polymer chain dynamics. Though the ideal chain situation is not encountered in practice, the physical concepts arising from the single chain such as the radius of gyration are applicable under specific solvent-polymer interactions and in polymer melts.

It is apparent that a single chain does not exist and polymers are ensemble of chains where it is important to consider inter- and intra-molecular secondary interactions. These secondary interactions can be suppressed in the presence of solvent. Thus, a single chain residing in the ensemble of chains interacts with both solvent and themselves. The relative strength of these interactions determines whether the repeating units effectively attract or repel one another.

Conformations of an ideal chain:

Polymer molecules in their melt and in solution can adopt a large number of conformations depending upon the number of degrees of freedom available e.g. bond lengths, bond angles and torsion angles. There are several models of ideal chains. Each model makes different assumptions about the allowed values of torsion and bond angles, ignoring the effect of interactions of repeating units and chains.

The model ignores the differences between the probabilities of different angles. It assumes that all the bonds are of fixed length and all the angles are equally likely and independent of each other. Thus, the path in space is a random walk, Figure 1.1 *[2-4]*.

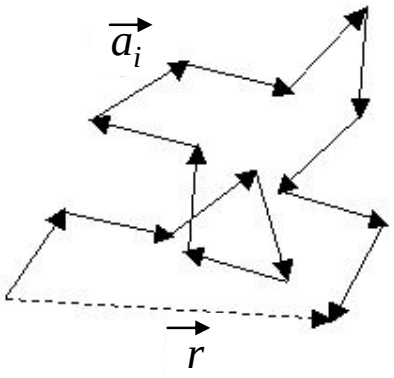

Figure 1.1. Schematic representation of freely jointed chain model of a polymer.

In this model, the polymer chain is considered to be made up of *N* links and each link is of the length, *a*. The end to end vector *r* will be sum of *N* jump vectors a_i, representing the direction and size of each link,

$$r = a_1 + a_2 + ... + a_N = \sum_{i=1}^{N} a_i \qquad \text{…(1.1)}$$

The mean end-to-end distance is,

$$< r.r > = < (\sum_{i=1}^{N} a_i).(\sum_{j=1}^{N} a_j) > \qquad \text{…(1.2)}$$

For *N* cases where *i=j*,

$$< r^2 > = Na^2 + < (\sum_{i \neq j} a_i.a_j) > \qquad \text{…(1.3)}$$

As the links are freely jointed, the directions are completely unrelated hence cross terms disappear on taking the average. Hence,

$$< r^2 > = Na^2 \qquad \text{…(1.4)}$$

The overall size in random walk is proportional to square root of the number of steps, *N*. In the limit of large *N*, the end to end distance follows a Gaussian distribution.

There are several models; like freely rotation chain models *[4]*, worm-like chain models *[7]*, hindered rotation model *[2,3]* etc. describing several modes of ideal chain. Each model makes different assumptions about the allowed values of torsion and bond angles. However, every model ignores interactions between repeating units separated by large distance along the chain.

The end-to-end distance $<r^2>$ is convenient measure for the average dimensions but is not experimentally measureable. An experimentally measurable parameter is the radius of gyration, $<r_g^2>$, defined as the averaged square distance from all repeating units to the centre of mass of the polymer, and for an ideal linear chain is given by,

$$< r_g^{\,2} > = Na^2 / 6 \qquad \text{…(1.5)}$$

1.1.2 Real polymer chain:

1.1.2.1 Short range effects

Real chains have interactions between repeating units. The links in real polymer chains are not free to rotate and have definite bond angles. The freely jointed chain model is unrealistic. Thus, in the treatment of freely jointed chain model it is important to consider the cross-terms which describe the correlations of neighbouring bonds. The presence of these correlations does not alter the basic random walk feature of the polymer chain statistics and simply alters the effective step size.

In a model where the bond is free to rotate but has a definite bond angle θ, the cross-terms of equation (1.3), $< (a_i . a_{j-1}) >= a^2 \cos\theta$ can be found. In general, it can be written as $< (a_i . a_{j-m}) >= a^2 \cos^m \theta$. As $\cos\theta$ is always less than unity, the correlation always dies away along the chain. This means that the chains can be broken into subunits, whose size can be larger than the range of the correlations.

For example, if there are *g* links in one of these new subunits, whose vector written c_i then the end to end distance is given by,

$$< r^2 >= \frac{N}{g} < c^2 >= Nb^2 \qquad \ldots(1.6)$$

Where *b* is an effective repeating unit size; the statistical step length. In practice, the effect of correlations along the chain is often characterised in terms of characteristic ratio C_∞,

$$c_\infty = \frac{b^2}{a^2} \qquad \ldots(1.7)$$

The characteristic ratio, or statistical step length, can be calculated from chemical details of the polymer, or experimentally, and is different for polymers with different chemical structures.

1.1.2.2 Long range effects

In short range effects, interactions between the neighbouring links are accounted for, but interactions between the distant points on the chain are neglected. However, this is not true as repeating units have definite volume and no two repeating units can take the same place at the same time. A chain cannot intersect to itself which gives rise to a self-avoiding walk. For a self-avoiding walk, end-to-end distance is given as,

$$< r^2 >^{1/2} = aN^{\nu} \qquad \ldots(1.8)$$

where exponent *v* is greater than *0.5,* which simply means that the excluded volume effect increases the size of polymer chain (swell) over its random walk value. Flory calculated the value of exponent as *3/5* with the assumption that repeating units are uniformly distributed within a given volume with no correlations between them. The Flory's value of the exponent is in close agreement with both experiments and with more sophisticated theories (renormalization group theory *[8,9]*, exact enumerations and computer simulations) which estimate a more accurate value of exponent, *0.588 [2]*.

1.1.2.3 Real chains in solution

In all the above models, the polymer chain is hypothesised as an isolated chain present in a vacuum. However, in reality this is not true and there are always energetic interactions between neighbouring polymer segments or with neighbouring solvent molecules. Depending upon the balance between the attractive and repulsive interactions between repeating units and solvent molecules, the chain can adopt various sizes.

For a condition when repulsive effect due to excluded volume effect (long range interaction) cancels out the attractive effect of the polymer/solvent interactions, the polymer chain follows ideal random walk, with $r \sim N^{0.5}$. This situation is known as the θ- condition, corresponding to a particular θ-temperature of a given solvent *[2-4]*.

For a good solvent, the attractive effect of the polymer-solvent interactions is stronger and the excluded volume is positive, leading to chain swelling. The polymer expands with $r \sim N^{3/5}$ and this happens at a temperature higher than the θ-temperature for corresponding solvent.

For a poor solvent, the attractive effect of the polymer-solvent interactions is weaker and the excluded volume is negative, leading to chain collapse. The chain collapses to globular conformation and the size is smaller than the ideal size. This happens at a temperature lower than the θ-temperature of a given polymer-solvent pair.

Depending upon the balance between the attractive and repulsive interactions between repeating units and solvent molecules, the polymer can undergo transition from an expanded chain, or coil, to the theta temperature and then to a collapsed coil.

1.1.2.4 Real chains in the melt

In the case of chains in a dilute solution, polymers do not follow the ideal random walk, which is because of excluded volume interactions and this leads chains to swell. If the concentration is increased, finally reaching to a condition of polymer melts where a chain molecule is surrounded by similar molecules of its own kind. At first glance, the situation looks more complicated. However, things become simpler and chains in a melt follow ideal random walk statistics. This is due to compensation of long range excluded volume interactions of the same chain by the interactions with neighbouring segments belonging to other chains. This was postulated by Flory and known as 'Flory ideality hypotheses'. This hypothesis was validated by Cotton *et al. [10]* using the neutron scattering technique and can be seen in Figure 1.2. However, a recent study by Wittmer *et al. [11]* showed that polymer chains in the melt are not random walk and related it to interplay of chain connectivity and the incompressibility of the melt system, which generates an effective repulsion between chain segments.

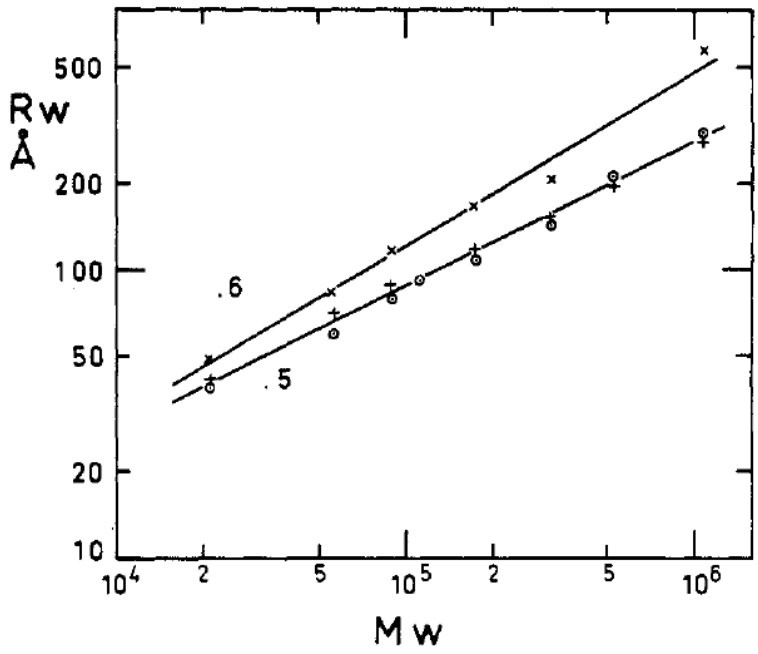

Figure 1.2. Log Rw (radius of gyration) plotted against log Mw. The experimental data were obtained for a) a good solvent shown by the cross symbols and b) θ -solvent shown by the plus symbol, and c) the melt by the open symbol. The slopes of 0.6 and of 0.5 were obtained by best fits [10].

1.1.3 Rubber Elasticity:

A rubber, above its glass transition temperature, is defined as a polymer melt in which cross-links (chains are covalently bonded) are randomly placed between adjacent polymer chains which bind the chains together to form a macroscopic network *[2,12]*. Rubbers are unique in their ability to deform reversibly to several times their size. The large deformability of networks is associated with entropic elasticity of the polymer chains present in the network.

1.1.3.1 Rubber elasticity (chemical bonding)

Affine and phantom network models:

The affine network model *[2,13]* assumes an affine deformation which means that deformation of each network strand is the same as the bulk deformation applied on the entire network. The model was originally proposed by Kuhn *et al. [14]*. The crosslinks are assumed to be fixed in space at positions exactly defined by the bulk deformation ratio, λ. In the phantom network model,

fluctuation of the crosslinks about their average affine deformation positions is allowed. It is important to emphasize that both models assume that the chains of the network behave like phantom chains, i.e. the dimensions of these chains are unperturbed by excluded-volume effects.

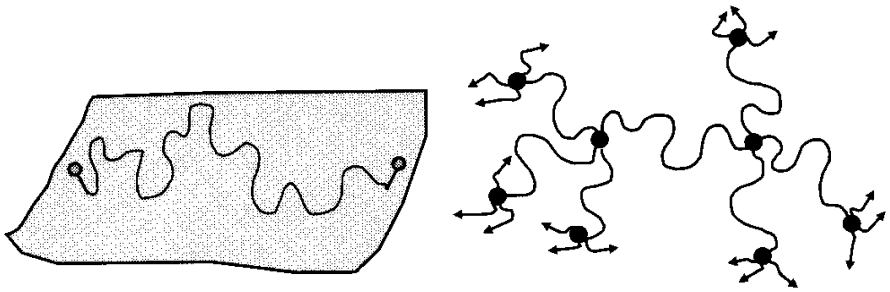

(a) **(b)**

Figure 1.3. (a) Affine network model - the ends of each network strand are fixed to an elastic background, (b) Phantom network model- the ends of network strands are joined at crosslink junctions that can fluctuate. Circles are crosslink junctions and arrows denote attachments to the rest of the macroscopic network [2].

Figure 1.4 shows schematically the difference between the affine network model and the phantom network model. The affine network model assumes that the junction points (i.e. the crosslinks) have a specified fixed position defined by the bulk deformation ratio. The chains between the junctions points are, however, free to take any of the great many possible conformations. The junction points of the phantom network are allowed to fluctuate about their mean values and the chains between the crosslinks to take any of the great many possible conformations.

The modulus of all the models, $G_{x,}$ as a network of strands with apparent molar mass M_x is given by,

$$G_x = \rho RT/M_x \qquad \ldots(1.9)$$

For the affine network model, M_x is the actual strand molar mass whereas the phantom network model requires a longer combined strand length.

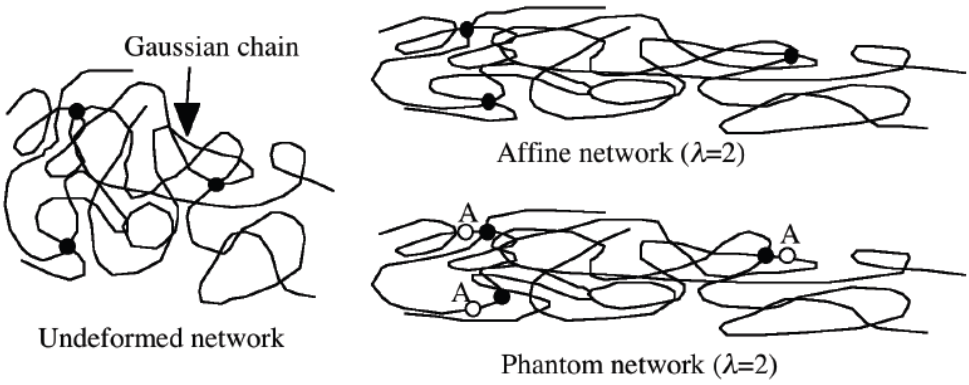

Figure 1.4. Schematic comparison between the deformation of a network, in the affine network model and the phantom network model. The unfilled circles indicate the position of the crosslinks assuming affine deformation (phantom network) [2].

1.1.3.2 Entangled rubber elasticity (physical bonding)

The modulus in many real rubber networks is much higher than the predictions of the affine and phantom network models. In both these models, repeating units other than chain ends do not feel any constraint. However, in reality, the network chains impose topological constraints on as they cannot cross each other, Figure 1.5. These topological constraints are called entanglements that raise the modulus of the network. A great deal of research has undergone to understand the effect of entanglement in polymers *[5,15,16]*.

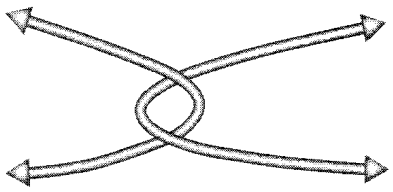

Figure 1.5. Sketch representing an entanglement formed due to the topological constraints in real networks.

The multi-body problem of entanglement has been reduced to the collective effect of all the surrounding chains on a given chain segment by introducing a tube-like region by Edwards *[7]*. Each repeating unit is constrained to the primitive path, but can fluctuate due to thermal energy. In the affine and phantom

models, the repeating units near to the crosslink points can fluctuate to the order of the unperturbed strand size. However, due to entanglement the network strand can only fluctuate transversely to a confining tube diameter *a*, Figure 1.6.

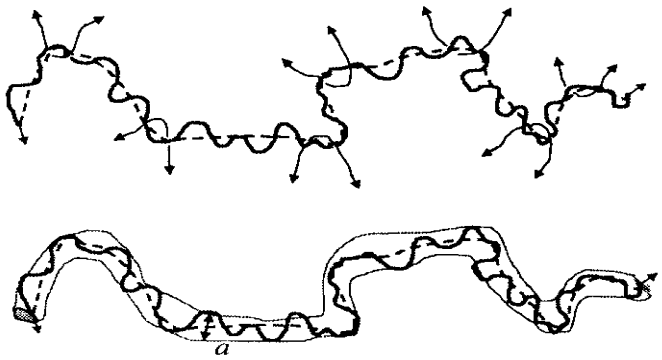

Figure 1.6. A chain or network strand (thick curve) is topologically constrained to a tube-like region by the surrounding chains. The primitive path is shown as the dashed curve [2].

The rubbery plateau modulus of a high molecular weight polymer melt is given by,

$$G_e = \rho RT/M_e \qquad \ldots(1.10)$$

where M_e is molar mass between entanglements.

The modulus is governed (a) by the crosslinks for low molar mass strands between crosslinks ($G \sim G_x$ for $M_x < M_e$) and (b) by entanglements for high molar mass strands between crosslinks ($G \sim G_e$ for $M_x > M_e$). For very long strands the modulus becomes nearly independent of the molar mass.

1.1.4 Dynamics in polymer melts:

1.1.4.1 Chain dynamics of a single chain

The first coarse grain models developed to understand the viscoelastic properties of polymers were for an isolated polymer chain and thus applicable to dilute polymer solutions. One of the early successful molecular models to understand polymer dynamics was developed by Rouse *[17]*. In this model, the polymer chain is represented by beads which are connected by springs, Figure 1.7. It is assumed that the polymer chain moves freely in the surrounding

environment presented by other chains and does not consider the hydrodynamic effect. In reality, the hydrodynamic interaction between the sub molecules has significant effects on the chain dynamics *[18]*. However, surprisingly the Rouse model was found to describe well the viscoelastic behaviour of short, linear chains in concentrated systems *[2,5]*, despite the fact that this model is formulated for the isolated chain, not for mutually overlapping chains. This is because in polymer melts, hydrodynamic interactions are screened by the presence of the other chains.

The beads in the Rouse model only interact with each other through connecting springs. The vibration of these springs depends on its stiffness, the force constant, and is modified or damped by frictional forces acting upon the beads. There are no hydrodynamic interactions between beads. The frictional forces are due to contacts with other polymer chains.

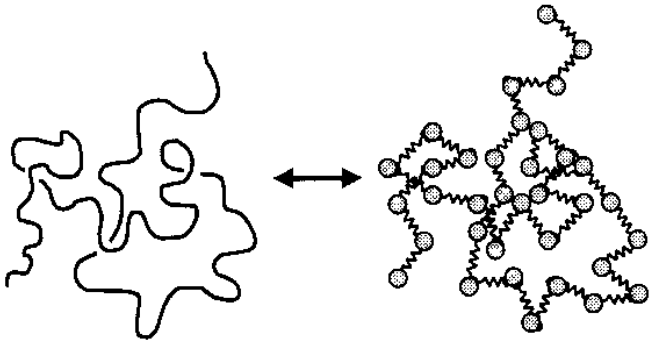

Figure 1.7. Schematic for the Rouse model. A polymer chain of N repeating units is mapped onto a bead-spring chain of N beads connected by springs [2].

The total friction coefficient of the whole Rouse chain is the sum of the contributions of each of the beads,

$$\varsigma_R = N\varsigma \qquad \ldots(1.11)$$

where ς is the individual friction coefficient for each bead.

The diffusion coefficient of the Rouse chain is given as,

$$D_R = \frac{kT}{\varsigma_R} \qquad \ldots(1.12)$$

The polymer diffuses a distance of the order of its size during a characteristic time, the Rouse time

$$\tau_R = \frac{r^2}{D_R} = \frac{\varsigma}{kT} Nr^2 \qquad \ldots(1.13)$$

Where r is end to end distance of the chain defined as in equation (1.4). The Rouse time has a great significance in polymer dynamics. On a time scale shorter than the Rouse time polymer chains show viscoelastic modes such as elasticity. For a higher time scale than the Rouse time, polymer chain moves diffusively and exhibits the response of a simple liquid (viscous). The Rouse model also brings out the linear dependence of the zero shear viscosity on the polymer chain length.

1.1.4.2 Chain dynamics in polymer melt

Probably the most fundamental feature of polymers noticed first was the dependence of some viscoelastic quantities (e.g. zero-shear viscosity, η_0) on the chain molecular weight, M_W.

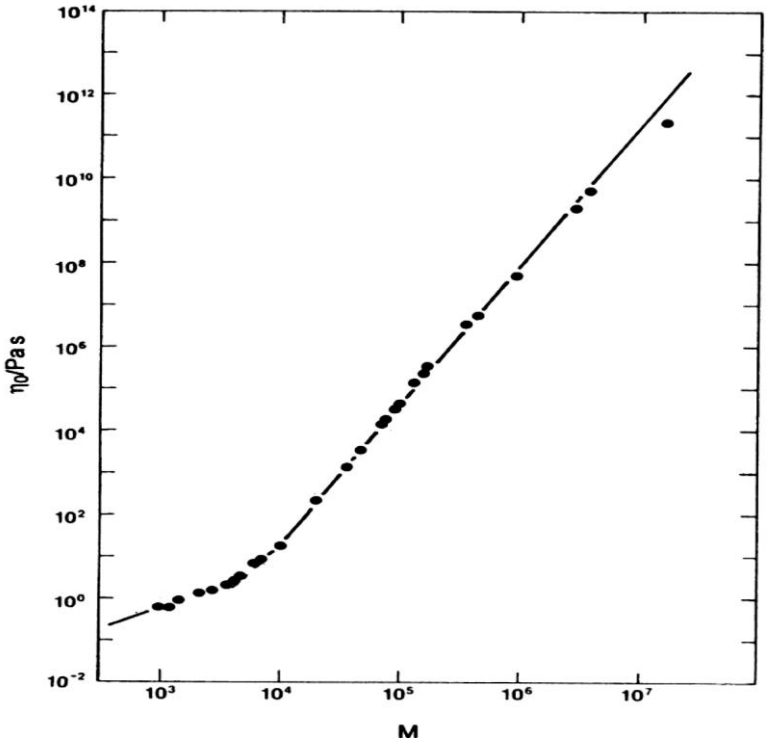

Figure 1.8. Molecular weight dependence of the zero-shear viscosity, η_0, in a bulk, monodisperse linear polybutylene (PB) at 25°C. Two solid lines indicate the power-law relationships $\eta_0 \alpha M$ and $\eta_0 \alpha M^{3.4}$ [19].

For long linear chains in concentrated polymer systems, early experiments *[4,5]* revealed that the zero-shear viscosity increases in proportion to $M^{3.5\pm0.2}$, Figure 1.8. This power law scaling of ~3.5 of zero shear viscosity to the molecular weight is not found for short chains (up to a critical molecular weight, M_c), is attributed to dynamic interactions between long chains referred to as entanglement *[4,5]*. The universality in the slow viscoelastic relaxation of long chains indicates that the entanglement is related to the chain un-crossability, not to specific interactions (such as local attractions) that change with the chemical structure of the chains. The entanglements are not permanent and can disentangle with a characteristic time scale, τ_T. The most successful existing model of entangled polymers is the Edwards tube model *[20]*. This model considers the complicated multi-body problem of topological constraints arising from surrounding chains to a tube-like region, confining the motion of any long chain within the tube. This simplifies the multi-body problem into two simpler problems: (a) motion of a chain in its tube and (b) the motion of the tube due to motion of the surrounding chains in the entangled system, Figure 1.6.

De Gennes *[21]* proposed a simple yet elegant molecular picture for the dynamics of entangled chains. For a linear chain trapped in a fixed (cross- linked) network, he considered that the large scale motion of the chain is limited in the direction of the chain backbone because of the topological constraint from the network that disturbs the lateral chain motion over distances larger than the network mesh size. The resulting curvi-linear diffusion along the chain backbone is referred to as reptation (snake-like movement). Reptation of polymer chain in confining tubes can be nicely visualized in Figure 1.9.

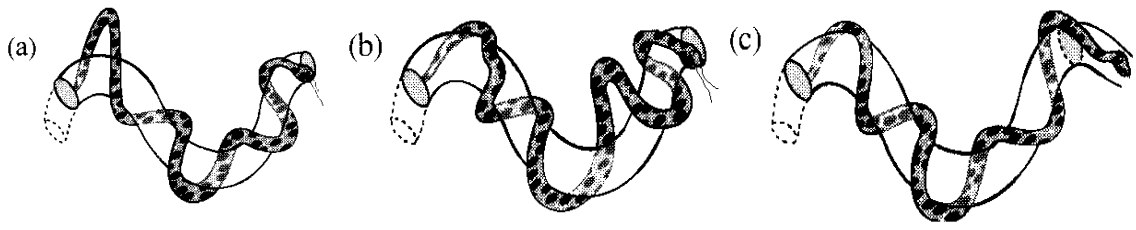

Figure 1.9. Reptation steps: (a) formation of a loop at the tail of the snake and elimination of the tail segment of the confining tube; (b) propagation of the loop along the contour of the tube; (c) release of the loop at the head of the snake and formation of a new section of the confining tube [2].

Doi and Edwards *[20,22-26]* extended this reptation picture to polymer melts/solutions and developed a model that enables consistent calculation of various dynamic properties of entangled linear chains at equilibrium as well as under flow. Chains in entangled melts/solutions form a dynamical mesh to mutually constrain their large scale motion. For a given chain (probe) in this mesh, the Doi–Edwards (DE) model assumes that the large scale motion is constrained in a tube-like region surrounding the probe backbone and this constraint survives (i.e. the tube is fixed in space) on a time scale of the probe relaxation. For this motion at equilibrium, the DE model introduces a further approximation that the probe contour length measured along the tube axis does not fluctuate with time. For this case, reptation is only possible at large scale motion of the probe. This motion is described in terms of a few, well defined molecular parameters, such as tube diameter. All dynamic quantities corresponding to this motion, i.e. those in the linear response regime are readily calculated. Under large strains/fast flow, the probe has largely distorted conformations and exhibits non-equilibrium motion. However, non-trivial differences were also observed e.g. the observed η_0 of linear chains is proportional to $M^{3.5\pm0.2}$ while the DE model predicts $\eta_0 \alpha M^3$.

Extra relaxation mechanisms by contour length fluctuation (CLF) *[23,27]* and the tube motion that allows a large scale lateral motion of the chain were incorporated in later models. The CLF concept *[6,28,29]* was naturally incorporated in the DE model that originally considered a flexible probe chain (Rouse chain) constrained in the tube. The latter concept of tube motion *[29-33]* was also introduced for the chains in entangled melts/solutions because the chains entangling with a given probe chain can exhibit the motion equivalent to the probe motion. For example, if a linear probe chain in mono-disperse systems reptates in its tube, the surrounding (tube-forming) chains equivalent to the probe should also reptate in their own tube to induce, in principle, the motion of the tube for the probe. The tube motion allows large scale motion of the probe in a direction lateral to its backbone to induce the probe relaxation *[6,15,28,29]*. This type of probe relaxation is referred to as the constraint release (CR) relaxation. This relaxation mode was later extended as double reptation specially in bi-modal blends *[34]*. Chain length fluctuation explains the discrepancies between basic

theoretical prediction (by DE model) and experimental results, e.g. molecular weight dependence of zero-shear viscosity; whereas, constraint release significantly modifies the relaxation spectrum *[35]*.

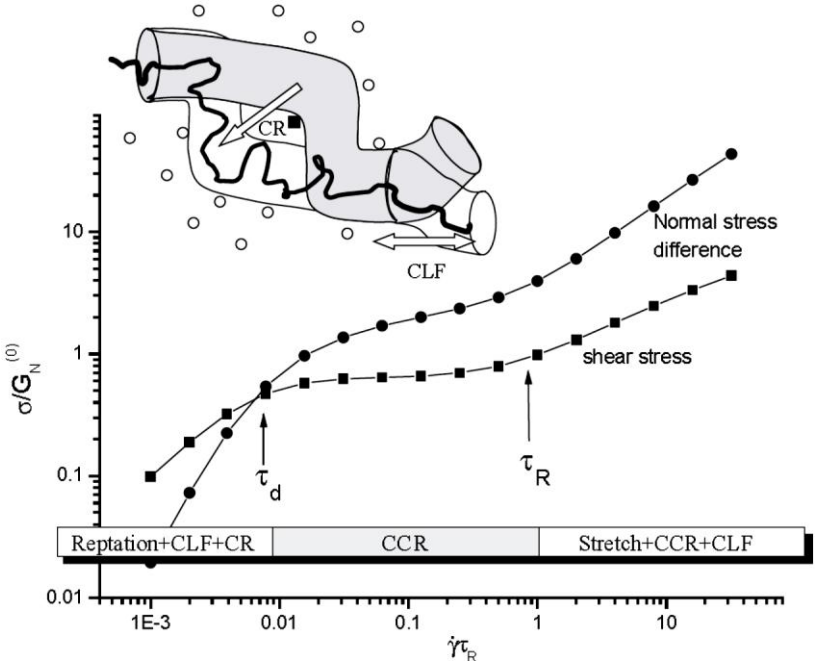

Figure 1.10. Schematic illustration of the shear rates at which the various tube-dynamic processes dominate. Plotted are both the shear stress σ_{xy} and normal stress difference $\sigma_{xx} - \sigma_{yy}$ with shear rate, where x and y are Cartesian components. Reptation (moderated by CLF) dominates a pseudo-Newtonian regime at low rates, until CCR causes the shear stress nearly to plateau when shear rates are faster than reptation. At high rates faster than the slowest CLF mode, the chains start to stretch and shear stress rises again. Inset: The three physical processes of polymer dynamics in a constraining tube are shown. Under reptation, the whole chain takes diffusive steps along the tube in a random direction (solid line). Under CLF, the chain end explores new tube configurations through longitudinal fluctuations of the total entangled tube length, but without requiring centre-of-mass (reptation) motion. Under CR, an entanglement with a neighbouring chain (shown by the solid square) may disappear, allowing effective conformational relaxation of that part of the tube, again without reptation of the test chain itself. Tube configuration before relaxation is shaded; after relaxation, light [32].

Under large shear (in the nonlinear range), earlier stretching of the chains was considered and accounted for flows faster than the reciprocal of the Rouse

time *[36,37]*. Later convective constraint release (CCR) *[38-40]* was added with chain stretch in the model to account for the problem of excessive shear thinning predicted by the DE theory *[35,41]*. The different tube-dynamic processes involved during flow are summarised in Figure 1.10.

The background and earlier work in the area of the non-linear rheology using large amplitude oscillatory shear (LAOS) is discussed separately in the beginning of chapter 3.

1.2 Polymer crystallisation:

Polymer crystallisation is a transition where randomly coiled polymer chains go to a perfectly ordered state and is one of the exciting phenomena in polymer physics *[42,43]*. Polymer crystallisation has puzzled scientists for many years and there has been rigorous debate *[44-52]* on the process by which a polymer crystallises, and there is considerable disagreement on the route taken to crystallisation. The prerequisite for crystallisation is that the chains are linear and stereo-regular.

1.2.1 Crystallisation from dilute solutions

Originally, it was believed that polymers being long chain molecules, highly entangled in their melt state, cannot form well-defined crystallites upon cooling from their melt. It was believed that most segments of polymer chains come together to form the so-called fringed-micellar crystals, first proposed by Herman *et al. [53]*, Figure 1.11a; a logical conclusion in view of the fact that the long chain molecules are highly entangled in the polymer melt. During cooling the long polymer chains aligned and pack themselves into ordered arrays. These ordered arrays are called crystallite and separated from each other by the amorphous regions. As the polymer chain length can be much longer than the crystal thickness, a chain can participate in the formation of many crystallites crossing many amorphous regions.

In the late 1950s, folded-chain crystals were discovered by Keller *[54]*, Fischer *[55]*, Till *[56]* and Jaccodine *[57]* by crystallising linear polyethylene from dilute solution. With the help of electron-diffraction experiments, Keller *[54,55]*

showed that the long polymer chains are folded into platelet (lamellar) crystals, where crystallites form thin platelets (lamellae) upon which polymer chains align back and forth in the direction perpendicular to the largest dimension (plate), Figure 1.11b. The thickness of the lamellae can be in the order of 10nm whereas the lateral size is at least an order of magnitude higher in μm. During crystallisation from the melt, with lamellae in the nucleus, crystals can further grow into large structures known as spherulites where between each lamellae amorphous regions can reside. However, another model known as the switchboard model, suggested that the chain does not re-enter (or irregular entry) the same crystallites where its adjacent chain segment crystallises but crosses through the amorphous region to another lamellae formation *[58]*. All the models extensions of previous and are elegant; however, actual crystal morphology is more complicated and depends on several parameters during crystallisation and on chemical structure.

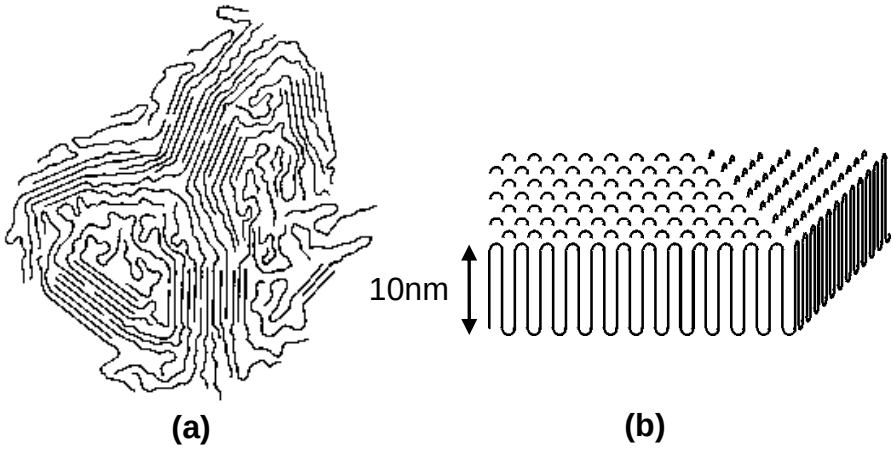

Figure 1.11. (a) Schematic representation of the fringed micelle concept and (b) folded chain crystals [59].

Crystallisation from very dilute solutions with concentrations < φ* (overlap concentration); the chains in solution are completely disentangled to start with, facilitating the development of regular crystallites. Many studies have shown that low molecular weight PE chains form platelet single crystals upon crystallisation from a dilute solution *[54,55,60-65]*. These single crystals are thin, in the order of 10 nm, and at least an order of magnitude larger in the lateral directions. The chains in these crystals are folded along the lateral faces of the growing lamellae,

thereby subdividing the crystal in different sectors. Further, Toda *et al. [66]* observed that within a polyethylene single crystal, polymers chains tilt at an angle of 10-17° to the folding surface of lamellar crystals. The tilting direction can be different for each growth sector leading to characteristic tri-dimensional forms (Figure 1.12c).

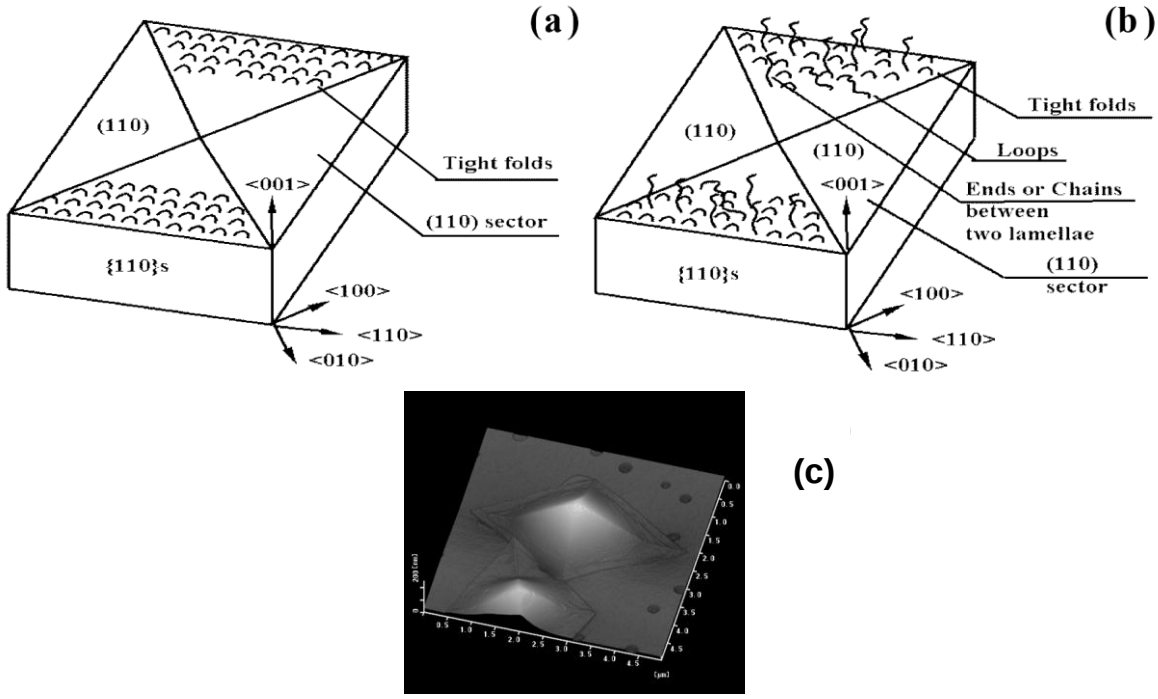

Figure 1.12. (a) Sketches of the fold surface organization with tight adjacent re-entrant folds [67] and (b) loose folds of the switchboard concept [58,68] (c) AFM topographic image of polyethylene single crystals of 30 kg/mole grown from dilute solution. In the picture crystals having convex hollow pyramidal type morphology is shown as an example [66].

1.2.2 Crystallisation from the melt

Crystallisation of polymer chains from the melt (concentrations > φ*) is not as simple as dilute solution where chains are separated from each other (disentangled). During crystallisation from the melt, the polymer chains must disentangle from the highly entangled network to achieve a regular conformation; the chain segments align parallel to each other and bend to form folded-chain crystals. Although, long polymer chains upon crystallisation have the tendency to form folded-chain crystal structures, but due to topological constraints such as entanglement, cannot form a regular chain folded crystal compared to their solution route. On crystallisation from the melt, spherulites that are aggregates of

folded-chain crystals are formed *[69-72]* . During crystallisation from the polymer melt at rapid cooling rates, randomly aligned and entangled chains may remain frozen in a disordered state (lesser time for disentanglement of the chains) and the solid will have a disordered structure. However, upon slow cooling, some polymer chains acquire ordered chain conformations and align in plate-like crystalline lamellae. In real polymer processing practice, due to variable cooling rate, the morphology becomes rather complex. Hence, final properties of the product depend on the complex morphology generated due to the processing conditions (crystallisation kinetics). Depending upon the molecular characteristics (such as Mw and molecular weight distribution) of polymer and crystallisation conditions (such as temperature and cooling rate), several kinds of morphology have been reported *[73-76]*.

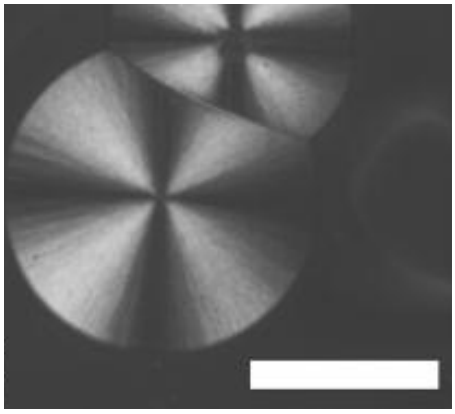

Figure 1.13. Spherulites of poly(vinylidene fluoride) taken by polarised optical microscopy. Bar represents 100 μm. Adapted from Toda et al. [77].

Orientation induced crystallisation:

During real polymer processing conditions (involving large shear and extension flow), the morphology generated does not depend upon the cooling rate alone, but also the flow (stretching of chains) involved. Flow in the melt (and solution) can lead to local ordering of the chains causing a decrease in the entropic barrier for the nucleation and, hence, increasing the crystallisation rate (higher crystallisation temperature) of the chains *[78]*. The high molecular weight component stretch due to their slower relaxation and forming extended chains which act as nuclei for lamellar growth of un-oriented low molecular weight chains. Thus, the developed morphology is known as shish-kebab morphology *[79-82]*.

1.2.3 Crystallisation during polymerisation

Unlike crystallisation from solution and melt, crystals can also form during polymerisation and are generally termed as nascent crystals (as-polymerised reactor powders). Crystallisation during polymerisation can proceed through different paths as depicted in Figure 1.14. Like crystallisation from solution and melt, crystal morphology depends on several coupled parameters arising during polymerisation, leading to numerous morphology developments, such as; fibrous crystal formation *[83-86]*, needle-shaped crystals under pressure in gas, liquid and solution phase polymerisation *[87]*. Crystallisation in heterogeneous and soluble catalytic systems produces chain-folded dendrites to a spherulitic morphology *[88]*. It is believed that in case where folded chain crystals are formed, crystallisation starts after completion of the polymer chain, similar to crystallisation from solution *[71,89,90]*. In a reaction at a higher concentration of catalyst, Keller *[91]* found a composite structure similar to the shish-kebab crystals. Formation of extended chain crystallisation was also reported by Chanzy *et al. [92]* using a catalyst supported on glass.

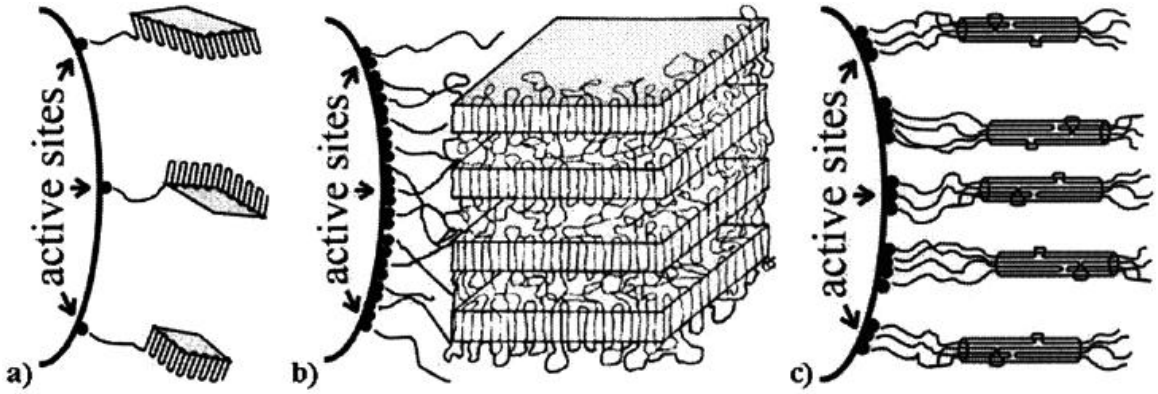

Figure 1.14. Schematic representation of crystallisation during polymerisation. (a) low density of active catalyst sites having no interaction between them, resulting in monomolecular metastable folded-chain crystals, (b) highly entangled molecules and folded-chain crystals forming due to high density of active catalyst sites with high polymerisation and low crystallisation rate; and (c) intermediate density of active catalyst sites and equal rate of polymerisation and crystallisation may result in less entangled molecules and extended chain crystals. Reproduced from Loos et al. [93].

Numerous studies *[89,90,94-107]* have been performed on crystal morphology produced during polymerisation. In polyolefin polymerisation, catalysis can proceed homogeneously through a dissolved initiator or heterogeneously on the solid catalyst particle surface. In a homogeneous reaction, crystallisation proceed after active polymer molecules (oligomers) form nucleates, whereas, in the heterogeneous reaction, the catalyst particle itself can serve as a primary heterogeneous nucleus for crystallisation *[88]*. Polymerisation of ethylene with a Ziegler-Natta type catalyst at low polymerisation temperature yields fibrous and chain folded lamellae *[90,94,108-110]*. Georgiadis *et al.* proposed a crystal growth mechanism during polymerisation; crystallisation proceeds after formation of the chains at higher polymerisation temperatures, whereas simultaneous polymerisation and crystallisation occurs for lower polymerisation temperatures *[110]*. The crystal morphology produced during polymerisation will depend on several parameters (coupled) such as polymerisation temperature, heterogeneous or homogeneous polymerisation, solvent, nucleation barrier, catalyst concentration, crystallisation rate, polymerisation rate. The morphology produced also has implications for the product properties of the polymer. For example, Smith *et al. [111-113]* showed the possibility of producing easily process-able ultra-high molecular weight polyethylene (UHMw-PE) in its solid-state into high strength/high modulus films, tapes and fibre; using controlled polymerisation conditions.

1.3 Melting in semi-crystalline polymers

In the previous section, polymer crystallisation and arising morphologies in quiescent and flow conditions have been addressed. Crystal morphology will depend on several crystallisation parameters which eventually decide whether the chains are shared among many crystallites through amorphous region or fold back into the same crystallite causing adjacent or non-adjacent re-entry, for example. See Figure 1.18. An intermediate ordered interphase exists between crystalline and amorphous phases which has a profound effect on melting of semi-crystalline polymers *[114-121]*. In the literature, this interphase is also referred as partially ordered component, rigid amorphous, non-crystalline, intermediate etc. Thus, polymer crystals which can take a large range of

morphologies and structures should be carefully identified before trying to understand their melting aspects *[122]*.

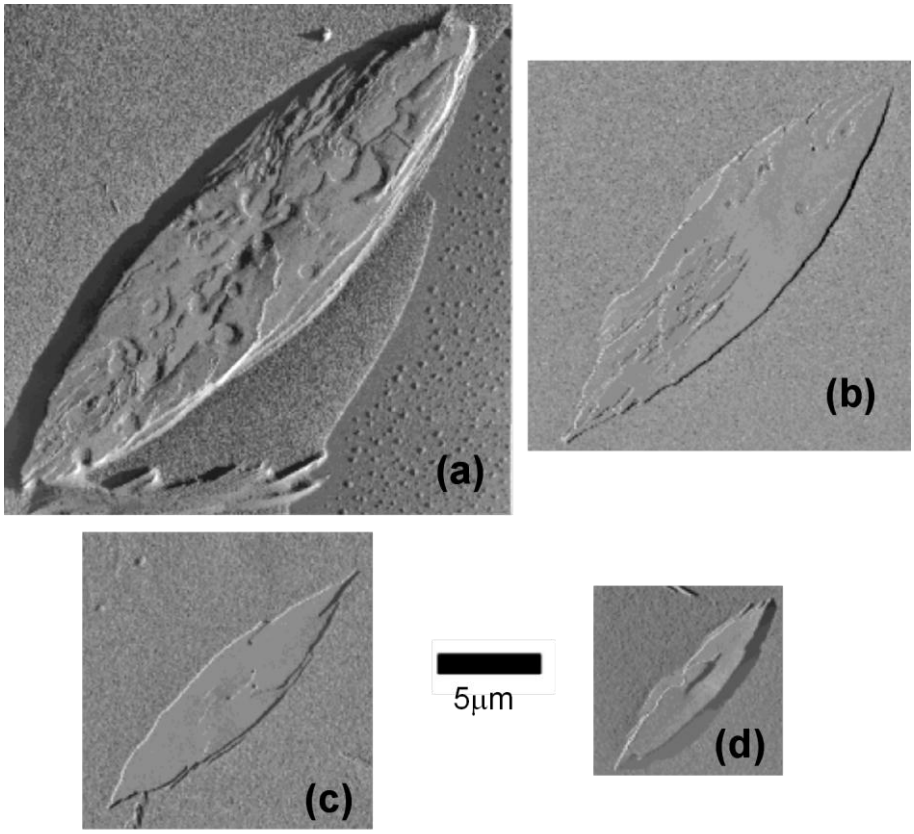

Figure 1.15. Atomic force microscopy (AFM) images of PE crystals (Mw = 32,100 g/mol and Mw/Mn = 1.11): (a) grown from the melt at 128.5°C and melted at 134.5°C for (b) 5 s, (c) 10 s, and (d) 15 s. Reproduced from Toda et al. [77].

Hellmuth *et al. [123]* were first to report sufficiently slow melting of large equilibrium crystals of linear macromolecules. An increase in melting temperature with increasing heating rate was observed, suggesting a superheating effect. Later Prime *et al. [124]*, with the help of electron microscopy and slow melting (near melting temperature), followed the melting of extended chain polyethylene crystals, and were able to observe various stages of melting. These authors found the melting to proceed by melting of low molecular weight crystals surrounding the large extended chain lamellae. After melting of the surrounding crystals, the extended chain crystals were found to break around amorphous phases into smaller parts followed by melting from the outer surfaces towards the interior of the crystal. The top of the lamellae surface was found to remain intact during melting of the extended chain crystals. Similar observations were also

made by Kovacs *et al. [125]* on folded and extended chain crystals of poly(ethylene oxide) and recently by Toda *et al. [77]* on single crystal of polyethylene using direct microscopy and AFM. See Figure 1.15. It was concluded that the melting of equilibrium crystals proceed by layer after layer, starting at the lateral crystal surfaces and making its way towards the core of the crystal in the directions perpendicular to the chain. These findings lead Toda and co-workers *[77]* to consider the presence of a nucleation barrier during melting. See Figure 1.16.

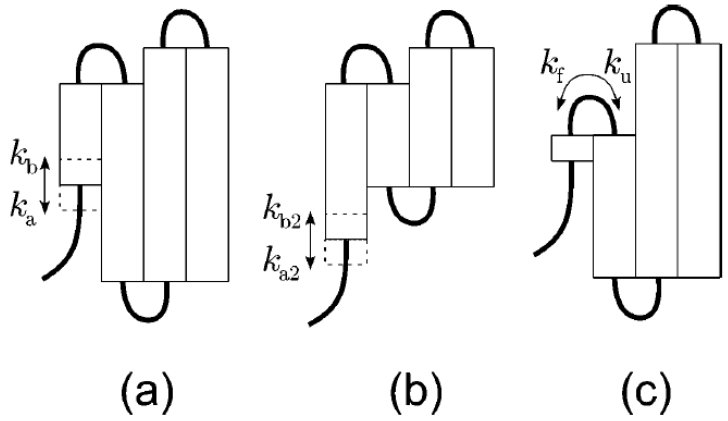

Figure 1.16. The processes at the melting/crystallisation tip of a stem: advance and reverse processes for the stem shorter (a) and longer (b) than the preceding stem, and the processes of folding and unfolding in (c). K_a and K_b are rate of addition and removal of a growth unit, respectively. K_{a2} and K_{b2} are rate of addition and removal of growth unit at the edge with the penalty of creating new side surfaces, respectively. K_f and K_u are rate of folding and unfolding of a chain, respectively. Reproduced from Toda et al. [77].

Recently, following the concept of a single chain forming a single crystal (monomolecular), with the help of controlled synthesis it has been possible to achieve such a distinct morphology in linear polyethylene having molecular weight greater than a million g/mol. For example, a polymer single crystal having dimensions 20 x 20 x 12 nm will be able to accommodate a chain of molecular weight 2.8 x 10^6 g/mol. This is shown in a simple calculation below. Such a distinct morphology has been confirmed by electron microscopy as well as X-ray diffraction data. These monomolecular crystals, similar to the studies reported by the others, show a unique melting behaviour that has been investigated by

Rastogi and co-workers. These authors *[117,118,126,127]* have shown a heating rate dependence on the melting process of these monomolecular crystals.

Considering lamellae dimension size = 20 x 20 x 12 nm and 100% crystallanity:

Mass of one chain of Mw ~ 2.8 million g/mol	=	2.8×10^{6}	/	6.02×10^{23}	=	4.65×10^{-18} g
Volume of crystal in cm^3 with 20 x 20 x 12 nm	=	4.8×10^{3}	x	1.00×10^{-21}	=	4.8×10^{-18} cm^3
Density of crystal in g/cm^3					=	1.00
Mass of chain residing in one crystal volume (100% crystalline)					=	4.8×10^{-18} g

However, in normal practice, the melting process in semi-crystalline polymers can be more complicated due to the presence of chain ends in the other crystal or non-adjacent chain folding. Restriction in detachment of the chain end can arise due to its incorporation in other crystals or in the same crystal by folding back through tight or loose folds (loops); restricting further sequential melting *[122]*, involving detachment of chains from the crystal surface as depicted in the single crystals.

Measurement of the melting temperature in semi-crystalline polymers is also complicated as it is generally not feasible to achieve crystals in the equilibrium state to get slow melting for the precise measurement of data. Hence several extrapolation methods have been devised to calculate the equilibrium data from metastable and small crystals of these semi-crystalline polymers *[122]*. Metastable crystals can be seldom measured at their equilibrium even after annealing or heating with slow heating rates. For example, in chain-folded crystals from solution melting temperature increases with decreasing heating rates due to simultaneous reorganisation processes (crystal perfection) *[123,128,129]*. Extended chain crystals melt at higher temperatures with increasing heating rate due to superheating (supplying heat to the crystals faster than the crystal can melt) and depends upon the melting velocity *[122,123,130]*. However, conventional differential scanning calorimetry (DSC) shows an increase in peak melting temperature with heating rate even for a pure metal standard

such as Indium. This artefact can result from instrumental measurement delay depending on thermal contact between sample pan and the sample temperature monitoring point itself *[131,132]*. Hence, it is also important to evaluate the apparent shift due to the instrumental delay in measured temperature during the melting region of the polymer crystals. An empirical method of temperature calibration can be used by using the onset temperature of melting of standard materials at the respective heating rates. However, Schawe *[133]* showed that the apparent shift due to instrumental delay also depends upon the peak height and slope during melting of the polymer crystals, hence the shift cannot simply be corrected by empirical method. Recently, Danley *et al. [132]* showed that by knowing instrumental coefficients pre-determined by a standard sample, it is possible to plot true heat flow from the sample against the true sample temperature to calibrate the instrumental thermal delay accurately. Alongside the instrumental delay and the reorganisation process (melting kinetics), the melting temperature can also increase (a) with increasing molecular weight; (b) with a decrease in entropy of the amorphous phase; (c) normally with increasing pressure *[122]*. Molecular weight distribution also plays an important role where polydispersity will broaden the melting peak of the polymer caused by distribution of crystal sizes.

Melting in solids is defined as a first-order transition (sharp) at the intersection of the Gibbs free energy of the solid and the liquid states, which is only true if one considers equilibrium and infinite size of the phases involved. However, these conditions are not met in semi-crystalline polymers such as polyethylene, either crystallised from solution or the melt. These polymers possess lamellae crystal thickness of finite dimensions (10-30 nm) with lateral dimensions of at least an order of magnitude larger *[54-56,134-136]*. The Gibbs-Thompson equation in its simple form has been widely used to describe quantitatively the maximum melting temperature correlating the lamellae thickness *[118,137,138]*;

$$T_m = T_m^{\infty}[1 - \frac{2\sigma_e}{l.\rho.\Delta H_m} - \frac{2\sigma}{A.\rho.\Delta H_m} - \frac{2\sigma}{B.\rho.\Delta H_m}] \qquad \ldots(1.14)$$

where T_m is the experimentally determined melting temperature, T_m^{∞} is the equilibrium melting temperature for an infinite size crystal (141.5°C for

polyethylene *[126,139]*), σ_e is the surface free energy for the folded planes, σ is the surface free energy of the lateral planes, l is the crystal lamellae thickness, ρ is the crystal density and ΔH_m is the heat of fusion per unit mass, where A and B are the lateral crystal dimensions. Normally A and B terms are neglected as the lateral dimensions are an order of magnitude higher than the crystal thickness, l. For crystal of infinite l, the melting temperature reaches an equilibrium melting temperature. However, the above form of the Gibbs-Thompson equation does not predict the correct melting temperature for a given crystal thickness such as in case of nascent UHMw-PE polymers *[59,118,126,127]*, where A and B cannot be fully neglected due to their finite size.

Höhne *[137]* proposed a modified form of equation (1.14) and is given in equation (4.2) to deduce the melting point of polyethylene (even its oligomers) by using the number of CH_2 groups involved in melting rather than the thickness of the lamella l, which describes the melting behaviour of linear, cyclic and folded alkanes with the same set of parameters as well as all types of polyethylene. This simple and elegant approach describes a melting point mainly by the number of CH_2 units which the molecule feels dynamically during its conformational change and constraints felt due to crystal morphology (tight or loose folds in amorphous region). Also, the increase in the melting temperature with increasing heating rate simply cannot be explained by existing thermodynamic concepts alone without invoking melting kinetics.

Rastogi and co-workers *[59,117,118,127,140]* with the help of annealing below the peak melting temperature were able to show the involvement of different melting processes in UHMw-PE polymers having different morphologies, Figure 1.17. These authors identified three different energies which correspond to (a) detachment of a chain segment of ~28 nm (roughly equal to one chain stem) at the lateral surface of lamellar crystal; (b) simultaneous detachment of three stems from the crystalline substrate and their co-operative diffusion; whereas, (c) involves breakdown of the crystal by simultaneous randomisation of at least 7-8 stems. In nascent disentangled UHMw-PE samples, melting can proceed by consecutive detachment of single chain stems. However, such a possibility is not available in nascent entangled UHMw-PE samples due to topological constraints

present in these entangled samples. Later these authors showed that by using controlled (slow) heating in disentangled UHMw-PE, it is possible to obtain a new (heterogeneous) long-lived melt state which possesses reduced melt viscosity, providing enhanced draw-ability on crystallisation *[117,118,126,140]*.

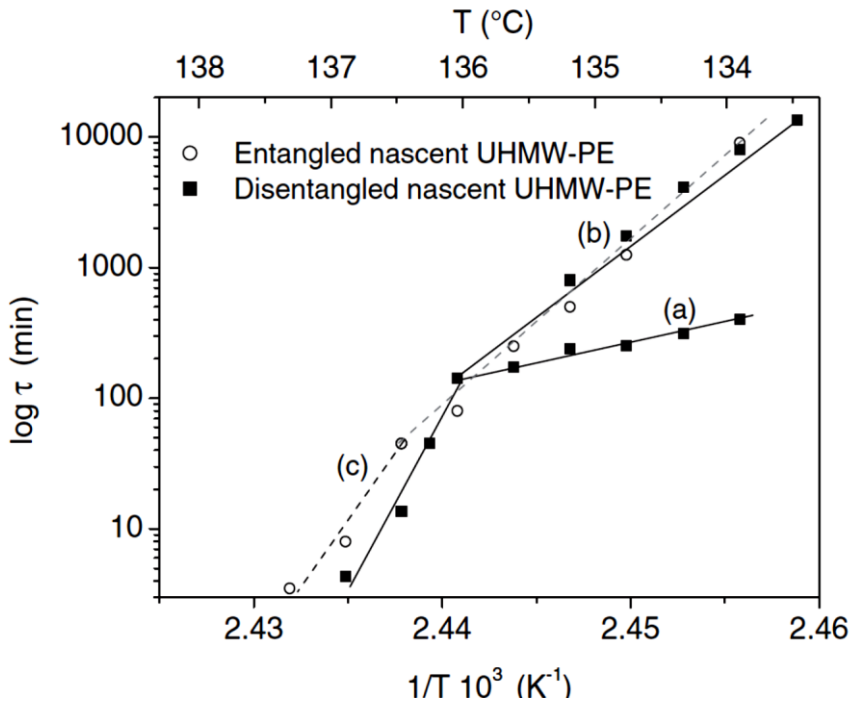

Figure 1.17. Arrhenius plot for the time constants determined from the melting rate at different annealing temperatures (below peak melting temperature) for the nascent entangled and disentangled UHMw-PE samples. (a) Detachment of a chain segment of ~28 nm at the lateral surface of lamellar crystal, (b) simultaneous detachment of three stems from the crystalline substrate and their co-operative diffusion, and (c) breakdown of the crystal by simultaneous randomisation of at least 7-8 stems. Reproduced from Lippits et al. [127].

1.4 Crystallisation and disentanglement:

In early 1930s, Carothers *et al. [141]* formulated and predicted conditions for achieving high strength oriented fibres, consisting essentially of a single crystal where the long molecules are in the ordered array with the fibre axis. The high strength in the direction of the fibre axis is due to the high cohesive forces of the long chains. However, in actual fibres a large number of molecules fails to align them completely with respect to ordered structure mostly due to constrains such as entanglements; leading to lower mechanical values than the theoretically

predicted. Although oriented fibres are not expected to arise in any process of spontaneous crystallisation under the ordinary conditions, post stage such as cold drawing (crystallisation under deformation) could be employed for the formation of orientated fibres with high strength *[141]*.

Treloar *[142]* and Frank *[143]* showed that theoretically attainable uni-directional Young's modulus for extended polymeric chains of polyethylene to be 180 GPa and 220 GPa, respectively. Later Capaccio *et al. [144-146]* using melt-spinning and followed by solid-state drawing were able to achieve highly oriented polyethylene fibres having a Young's modulus of the order of 70 GPa. However, melt-spinning and drawing did present a problem with increasing molecular weight as the viscosity increases. Pennings *et al. [147]* demonstrated the formation of shish-kebab type fibrils via a solution method alternative to melt-processing. However, a maximum modulus of 25 GPa was achievable as the fraction of extended chains could not be formed large enough *[148]*. The authors *[149,150]* were also able to produce orientated polyethylene crystals from UHMw-PE using a so-called surface-growth technique and achieve a maximum Young's modulus of around 100 GPa.

Smith *et al. [151-153]* by using crystallisation from semi-dilute solutions showed remarkable high drawability in the solid state to achieve ultra-high strength in so obtained dry film of polyethylene, due to the reduced number of entanglements. This has served as the basis for the development of the process of solution-spinning of ultra-high-molecular-weight PE (UHMw-PE) at DSM®, 1979. The fibres spun from semi-dilute UHMw-PE solutions, after removal of the solvent, can be drawn to high draw ratios (above 100) into fibres and tapes *[153]*. The thus obtained fibres possess a tensile strength of greater than 3 GPa and a Young's modulus greater than 100 GPa, which approaches the theoretical value for the fully extended chain crystals. The success of solution spinning for UHMw-PE was associated with the reduction in the number of entanglements in the amorphous region of the crystals and morphology formed, providing ease in solid-state processing.

1.4.1 Disentanglement via solution route

Crystallisation in semi-crystalline polymers is the reverse process of melting which demands polymer chains to free themselves from their entangled network by a process of reeling-in onto the crystal surface. By tuning the parameters which enhances crystallisation also promotes lesser entanglement formation in the semi-crytsalline polymer, which in turn also determines the processability and mechanical properties of the product *[1,111-113,151,152]*. Reduction in entanglement (disentanglement) in polymer is desired for their processability in solid-state, which decreases with increasing number of entanglement. However, it is also critical to have some entanglements between crystals, otherwise the polymer becomes brittle due to the absence of cohesion between crystals. Slow cooling allows more time for chains to reel out from the entangled network to form crystals, with lesser entanglement than residing in the amorphous region.

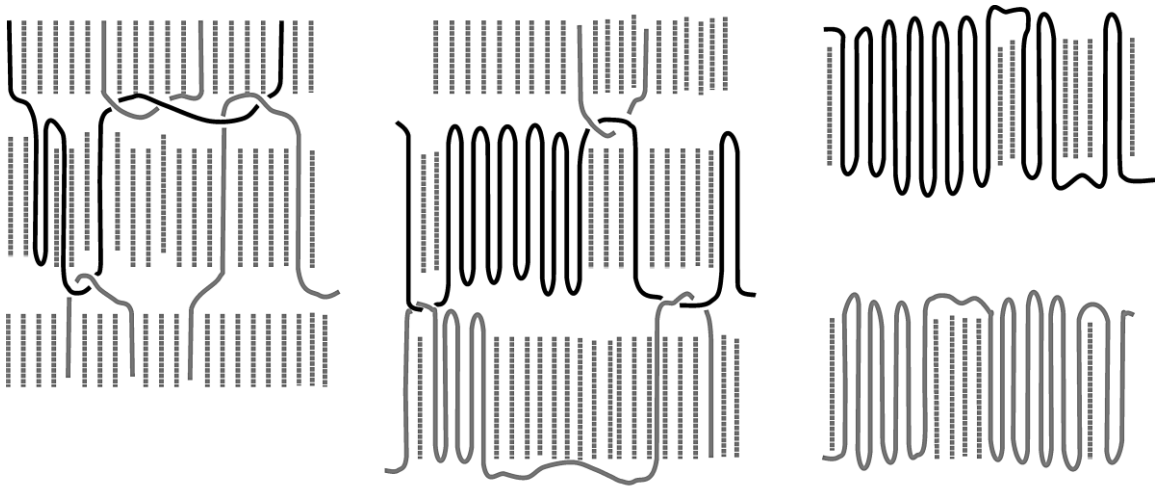

a) Melt b) Solution φ> φ* c) Solution φ< φ*

Figure 1.18. 2-D schematic representation of the chain trajectory upon crystallisation from melt (a); semi-dilute solutions (b); and dilute solutions (c); φ is the critical overlap concentration for polymer chains. Reproduced from Lemstra et al. [154].*

The number of entanglements left over after crystallisation can be minimised by reducing the number of overlapping polymer chains to start with. The number of entanglements (overlap) is less in solution of the polymer compared to its melt state and can have dependent crystal morphology. See

Figure 1.18. In the limit of dilute solutions where the polymer concentration φ is lower than φ*, no chain overlap and individual folded-chain single crystals can grow, possessing no or very low entanglement in the amorphous region of the crystals. Semi-dilute solutions (φ > φ*) also form folded-chain crystals but with increased number of entanglements in amorphous region of the crystals. Crystallisation from the equilibrium melt state (with maximum overlap) will have the maximum number of entanglements present in the amorphous region of the crystals. It is important to note that the final number of entanglements in the amorphous region of the crystals formed after crystallisation will depend on several parameters controlling the crystallisation of the chains themselves viz. cooling rate, solvent evaporation rate etc.

1.4.2 Disentanglement via direct polymerisation route

The solution crystallisation route to obtain disentangled polymers requires use of more than 90% of solvent; the disposal or recycling of which becomes cumbersome with environmental issues. Smith et al. *[111-113]* showed the possibility of producing disentangled UHMw-PE using controlled synthesis conditions where the polymerisation temperature was lower than the crystallisation temperature favouring formation of crystals before entanglement formation between growing chains can take place. However, a heterogeneous catalytic system is used in the conventional synthesis of the UHMw-PE (slurry process) where active sites are closely placed and polymerisation conditions are optimised to maximize the yield; leading to overlap of the growing polymer chains during polymerisation and entanglement formation.

The direct synthesis route using a homogeneous catalytic system to obtain disentangled polymers is a more elegant and promising route to control the entanglement in the polymer. In the homogeneous synthesis route, a single site catalyst is diluted to a level where growing chains from the active site of the catalyst do not see each other and polymerise at temperature lower than the crystallisation temperature *[155-158]*. The low temperature used for synthesis supports a faster rate of crystallisation of the growing chains as compared to the rate of polymerisation, with increased possibility of achieving monomolecular crystals growing from a single site catalyst. These UHMw-PE reactor powders

often referred to as 'nascent' UHMw-PE, can be remarkably ductile in the solid state *[111,156,157,159]*. With all practical complications involved in any synthesis, the polymers are not fully disentangled and have some amount of entanglement in them. However, the number of entanglements present in the polymer is much lower than those of commercial polymers synthesised using a Ziegler-Natta catalyst and a slurry process. The reduced number of entanglements in nascent polymers is clearly evident by their easy draw-ability in the solid state as compared to their conventional commercial counterparts. See Figure 1.20. Films from the reactor powders, in the same manner as solution cast UHMw-PE, could be drawn easily into high-modulus structures *[1,112,118,160]*. Figure 1.19 shows a possible route for the formation of crystals during polymerisation, simultaneously avoiding entanglement formation.

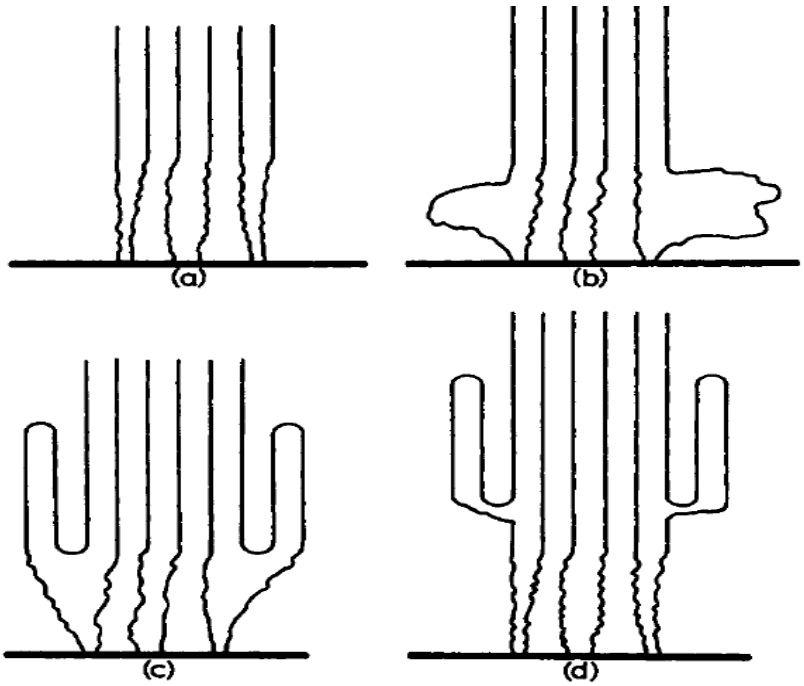

Figure 1.19. Schematic diagram showing a fibril composite structure evolving in a Ziegler (catalyst surface) synthesis because of the unequal chain growth rates on adjacent catalyst sites due to monomer feeding difference. (a) Fibrous crystals are formed by coalescence after they become insoluble beyond a certain chain length, (b) The active sites at the centre starve as compared to sites at the periphery. Hence, the faster growing chains at periphery bulge as one end fixed to catalyst and other to fibril, (c) the large bulge crystallise by folding, and (d) and as the folded portion advance farther from catalyst site, the monomer feed to extended chain portion at the centre gets easier. Adapted from Keller et al. [94].

1.4.3 Disentanglement and ease in processability

Crystallisation is an inherent chain-disentangling (removal of chain constraints) process and upon cooling from melt or solution, the long chain molecules withdraw from the entangled network in order to form a crystalline structure. It is understood that the entanglement network of a molten system is preserved into the solid state upon cooling to an extent depending upon the type of polymer; amorphous or crystalline. Entanglement in the network of polymer chains is responsible for the solid state mechanical properties of the amorphous polymers. The entanglement points act like physical crosslink points in the network and the molecular weight between two entanglement points, M_e governs the deformation behaviour for the material. The value of M_e is dependent on the polymer chemical structure and can be derived from the plateau modulus (G_N^0) through rheology by using equation,

$$G_N^0 = g_n \rho RT / M_e \qquad \ldots(1.15)$$

Where, g_n is a numerical factor (1 or 4/5 depending upon convention *[3]*), ρ is the density, R the gas constant and T the absolute temperature. The plateau modulus is an intrinsic property arising from the elastic response of the entangled polymer melt and is independent of the total number of entanglement per chain, which increases with the molecular weight.

In the case of semi-crystalline polymers, the entanglement density (or M_e) can change significantly during crystallisation. The long chain molecules are withdrawn from the entanglement network to form a crystalline structure (crystalline zones are void of entanglement). The extent of crystallisation (disentanglement) is dependent on the crystallisation conditions. In general, lower super cooling promotes disentanglement during crystallisation. As seen in earlier sections of the thesis, two effective ways of achieving disentanglement are by (a) crystallisation from dilute solution and (b) crystallisation during polymerisation. These two cases present the possibility of achieving nearly complete disentanglement in the solid state. A strong influence of higher entanglement density on the solid state deformation between melt-crystallised and solution-cast

polymer films, below the melting point and above the alpha relaxation temperature, can be seen from Figure 1.20 *[161]*. The easy draw-ability of the solution cast film over the melt crystallised sample can be observed. The strain hardening feature in the melt crystallised film is associated to the presence of entanglement in the amorphous regions of the semi-crystalline polymer. Detailed studies performed by Rastogi *et al. [161]* on solution crystallised polymer films show a regular stacking of crystals.

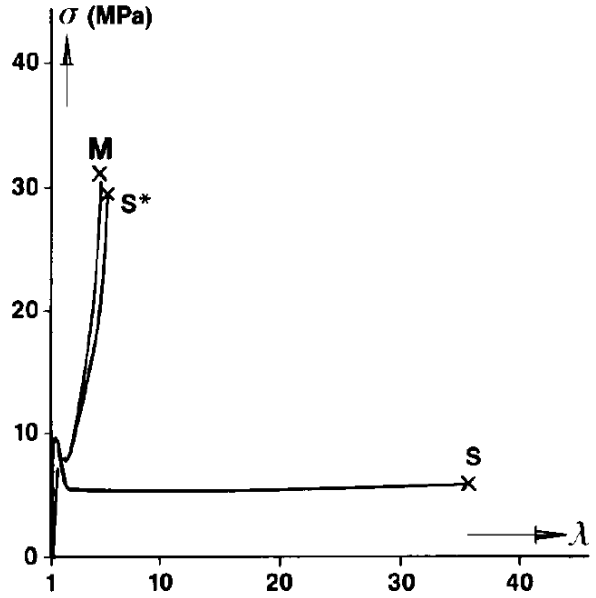

Figure 1.20. Nominal stress-strain curves of UHMw-PE at 90°C for melt-crystallised (M), solution-cast (S) film and re-crystallised film of solution-cast from 1 minute in the melt at 150°C (S). Reproduced from ref [162].*

Absence of strain hardening in solution crystallised film facilitates easy draw-ability and to achieve a very high draw ratio, leading to superior mechanical properties for applications such as fibres. In the direct synthesis route to achieve disentanglement, where a single site catalyst in dilute solution can be used ideally to produce single chain forming single crystal at lower polymerisation temperatures. The controlled synthesis gives a disentangled nascent system, where the entanglements reside in the amorphous regions. This system is similar to the solution cast films (although crystal morphology is very different) and can be deformed in the solid state. A recent study by Rastogi *et al. [1]* shows easy processability of disentangled UHMw-PE using direct synthesis, even extending Young's modulus (> 165 GPa) beyond that of solution-spun fibres (~130 GPa).

1.5 Outstanding issues and scope of the thesis:

In the recent past, several pioneering works *[59,156,157,163]* on disentangled UHMw-PE obtained using the direct synthesis route have been undertaken at the University of Eindhoven and Loughborough University. Although, these works touched upon several key aspects in synthesis, melting and melt dynamics of disentangled UHMw-PE; understanding of the disentangled state produced during polymerisation and its relation to the synthesis conditions and molecular characteristics such as molecular weight has been lacking. In this thesis, UHMw-PE synthesised via the direct synthesis route described by Talebi *[157]* has been extended to understand the relationship between synthesis conditions and the disentangled state. The synthesised polymer is used for studying melting, crystallisation and melt dynamics in the linear and non-linear viscoelastic responses. For simplicity, the polymers achieved by this route have been mentioned as nascent disentangled. However, in reality, this may not be a fully disentangled system.

1.5.1 Effect of polymerisation conditions on entanglement density in disentangled UHMw-PE

Thanks to the synthesis capabilities available in our group at Loughborough University, disentangled UHMw-PE samples with narrow polydispersity have been synthesised under controlled conditions. For this purpose a single-site catalytic system was used. By judiciously selecting the polymerisation conditions, it has been illustrated how the disentangled state (morphology) is influenced by the balance between the crystallisation rate and the polymerisation rate. The following studies were carried out using melt rheology within the linear viscoelastic regime of polymer melt.

- Entanglement formation in the nascent disentangled polymer melt.
- Effect of polymerisation time on molecular weight and its influence on entanglement density.
- Effect of synthesis temperature on entanglement formation.
- Crystallisation from the metastable melt state.
- Effect of molecular weight distribution on entanglement formation.

1.5.2 Non-linear melt rheology behaviour of UHMw-PE

Disentangled UHMw-PE has been seen as a promising material to be processed via melt route due to the reduced number of entanglement (resistance to flow), where the melt will require a sufficiently long time to establish the equilibrium (fully entangled) melt state. However, ease in processability and high draw-ability in the solid state of disentangled UHMw-PE is lost, almost immediately, after reaching the melt state. See Figure 1.20 *[162]*. Very few studies of the non-linear melt dynamics of disentangled UHMw-PE have been carried out in the past which could give an insight into correlating entanglement with the underlying dynamics during large scale flow *[157]*. In this respect, disentangled UHMw-PE gives a unique opportunity to follow the effect of entanglements on the non-linear melt rheology of polymers in general. The following studies have been performed.

- Non-linear melt rheology behaviour of entangled and disentangled UHMw-PE under large amplitude oscillatory shear (LAOS).
- Effect of entanglement density on the non-linear behaviour using LAOS.
- Effect of large shear on the entanglement density (or entanglement molecular weight).
- Effect of deformation rate on the non-linear behaviour in LAOS.
- Effect of molecular weight on the non-linear behaviour in LAOS of disentangled UHMw-PE.

1.5.3 Effect of entanglement (amorphous region) on melting and crystallisation

The melting behaviour of semi-crystalline polymers is complicated due to the influence of topological constraints in amorphous regions of crystals which influences the melting of the polymer *[117,118,161,163,164]*. The melting temperatures of solution, nascent and melt-crystallised samples of same polymer having approximately similar crystal thickness are distinctively different and cannot be explained by the Gibbs-Thomson equation alone. See equation (1.14) *[59,117,137,165]*. A negative or positive heating rate dependence of melting temperature can arise from crystal reorganisation or a superheating effect *[123]*. However, a non-linear heating rate dependence of the melting temperature

cannot be explained by a superheating effect alone, and melting kinetics plays an important role *[118,126,127]*.

In this thesis by selecting UHMw-PE samples, based on the understanding of morphology (entanglement and topological constraints in the amorphous region of crystals); melting aspects of nascent disentangled, entangled and melt-crystallised UHMw-PE samples are investigated with the help of DSC and temperature modulated DSC (TM-DSC). Following studies were performed.

- Effect of topological constraints on the melting temperature.
- Non-linear heating rate dependence of the melting temperature in nascent disentangled, nascent entangled and melt-crystallised samples.
- Effect of molecular weight on the non-linear heating rate dependence of the melting temperature.
- Melting in nascent disentangled and entangled UHMw-PE samples close to (below) the peak melting temperature.
- Characteristic melting time of nascent disentangled crystals using TM-DSC.
- Characteristic melting time with increasing entanglement in melt-crystallised UHMw-PE samples.

Although, most of the studies performed in this thesis are on UHMw-PE samples; many of the results and the understanding from this work can be extended and applied to flexible polymers in general. The high molar mass provides an experimentally accessible time to follow entanglement formation due to the consequent slower chain dynamics.

Chapter 2

Heterogeneity in the distribution of entanglement density during polymerisation in disentangled Ultra High Molecular Weight Polyethylene

Ultra High Molecular Weight Polyethylene (UHMw-PE) is an engineering polymer that is widely used in demanding applications because of its un-paralleled properties such as high abrasion resistance, high-modulus and high-strength tapes and fibres, biaxial films etc. In common practice, to achieve the uniaxial and the biaxial products, the solution processing route is adopted to reduce the number of entanglements per chain, such as found in Dyneema® from DSM®. Another elegant route to reduce the number of entanglements to ease solid-state processing is through controlled polymerisation using a single-site catalytic system. In this chapter, how different polymerisation condition, such as temperature and time control molecular weight and the resultant entangled state in synthesised disentangled UHMw-PE is addressed. Linear dynamic melt rheology is used to follow entanglement formation in an initially disentangled melt. With the help of rheological studies, heterogeneity in the distribution of entanglements along the chain length and the crystal morphology produced during polymerisation is considered. Due to the living nature of the catalytic system, with increasing polymerisation time molecular weight increases whereas the number of entanglements per unit chain decreases. These findings suggest that most of the entanglement is established at the initial stages of polymerisation and there is a heterogeneous distribution of entanglements. The effect of molecular weight, molecular weight distribution and temperature on the rate of entanglement formation is also presented.

2.1 Introduction

The mechanical properties in polymers are strongly dependent on molecular characteristics. For example, in linear polyethylene, with increasing molecular weight from several hundred thousand g/mol to a million g/mol or above, mechanical properties such as tensile strength, modulus, abrasion resistance increase to an extent that the polymer normally used in commodity applications becomes applicable for demanding applications, that include prostheses, light weight strong fibres and tapes for ballistic applications, ropes for replacement of steel cables etc. However, increased molecular weight of the polymers also adversely affects their processability, mainly due to the reduced number of chain-ends and increased number of entanglements per chain. Thus it has been always a quest to find a balance between ease in processing and the acquired mechanical properties of higher molecular weight polymers.

Smith and Lemstra *[151,152]* have shown improved processability of Ultra High Molecular Weight Polyethylene (*UHMw-PE*) by reducing the entanglement (density) by dissolution of the polymer (less than 5 weight %) in a solvent, such as decalin or xylene. Later, Smith *et al. [111,112]* also showed the possibility of synthesising disentangled *UHMw-PE* under controlled synthesis conditions where the polymerisation temperature was lowered to an extent that the crystallisation rate is favoured over the polymerisation rate, thus avoiding entanglement formation. For their studies, the authors made use of a supported vanadium catalyst, where the polymerisation was performed below -20°C. Due to the low polymerisation temperature the polymer yield was low. However, it was shown that the synthesised polymer can be compressed and drawn uni-axially to make fibres below the equilibrium melting temperature of linear polyethylene. Considerable studies have been performed to understand the morphology developed during polymerisation of the semi-crystalline polymers, which are generally synthesised at a temperature below their melt-crystallisation temperatures *[89,90,94-107,112,155,166]*. Although, most of these studies have been performed on samples synthesised using heterogeneous catalytic systems, it is interesting to see the influence of polymerisation conditions on the morphology of nascent (as-synthesised reactor powder) crystals.

Normally in commercially synthesised polymers, where a heterogeneous Ziegler-Natta (Z-N) catalyst is used, the crystallisation rate is slower than the polymerisation rate. Moreover, in a heterogeneous catalytic system, the active sites are tethered on a support and are close to each other which is likely to have a higher probability of finding the neighbouring growing chains. This result in the entanglement formation during synthesis of the polymer chains after the chains have grown beyond a critical chain length or entanglement molecular weight. In contrast to the heterogeneous synthesis, in the homogeneous synthesis, the catalyst and co-catalyst are dispersed in the polymerisation medium (solvent) where active sites are separate on the molecular level and far from each other depending upon their concentration. Thus, the homogeneous synthesis provides an opportunity to control the polymerisation rate, crystallisation rate and desired separation between the polymerisation sites to tailor the entangled state in the synthesised polymer. Such a possibility results in the formation of disentangled polyethylene; ultimately resulting into a "single chain forming single crystal" *[59,156-158]*.

Recently, in our group by using a single-site homogeneous catalytic system, disentangled UHMw-PE were synthesised by following the concept of single-site forming single crystal, separating the active sites in the solvent to an extent that the growing chains do not overlap during polymerisation at low polymerisation temperature *[160]*. This novel synthesis also presents the possibility of synthesising UHMw disentangled polymers with narrow polydispersity that could be deformed in the solid state to obtain high-modulus, high-strength tapes *[167]*. The synthesised *UHMw-PE* also provides opportunity to investigate entanglement formation during polymerisation, and chain dynamics arising on melting of the disentangled crystalline state. Lippits *et al. [59,157,167]* have studied the entanglement formation in such disentangled *UHMw-PE* and have shown the effective use of rheology to follow the entanglement formation.

In this chapter, the series of *UHMw-PE* samples studied were synthesised using a single site catalyst reported by Fujita and co-workers in dilute solution for different polymerisation times and temperatures *[168]*. The rheological tests were performed to unravel the influence of polymerisation conditions on the entanglement formation during polymerisation. Dynamic melt rheology as a

technique to characterise the molecular weight (Mw) and molecular weight distribution (MWD) of *UHMw-PE* has been used, which was demonstrated earlier by Talebi *et al. [169]*. Dynamic melt rheology is used to understand the morphology produced during the synthesis and its effect on entanglement formation.

2.2 Experimental section:

2.2.1 Synthesis of disentangled *UHMw-PE*

Disentangled UHMw-PE samples used in this thesis were synthesised in our group at Loughborough University by Dr. Yohan Champouret and the procedures used are described here. All the manipulations of air and moisture-sensitive products were carried out under a dry nitrogen or argon atmosphere using a dry-box (MBraun Unilab) and/or standard Schlenk line techniques *[157]*. The bis(phenoxyimine) titanium dichloride complex, [3-*t*-Bu-2-O-$C_6H_3CH=N(C_6F_5)]_2TiCl_2$, was purchased from MCAT and was used as received. Methylaluminoxane (MAO, 10% weight in toluene) and dry toluene were used as received from Aldrich. All the other chemicals were commercially available and used as received. Ethylene (polymer grade) was purchased from BOC and used as received.

Ethylene Polymerisation: All polymerisations were conducted using similar experimental conditions. A typical experiment is described here as a representative example. An oven dried 5-necked round-bottom flask equipped with magnetic stirrer bar, thermometer probe and sintering cannula were previously dried under vacuum for 30 minutes and backfilled with nitrogen. Dry toluene was introduced to the reaction flask, followed by 1 ml of MAO, and dry nitrogen was bubbled through the solvent for 30 minutes under stirring. The nitrogen was then replaced by ethylene gas which was left bubbling through the solvent. After 30 min, the desired amount of MAO (minus 2 ml) was introduced and the reaction flask was then heated to the desired temperature. When the requisite temperature was reached, the polymerisation was initiated by addition of the pre-catalyst $[3\text{-}t\text{-Bu-2-O-}C_6H_3CH=N(C_6F_5)]_2TiCl_2$ previously dissolved in 2 ml of toluene and activated by 1 ml of MAO solution. After the required

polymerisation time, the polymerisation was quenched by addition of an acidified MeOH solution. The resulting polyethylene was filtered, washed with copious amounts of methanol/acetone and dried overnight in a vacuum oven at 40°C.

N-(3-tert-butylsalicylidene)-2,3,4,5,6-pentafluoroaniline[3-*t*-Bu-2-O-$C_6H_3CH=N(C_6F_5)]_2TiCl_2$ precatalyst was used for the preparation of a range of *UHMw-PE*. Typically, [3-*t*-Bu-2-O-$C_6H_3CH=N(C_6F_5)]_2TiCl_2$ was treated with 1100 equivalents of MAO in toluene under atmospheric pressure of ethylene with the temperature and time being the only parameters that were variable during the polymerisation reaction (Figure 2.1 and Table 2.1).

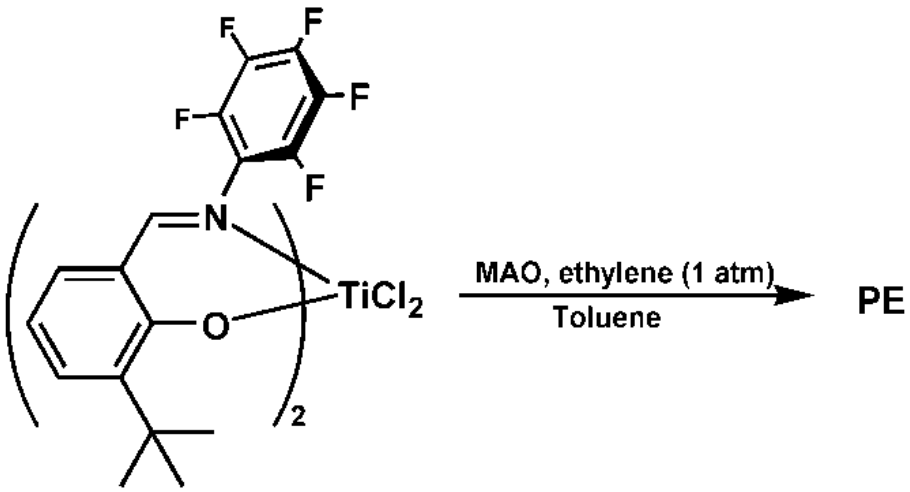

Figure 2.1. Ethylene polymerisation using [3-t-Bu-2-O-$C_6H_3CH=N(C_6F_5)]_2TiCl_2$/MAO.

2.2.2 Synthesised disentangled *UHMw-PE* used in this thesis

Table 2.1. Polymers used in this thesis, synthesised at different polymerisation temperatures and times. Synthesis conditions: co-catalyst = MAO (Al:Ti = 1100:1), ethylene pressure 1 atmosphere, polymerisation medium was toluene. After polymerisation for the desired time the reaction was quenched with a HCl/MeOH solution and the polymer was filtered, washed and dried in a vacuum oven at 40°C. The sample nomenclature reflects information on the polymerisation temperature and time, where time was measured from immediately after addition of the activated catalytic system.

Sample	$[C_{Cat}]$ (mM)	Toluene (L)	Temp (°C)	Time (min)	Yield (g)	Activity ($Kg_{PE}.mol_{cat}^{-1}.h^{-1}$)	Activity/[Ethylene] ($Kg_{PE}.mol_{cat}^{-1}.h^{-1}).(mol.l^{-1})_{ethylene}$
dPE_10C_1’	0.012	1.5	10	1	3.1	10330	61850
dPE_10C_2’	0.012	1.5	10	2	4.7	7830	46890
dPE_10C_5’	0.012	0.5	10	5	4.1	6200	49100
dPE_10C_10’	0.012	0.5	10	10	5.2	5200	31140
dPE_10C_20’	0.012	0.5	10	20	10.1	5050	30240
dPE_10C_30’	0.012	0.75	10	30	11.4	2530	15150
dPE_20C_30’	0.012	0.75	20	30	23.9	5310	37130
dPE_30C_30’	0.012	0.75	30	30	36.4	8090	65240
dPE_40C_30’	0.012	0.75	40	30	22.1	4910	45460
dPE_70C_30’	0.012	0.75	70	30	2.8	620	8210

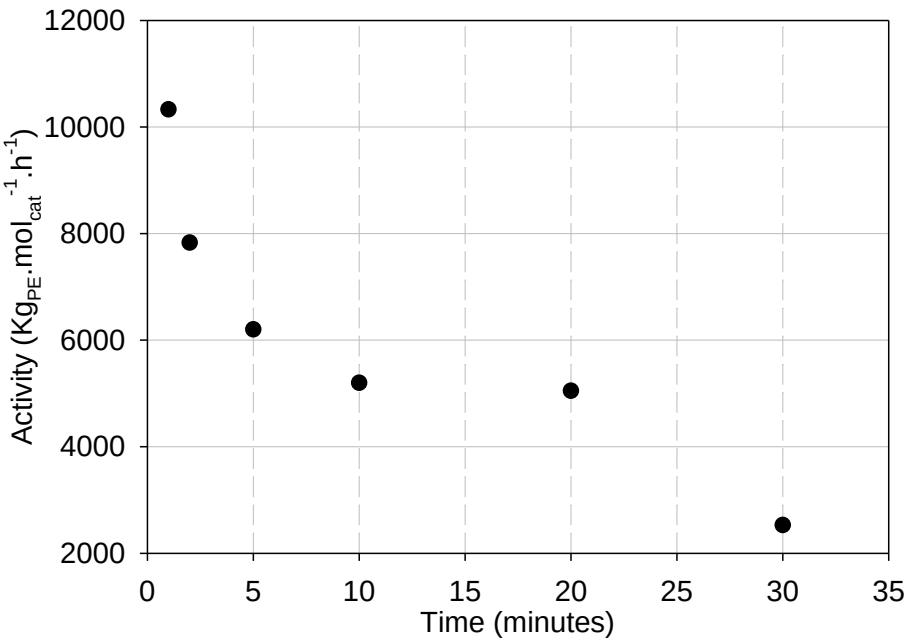

Figure 2.2. For the same polymerisation temperature of 10°C and polymerisation conditions, the activity of the catalyst, [3-t-Bu-2-O-$C_6H_3CH=N(C_6F_5)]_2TiCl_2$/MAO, decreases with increasing polymerisation time. The catalyst activity varies from 10330 – 2530 Kg.mol^{-1}.h^{-1} in toluene, as summarised in Table 2.1 and Figure 2.1. The decrease in activity could arise from heterogenisation of the catalyst, an increase in the viscosity of the polymerisation media due to precipitation of polymers, the introduction of traces of catalyst poison with the ethylene feed, etc.

From Figure 2.3, an increase in catalyst activity is noticeable from 10°C to 30°C. However, above 30°C the catalytic activity decreases. The reason for the decrease in the activity, with increasing polymerisation temperature, could be the same as mentioned above in the caption of Figure 2.2. In addition, because of the decrease in the solubility of ethylene with increasing temperature the catalyst activity is also likely to decrease *[157,169]*. Furthermore, Mitani *et al. [170]* suggested that chain termination or chain transfer and/or catalyst deactivation is not negligible at temperatures above 50°C.

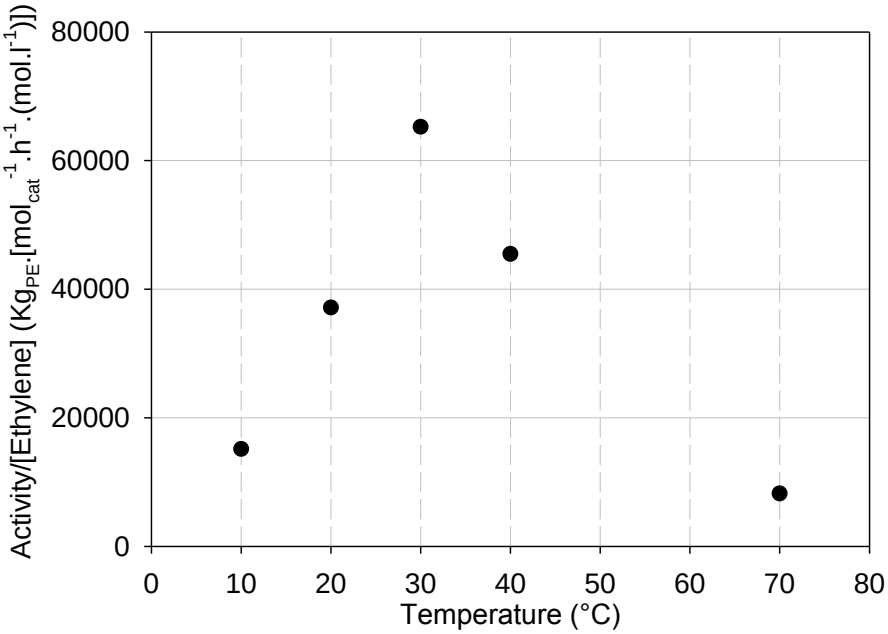

Figure 2.3. Catalyst activity/[Ethylene] [171,172] for ethylene polymerisation using [3-t-Bu-2-O-C_6H_3CH=N(C_6F_5)]$_2TiCl_2$/MAO was obtained at different temperatures for the same polymerisation time of 30 minutes. The concentration of ethylene in toluene was calculated according to Henry's law: $\Phi_{ethylene} = p_{ethylene} * H_0 \exp(\Delta H_L/RT)$ with $\Phi_{ethylene}$ = ethylene concentration (mol.L^{-1}); $p_{ethylene}$ = ethylene pressure (atm); H_0 = Henry coefficient = 0.00175 mol.L^{-1}.atm^{-1}; ΔH_L= enthalpy of solvation for ethylene in toluene = 2569 cal.mol^{-1}; R = 1.989 cal.mol^{-1}.K^{-1} and T = polymerisation temperature (K).

2.2.3 Rheometry:

2.2.3.1 Sample preparation for the rheological studies

The nascent powder obtained from the reactor was mixed with an anti-oxidant (Irganox 1010) of 0.7% by weight to prevent any degradation over the long rheological experiments. To have homogeneous mixing of the antioxidant with the powder, the antioxidant was first dissolved in acetone and subsequently mixed with the nascent *UHMw-PE* powder submerged in acetone. After mixing, the powder was dried overnight in a vacuum oven at 40°C. The dried powder was compressed into a plate of diameter 40-50 mm and thickness 0.6-0.7 mm at 125°C, under the force of 20 tons for an average time of 25 minutes. From the compressed plate several discs of 12 mm diameter were cut, using a metal punch, for rheology experiments.

2.2.3.2 Experimental protocols for the rheological studies

All the rheological studies were performed on a strain controlled rheometer, an ARES, TA Instruments, USA. In all the rheological studies, discs of 12 mm diameter were used to avoid excessive force to the rheometer transducers that the rubber-like melt state of the UHMw-PE imposes. The disc between the parallel plates of the rheometer was heated to 110°C under a nitrogen environment in a convection oven to prevent thermo-oxidative degradation. From 110°C to 130°C, the sample was heated rapidly (~30°C/min). After waiting for thermal stabilisation at 130°C (~2 minutes), the sample was compressed with a compressive (normal) force of ~400 grams. The auto normal force function, maintaining the constant force of ~400 grams, was chosen throughout the experiment. The sample was heated at 10°C/min from 130°C to 160°C. The dynamic amplitude sweep (DAS) test was performed at a fixed frequency of 100 rad/s to determine the linear viscoelastic (LVE) regime. The dynamic time sweep (DTS) test was performed to follow the entanglement formation at a fixed frequency of 10 rad/s (in the rubbery regime) and strain of 0.5% in the linear viscoelastic regime of the polymer *[59,157,167]*. Experimental protocols for various rheology experiments are discussed further in the following paragraphs and the sequence used has been schematically shown in Figure 2.4.

- *Sample loading:* Due to the high stiffness of the sample, a disc diameter of 12 mm was loaded in parallel plate geometry at 110°C. Sample was then heated fast (~20-30°C/min) to 130°C. After waiting for thermal stabilisation at 130°C (~2 minutes), the sample was loaded with a compressive (normal) force of ~400 grams to maintain the same contact during all the rheological tests. The auto normal force function (maintaining a constant force by changing the gap) available in the rheometer was chosen for all the tests (except DAS and DFS) to maintain the same contact force on the sample. The auto normal force function is useful and ensures similar contact between the sample and the plate during very long experiment times. The normal force on the sample initially increases due to the melting and expansion of the sample. However, it decreases during the modulus build-up (DTS) experiments due the free volume reduction owning to

entanglement formation or to melt flowing out of the edge of the sample causing loss in contact between sample and the plate over very long experimental times.

- *Heating sample to observation temperature:* The sample was heated at the chosen heating rate (10°C/min) to the observation temperature (160°C/min) for the study of entanglement formation under the auto normal force of ~400 grams. The viscoelastic response of the material was followed during heating by applying strain of 0.5% and the frequency of 10 rad/s. It is important to apply the auto normal force function during this heating step to avoid excessive force on sample which occurs due to expansion in the sample while the sample melts.

- *Dynamic Amplitude Sweep (DAS):* After reaching the observation temperature (160°C), the dynamic amplitude sweep was performed to identify the linear viscoelastic (LVE) regime. All the rheological tests were performed within the LVE regime (due to complications involved at higher strains in LVE regime such slippage and secondary flows) of the material. In this test, the strain was varied from 0.1 to 100% at a fixed frequency of 100 rad/s. However, if enough care is taken then the dynamic amplitude sweep can provide in-depth information about the microstructure and underlying dynamics in materials and is discussed in detail in chapter 3. This test is also referred as the large amplitude oscillatory shear (LAOS) and used in this thesis to maintain the consistency with earlier work by researchers *[173]* in chapter 3 to understand the effect of entanglement on the melt dynamics under large shear deformation.

- *Dynamic Frequency Sweep (DFS):* Dynamic frequency sweep experiments within the LVE regime were performed to follow the response of the polymer at different frequencies (length scales). A frequency from the plateau (rubbery) region of the polymer was chosen to follow the entanglement (modulus build-up) in dynamic time sweep (DTS) experiments. The frequency has been varied from 100 to 0.001 rad/s at a fixed strain of 0.5% (strain chosen from DAS, within the LVE regime). The dynamic frequency sweep was also performed on a fully entangled melt (the thermodynamically stable state) for the characterisation of molecular weight (Mw) and molecular weight distribution (MWD). A method to

obtain Mw and MWD data from dynamic frequency sweep data is described in detail in section 2.3.6 *[169]*.

- *Dynamic Time Sweep (DTS):* Modulus build-up in the melt as a function of time was followed using the dynamic time sweep (DTS) experiment by applying a fixed frequency (from the plateau region) and a strain within LVE regime. The elastic modulus in the plateau regime reflects the entanglement density in the melt. See equation (2.1). The increase in plateau modulus relates to the increase in entanglement density (M_e), i.e. the decrease in entanglement molecular weight. A frequency of 10 rad/s (within plateau modulus from DFS) and a strain of 0.5% (within LVE) at 160^0C was chosen to follow the entanglement formation. The NonLinMon parameter, which is ratio of intensity of the 3rd harmonic over the 1st harmonic, generated by the rheometer is monitored to check for any slippage (non-linearity) during the experiments. NonLinMon needs to be very small (<0.001), which confirms the linear viscoelastic regime and the absence of artefacts such as slippage and contact problems between the sample and the plates.

- *Crystallisation during Cooling (CC):* To understand the effect of entanglement on crystallisation of polymers, single point dynamic oscillatory experiments during cooling were performed. After reaching the fully entangled melt (or partially entangled), the sample was cooled from its observation temperature to 140°C at 5°C/min, from 140°C to 135°C at 1°C/min and finally cooling from 135°C to 110°C at 0.1°C. During the entire cooling, a frequency of 10 rad/s and a strain of 0.5% were applied to follow the changes in the viscoelastic response of the polymer. The modulus response is very different for polymers in their melt and solid state (from melt to solid). With decreasing temperature, at the on-set of phase change, from the melt to the solid, the modulus and the phase angle at a given frequency and strain increase strongly.

The rheological measurements using different normal force other than 400 grams were also carried out and values were found to be independent of the used force upto 600-700 grams.

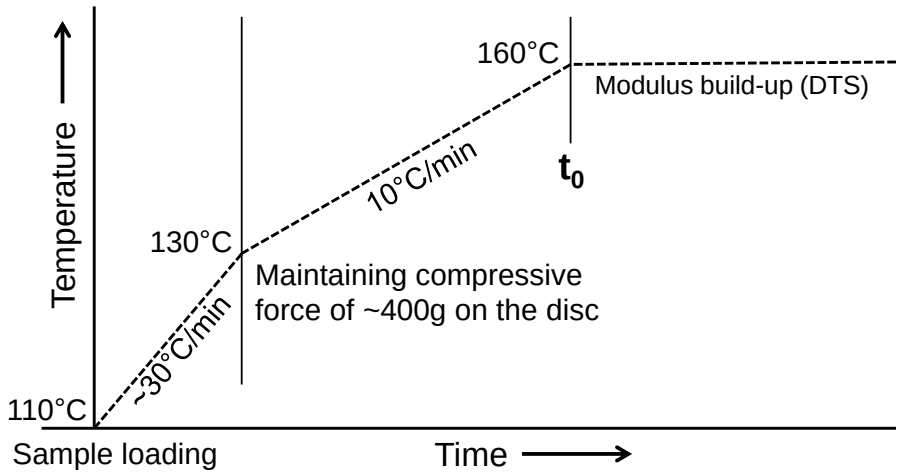

Figure 2.4. Schematic diagram for the rheological experiment protocol used to follow modulus build-up (entanglement formation) at 160°C for the samples synthesised at different polymerisation times and temperatures, as depicted in Table 2.1. Time t_0 in Figure represents the start of the data collection after thermal stabilisation i.e. 100 seconds after reaching 160°C.

2.3 Results and discussion:

To follow the influence of synthesis conditions on the entangled state rheological studies were performed systematically on the synthesised polymers. All samples for the rheological studies were synthesised using the same catalytic system where the variable parameters during polymerisation were: time and temperature as listed in Table 2.1. The two parameters were varied to understand their effects on the entanglement formation during synthesis.

2.3.1 Morphology of nascent disentangled *UHMw-PE* synthesised at different temperatures

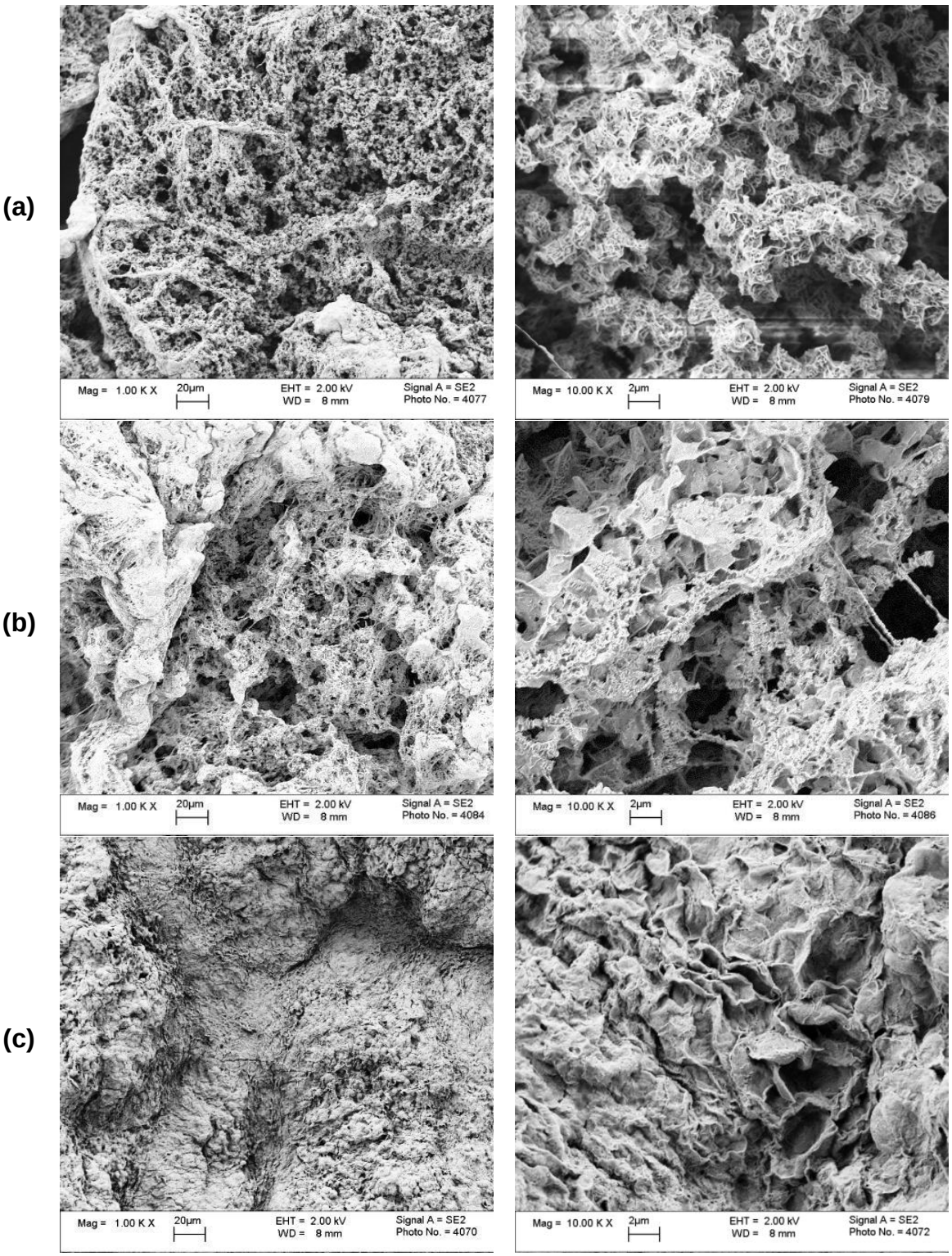

Figure 2.5. Scanning electron micrographs of the nascent (direct from the reactor) samples synthesised at different temperatures (a) 10°C, (b) 40°C and (c) 70°C.

Investigations on morphologies of nascent reactor powders were carried out with a high resolution FEG SEM (Carl Zeiss Leo 1530 VP) operated at 5kV. As-polymerised particles were carefully deposited on SEM stubs and the samples were coated with gold by a sputtering technique.

Scanning electron micrographs (SEM) of the nascent powders for the samples synthesised at different temperatures are shown in Figure 2.5. Randomly ordered stacks of single chain crystals, distributed throughout the bulk; single crystals in higher resolution SEM images can be seen in Figure 4.5. However, these randomly ordered stacks of single chain crystals are lost and form aggregates throughout the bulk with increasing temperature of synthesis, Figure 2.5b-c. The loss of stacks of crystal morphology and its aggregate formation is greatest at the highest synthesis temperature and can be significantly observed in the sample synthesised at 70°C where the bulk is a lump of large aggregates, Figure 2.5c. The bulk morphology of the samples goes from (a) a free powder-like material to (b) a flake-like material to (c) a lump of flake-like morphology with increasing synthesis temperature.

Even simple micrographs show a profound effect of polymerisation temperature on the morphology of the bulk powder produced during polymerisation. High resolution micrograph for crystal morphology of synthesised disentangled *UHMw-PE* (by homogeneous polymerisation) is shown and compared with commercially available *UHMw-PE* (heterogeneous polymerisation) sample in chapter 4. However, to understand, in detail, the effect of polymerisation conditions on entanglement and the resulting morphology, rheological studies were carried out and are discussed in the following sections. It is expected that the changing morphology of the samples with the different polymerisation temperatures will also have implications on the rate of the entanglement formation. The sample morphology itself depends on rate of crystal formation during polymerisation, which itself depends on several reaction parameters which are also discussed in the following sections.

2.3.2 Entanglement formation in a nascent disentangled polymer

Figure 2.6 shows dynamic time sweep data at 160°C for the sample dPE_10C_5', synthesised at 10°C for 5 minutes. All the modulus build-up data

discussed in this thesis were carried out at 160°C. The modulus build-up rate (entanglement formation) is independent of temperature above 160°C which was therefore, chosen as a reference temperature. Modulus build-up at various temperatures is shown in Appendix 2 at the end of this thesis. Data collection was started after thermal stabilisation of the sample i.e. after leaving the sample for 100 seconds at 160°C, as depicted in Figure 2.4. Figure 2.6 shows that the elastic modulus (G') increases with the increasing annealing time at 160°C. The elastic modulus for a thermodynamically stable polymer melt is related to the average molecular weight between entanglements (or average entanglement density in the melt) by equation (2.1).

$$G_N^0 = g_n \rho RT / M_e \qquad \ldots(2.1)$$

G_N^0 is the plateau modulus (in the rubbery regime), g_n is a numerical factor (1 or 4/5 depending upon the convention *[3]*), ρ is the melt density, R is the gas constant, T is the absolute temperature, and M_e is the molecular weight between entanglements.

Thus, in the melt state at a fixed temperature, the increasing elastic modulus relates to its increasing entanglement density i.e. decrease of the average molecular weight between entanglements. From Figure 2.7, it is apparent that the initial modulus just after melting is ~1 MPa. The modulus increases with time till it reaches a maximum value of ~1.8 MPa, G'_{max}, the maximum plateau modulus value for a thermodynamically stable polyethylene melt. The time required for a disentangled polymer to reach 98% of its maximum plateau modulus is termed the total build-up time (t_m) *[59,157,167]* and is around 15,000 seconds for the dPE_10C_5' sample. Though equation (2.1) presents a relationship between the elastic modulus and the molecular weight between entanglements in a thermodynamically stable state, for simplicity its application to the data shown in Figure 2.6 suggests a varying molecular weight between entanglements with annealing time i.e. a thermodynamically metastable melt state where the rheological concepts for the thermodynamically stable melt state may not hold.

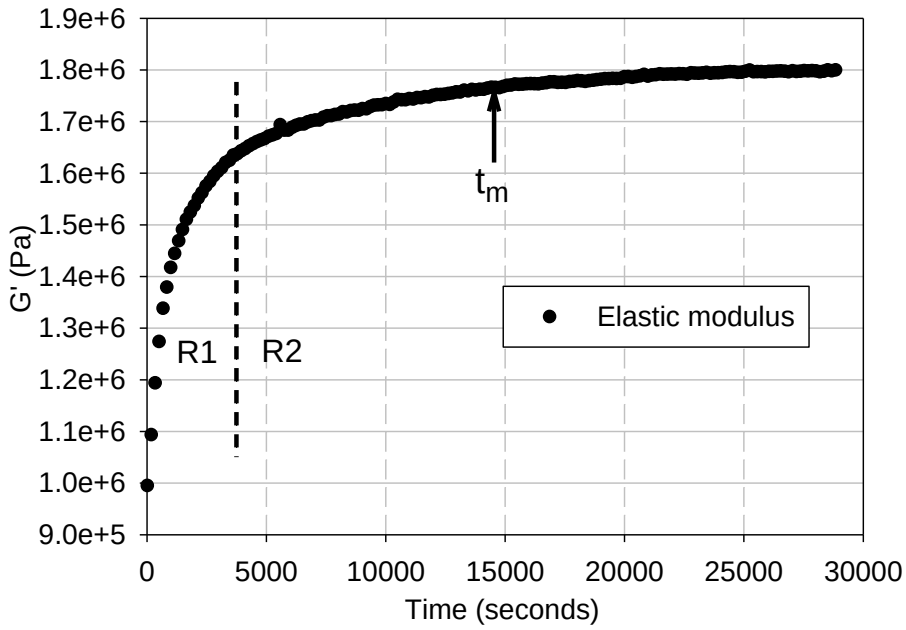

Figure 2.6. Dynamic time sweep test at 160°C on the disentangled dPE_10C_5' sample, at a constant frequency of 10 rad/s and a strain of 0.5%. The modulus build-up with the increasing annealing time represents the increasing entanglement density (decreasing M_e) in the polymer melt. See equation (2.1). The modulus build-up is divided into two regions, R1 and R2. Region R1 is defined where 80% of the total modulus build-up occurs in 20% of the total entanglement time (t_m). The remainder of the modulus build-up in the 80% of the time is associated with the region R2.

The two regions illustrate differences in the rate of entanglement formation. In the region R1, the rate of modulus build-up is faster and is associated with the entanglement formation by faster mixing of the polymer chains through the chain explosion process on melting *[126,174]*. However, in region R2, the entanglement formation is slower and predominantly governed by the reptation dynamics. After the modulus reaches to a plateau value of G'_{max} (1.8-1.9 MPa), the initially disentangled melt achieves thermodynamic equilibrium and no further increase in the modulus occurs.

Figure 2.7 shows plots for the absolute values of the elastic modulus along with the normalised elastic modulus (G_N^t). The modulus is normalised by the maximum plateau modulus (G'_{max}) in the modulus build-up and is given by equation (2.2).

$$G_N^t = G'_t / G'_{\max} \qquad \ldots(2.2)$$

Where, G_N^t is the normalised elastic modulus at time t, G'_t is the absolute value of elastic modulus at variable time *t*. The data chosen are the same as shown in Figure 2.7. To accommodate a long experimental time along the x-axis the chosen graphic representation in this thesis, in most places, is semi-log plot as shown in the inset of Figure 2.7.

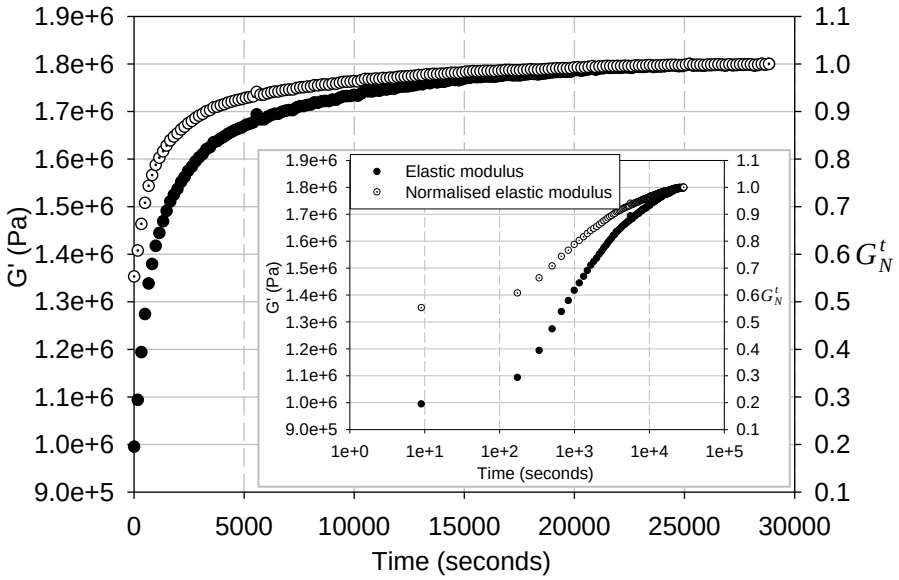

Figure 2.7. Absolute values of the elastic modulus (G') and the normalised elastic modulus (G_N^t) obtained on annealing the sample dPE_10C_ 5' at 160°C. Inset picture is the semi-log plot of the same data. Scaling for the Y-axis of G_N^t is chosen to show data points of the two moduli together.

In a thermodynamically stable melt, the chains acquire the maximum number of entanglements at G'_{max}. Thus, at any given time *t*, G_N^t represents the number of entanglements present (entanglement density or M_e) and is a fraction of the total number of entanglements possible in a thermodynamically stable melt for a given molecular weight. Hence, G_N^t is used as a measure of fraction of the total number of entanglements present in the melt state at any given time, *t,* with respect to its thermodynamically stable state. The higher value of G_N^t reflects the higher entanglement density and lower molecular weight between entanglements (M_e). At unity, the melt is thermodynamically stable and achieves maximum entanglement density i.e. equilibrium entanglement molecular weight (~1800 g/mol in case of PEs *[2,3]*).

To strengthen the evidence that the increase in elastic modulus is due to entanglement formation and not any artifact due to a contact problem between the sample and the rheometer plates, multiple modulus build-up tests on the same polymer disc were performed. See Appendix 1. To strengthen further the concept that the increase in modulus is due to entanglement formation; studies on crystallisation with increasing annealing time were performed and are presented in next section.

2.3.3 Effect of entanglement on polymer crystallisation

To study the effect of the polymer entanglement on its crystallisation, modulus build-up experiments during cooling (CC) using rheology were performed on a synthesised disentangled UHMw-PE sample with increasing annealing time (increasing entanglement). The number of entanglements was varied by keeping the sample for varying times (t_0, t_1, t_2…) in the melt (160°C) and on-set of crystallisation temperature were studied by performing single point dynamic experiment during cooling. With increasing time in the melt, the extent of entanglement increases, Figure 2.6 and Figure 2.8.

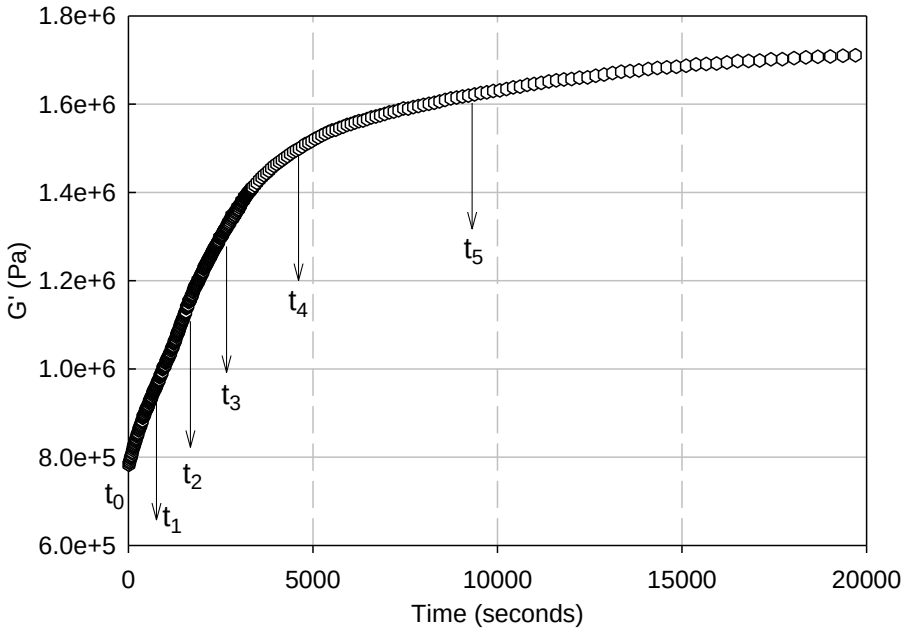

Figure 2.8. Dynamic time sweep test at 160°C on the disentangled sample dPE_10C_10', at a constant frequency of 10 rad/s and a strain of 0.5%. From time t_0 to t_5, the number of entanglements increases. The sample was cooled after time t and the on-set of crystallisation was studied. See Figure 2.9

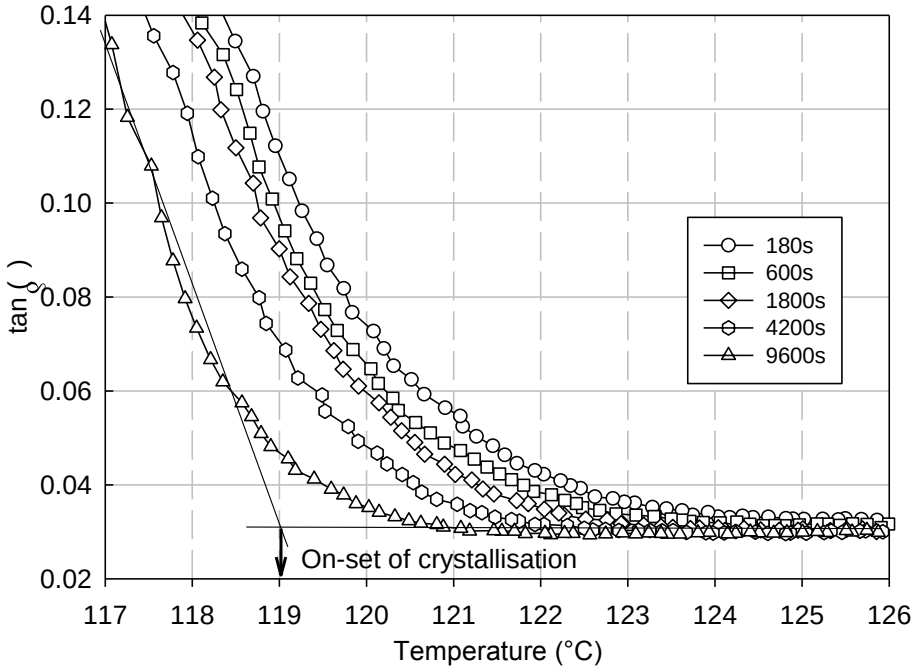

Figure 2.9. Phase angle as a function of temperature at a cooling rate of 1°C/min to study the effect of increasing entanglement on the on-set temperature of crystallisation during cooling experiments using rheology for sample dPE_10C_10'. Change in phase angle (tanδ) represents the phase transition in the polymer from the melt to the solid state.

Table 2.2. On-set crystallisation temperatures at a cooling rate of 1°C/min after annealing the sample dPE_10C_10' for various times in the melt at 160°C. Reproducibility between temperature peaks measured were ± 0.1°C/min. Also see Figure 4.18.

Melt time in seconds at 160°C	180	600	1500	4200	9600
On-set temp. of crystallisation (°C)	120.8	120.5	120.3	119.9	119.0

In Figure 2.9, the on-set of crystallisation temperature for samples can be seen decreasing from time 't_0' to time *'t'* ($t > t_0$). The on-set crystallisation temperature for different annealing time is tabulated in Table 2.2. The decrease in on-set crystallisation temperature for the melt staying for longer annealing times in the melt state is due to the increasing entanglement *[59,140]*. Crystallisation requires disengagement of chains (reeling out) from entangled network which gets difficult and slow with increasing number of entanglements. This result is also supported by the increasing elastic modulus with increase in

entanglement. However, one can co-relate the decrease in on-set crystallisation temperature with annealing time to the memory effect as well *[88]*. The memory effect can be avoided by annealing the sample at even higher temperature. Effect of increasing annealing time on the on-set crystallisation temperature is further supported using DSC in chapter 4, where no contact problem similar to rheology arises.

2.3.4 Effect of annealing temperature (in melt) on entanglement formation

To study the effect of selected observation temperatures on modulus build-up rate (entanglement formation), several DTS experiments were performed at different temperatures on the synthesised disentangled sample dPE_10C_10', annealed for a fixed melt time of around 50,000 seconds (the observation time at a given test temperature). After 50,000 seconds of annealing time at the observation temperature, the crystallisation experiment under a cooling rate of 0.1°C/min was performed to study the on-set crystallisation temperature (number of entanglements) for the corresponding melt temperatures.

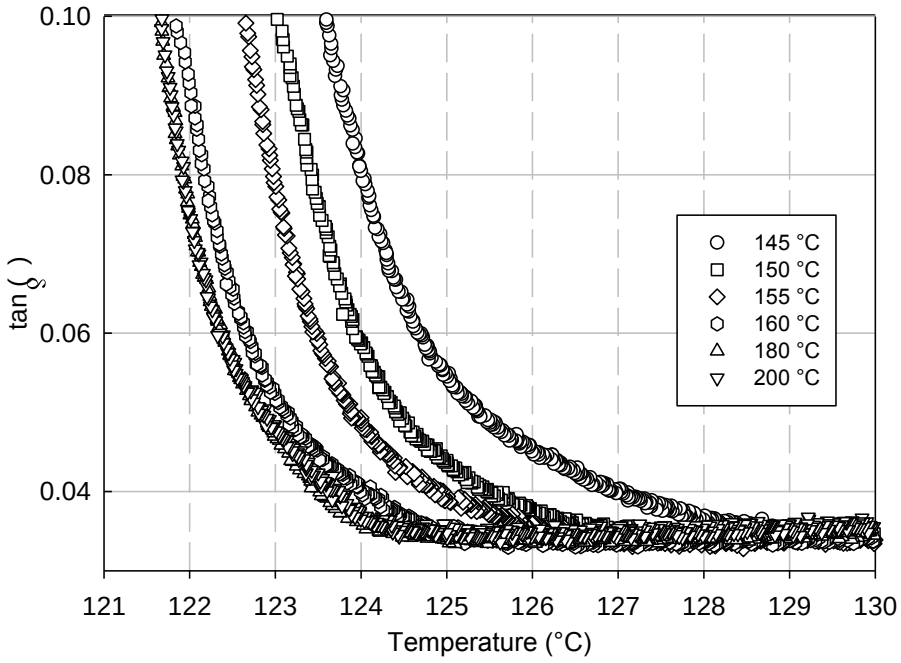

Figure 2.10. On-set crystallisation temperature of synthesised disentangled sample dPE_10C_10' after annealing for 50,000 seconds at various observation temperatures (145, 150, 155, 160, 180 and 200 °C) under a cooling rate of 0.1°C/min. Modulus build-up at different observation temperatures are given in Appendix 2.

It can be seen from Figure 2.10 that on-set crystallisation temperature decreases with increasing examined annealing temperature. In all the experiments the samples were annealed for 50,000 seconds, but, at different annealing temperatures. In the earlier section 2.3.3, a decrease in on-set crystallisation temperature with increases in entanglement was observed. A decrease in the on-set crystallisation temperature with increasing observation temperature implies that at higher temperature entanglement formation is faster, leading to the formation of a larger number of entanglements within the same annealing time. The entanglement formation rate can be associated to the free volume in a polymer melt available at a given temperature *[2]*. The free volume in the melt is smaller at lower annealing temperature and hence the diffusion of chains (mixing and reptation) required for entanglement formation is also slower compared to a higher annealing temperature. However, the entanglement formation rate becomes relatively independent of temperature after a certain temperature (160°C), as no appreciable decrease in the on-set crystallisation temperature can be seen from 160-200°C. Whereas even in a smaller temperature difference (140-160°C), decrease in on-set crystallisation temperature is about 2-2.5°C. See Figure 2.10

After establishing the concept of following entanglement formation using modulus build-up, the entangled state of the synthesised polymer at different polymerisation times and temperatures are now addressed in following sections.

2.3.5 Effect of polymerisation time on entanglement formation

Figure 2.11 shows comparison of the normalised modulus build-up (G_N^t) on annealing at 160°C for the samples synthesised at 10°C for different polymerisation times. The total entanglement time (t_m), increases with the increasing polymerisation time. For example, to reach the maximum modulus it takes about one thousand seconds in the sample synthesised for two minutes compared to a week required for the modulus build-up in the sample synthesised for thirty minutes. Consistent decrease in the normalised modulus at t_0 suggests a decreasing density of entanglement in the nascent polymer with increasing polymerisation time.

For a pure living catalytic system, the molecular weight increases linearly with the polymerisation time *[170]*. For a thermodynamically stable melt, the number of entanglements per chain increases with increasing molecular weight as the equilibrium entanglement molecular weight (M_e) is considered to be intrinsic for a given polymer *[3-5,15]*. Hence, higher molecular weight sample will require more time to reach the thermodynamically stable state from its disentangled state.

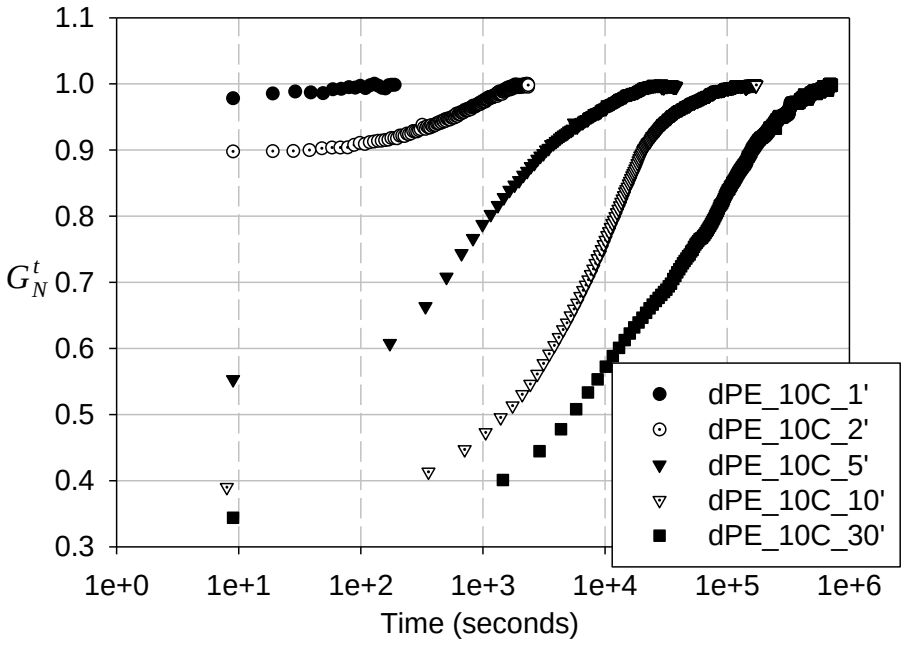

Figure 2.11. Dynamic time sweep at 160°C for the samples synthesised at 10°C for varying polymerisation times. G_N^t is the normalised elastic modulus, normalised by G'_{max} (maximum plateau modulus in the modulus build-up).

To get a molecular insight on the synthesised polymer, it is important to determine the molecular weight (Mw) and the molecular weight distribution (MWD). For the purpose molecular rheology was applied as a tool described in the following section.

2.3.6 Mw and MWD determination using dynamic melt rheology

Using a standard gel permeation chromatography (GPC) technique, it is not easy to determine the molecular weight (Mw) and molecular weight distribution (MWD) of polyethylene exceeding a molecular weight, $M_{W,}$ > 1 million g/mol *[169]*. Following the methods described by Mead *[175]* and Tuminello *[176]*, from dynamic melt rheology, Mw and MWD data can be numerically synthesised. Viscosity models *[177,178]* and modulus models *[175]* are generally used to synthesise numerically the Mw and MWD from the melt dynamic rheology data. In the viscosity model the Mw and MWD are computed from the rheological behaviour of the material's viscosity dependence on the shear rate *[177,178]*. However, the modulus model describes the viscoelastic properties for polymers with high molecular weight components, and is more suitable for the high Mw polymers synthesised in this thesis. The modulus model is presented in terms of the relaxation modulus which takes the relaxation spectrum from the time domain of the material and converts it into the molecular weight domain *[169]*. The MWD curve is then obtained through regularised integral inversion.

One of the most successful algorithms in predicting the molecular weight distribution of nearly monodisperse, broad and bimodal polymer melt was developed by Mead *[175]*. This algorithm has been commercialised by Rheometric Scientific for incorporation in their Orchestrator software and used here for the determination of Mw and MWD. Tuminello *[176]* and Talebi *et al. [169]* have shown the usability using melt rheology to determine Mw and MWD of a series of polymers having molecular weights ranging between 35,000 and 10 million g/mol. A dynamic frequency sweep within the linear regime, at 160°C, was performed on a thermodynamically stable melt obtained after reaching G'_{max}. This is considered to be the requisite as all theoretical models are applicable on the thermodynamically stable melt state *[169]*.

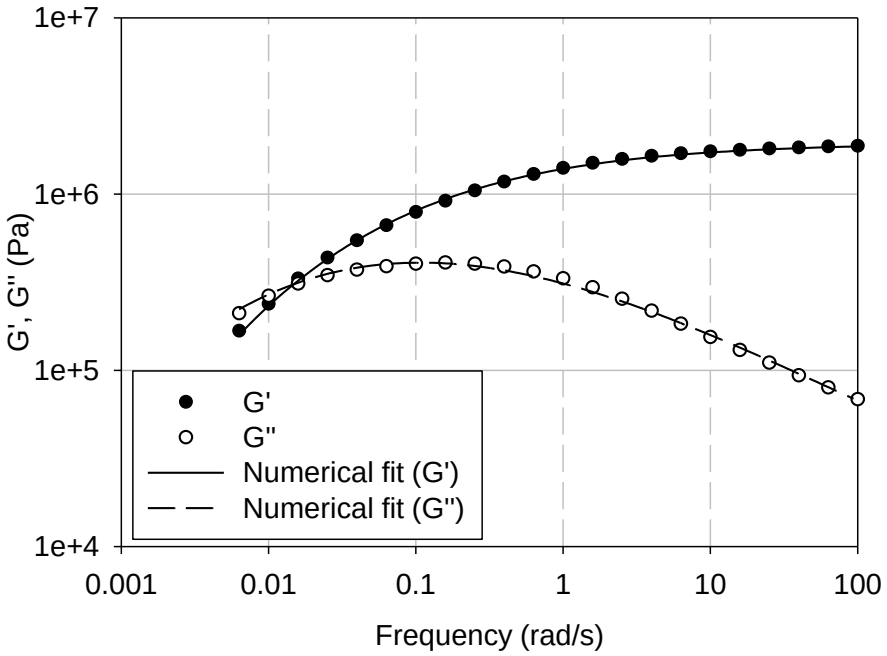

Figure 2.12. An example of dynamic frequency sweep data (performed on a sample of dPE_10C_5' at 160°C, and at a constant strain 0.5%) along with the numeric fit to obtain Mw and MWD. For the numerical fit the Orchestrator software's in-build analysis tool was used.

The numerical fit of molecular weight and molecular weight distribution to the dynamic frequency sweep data at 160°C for sample dPE_10C_5' is shown in Figure 2.12. A numerically synthesised MWD curve for such a fit is shown in Figure 2.13b along with the other samples synthesised for different polymerisation times. Thus, the determined Mw and MWD values of the synthesised samples are summarised in Table 2.3. From the data, it is evident that the molecular weight increases with the increasing polymerisation time. However, the increase is not linear (Figure 2.13a) as the catalyst activity decreases with the increasing time. See Figure 2.2.

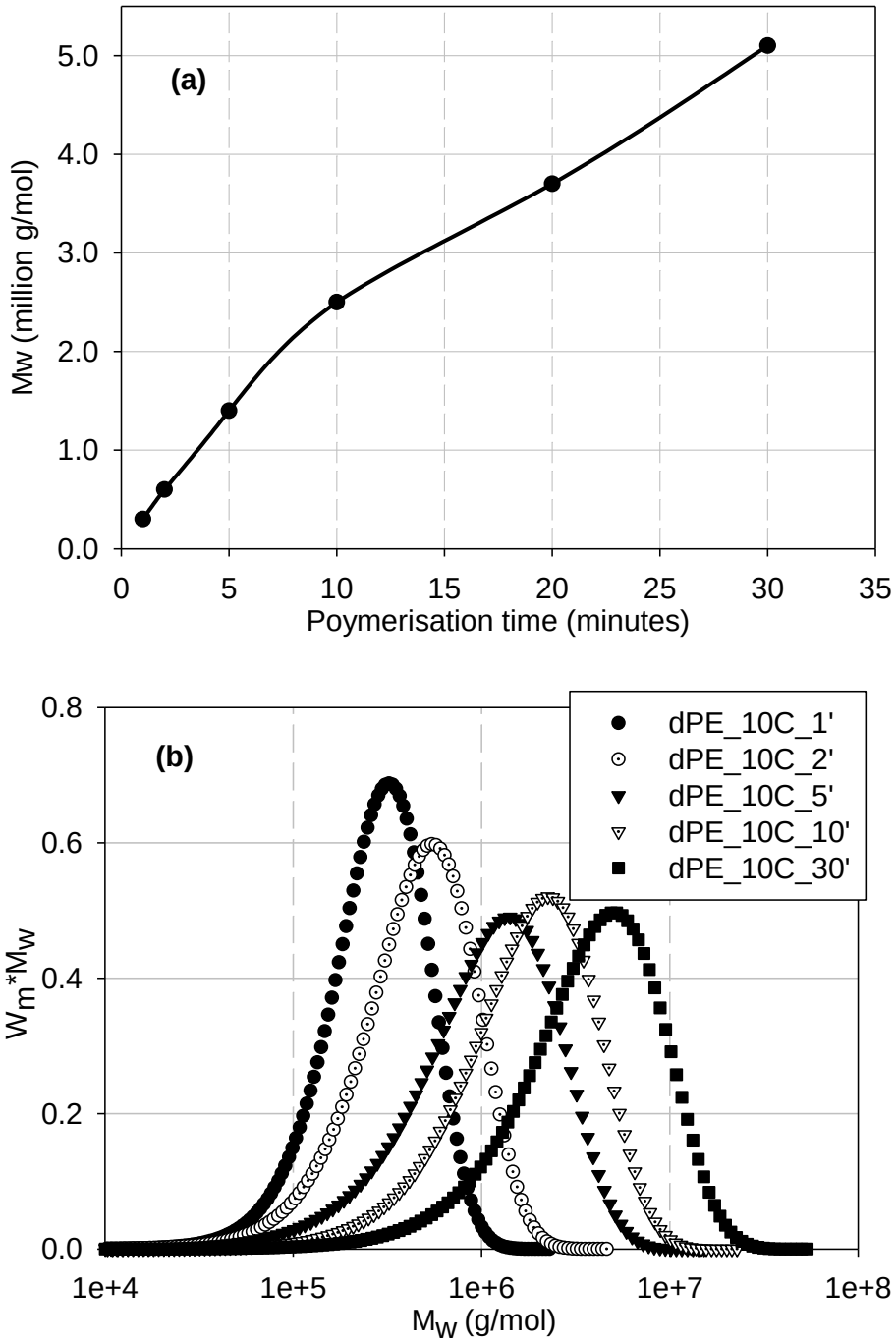

Figure 2.13. Numerically synthesised (a) Mw and (b) MWD curves using TA Orchestrator software's in-built analysis for Mw and MWD determination for a series of samples synthesised for the different polymerisation times listed in Table 2.3.

Table 2.3. Mw and MWD along with the total entanglement build-up time, t_m for samples synthesised at 10°C for varying polymerisation time.

Samples	Mw (million g/mol)	MWD	Total entanglement time, t_m (s)
dPE_10C_1'	0.3	1.4	20
dPE_10C_2'	0.6	1.7	1,220
dPE_10C_5'	1.4	2.5	14,260
dPE_10C_10'	2.5	2.4	64,640
dPE_10C_20'	3.7	2.8	120,500
dPE_10C_30'	5.1	2.5	423,430

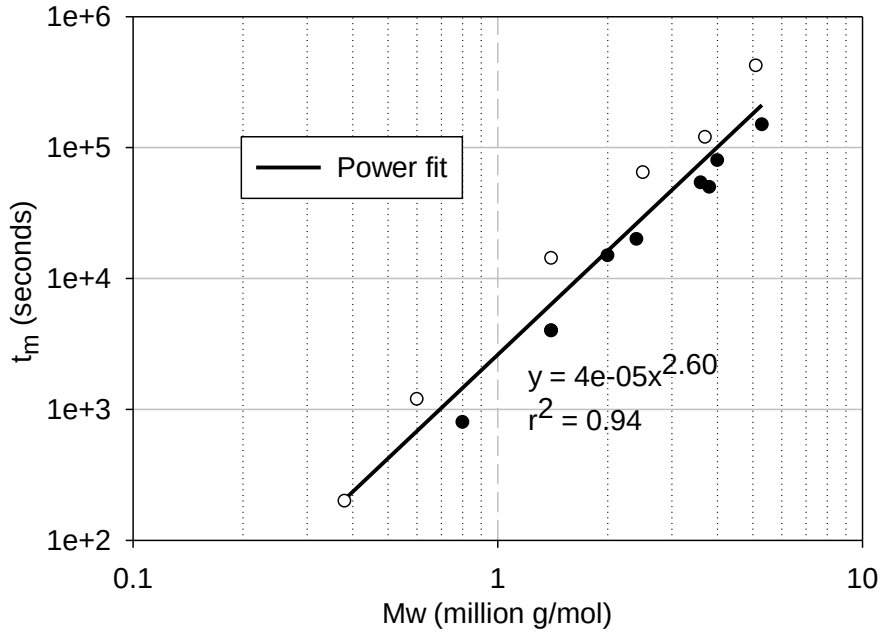

Figure 2.14. Total entanglement time (t_m) for the different molecular weights. The total entanglement time scales t_m with the power of ~2.6 with the molecular weight. These observations are in accordance with the earlier data reported by Lippits [59] and Talebi [157]. Open symbols are data obtained from the study in this work whereas the filled symbols are data obtained from previous studies.

Figure 2.11 shows that the total entanglement build-up time, t_m increases with the samples synthesised at longer polymerisation times (higher molecular

weight) and has been tabulated in Table 2.3. The total entanglement time scales with the power of ~2.6 to the molecular weight, see Figure 2.14. The lower scaling of ~2.6 compare to the ~3.0 in reptation time (of *UHMw-PE*) in a thermodynamically stable melt, can be associated with (a) faster entanglement formation due to a physical mixing process immediately after melting of the disentangled crystals *[126,174]*, and (b) faster reptation dynamics arising in the initially "disentangled" melt state having a lesser number of entanglements. A similar lower scaling of total entanglement time to the molecular weight has been reported in earlier work *[59,157]*.

2.3.7 Effect of polymerisation time on the entangled state of the nascent polymer

In Figure 2.11, it can be seen that G_N^t at time t_0 decreases with the increasing molecular weight. For *t*=0, the $G_N^t = G'_t / G'_{\max}$ can be modified as,

$$G_N^{t=0} = G'_{t=0} / G'_{\max} \quad \ldots(2.3)$$

Where, $G_N^{t=0}$ is the normalised elastic modulus at time t_0, $G'_{t=0}$ is the absolute value of elastic modulus at time t_0.

$G_N^{t=0}$ gives an estimate of the entanglement density at time t_0 which represents a fraction of the total entanglements present in a nascent polymer immediately after melting. Some entanglement formation in the process of heating from 140°C to 160°C cannot be ignored. However, compared to the time required for the complete modulus build-up that exceeds several hours depending on the molecular weight, hundreds of seconds lost in the process of heating above the equilibrium melting point and temperature stabilisation are relatively small. In Figure 2.15, $G_N^{t=0}$ can be seen decreasing with the increasing molecular weight. It is counter-intuitive to see that the higher molecular weight nascent samples have lower entanglement density (higher M_e) compared to the lower molecular weight nascent samples of similar MWD. The possible causes for such behaviour are further discussed in the following paragraphs.

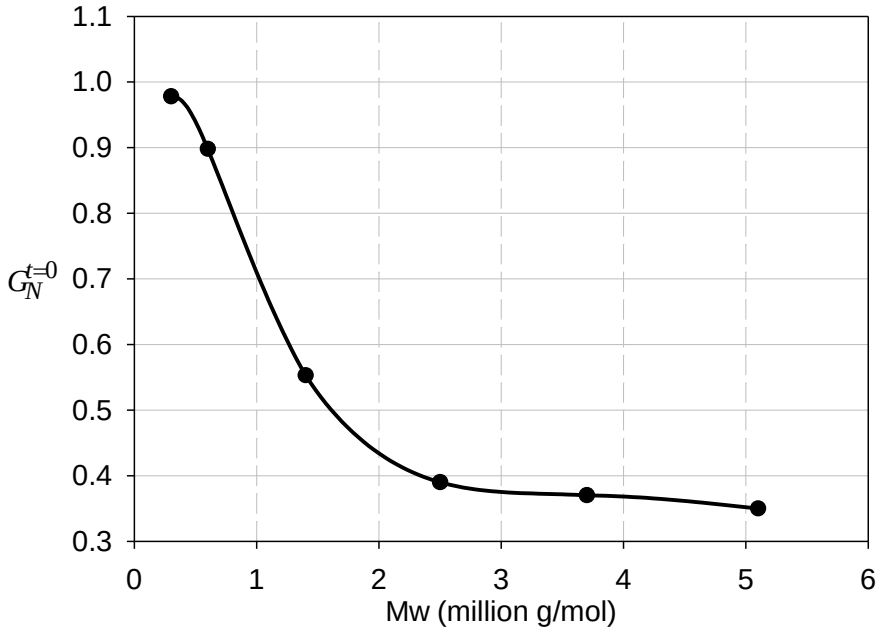

Figure 2.15. Normalised storage modulus immediately after melting of samples having different molecular weights. The modulus characterises the inverse of molecular weight between entanglements.

The novel synthesis of the disentangled polymers is based on the conditions where the catalyst concentration is so low that growing chains from the single-site catalyst do not see each other and hence present a lesser probability for the overlapping of the growing chains to avoid entanglement formation *[59,111,112,155-158]*. Another important factor in the synthesis of disentangled polymers is the lower polymerisation temperature than the crystallisation temperature of polymer. Therefore, the final entangled state of the nascent polymer (morphology) will be combined effect of polymerisation and crystallisation kinetics. For example, the polymerisation temperature determines the catalyst activity (rate of polymerisation) and also the crystallisation rate of the growing chains. At higher polymerisation temperatures, catalyst activity normally increases causing an increase in the polymerisation rate. However, at the same time the increased temperature also causes a decrease in the crystallisation rate of the growing chains. It is anticipated that the faster crystallisation rate would suppress overlapping of chains and would result into a lesser entangled nascent state. Thus, the resultant entangled state is the balance between the rates of polymerisation and crystallisation. From Figure 2.2, it is apparent that the catalyst activity decreases substantially after 5-10 minutes of polymerisation. The

decrease in catalyst activity, i.e. polymerisation rate, will favour less entanglement formation as the crystallisation rate at the fixed temperature will remain the same. In this respect, the observed decrease in $G_N^{t=0}$ (i.e. decreasing entanglement density) depicted in Figure 2.16, with increasing polymerisation time is in accordance with the decreasing catalyst activity shown in Figure 2.2.

Although the reactor bath for the polymerisation was maintained at 10°C, this does not imply that the temperature achieved at the very local site of the catalyst where polymer chain is growing will be the same. In very early stages of polymerisation i.e. immediately after injection of the catalytic system in the ethylene saturated solvent, the local temperature at the catalyst site can be much higher than the desired polymerisation temperature due to heat release on polymerisation and crystallisation. However, as time lapses with polymerisation, the local and global temperature of reaction equilibrates to the set polymerisation temperature. At a fixed temperature, the crystallisation rate of the growing chains also starts increasing over the polymerisation rate due to the decreasing catalyst activity that may arise due to difficulty in ethylene diffusion to the active site. The gradual decrease in the polymerisation rate while the crystallisation rate remains same, at a fixed temperature with increasing polymerisation time, leads to lesser probability of entanglement formation.

The higher value of $G_N^{t=0}$ for lower molecular weight samples highlights the fact that the entanglement density is higher in these samples than the high molecular weight samples synthesised for longer polymerisation times. Higher entanglement density in low molecular weight samples is caused by the higher probability of the entanglement formation due to the higher catalyst activity (polymerisation rate) and higher temperature (lower crystallisation rate) at the local sites of the catalyst in the initial stages of polymerisation. With increasing polymerisation time, the catalyst activity slows down effectively and crystallisation of the growing chains increases as the polymer chains grow. This leads to a scenario where one end of the chain has a higher entanglement density (lower M_e) compared to the other end which has grown at the later stages of polymerisation, causing a heterogeneous distribution of the entanglement density in the amorphous regions of the crystal. On melting of the nascent disentangled

polymers, having heterogeneity in the distribution of entanglements, the heterogeneity is slowly lost because of physical mixing and reptation dynamics as chains approach the thermodynamically stable melt state (homogenous melt). The average molecular weight between entanglements is higher in the higher molecular weight nascent disentangled samples compared to the lower molecular weight samples. The entanglement density produced during the polymerisation can also depend upon several parameters such as the polymerisation temperature, catalyst activity, heat and mass transfer within the bulk of reaction, solubility of ethylene in the solvent used etc *[157]*. What follows are the observations on the samples synthesised at higher temperatures while keeping the same polymerisation time and other synthesis conditions.

2.3.8 Effect of polymerisation temperature on entanglement molecular weight

In the sections above, it is hypothesised that during polymerisation, especially at the initial stages, higher temperature at local catalyst site may increase the entanglement formation. To recall, the entanglement density decreases with increasing polymerisation time or increasing molecular weight. To have further insight on the influence of polymerisation temperature on the entanglement formation, polymerisation temperature was varied while maintaining the same polymerisation time and other polymerisation conditions (solvent, pressure, catalyst concentration etc). The effect of polymerisation temperature on the rate of entanglement formation is shown in Figure 2.16, where entanglement formation occurs faster in samples synthesised at higher temperatures. Figure 2.17 shows that the samples synthesised at higher temperatures have higher $G_N^{t=0}$, thus higher entanglement density. The presence of high entanglement density in the nascent polymer also promotes faster entanglement formation on melting and subsequently reduces the total entanglement time, t_m. The Mw and MWD of the samples along with their total entanglement build-up time are tabulated in Table 2.4. From Table 2.4 and Figure 12 it is apparent that though the samples dPE_10C_30' and dPE_40C_30' have the similar molecular weight and molecular weight distribution, the time required for the modulus build-up of the sample dPE_10C_30' is much larger than the sample dPE_40C_30'. The distinction in the modulus build-up time is attributed to

the higher initial entangled state ingrained in the sample dPE_40C_30' due to its higher polymerisation temperature (faster polymerisation and slower crystallisation rate). It is also to be realised that the modulus build-up time, entanglement formation, in these samples are also influenced by factors such as MWD, the entanglement density present due to different crystallisation rate and catalyst activity (Figure 2.3) at different polymerisation temperatures. Effect of MWD on entanglement formation is discussed in next section.

From Figure 2.17, it is apparent that $G_N^{t=0}$ increases with increasing polymerisation temperature and becomes almost constant at higher polymerisation temperatures. Though the reduction in catalyst activity above 30°C (Figure 2.3) will favour the disentangled state, at the same time the reduced crystallisation rate at the higher temperature will favour entanglement formation. Thus, the net effect of increasing polymerisation temperature, above 30°C, on the change in entanglement density is negligible.

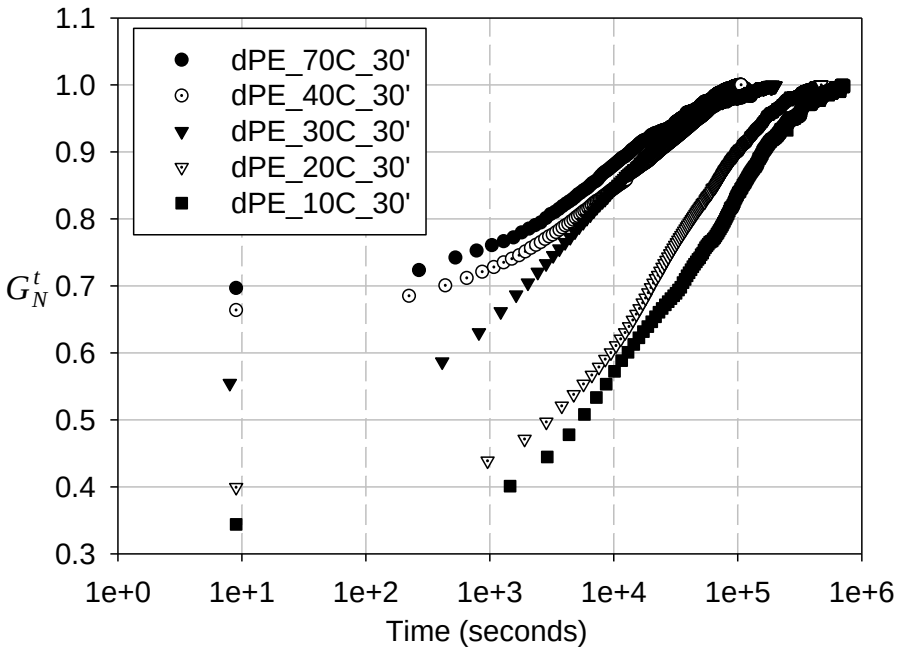

Figure 2.16. Normalised elastic modulus for dynamic time sweep at 160°C for different polymer samples synthesised at different polymerisation temperatures. It can be seen that the starting value of G_N^t at t_0 decreases for the polymer samples synthesised at lower temperatures.

Table 2.4. Mw and MWD of samples synthesised at different temperatures for a fixed polymerisation time of 30 minutes. Due to the extremely broad molecular weight distribution of the sample dPE_70C_30', it was not possible to determine a reliable molecular weight.

Samples	Mw (million g/mole)	MWD	Total entanglement time, t_m (s)
dPE_10C_30'	5.1	2.5	423,430
dPE_20C_30'	6.3	2.4	266,310
dPE_30C_30'	4.7	2.9	88,450
dPE_40C_30'	5.2	3.1	72,270
dPE_70C_30'	--	--	62,470

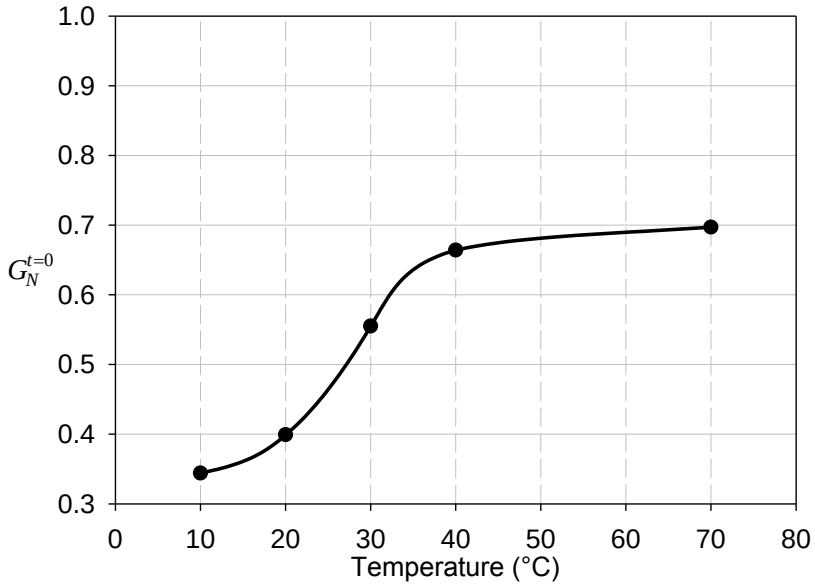

Figure 2.17. Normalised storage modulus at time t_0 (after melting) for nascent disentangled samples synthesised at different temperatures which represents the initial entanglement density present in the sample.

2.3.9 Effect of MWD on entanglement formation

Figure 2.18 shows the effect of MWD on entanglement formation in disentangled samples of similar Mw, but different MWD, synthesised at the same temperature of 10°C. It can be seen that the modulus builds up is faster for the samples having higher MWD. It is already noted that higher Mw samples (chains) have a lower entanglement density. In a broad MWD sample with similar Mw as

of a narrow MWD samples, overall entanglement density ($G_N^{t=0}$) is higher due to presence of the lower molecular weight components, Figure 2.18. However, it is not easy to synthesise disentangled *UHMw-PE* having the same Mw, but different MWD. Hence, samples having two different Mw and MWD were physically mixed by hand (1:1 ratio by weight) and used for the rheology study of lower or higher components (chains) on entanglement formation rate, Figure 2.19.

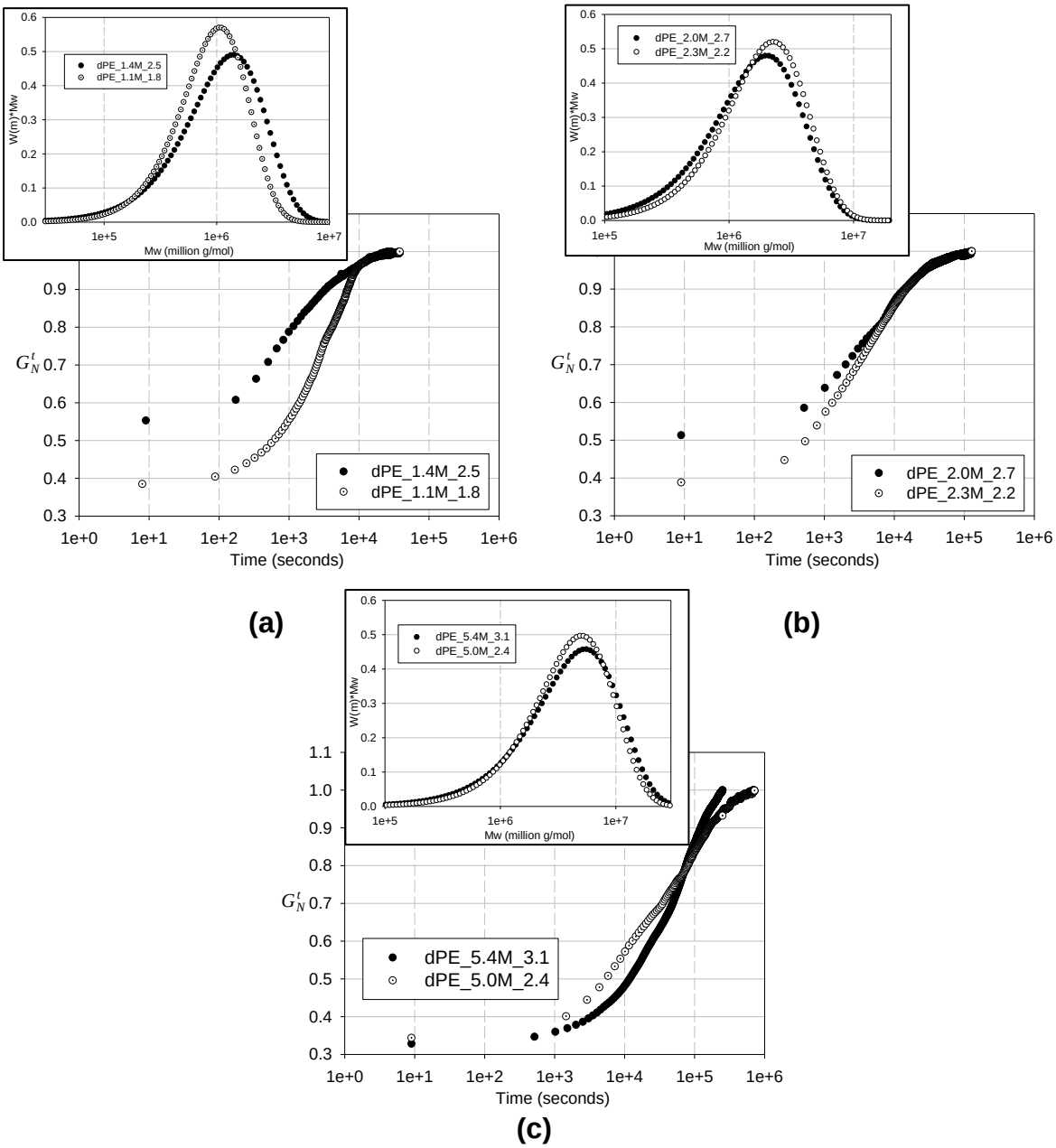

Figure 2.18. Normalised modulus build-up at 160°C for synthesised disentangled UHMw-PE (synthesised at 10°C) of similar Mw, but having different MWD. Inset Figures show numerically synthesised MWD curve of the sample. Middle terms in the sample names (legends) represent Mw in million g/mol whereas the last terms are MWD.

Figure 2.19 shows the entanglement formation in the synthesised disentangled samples of different Mw and MWD. Sample dPE_3.4M_2.9 was obtained by physically mixing the samples dPE_2.5M_2.1 (low Mw) and dPE_5.9M_3.3 (high Mw) in ratio of 1:1 by weight. Addition of higher Mw components affects the entanglement formation rate as can be seen from modulus build-up in dPE_3.4M_2.9 compared to other samples. Also, by the addition of high Mw components having a lower entanglement density, mixed sample dPE_3.4M_2.9 shows overall lower entanglement density, can be thought as dilution of entanglement density. However, faster reptation dynamics due to large number of chain ends from the low Mw components helps in the overall faster entanglement formation. The modulus build-up time does not change much for samples for lower Mw, Figure 2.18a and Figure 2.18b. However, a large difference in the total entanglement times can be seen for the sample with the higher Mw, Figure 2.18c and Figure 2.19. The total entanglement time (t_m) for the sample obtained after mixing of samples of different Mw, is in between the times of the two original samples.

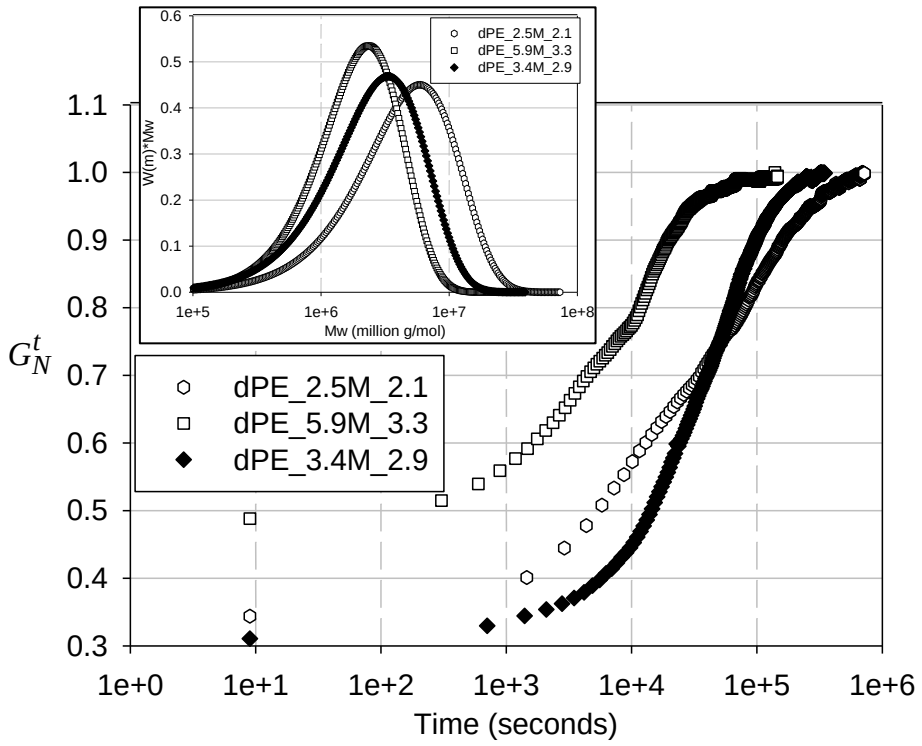

Figure 2.19. Normalised modulus build-up at 160°C for synthesised disentangled UHMw-PE (synthesised at 10°C) having different Mw. Sample dPE_3.4M_2.9 was obtained by physical mixing of sample dPE_2.5M_2.1 and dPE_5.9M_3.3 in ratio of 1:1 by weight.

In addition to the concepts summarised on the entanglement formation with polymerisation time and polymerisation temperature based on the experiments in this chapter, crystallisation at the later stages of polymerisation will also be favoured due to suppression of the nucleation barrier, once the crystal is nucleated due to the growing chains.

2.4 Summary

In this chapter it is conclusively shown that melt rheology can be effectively used as a tool to assess qualitatively the entangled state in the synthesised nascent polymer. One of the important conclusions is that entanglement formation and its distribution along the chain length, which in turn controls the morphology of the sample, continues after the initiation of the chain growth and depends on the polymerisation conditions. Based on various observations and results from numerous experimental data in this chapter, a schematic drawing hypothesising entanglement formation during polymerisation time lapses is shown in Figure 2.20.

Experimental findings on entanglement formation and distribution as function of polymerisation conditions are summarised in Figure 2.21. All the observations from this chapter are summarised below,

- Entanglement formation in a melt of disentangled *UHMw-PE* can be followed by using dynamic melt rheology, Figure 2.6. Entanglement formation consists of two regions, R1 and R2. In region R1, entanglement formation proceeds by mixing of the chains through the chain explosion process after melting whereas, in region R2, entanglement formation is slow and mainly governed by reptation dynamics, Figure 2.6.
- The on-set crystallisation temperature decreases with increasing number of entanglements (annealing time in the melt) in a given polymer, Figure 2.9.
- Entanglement formation rate is dependent on the observation temperature up to a certain temperature (160°C for the synthesised disentangled *UHMw-PE* samples used here), above which the rate is independent of temperature, Figure 2.10.

- The entanglement formation rate is faster for disentangled polymers synthesised at lower polymerisation times (lower molecular weight) and having higher entanglement density, Figure 2.11, Figure 2.15, Figure 2.16, Figure 2.17 and Figure 2.19. The total entanglement build-up time scales as ~2.6 with the molecular weight, Figure 2.14
- Entanglement distribution along the entire chain length in a synthesised disentangled *UHMw-PE* sample is heterogeneous where the maximum density resides along the part of the chain produced during the initial stages of polymerisation, Figure 2.15 and Figure 2.17. The decrease in entanglement density with increasing molecular weight (or polymerisation time) can be explained because of the favoured crystallisation rate over the polymerisation rate with increasing polymerisation time.
- For the same polymerisation conditions, with time the crystallisation rate is anticipated to gain the upper hand over the polymerisation rate because of (a) the suppression in the nucleation barrier due to crystallisation of the chains synthesised at the earlier stages, (b) the decrease in catalyst activity due to the difficulty in diffusion of ethylene to the active centre, and (c) the decrease in the temperature difference at the catalyst and its surroundings due to exothermic polymerisation.
- These concepts were further strengthened by experiments performed at different polymerisation temperatures where the entanglement density is higher for higher polymerisation temperature, Figure 2.17.
- Entanglement formation rate overall increases with addition low molecular weight components (broader MWD) whereas higher molecular weight component (which has lower entanglement density) decreases the overall entanglement density in the melt, Figure 2.19.

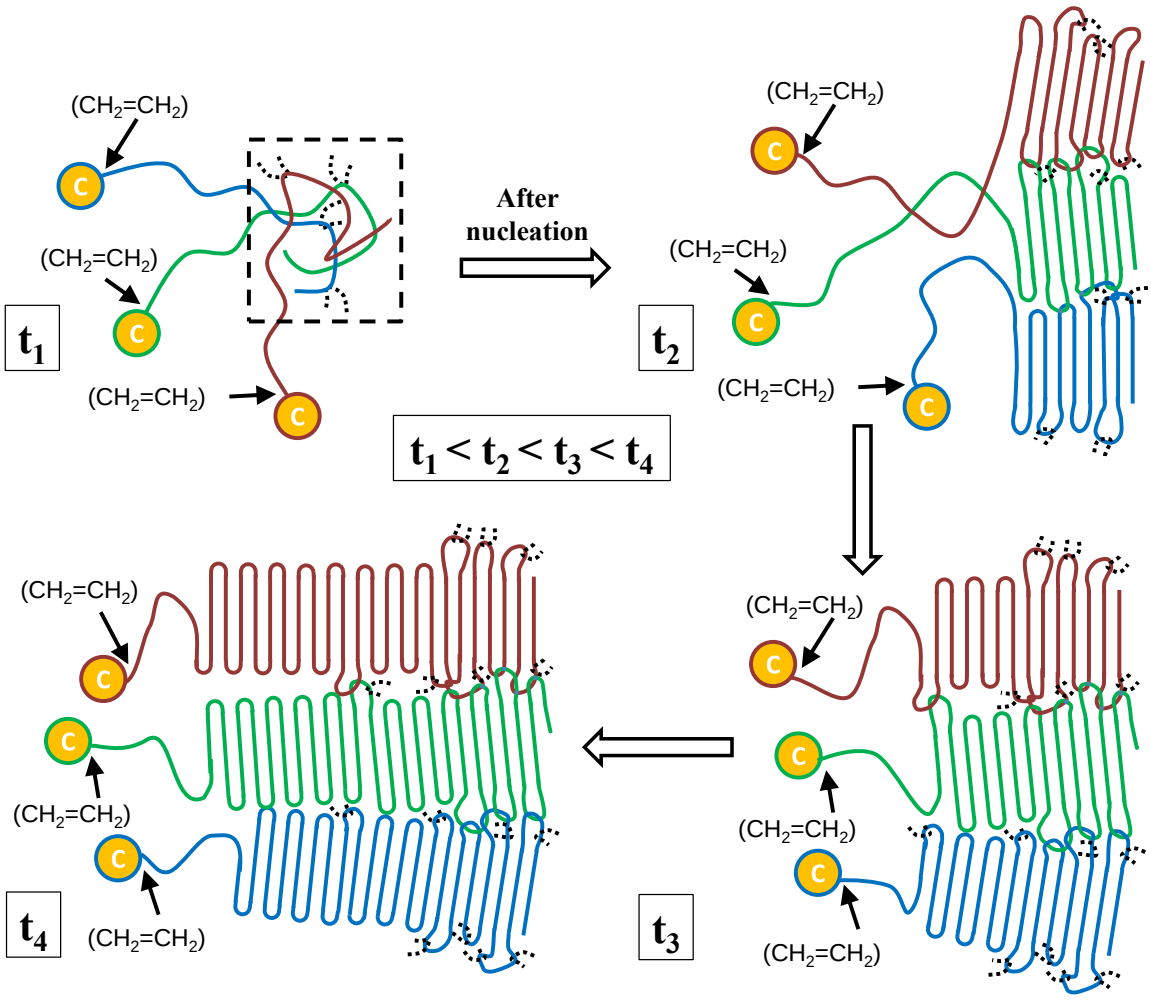

Figure 2.20. A schematic drawing showing chain growth from three different catalytic sites, where entanglements are realised at the initial stages of polymerisation prior to crystallisation. Dotted black loops represent entanglement formation from the neighbouring chains other than polymer chains represented by red-blue-green. The discontinuous rectangular box represents entanglement formation prior to crystallisation.

Figure 2.20 shows entanglement formation during polymerisation, prior to crystallisation as the chains grow in length they will have a strong probability to find each other and entangle, time t_1. (Even at very dilute catalytic concentrations, if the chains do not find each other they will have the tendency to form intramolecular entanglements, prior to nucleation). Further, at time t_2, considering polymerisation to be an exothermic process, at a distance from the catalytic site the temperature would be lower and the chains will tend to crystallise. The crystallisation (or nucleation at this stage) will push entanglements into the amorphous regions. At the depicted time t_3, the crystallised domains will suppress

the nucleation barrier and the growing chains from the same catalytic site will crystallise faster. With increasing polymerisation time, t_4, the catalyst will be surrounded more and more by the crystallised polymer, and ethylene diffusion will become difficult and thus the polymerisation rate will decrease constantly giving the upper hand to the crystallisation of the growing chains. This process in a single site catalytic system would ultimately favour the formation of disentangled polyethylene with increasing molecular weight, i.e. reduction of entanglement density with increasing chain length.

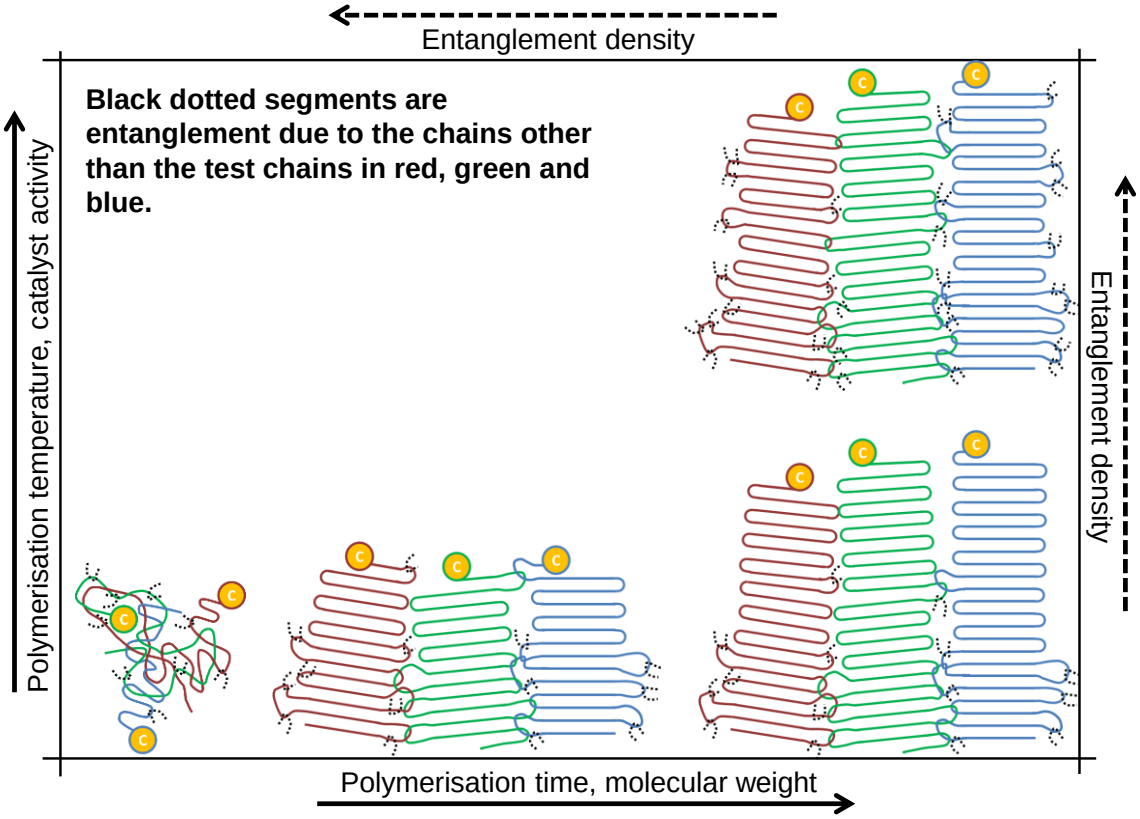

Figure 2.21. A sketch summarising the effect of polymerisation conditions and parameters on entanglement formation and distribution during polymerisation of disentangled UHMw-PE using a homogeneous synthesis. Dotted black loops represent entanglement formation from the neighbouring chains other than polymer chains represented by the red-blue-green solid lines.

Chapter 3

Non-linear viscoelastic response of Ultra High Molecular Weight Polyethylene; Large Amplitude Oscillatory Shear (LAOS)

Frequency dependent elastic and viscous modulus determination using oscillatory rheometry within the linear viscoelastic regime is commonly used for studying several classes of complex fluids, viz. biological macromolecules, surfactants, suspensions, emulsions, polymer melts etc. [179-181]. Application of oscillatory rheometry within the linear viscoelastic regime is due to well-developed molecular theories [3,5,15,16] that help in the understanding of the underlying microstructure of these complex fluids. However, due to the requisite small deformation in the linear viscoelastic regime, it is not possible to provide any information on the dynamics and microstructure that can develop under large deformation that the polymer experiences during real processing conditions. Recently, there has been growing interest in large amplitude oscillatory shear (LAOS) rheometry that is capable of differentiating materials having identical linear viscoelasticity responses [173,182-184]. To recall, in the previous chapter of this thesis, heterogeneity in the distribution of entanglements over chain length in the metastable melt state of disentangled UHMw-PE samples has been established. In this chapter, the influence of entanglement on the relaxation behaviour is investigated. For the purpose LAOS is applied and the non-linear viscoelastic regime is explored. A remarkable feature of overshoot in loss (viscous) modulus with increasing deformation (strain) in UHMw-PE melt is observed. This observation is characteristic of colloidal systems [173,185]. By carefully designing the LAOS experiments, the difference in LAOS behaviour of the metastable and thermodynamically stable melt of UHMw-PE was studied. Effect of frequency and molecular weight of the polymer on LAOS behaviour is also summarised.

3.1 Introduction

Recent developments on disentangled ultra-high molecular weight polyethylene (UHMw-PE), synthesised using controlled chemistry have opened new possibilities of achieving higher mechanical properties in uniaxial and biaxial drawn films. The increase in tensile strength, tensile modulus also comes with ease in solid state processability without using any solvent *[1]*. Such disentangled materials not only show promising commercial advantages, they also present opportunities in understanding of chain dynamics during the formation of the thermodynamically stable melt state. The time needed for the metastable melt state, obtained after melting of the disentangled crystals, to reach the thermodynamic stable melt (t_m) where entanglements are homogeneously distributed shows molecular weight (M_w) dependence, $t_m = M_w^{\sim 2.6}$, see chapter 2. The heterogeneous distribution of entanglements in the solid and amorphous regimes of the semi-crystalline polymer influences solid state deformation *[1,118,151,152]*. Heterogeneity in the distribution of the entanglements, during solid to liquid transition on melting, has an influence on heating rate dependence of melting i.e. the kinetics involved in melting process, see chapter 3. For example, detachment of the number of chain stems from the crystal surface, and their reeling into the melt state, is strongly dependent on the heating rate. Further, disentangled polymers using controlled slow heating are capable of producing a new melt state (heterogeneous melt) possessing a lower modulus which can facilitate melt processing *[127]*. In chapter 2, the heterogeneous distribution of entanglements in disentangled UHMw-PE, synthesised using homogeneous catalytic system is studied in the linear viscoelastic regime.

It is a common practice to measure the frequency dependence of the elastic modulus (G') and the viscous modulus (G'') in the linear viscoelastic regime. Normally, in such frequency dependent rheological experiments, small amplitude strains within linear viscoelastic (LVE) regime are used. Oscillatory experiments performed under small amplitude strain provide information on viscoelastic behaviour of the material. However, the deformation conditions in such experiments are not sufficient to replicate the large deformation (shear) experienced by materials during actual processing conditions, viz. injection

moulding, extrusion, fibre spinning etc. Hence, non-linear rheological experiments, involving high deformation, such as step shear rate experiments are performed to obtain information on shear viscosity at relatively large deformations. These studies are of relevance in measuring the flow ability (processability) of polymers. However, it is not possible to achieve steady state data due to higher shear rates as viscoelastic materials having slower relaxation dynamics do not have enough time to relax. Unlike in the case of oscillatory linear viscoelastic experiments, where theoretical models have been rigorously validated with large experimental data sets and thereby provide molecular insight during deformation. The lack of validation of the theoretical models with large amplitude oscillatory shear data leaves uncertainty in the understanding of the structural changes during deformation.

Recently, there has been growing interest in large amplitude oscillatory shear (LAOS) experiments where varying strains (beyond LVE, G' and G" are dependent on strain) is applied at a fixed frequency; which is useful for characterising a broad range of complex fluids. Payne studied the non-linear behaviour of carbon black particle filled natural rubber systems and reported dynamic stress softening, known as the Payne effect or the Fletcher-Gent effect *[186,187]*. Giacomin *et al. [188-194]* studied viscoelastic behaviour of various polymer melts under large shear. They investigated large shear behaviour by using waveform analysis, a Fourier transform (FT) and constitutive modelling. Researchers have used these two data analysis methods viz. Fourier transformation and stress waveform analysis for investigating the non-linear characteristics of various viscoelastic materials under oscillatory shear *[186,187,195-201]*. One of the inherent problems with the LAOS experiment is that data generated at high shear includes higher harmonic responses, and is also contaminated with electrical and mechanical noise. Wilhelm *et al. [202-205]* developed a highly sensitive LAOS method by data oversampling using a high performance Analog-to-Digital Converter (ADC) card, mechanical and electrical shielding and a special FT algorithm. The developed method has been able to attain a signal to noise of the order of 10^5, an improvement of 2-3 decades over previous methods. This method has been commercialised in new rheometers, such as the ARES-G2 manufactured by TA Instruments and has been used in

this study for the confirmation of non-linearity (higher harmonic intensities) under high deformation. Cho *et al. [206]* proposed a new non-linear stress decomposition (SD) method where a non-linear stress is decomposed into a superposition of elastic and viscous contributions. Hyun *et al. [207]* recently proposed and used a new non-linear coefficient, Q, as a function of strain and frequency to distinguish the non-linear responses of linear polystyrene and comb polystyrene. These new developments in LAOS experimental methods and analysis of the non-linear rheology data are bringing some physical interpretation of non-linear stress response for understanding material behaviour. Very recently, Hyun *et al. [173]* published a detailed review on progress in experiments and analysis of LAOS.

LAOS experiments are normally performed by applying varying strains at a fixed frequency and are minimally used to establish the linear viscoelastic (LVE) regime where dynamic frequency sweep experiments are performed. In LAOS experiments at larger strains, viscoelastic responses such as G' and G'' lose their exact mathematical meaning (based on linear rheology theory) as the stress response is no longer sinusoidal. However, if enough experimental care (such as avoiding slippage) is taken then the LAOS behaviour of a material can provide some useful additional information. Hyun *et al. [208]* have judicially used LAOS to classify complex fluids based on their viscoelastic response to large strains. These authors summarised the different features of LAOS behaviour beyond the LVE regime: type-1, strain thinning (G', G" both decreasing); type-2, strain hardening (G', G" both increasing); type-3, weak strain overshoot (G' decreasing, G" increasing followed by decreasing) and type-4, strong strain overshoot (G', G" both increasing followed by decreasing). The type of LAOS features exhibited by the investigated materials showed a dependence on the interactions between its micro-structures. For example, type-1 (strain thinning) behaviour is observed in polymer solutions and melts where chain orientation (alignment of microstructures) in the flow direction helps in the reduction of local drag causing a continuous decrease in G' and G" with increasing strain. A solution with weaker structural complexes (such as a xanthan gum solution) exhibited the type-3 feature (weak strain overshoot) due to the resistance offered by the complex

structure against deformation, where to a certain applied strain G" increases, and above which it decreases.

In this chapter, conventional LAOS experiments (without FT and SD analysis) are used to understand rheological properties of linear UHMw-PE polymers, while moving from the linear to the non-linear viscoelastic regime. For the studies, commercially available UHMw-PE and the disentangled UHMw-PE synthesised as described in previous chapter were used. The disentangled UHMw-PE allowed following the influence of entanglements (during modulus build-up) on LAOS behaviour during large deformation. The effects of frequency, molecular weight (Mw) and annealing time (in the melt) to elucidate the effect of entanglement on the rheological behaviour under large deformation are also presented.

3.2 Materials and experimental protocols:

3.2.1 Materials and sample preparation

All the disentangled ultra-high molecular weight polyethylene (UHMw-PE) samples used in this chapter were synthesised using the synthesis conditions described in chapter 2. A commercially available grade of UHMw-PE from DSM® was used to understand the difference in the non-linear behaviour between entangled and disentangled melts. Different molecular weights (Mw) of disentangled UHMw-PE samples were synthesised using the same catalyst system and reaction conditions, except for the polymerization time. The nascent polymers (obtained directly from the reactor) were mixed with anti-oxidant (Irganox 1010), 0.7% by weight, to prevent any oxidation over the long experimental time. To have homogeneous mixing of the antioxidant with the powder, the antioxidant was first dissolved in acetone and subsequently mixed with the nascent UHMw-PE powder covered in acetone. After mixing, the powder was dried overnight in a vacuum oven at 40°C.

Sample preparation for the rheological studies: The dried powder (with anti-oxidant) was compressed into a plate of diameter 40-50 mm and thickness 0.6-0.7 mm at 125°C, under a force of 20 tons for an average time of 25 minutes.

From the compressed plate, several discs of 12 mm diameter were cut using a metal punch for rheology experiments.

Table 3.1. List of UHMw-PE samples used in this chapter. Molecular weight (Mw) and molecular weight distribution (MWD) were measured using melt rheology as described in chapter 2. Samples with prefix 'd' before PE in the sample names are disentangled (synthesised) UHMw-PE whereas sample with prefix 'e' is the commercial entangled UHMw-PE obtained from DSM®. The middle term in the sample name is the molecular weight of the sample in million g/mole whereas the last term is molecular weight distribution.

Sample name	Mw (million g/mol)	MWD
dPE_0.3M_1.5	0.3	1.5
dPE_0.5M_1.7	0.5	1.7
dPE_0.8M_1.8	0.8	1.8
dPE_1.1M_1.8	1.1	1.8
dPE_3.4M_2.5	3.4	2.5
ePE_3.7M_8.4	3.7	8.4

3.2.2 Experimental protocols for the rheological studies

All the rheological studies were performed using a strain-controlled rheometer, ARES, TA Instruments, whereas a more modern ARES-G2 was used for validation of higher harmonic moduli intensities (to ensure $I_3/I_1 < 0.15$) during large deformations. Experimental conditions and protocols used are summarised here. For more details on specific experiments, also see chapter 2.

In all rheological studies, discs of 12 mm diameter were used to avoid excessive force to the rheometer transducers that the rubber like melt state of the UHMw-PE imposes. To prevent thermo-oxidative degradation all experiments were performed in a nitrogen environment. After preheating the disc between the parallel plates of the rheometer to 110°C, the sample was heated from 110°C to 130°C rapidly (~30°C/min). After waiting for thermal stabilisation at 130°C (~2 minutes), the sample was compressed under a normal force of ~400 grams. The auto normal force function, maintaining the constant force of ~400 grams, was chosen throughout the experiment (for example dynamic time sweep). From

130°C to 160°C, the sample was heated at 10°C/min. At a fixed frequency of 100 rad/s, the Dynamic Amplitude Sweep (DAS) test was performed to determine the LVE regime. DAS was also performed at various frequencies for LAOS studies. Dynamic Time Sweep (DTS) test was performed to follow the entanglement formation at a fixed frequency of 10 rad/s and a strain of 0.5% within the LVE regime of the polymer *[59,157,167,209]*. The Dynamic Frequency Sweep (DFS) test was performed for 0.5% strain (within LVE) at 160°C. All rheological studies were performed at 160°C. Test protocols and steps involved are also schematically represented in Figure 3.1.

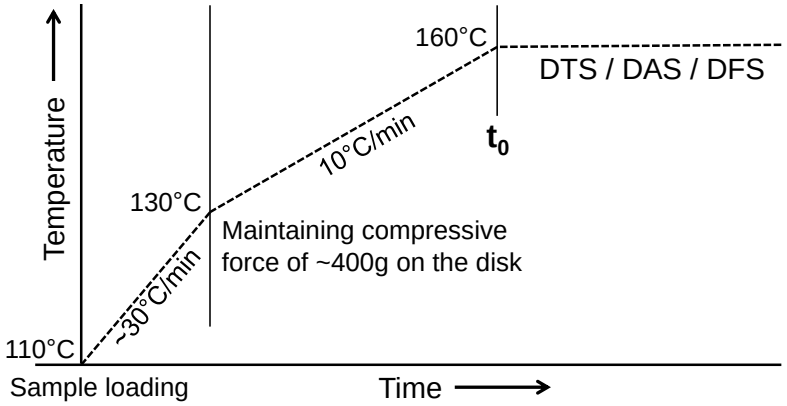

Figure 3.1. Schematic diagram for the rheological experiment protocol used to perform various rheological tests to observe modulus build-up (entanglement formation), linear and non-linear viscoelasticity at 160°C for all the samples. Time 't_0' in Figure represents the start of the data collection after thermal stabilisation i.e. 100 seconds after reaching 160°C.

To understand the effect of entanglement and large deformation on the linear viscoelastic response of different Mw samples, numerous combinations and sequences of (a) DAS (to observe LAOS behaviour), (b) DTS (modulus build-up to follow entanglement formation) and (c) DFS (to find the length scale probed at a used frequency during DAS in the corresponding sample) were used and are represented as a sequential scheme in an inset (rectangular box) of the respective Figures in this chapter. The following parameters were used for the experiments discussed in this chapter (unless mentioned otherwise).

a) Dynamic Amplitude Sweep (DAS): Frequency of 100 rad/s, at 160°C.
b) Dynamic Time Sweep (DTS): Frequency of 10 rad/s, strain of 0.5% (within LVE regime), at 160°C.
c) Dynamic Frequency Sweep (DFS): Strain of 0.5% at 160°C.

3.3 Results and discussion:

3.3.1 Non-linear behaviour of commercial entangled UHMw-PE in melt:

Figure 3.2 shows the dynamic amplitude sweep (DAS) data on the commercially available entangled UHMw-PE, Mw of 3.7 million g/mol and MWD ~ 8.4 (ePE_3.7M_8.4, Table 3.1). Figure 3.2a shows the absolute values of G' and G" (obtained directly from the rheometer) for varying applied strains at 160°C (at time t_0) and a frequency of 100 rad/s. It should be noted that the moduli measured under large strains do not have same meaning as described by linear viscoelasticity because the stress is no longer sinusoidal. Conventional rheometers (such as used in this study) cannot differentiate and eliminate response from the higher harmonic components generated at larger strains and report the data in the same way as in the linear viscoelastic regime. However, the third higher harmonic contribution at larger strain was not more than 10-15% (I_3/I_1 < 0.15) of the first harmonic response for all samples studied (see Appendix 5), and therefore, the higher harmonics that decay very fast can be neglected *[173,185,204,210]*. The moduli obtained from the first harmonic using Fourier transformation is not very different from the moduli obtained from the rheometer directly, and the type of LAOS behaviour is not affected *[208]*. For simple analysis, the data presented in this study is without any Fourier transformation. However, for accurate analysis Fourier transformation of the stress signal will be necessary. Figure 3.2b shows the normalised G' and G"; where the values of G' and G" at lowest strain (0.3%) are used for normalisation and have been used throughout the discussion.

3.3.1.1 Unusual Type-3 behaviour in polymer melt

Although the LAOS data presented in Figure 3.2 is on the melt of a homo-polymer linear PE, a striking feature of the G" peak (overshoot) is observed that is characteristic of colloidal systems *[173,185]*. In the literature, the G" peak in a LAOS experiment for a homo-polymer melt has never been reported and it is stimulating to observe behaviour ubiquitous to metastable complex fluids. Up to ~5% strain, the linear viscoelastic (LVE) regime is observed. Above ~5% strain, G' continuously decreases with increasing strain. However, G" shows a distinct

peak (overshoot) after LVE before decreasing at higher strains. A small dip in G", before the peak is also evident. In the nomenclature given by Hyun *et al. [208]*, polymer melts are classified as Type-1 complex fluids showing strain thinning. However, from Figure 3.2, UHMw-PE melt behaves similar to Type-3 systems such as xanthan gum solutions. Hyun *et al.* have associated the G" peak to a weak complex structure caused by molecular alignment and association arising due to hydrogen bonding *[208,211]*. However, UHMw-PE melt having linear chains, used in this study, are not expected to show any such association.

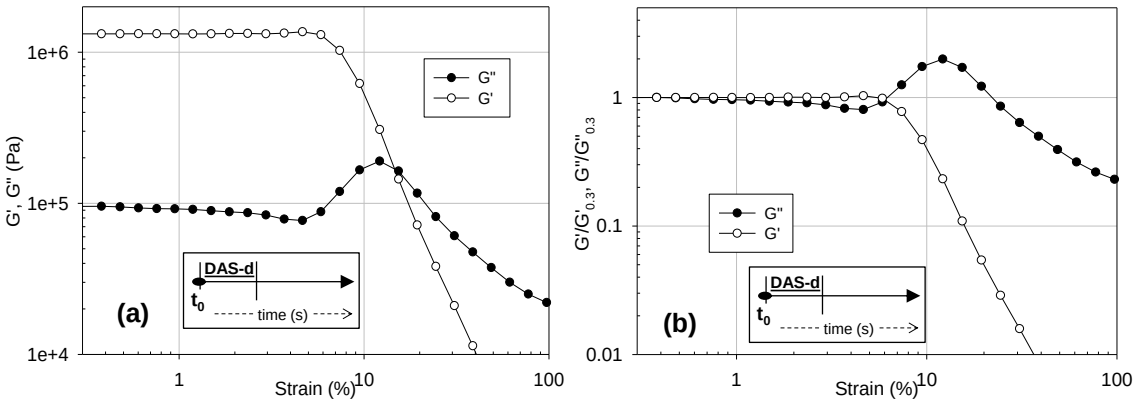

Figure 3.2. Dynamic amplitude sweep (DAS) on a commercial entangled UHMw-PE from DSM® (ePE_3.7M_8.4) at time t_0, 160°C and frequency of 100 rad/s. (a) Elastic (G') and viscous modulus (G") as a function of strain and (b) normalised elastic ($G'/G'_{0.3}$) and viscous ($G"/G"_{0.3}$) modulus as a function of strain. The data are normalised by G' and G" at lowest strain, in this case 0.3% strain.

Most likely in LAOS experiments on polymer melts, the G" peak at larger strains can be associated with the difference in relaxation (modulus) in the system caused by the large deformation. In polymer melt, under fast flow, entanglements may be removed (by convection) by a process known as convective constraint release (CCR), which in turn influences the chain relaxation *[41,212,213]*. In the case of the ePE_4M_8.4 sample, the broad polydispersity may also help in easy removal of entanglements due to the smaller chains (having faster relaxation) affecting the effectiveness of the entanglements along the chains. For an example, along the chain, entanglements formed due to low molecular weight chains will have a shorter tube renewal time compared to the entanglements formed by the large chains; entanglement removal due to chain renewal (even in slow flow) is known as constraint release (CR). The difference in

the effectiveness of entanglements is likely to develop heterogeneity (having different entanglement molecular weight, whether by CR or CCR) in the relaxation along the entire chain length in the normally seen homogeneous polymer melt, where entanglements are considered to be homogeneously distributed. Thus, similar to a xanthan gum solution, on application of LAOS to a polymer melt the G" overshoot arises due to the creation of different relaxation times (at a fix length scale i.e. frequency) along the same chain because of the removal of some entanglements, arising due to CCR. The peak in G" (type 3, overshoot) is predicted by the network model for LAOS, for a condition where creation and loss rate of network junctions (can be considered as entanglements) are positive, but the loss rate is higher than the creation rate parameter *[214]*. However, a more robust molecular model developed for fast flows may be able to predict the G" peak in LAOS test, such as the Rolie-Poly model *[215,216]*. A molecular model developed for polymer melts predicting type-3 behaviour would be much desired to get a further molecular insight in the relaxation dynamics involved, and is out of the scope of this thesis work.

Almost all the systems reported in the literature that show type-3 (G" overshoot) behaviour are two component systems having different relaxation times. One can see the system in an analogy of hard and soft spheres similar to filled rubber systems *[187,217]*. Babu *et al. [218]* reported DAS data on polypropylene (PP) and ethylene octane copolymer (EOC) based thermoplastic vulcanizates (TPV) where the un-crosslinked PP-EOC system shows type-1 (G' and G" decreasing). However, after crosslinking it exhibits type-3 (G" overshoot). With crosslinking of the EOC phase, the two phases of PP and EOC create a heterogeneous system having different relaxation domains; a reason for the G" peak. Miyazaki *et al. [185]* argued that the G" peak behaviour is universal despite the diversity in exhibiting systems and is common in metastable complex fluids.

In chapter 2, using linear melt rheology, the heterogeneity in the distribution of entanglements in synthesised disentangled UHMw-PE samples is recognised. The decrease in molecular weight between entanglements was followed with the increase in elastic modulus with time in dynamic time sweep experiments at a fixed frequency. Figure 3.3 shows a modulus build-up for sample ePE_4M_8.4. From the Figure, it is apparent that some increase in elastic (or storage) modulus

occurs with time. However, compared to the disentangled sample, the chain mixing region R1, where more than 80% of the increase in modulus occurs, is absent. For example, see Figure 3.7c. Thus, in Figure 3.3, entanglement formation by mixing of chains (through chain explosion, region R1) is missing and the entanglement formation mainly proceeds by reptation dynamics seen in region R2. The observed build-up in elastic modulus is extremely slow. However, it does suggest the presence of some heterogeneity in the melt arising due to its non-equilibrium state.

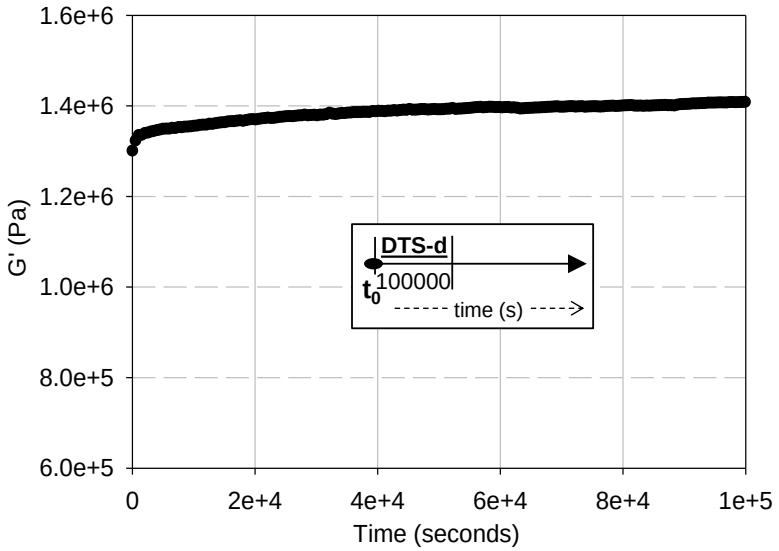

Figure 3.3. Modulus build-up in the commercially available entangled UHMw-PE from DSM® (ePE_3.7M_8.4) at 160°C, angular frequency of 10 rad/s and strain 0.5% (within LVE). The slow increase in elastic modulus (G') corresponds to the increasing number of entanglements with annealing time. When G' reaches a plateau at ~40,000 seconds, the melt reaches a thermodynamically stable (fully entangled) state. Beyond this annealing time, no increase in modulus is observed.

As discussed earlier, in the LAOS experiments, the difference in relaxation modulus due to the broad molecular weight distribution and entanglement removal by CCR in ePE_3.7M_8.4 sample may cause the G" peak. The difference in relaxation may arise due to heterogeneity in the distribution of entanglements, thus creating domains (zones) of different relaxation times (modulus). One can visualise the polymer melt as a two component system where a fast relaxing component forms a continuous phase (like the solvent in a colloidal system) and a slow relaxing component is dispersed as soft spheres, or vice-versa. Figure 3.3 shows entanglement formation, where the polymer melt

gradually transforms from a thermodynamically metastable to a stable state melt. The dynamics during entanglement formation, gives an opportunity to follow the influence of the non-equilibrium state of entanglement distribution on LAOS behaviour.

3.3.1.2 Influence of entanglement and MWD on LAOS behaviour of entangled UHMw-PE

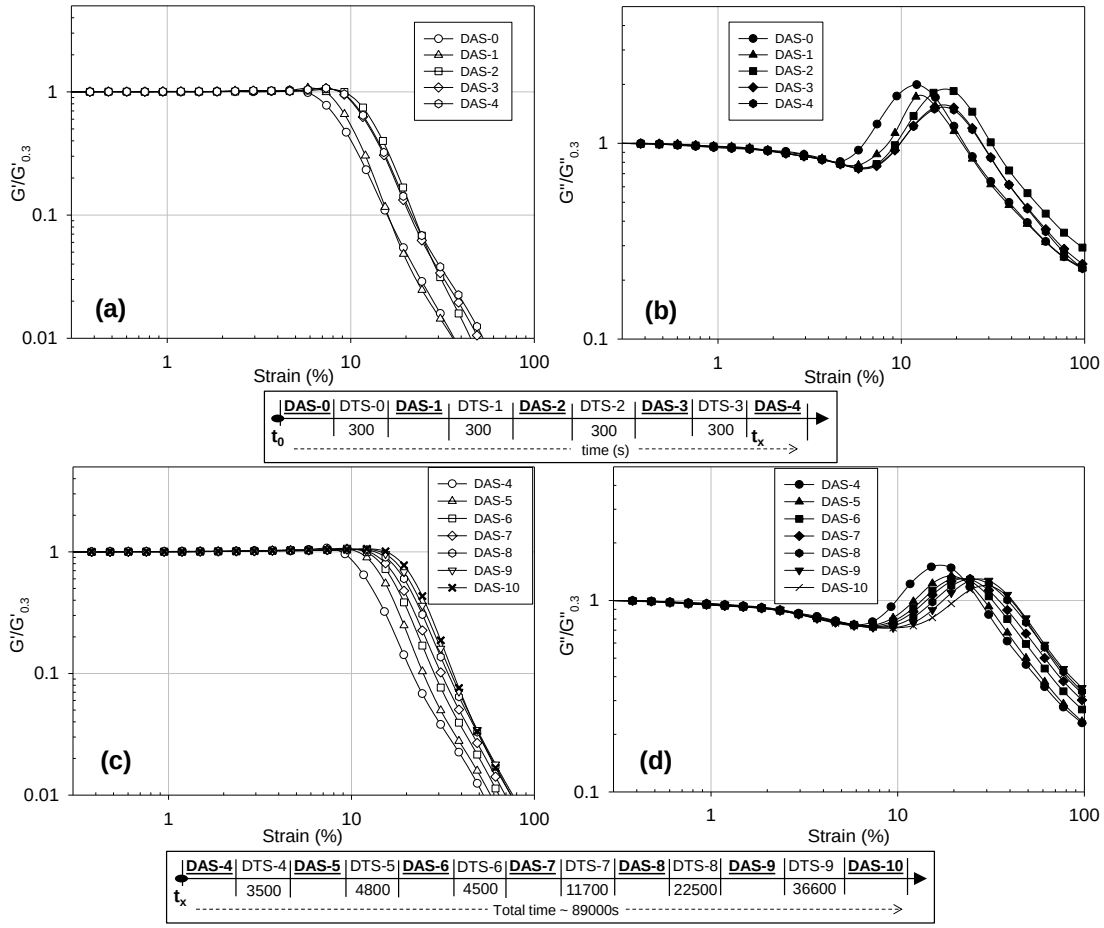

Figure 3.4. Dynamic amplitude sweep (DAS) data on the commercially available entangled UHMw-PE from DSM® (ePE_4M_8.4) at 160°C, frequency of 100 rad/s with increasing annealing time. (a) and (b) show normalised G' and G" data with respect to time t_0. (c) and (d) show normalised G' and G" data with respect to time t_x. The rectangular box below (or inset) in the Figure shows the sequence of the experiments performed where the horizontal axis represents time. Underlined experimental name (e.g. DAS-4, DAS-5 etc.) are shown in the corresponding Figure whereas the number below DTS (e.g. 300, 4500, 22500 etc.) experiment represents the annealing time between the DAS experiments. This scheme has been followed throughout the discussion.

Figure 3.4a and Figure 3.4b show the normalised elastic and viscous moduli at 160°C and a frequency of 100 rad/s for sample ePE_4M_8.4. Data collection was started after time t_0, where each Dynamic Amplitude Sweep (DAS) experiment was performed with an annealing time interval of 300 seconds. With increasing number of sequences, i.e. annealing time, the number of entanglement increases and the heterogeneity in distribution of entanglements reduces. It is apparent that the intensity of G" peak decreases with decreasing heterogeneity in distribution of entanglements in melt. The linear viscoelastic regime (LVE) also increases with increasing number of entanglements, Figure 3.4a. The onset and peak position of G" also shifts to higher strains, Figure 3.4b. The dip in G" before the peak also increases with increasing entanglement. *It is acknowledged that the LVE regime is larger for low molecular weight polymers (faster relaxation). However, it is counter-intuitive to observe increasing LVE regime as one would expect system to relax slower with increasing entanglement. This will be discussed further in following sections.*

Figure 3.4c and Figure 3.4d show the normalised G' and G" data after time t_x, which continues after DTS-3 (see rectangular box below Figure 3.4a and Figure 3.4b). Compared to Figure 3.4a and Figure 3.4b, the annealing times in Figure 3.4c and Figure 3.4d were much higher than 300 seconds between each DAS experiment. Similar trend of increase in LVE regime, onset and peak position of G" to higher strains with increasing annealing time was observed. However, the increase is less prominent at the high annealing times. The initially observed large decrease in G" peak intensity (Figure 3.4b) becomes less prominent with increasing annealing time (Figure 3.4d). As the melt approaches the thermodynamically stable state (fully entangled, see Figure 3.3); changes in G" peak intensity are no longer noticeable. However, even after annealing the melt for ~89,000 seconds, the presence of the G" peak is apparent. As discussed earlier, G" peak may arise due to entanglement removed by CCR at fast flow and its presence in sample ePE_4M_8.4 can be attributed to the broad molecular weight distribution facilitating entanglement removal. Whereas, the relatively large decrease in G" peak intensity, during the initial annealing time (until DAS-5), can be correlated with the substantial decrease in the heterogeneous distribution of entanglements across melt. Thus, in sample ePE_3.7M_8.4, the G" peak at

time t_0 (initial annealing time) is caused by the combined effect of the difference in relaxation rates of different domains; (a) heterogeneity in distribution of entanglement density and (b) CCR assisted by the broad molecular weight distribution. However, the intensity of the G" peak at any given time does not depend on the heterogeneity in the system alone, but also on the frequency used during the LAOS experiment and has been studied in the following section.

3.3.1.3 LAOS behaviour of entangled UHMw-PE melt at different frequencies

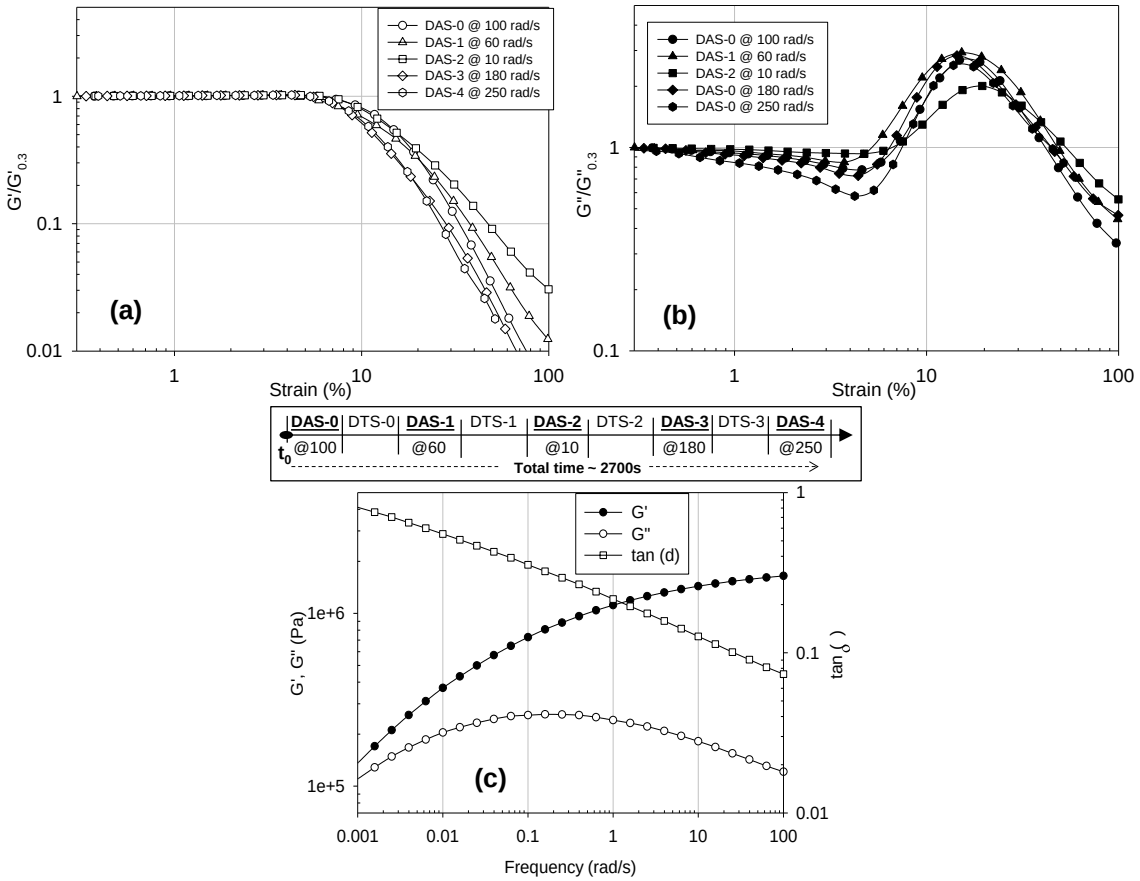

Figure 3.5. (a) and (b) show DAS (normalised G' and G") data on the commercially available entangled UHMw-PE from DSM® (ePE_4M_8.4) at 160°C and different frequencies. (c) shows the dynamic frequency sweep (DFS) at 160°C and 0.5% strain on the thermodynamic stable melt of ePE_4M_8.4.

Figure 3.5a and Figure 3.5b show normalised G' and G" in DAS experiments performed at various frequencies on sample ePE_4M_8.4 at 160°C. It is apparent that that the G" peak intensity decreases in the DAS experiments performed at lower frequencies. The dip in G", before the peak, also decreases

with decreasing frequency. The dip in G" can be associated with the stretching of the chains, which increases at higher frequencies allowing less time for the chains to relax. Though, the LVE regime remains the same at different frequencies, the slope of G' in non-linear regime increases with frequency, Figure 3.5a.

3.3.2 LAOS behaviour of laboratory synthesised disentangled UHMw-PE:

Compared to the commercially available polyethylene, the disentangled UHMw-PE, that has been characterised and reported in chapter 2, possess a relatively narrow polydispersity. On melting, the disentangled crystals form a thermodynamic metastable melt state in which the chains tend to entangle with time, where the time required for the disentangled melt to reach the thermodynamic stable state follows the power law ~2.6. In the following sections, LAOS behaviour of the disentangled polymer melt is reported.

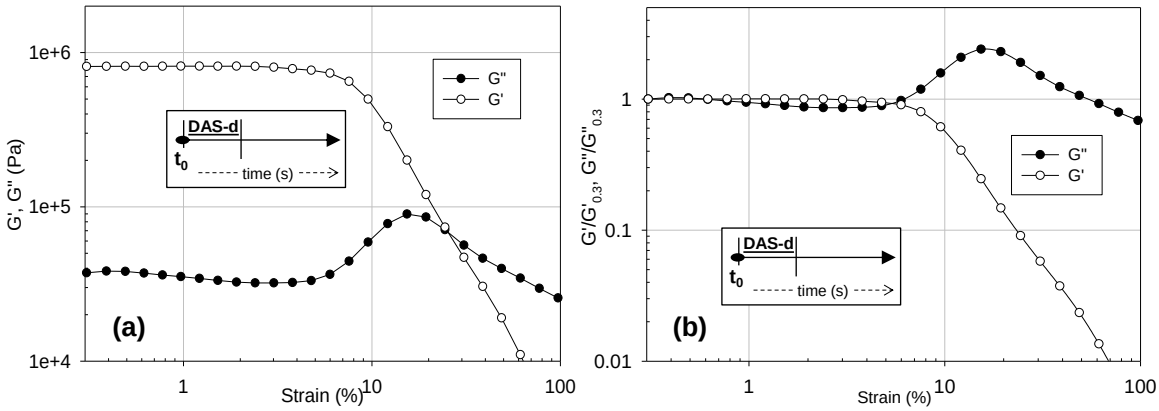

Figure 3.6. Dynamic amplitude sweep (DAS) on a synthesised disentangled UHMw-PE (dPE_1.1M_1.8) at time t_0, 160°C and a frequency of 100 rad/s. (a) Elastic (G') and viscous (G") modulus as a function of strain and (b) normalised elastic ($G'/G'_{0.3}$) and viscous modulus ($(G"/G"_{0.3}$) as a function of strain.

Due to the relatively narrow polydispersity of the disentangled UHMw-PE samples, it should be possible to suppress the effect of heterogeneity caused by the molecular weight distribution (assisting entanglement removal by CCR), that was apparent in the commercial sample. LAOS data of a disentangled UHMw-PE sample dPE_1.1_1.8 having a Mw of 1.1 million g/mol and a narrow MWD of ~1.8

is shown in Figure 3.6. Entanglement formation in the disentangled melt can be followed as an increase in the storage modulus with time.

Figure 3.6 shows features such as the G" peak (beyond LVE) and a dip before the peak at time, $t_{0,}$ immediately after melting at 160°C similar to the commercially available entangled sample ePE_3.7M_8.4 (Figure 3.2). However, unlike sample ePE_3.7M_8.4, the disentangled sample has a narrower MWD of 1.8. The G" peak in the case of sample ePE_3.7M_8.4 is a combined effect of heterogeneity in the relaxation (modulus) arising due to the distribution of entanglements and MWD assisting CCR in the melt. The narrow MWD of the disentangled UHMw-PE sample provides an opportunity to study the influence of increasing entanglement density and its homogenisation along the chain on LAOS behaviour of polymers. To some extent, the influence of a broad molecular weight distribution on CCR can be neglected in these polymers having relatively narrow polydispersity. At time $t_{0,}$ immediately after melting, the disentangled UHMw-PE is in a thermodynamically metastable state where the melt possess heterogeneous distribution of entanglements along the chain, and molecular weight between entanglements decreases with time. See chapter 2. With increasing annealing time, the metastable melt finally reaches a thermodynamic equilibrium state, where entanglements are homogeneously distributed and M_e is considered to be a constant for the polymer. The increase in number of entanglements, with increasing annealing time, can be followed in the sample by the modulus build-up, see Figure 3.7c. The melt reaches the thermodynamically equilibrium state (fully entangled) when the elastic modulus reaches the plateau value, ~30,000 seconds for sample dPE_1.1M_1.8 as seen Figure 3.7c.

3.3.2.1 Effect of number and distribution of entanglements on LAOS behaviour

Figure 3.7a and Figure 3.7b show a comparison of LAOS behaviour between disentangled (at time t_0) and fully entangled (after annealing 50,000 seconds) melts of the same polymer (two different discs taken from the same polymer), dPE_1.1M_1.8 at 160°C. Remarkably, in the fully entangled (thermodynamically stable) melt the G" peak does not appear (diffused) even though the disentangled melt (thermodynamically metastable with respect to the heterogeneity in the distribution of the entanglements) of the same sample shows

a prominent peak in G". This result is in agreement with the reduction of the G" peak in the sample ePE_3.7M_8.4, that also occurs due to increasing the homogenisation of the entanglements. However, in sample ePE_3.7M_8.4, the G" peak does not disappear due to CCR assisted by the broad MWD. Whereas, in the thermodynamically stable melt of the synthesised disentangled UHMw-PE sample dPE_1.1M_1.8, entanglement removal by CCR is suppressed due to its narrow MWD. Hence, the G" peak disappears in the thermodynamically stable melt having a homogeneous distribution of entanglements (equilibrium M_e) in the UHMw-PE sample with narrow polydispersity.

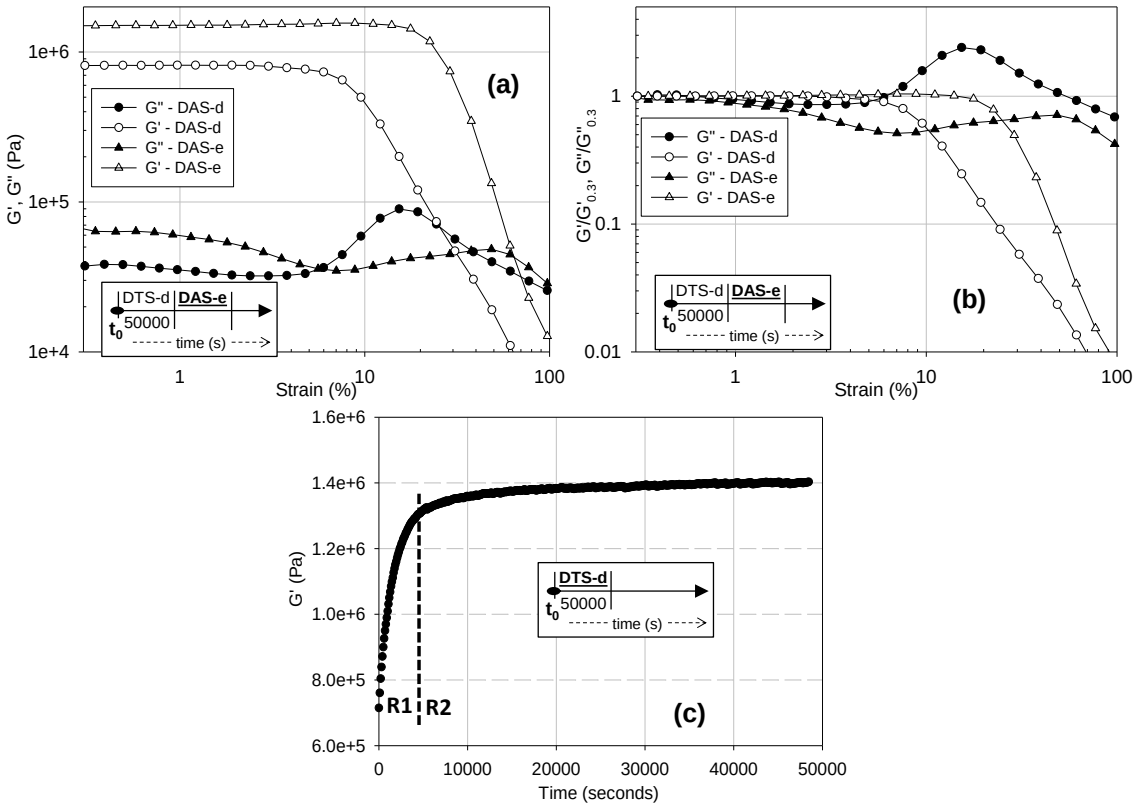

Figure 3.7. Comparison of the LAOS behaviour between disentangled (thermodynamically metastable, at time t_0) and fully entangled (thermodynamically stable, after annealing for ~50,000 seconds) melt at 160°C for sample dPE_1.1M_1.8. (a) Absolute value of G' and G"; (b) normalised G' and G" at 100 rad/s for the disentangled and the fully entangled melts of the same sample; (c) modulus build-up (entanglement formation) at 160°C. Entanglement formation occurs by a mixing process (through chain explosion) in the region R1, whereas by reptation dynamics in region R2. See chapter 2.

In Figure 3.7a, increases in G' and G" can also be seen at lower strain (< 3%, within the LVE regime) as expected with annealing time. See Figure 3.7c. The linear viscoelastic regime increases from the disentangled melt to the fully entangled melt, and is accordance with the observation on sample ePE_3.7M_8.4. It is believed that the decrease in G' after LVE is caused by chain orientation and subsequent loss (disengagement) of entanglements due to the large deformation imposed during the LAOS experiments. Hence, an increase in LVE regime can be associated with the need for even larger strains with increasing entanglement density to disengage the chains. It is known that the LVE regime is larger for low molecular weight polymers (faster relaxation). Thus, the increase in the LVE regime with increasing entanglement formation suggests that the more entangled melt relaxes faster than the disentangled melt, which at first sight may appear to be counter-intuitive. However, a closer look at the experiments suggests that the chosen frequency (100rad/s) is in the vicinity of the G' plateau and the G" minima and refers to the relaxation modes activated by CCR which is further suppressed by the stretch of the chains (increasing entanglements). As the number of entanglements increases, relaxation modes active due to CCR are suppressed *[2,3]*. In the following section, effect of large strain at constant frequency (100 rad/s) on G' and G" is further investigated.

3.3.2.2 Effect of large deformation on the LAOS behaviour during entanglement formation

Figure 3.8a shows a comparison between the modulus build-up in a disentangled melt (time t_0) and the thermodynamically stable melt (annealing time ~50,000 seconds) immediately after experiencing a large deformation (strain = 100% in experiment DAS-e). From the Figure, it is apparent that after the large deformation, the storage modulus of the equilibrium melt drops from 1.4 MPa to a lower value of 1.0 MPa. The cause for the decrease in modulus is correlated with the disengagement of chains (reduction in the number of entanglements) from the entangled network, CCR. However, the disentangled state obtained (DTS-e1) after high shear is different from the disentangled state (DTS-d at time t_0) achieved after melting of the nascent crystals. The disengaged chains by CCR, on the application of large strain, attains the equilibrium melt state much faster

than the disentangled melt from the nascent crystals. The short residence time of the metastable melt by CCR can be associated with partial disengagement of chains from the physical network that helps in fast restoration of the equilibrium state. To compare the structural differences in the equilibrium melt obtained before and after application of large strain, the experiments performed are summarised in Figure 3.8b and Figure 3.8c.

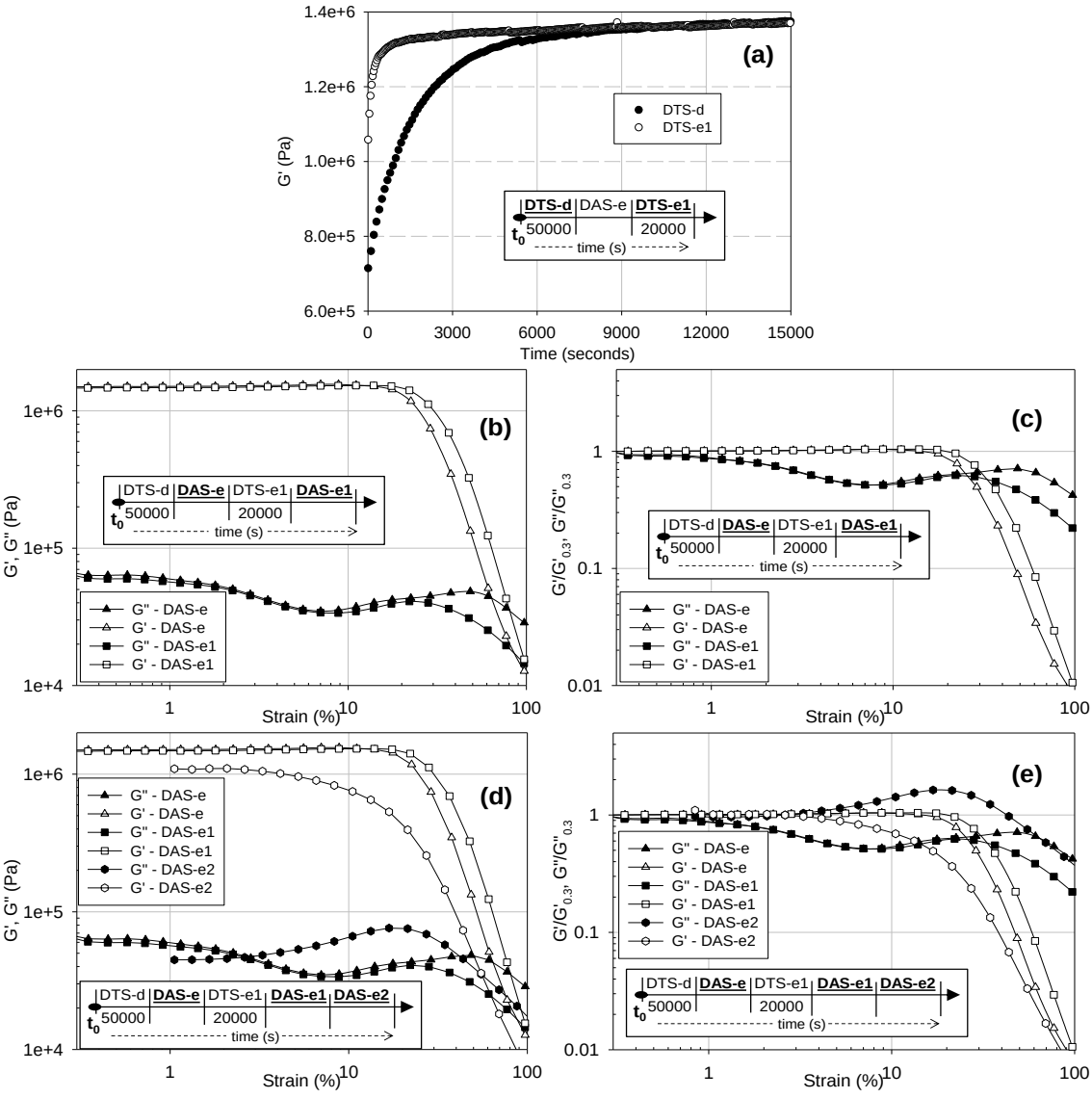

Figure 3.8. (a) Comparison between the modulus build-up in a disentangled melt with and without undergoing large deformation. (b) and (c) Comparison of LAOS behaviour between the thermodynamically stable melt after annealing for 50,000 and 70,000 seconds, respectively. (d) and (e) Comparison of the LAOS behaviour between the thermodynamically stable melt and melt immediately after experiencing a large deformation (strain) at 160°C for sample dPE_1.1M_1.8.

Figure 3.8b and Figure 3.8c show comparison between LAOS behaviour of thermodynamically stable melt obtained on subsequent annealing for 50,000 seconds (just after t_0) and 20,000 seconds (total 70,000 seconds after t_0). The second annealing step for 20,000 seconds was performed in the melt that experienced the large deformation after the first annealing step of 50,000 seconds. The chosen time of 20,000 seconds was sufficient for the non-equilibrium melt to reach the equilibrium state after the large deformation. The G" peak was not observed in the thermodynamically stable melt states, after either subsequent annealing for 50,000 seconds or 20,000 seconds.

However, between the two thermodynamically stable melt states obtained after the annealing steps, some small differences in the plateau regime of the LVE regime, combined with the decrease in G" at larger strains were observed (Figure 3.8b and Figure 3.8c). This difference can be associated with the melt state with an increasingly homogeneous distribution of entanglements with annealing time. The effect of large deformation causing disentanglement (by disengagement) of chains are further confirmed by performing a consecutive LAOS test immediately after melt has experienced the large deformation. See Figure 3.8d and Figure 3.8e. From these Figures it is apparent that G' and G" show lower values (in the LVE regime) due to disentanglement after experiencing the large deformation (100% strain in DAS-e1).

It is intriguing to see that the LAOS experiments are capable of picking up differences even between a thermodynamically stable melt (DAS-e1), which does not show the G" peak and the melt after experiencing a large deformation (in DAS-e1) showing G" peak and a reduced LVE regime (DAS-e2). The peak in G", in DAS-e2, is caused by the disengagement of already disentangled chains during the application of DAS-e1. These findings support ease in removal of entanglements (by CCR) on the application of DAS-e2, in the disengaged melt state generated immediately after DAS-e1. These results are in accordance with earlier observations on heterogeneity in the entanglement density in the polymer melt, that gives rise to variations in G" peak and the LVE regime in G'.

To investigate the influence of the disengagement process in region R1 (mixing region of disentangled chains) and R2 (chain dynamics in the disentangled melt), experiments were performed. These experiments have been tailored to give a molecular insight on differences in the metastable melt states.

3.3.2.3 LAOS behaviour in region R1 and R2 of metastable melt state

Entanglement formation in a synthesised disentangled UHMw-PE shows two different regions R1 and R2. See Figure 3.7. Region R1 is defined where 80% of the total modulus build-up occurs in 20% of the total entanglement time. The remainder of the modulus build-up in the 80% of the time is associated with region R2. The two regions illustrate the differences in the rate of entanglement formation. In region R1, the rate of modulus build-up is faster and is associated with the entanglement formation by the mixing of polymer chains through the chain explosion process on the melting of the crystals. In the region R2, the entanglement formation is slower and predominantly governed by the reptation dynamics.

Figure 3.9 shows the LAOS behaviour of the disentangled UHMw-PE melt at 160°C in region R1 and R2. Figure 3.9a and Figure 3.9b compares LAOS behaviour of the melt after annealing for time t_0, 4500 seconds (in region R1), 14000 seconds (in region R2). The G" peak decreases in region R1, whereas the onset of the G" peak and the LVE regime shift to higher strains. The G" peak further decreases and disappears in region R2 (DAS-2), although, LVE shifts to higher strains. Even further annealing of 50,000 seconds in region R2 (DAS-2 to DAS-3), LAOS behaviour does not change much and is comparable (Figure 3.9c and Figure 3.9d). The melt annealed for 68,000 seconds (DAS-3) and 50,000 seconds (DAS-e) in two different discs of sample dPE_1.1M_1.8 show comparable LAOS behaviour. See Figures 3.8, 3.9c and 3.9d. These results show conclusively that a thermodynamically stable melt with a narrow polydispersity having large number of entanglements (due to suppression of CCR) will not show the G" peak in LAOS.

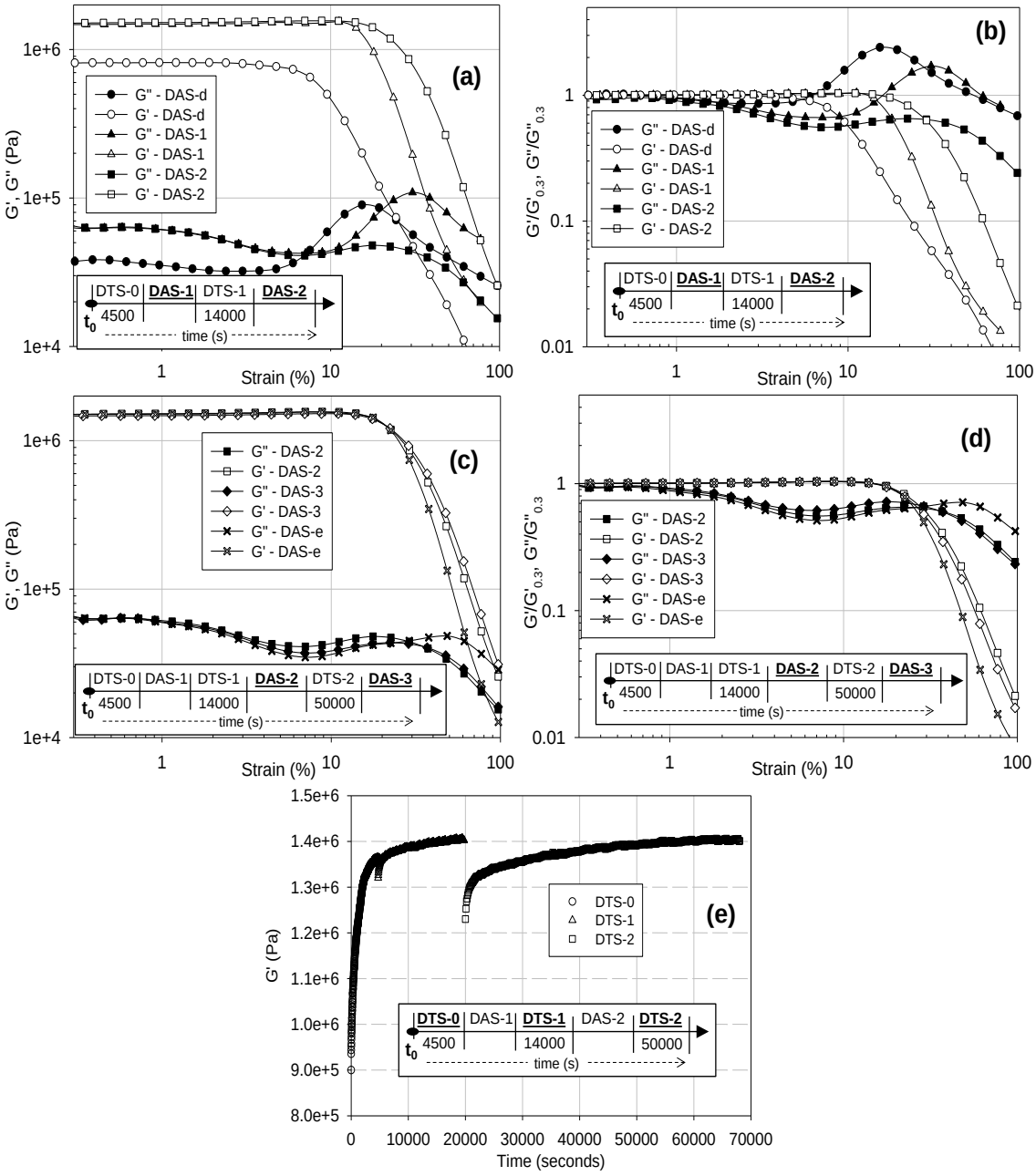

Figure 3.9. (a) and (b) Comparison of LAOS behaviour between dPE_1.1M_1.4 melt annealed for time t_0, in the region R1 (annealing time ~4500 seconds) and in region R2 (annealing time ~14000 seconds) at 160°C. (c) and (d) Comparison of LAOS behaviour between dPE_1.1M_1.4 melt annealed in region R2 for different times at 160°C. (e) Comparison of modulus build-up in a disentangled melt (time t_0) and entangled melt which has undergone a large deformation in region R1 and R2.

In Figures 3.9a and 3.9b, within region R1, G' and G" (in LVE regime) increase with annealing time where entanglement formation proceeds faster by mixing through chain explosion, leading to the decrease in the G" peak. However, the G" peak continues to decrease with annealing time in region R2, although, there is no appreciable change in G' and G" (in the LVE regime). These observations suggest that region R1 dominantly involves fast entanglement formation by the mixing of chains (from the disentangled melt) followed by region R2 where (dominantly) the homogenisation in the distribution of entanglements already formed in region R1 takes place.

Figure 3.9e shows a comparison between the modulus build-up in the disentangled melt (time t_0) and the relatively more entangled melt which has undergone a large deformation in regions R1 and R2. As discussed earlier, the disengagement of chains creates disentanglement in melt after it undergoes a large deformation. This can be seen as a reduction in G' and G" (Figure 3.8a). Similar observation can be seen in Figure 3.9e. However, the reduction in G' (DTS-1) is smaller, for the same deformation, if it is applied in region R1 as compared to region R2 of the melt (DTS-2), also see Figure 3.8a.

The larger reduction in G' due to large shear with increasing the number of entanglements can be associated with more effective disengagement of chains. In region R1, due to the lower number of entanglements (more heterogeneous distribution), the chains cannot effectively hold-on to each other to cause disengagement from other chains. The rate of modulus build-up after the large deformation (disengagement) is also faster in the melt having more entanglements (a less heterogeneous distribution of entanglements). See Figures 3.8a and 3.9e.

3.3.2.4 Continuous application of large deformation on LAOS behaviour in region R1 and R2 of metastable melt

Figure 3.10a-d show the effect of large deformation on the G" peak and the LVE regime of synthesised disentangled UHMw-PE sample dPE_1.1M_1.4 at 160°C in region R1 of entanglement formation. Entanglement formation is

followed (DTS) for 300 seconds between each alternating DAS experiment (DAS-0 to DAS-5). There is a delay of 10 seconds for data collection between each experiment. A relatively small decrease in the G" peak and a shift in the onset of the peak to higher strain was observed from DAS-0 to DAS-5 (Figure 3.10a and Figure 3.10b). However, for a similar total annealing time without experiencing any large deformation, the sample showed a considerable decrease in the G" peak and a shift in the onset of the peak to higher strain (Figure 3.9a and Figure 3.9b).

This difference in the changes in the G" peak with time suggests that by continuously applying a large deformation, it may be possible to suppress (slow down) the entanglement formation considerably. Hence, a relatively smaller and slower decrease in the G" peak (Figure 3.10b) and a small increase in the LVE (Figure 3.10d) regime was observed. This is further confirmed by following entanglement formation for 300s between each DAS experiment (Figure 3.10e), where, the melt gets disentangled (by disengagement) on the application of the large strain DAS experiments causing a decrease in the initial value of G'. Hence, slowing down the overall rate of entanglement formation and subsequently suppressing the rate for the homogeneous distribution of entanglements.

This gives a unique possibility where a disentangled melt can be maintained for a longer time by deforming (shearing) for continuously in region R1, having implications in the ease for melt-processing of disentangled UHMw-PE. However, eventually the melt will reach a fully entangled state even with continuous application of large shear, but it can give an extra window of processing time where disentangled melt can be processed relatively easier compared to its entangled state *[219]*. Such a possibility has been explored using a Multi Pass Rheometer described in Appendix 6.

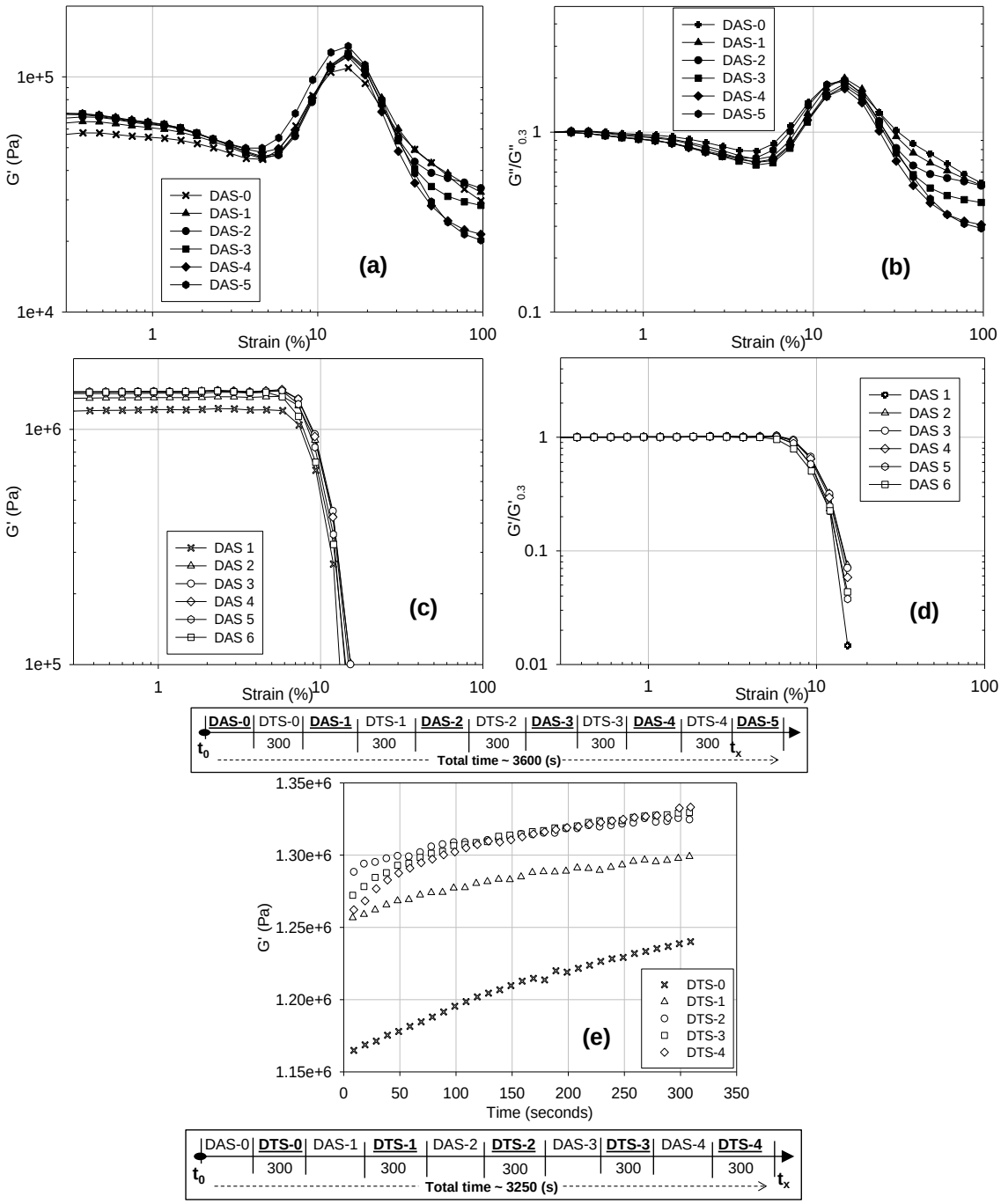

Figure 3.10. (a), (b) G" vs. strain; and (c), (d) G' vs. strain - (LAOS behaviour) for the melt of dPE_1.1M_1.4 undergoing continuous large deformation at an interval of 300 seconds in region R1 at 160°C. (e) Shows modulus build-up in the disentangled melt of dPE_1.1M_1.4 after undergoing a large deformation (shear) during a DAS experiment(s). The decrease in G', after alternate DAS experiment, shows a disentanglement process in the sample.

Figure 3.11 captures the transformation in LAOS behaviour from the thermodynamically metastable melt to the stable melt with increasing annealing time. Figure 3.11a and Figure 3.11b show a decrease in the G" peak and the shift in the onset of the peak to higher strain with increasing number of entanglements. The decrease in the G" peak suggests a reduction in the heterogeneous distribution of entanglements (suppressing CCR due to a decrease in the Rouse relaxation time). Figure 3.11c and Figure 3.11d show an increase in the LVE regime with increasing number of entanglements. Recalling Figure 3.4, in the sample ePE_3.7M_4 a negligible decrease in G" peak was observed due to the broad MWD of this sample, whereas the near disappearance of the G" peak with entanglement formation in the narrow molecular weight distribution polymer is similar to the findings discussed earlier (see Figure 3.7).

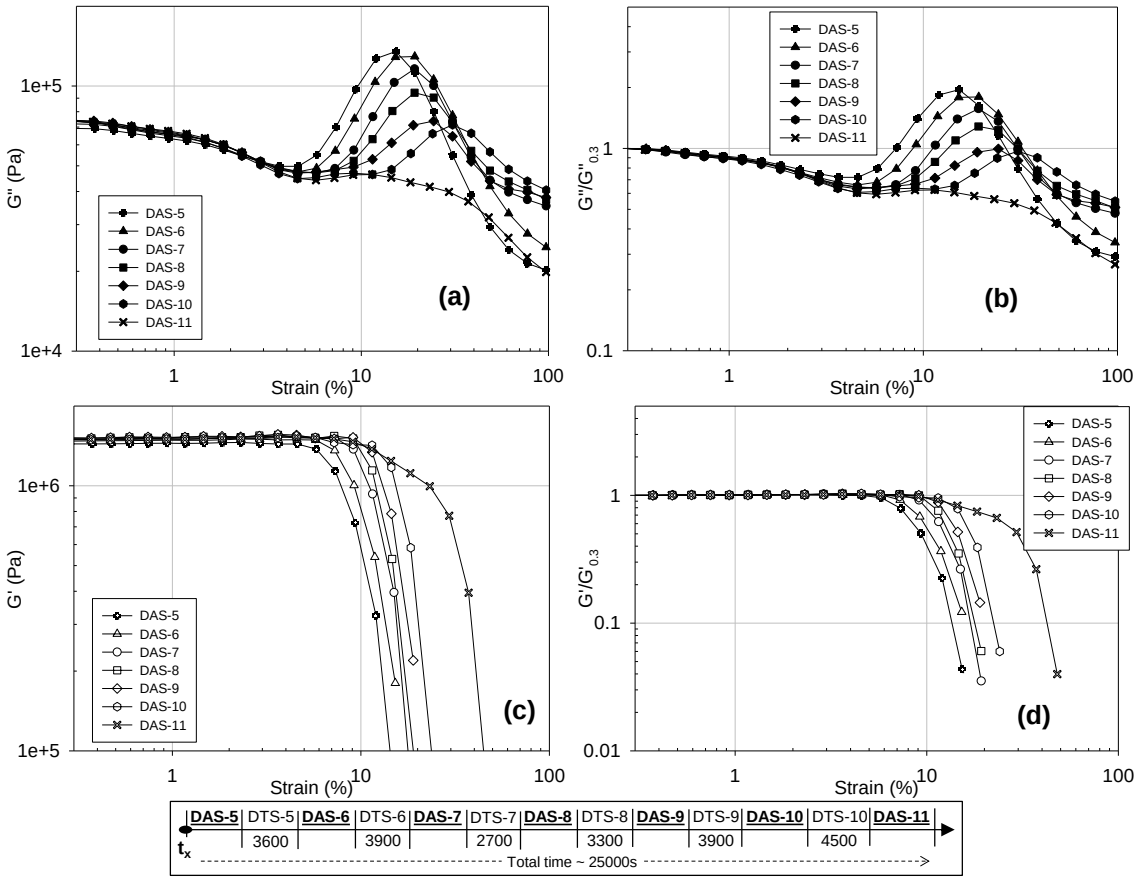

Figure 3.11. (a), (b) G" vs. strain and (c), (d) G' vs. strain – depicting LAOS behaviour of the disentangled melt in dPE_1.1M_1.4 during transformation of the melt from the disentangled (thermodynamically metastable) to the fully entangled (thermodynamically stable) state.

Figures 3.4 and 3.11 strengthen the idea that LAOS experiments are capable of capturing the underlying transformation (changes) in the microstructure of the polymer melt and it is useful to follow the polymer dynamics which cannot be captured by performing simple linear viscoelastic experiments, such as dynamic frequency sweep experiments. However, one may question why type-3 behaviour in a homo-polymer melt has not been observed in earlier work? A possible answer lies in the experimental protocols (also molecular weight of the sample) that have been used for LAOS study in past. In following sections this will become clearer from LAOS behaviour at different frequencies and molecular weights.

3.3.3 LAOS behaviour of disentangled melt at different frequencies

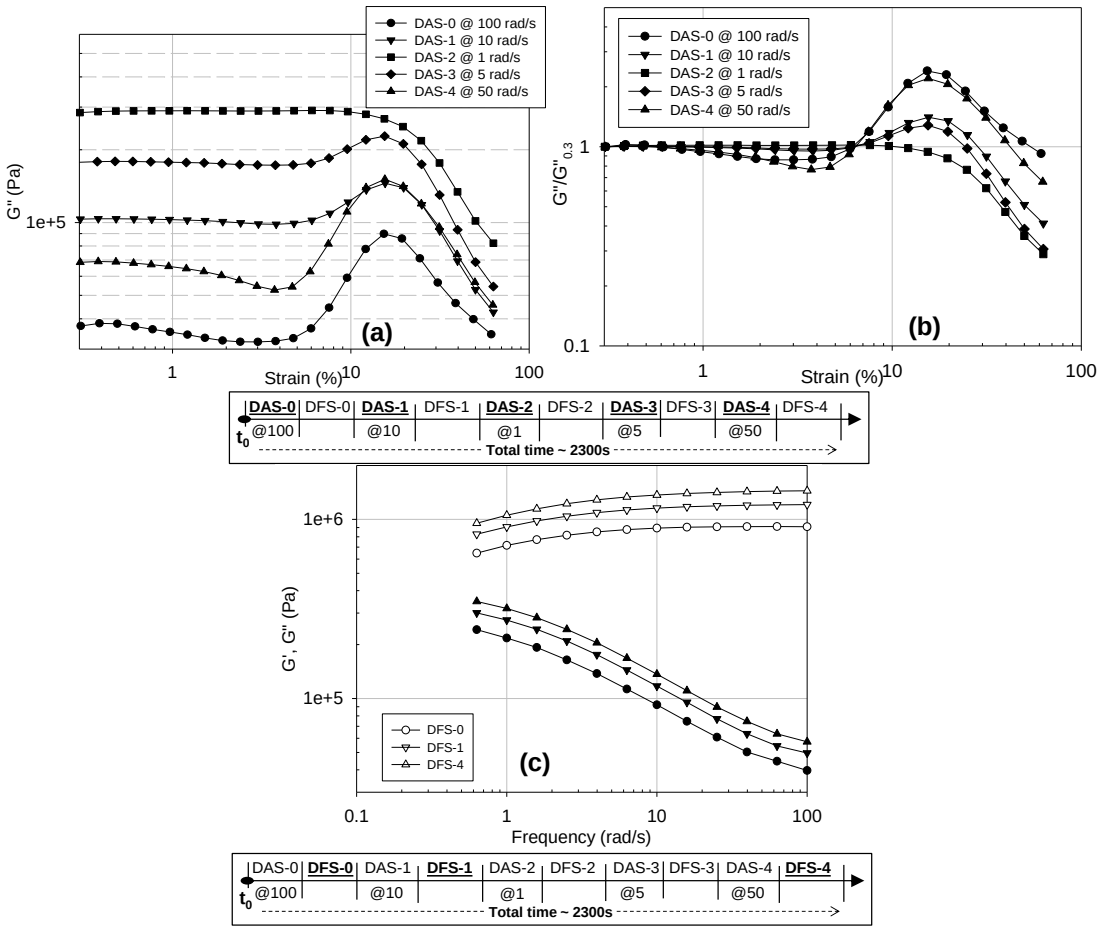

Figure 3.12. (a) and (b) show DAS (normalised G' and G") data on synthesised disentangled UHMw-PE sample dPE_1.1M_1.8 at 160°C and different frequencies. (c) Dynamic frequency sweep (DFS) at 160°C, 0.5% strain with increasing annealing time (entanglement formation) between DAS experiments.

Figure 3.12a and Figure 3.12b show LAOS behaviour of disentangled melt sample dPE_1.1M_1.4 at various frequencies. G" peak intensity reduces with decreasing frequency at which DAS is performed. Ultimately, no G" peak is observed for DAS experiment performed at 1 rad/s. It is important to note that for all the experiments at different frequencies, melt is still disentangled where G" peak can be observed e.g. both experiments DAS-1 (at 10 rad/s) and DAS-3 (at 5 rad/s) that are performed before and after DAS-2 (at 1 rad/s) show G" peak.

Similar behaviour of decrease in G" peak with decreasing frequency in LAOS experiments is seen for other complex fluids as well. Miyazaki *et al. [185]* claimed that G" peak in LAOS experiment is a universal behaviour and can be observed in a frequency regime where system is elastic, i.e. G' > G". Considering this definition for elasticity, frequency sweep data performed at 0.5% strain, shown in Figure 3.12c, confirms that within the spectrum of frequencies used for LAOS study (0.5 to 100rad/s) the system is elastic. However, G" peak is not observed for low frequencies, for example at and below 1rad/s. The absence of G" peak below 1rad/s and its appearance at and above 5rad/s, suggests that the requisite for the observation of G" peak is the frequency close to G" minima in Dynamic Frequency Sweep experiments.

Since most of the conventional rheometer cannot access frequency more than 500 rad/s, the frequency regime in polymer melt are restricted to terminal region or frequency lower than G" peak (tube renewal cross-over), for low molecular weight polymers, that have been often used for studies in past. UHMw-PE due to its very slow relaxation dynamics provides an opportunity to access the frequency regime (higher than frequency of G" peak and G' plateau in a frequency sweep) where G" peak during a LAOS experiment can be observed using a conventional rotational rheometer.

To investigate molecular weight dependence in the appearance of G" peak in LAOS experiments, a set of samples shown in Table 3.1, synthesised using the same catalytic system and conditions but different polymerisation time are chosen. These studies have been performed at same frequency.

3.3.4 LAOS behaviour of disentangled UHMw-PE for different molecular weights at a fixed frequency

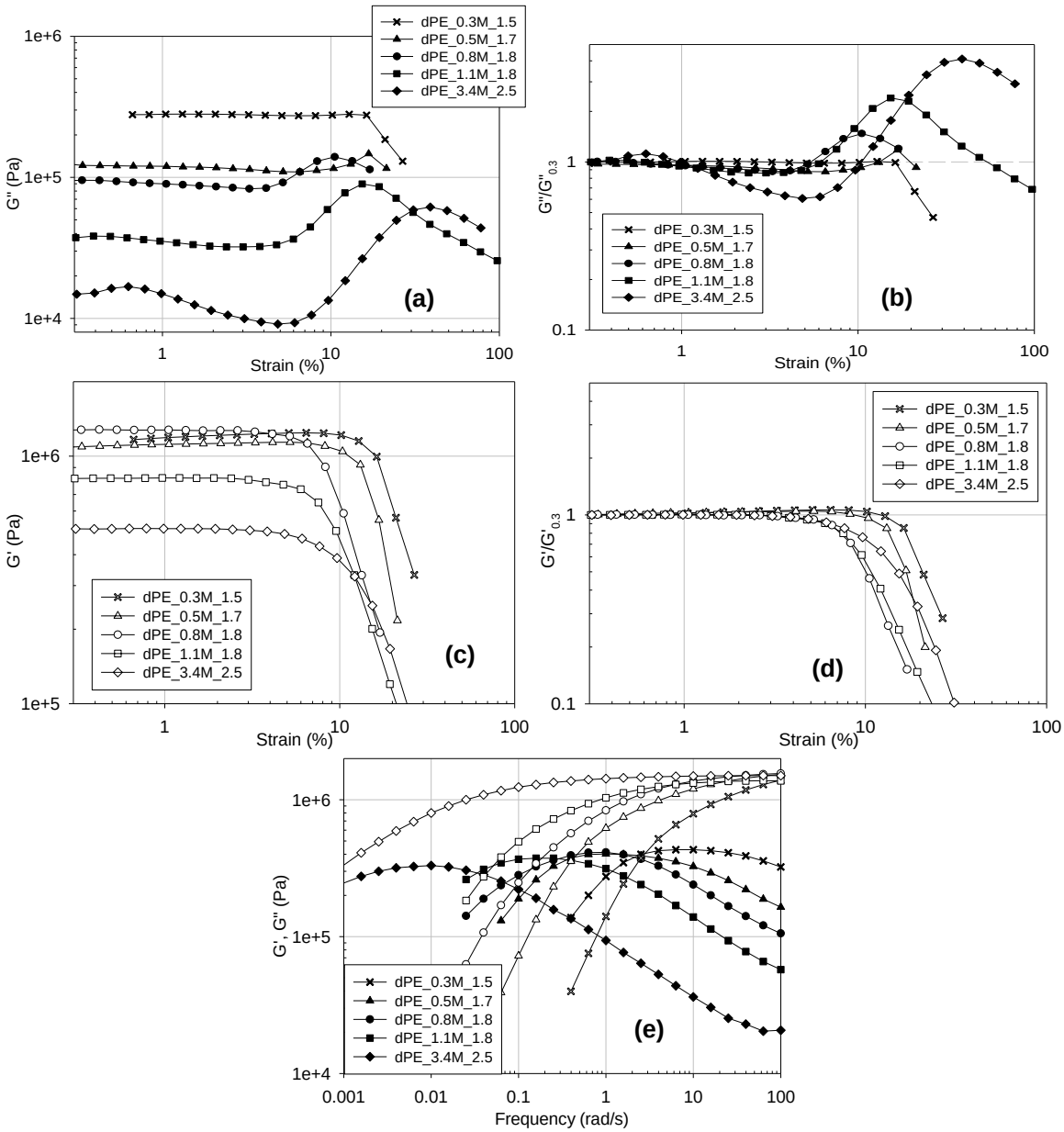

Figure 3.13. (a), (b) G" vs. strain and (c), (d) G' vs. strain - LAOS behaviour in disentangled UHMw-PE samples of different molecular weights at 160°C, frequency of 100 rad/s, at time t_0. (e) Comparison with frequency sweep for fully entangled (thermodynamically stable) melt of different molecular weights at 160°C, strain 0.5%. Table 3.1 lists the molecular weight and molecular weight distribution of all the samples.

Figure 3.13 shows the LAOS and frequency sweep data for the disentangled UHMw-PE samples having different molecular weights. Mw and MWD of the samples used have been listed in Table 3.1. Figure 3.13a and Figure 3.13b show the LAOS behaviour of the disentangled UHMw-PE samples having different molecular weights at time t_0 and frequency 100 rad/s. The G" peak decreases with decreasing molecular weight, similar to decreasing frequency (Figure 3.12a and Figure 3.12b). Sample dPE_0.3M_1.5 with lowest Mw of 0.3 million g/mol does not show any G" peak, whereas sample dPE_3.4M_2.5 with Mw of 3.4 million g/mol shows the maximum peak intensity. It should be noted that although for all samples in Figure 3.13, the frequency used for LAOS is in the regime where G' > G", the G" peak cannot be observed in the low Mw sample dPE_0.3M_1.5. According to a study reported in this thesis, the G" peak is observed in the frequency regime where G' plateau and G" minima (in frequency sweep) appears. Such a frequency regime is not available for low Mw samples using a conventional rheometer, where frequencies greater than 100 rad/s are not easily accessible. In low Mw samples, this experimental limitation is most likely to be the cause for absence of reports on the presence of the G" peak. Moreover a smaller LVE regime, with modulus against strain graphs, can be observed in high molecular weight samples compared to the low molecular weight samples. See Figure 3.13c and Figure 3.13d.

G" peak in polymer melt is further confirmed by performing LAOS study on polystyrene samples of 300,000 g/mol having the MWDs of 1.05 and 2.1, respectively. The polystyrene melt also shows a peak in G" in the LAOS experiments in the frequency regime close to the G' plateau and the G" minima frequency observed frequency sweep. The intensity of the G" peak decreases with frequencies away from the frequency of G' plateau and G" minima observed in a frequency sweep. LAOS data on polystyrene melt are presented in Appendix 5. By combining study performed on LAOS behaviour of polystyrene and the UHMw-PE polymer melt, it can be concluded that the peak in G" is a universal feature common to soft matter. For the observation one of the main requisites is the use of appropriate experimental protocol. For example, the judicious choice of frequency to explore LAOS in regime close to the G' peak and the G" minima.

The studies clearly show that the appearance of the G" peak is due to CCR in the polymer melt that arises on application of LAOS and can be used as a tool to give an insight into the breakdown of the polymer network that would be dependent on molecular characteristics such as molecular weight and molecular weight distribution. To have further insight, it is necessary to validate the hypothesis using recent molecular rheological models for high flow such as Rolie-Poly [215,216].

3.4 Summary

One of the striking conclusions from the study reported in this chapter is that nonlinear rheology can be used as a probe to investigate the heterogeneous distribution of entanglements that may be present either in the metastable melt or in a polymer melt having a broad molar mass distribution. The extent to which the network can be influenced by convective constraint release (CCR), on application of a large strain, is seen as G" peak in the LAOS experiment, which is a signature of glassy (metastable) systems.

Disentangled polyethylene having a relatively narrow polydispersity provides unique opportunity to follow changes in the linear viscoelastic regime of the storage modulus G', and the G" peak while the melt changes from a metastable to the thermodynamically stable state with an increasing number of entanglements. From the chosen frequency for nonlinear studies, it has been concluded that the Rouse relaxation time(s) decreases with increasing number of entanglements in the same polymer melt as it transforms from a metastable to a stable state.

Studies performed on different molecular weights suggest that the appearance of G" peak should be a universal phenomenon that will be observed on making a judicious choice of frequency i.e. at the plateau regime of G' and minimum in G" of the dynamic frequency data.

Influence of molecular weight distribution is also found to play an important role in the appearance of the G" peak. For example, UHMw-PE having a large number of entanglements in its thermodynamically stable melt state shows a

weak presence of the G" peak in contrast to the UHMw-PE having a similar molecular weight, but a broad molecular weight distribution. This difference in intensity is attributed to CCR that chains having different molar mass experiences on the application of the applied large strain at the fixed frequency.

The schematic picture that has evolved from the LAOS behaviour, in the metastable melt as it transforms into thermodynamically stable state, is depicted in Figure 3.14. The mentioned conclusions have been further illustrated:

- UHMw-PE melt shows a G" peak (type-3 behaviour) in LAOS which is a characteristic of colloidal (glassy) systems. See Figure 3.2 and Figure 3.6.
- The G" peak in LAOS experiment on polymer melts may arise due to the removal of entanglements by CCR, creating a heterogeneity in the relaxation of the system, due to the creation of non-equilibrium molecular weight between entanglements. See Figure 3.2 and Figure 3.4d.
- The intensity of G" peak in LAOS reduces with decreasing heterogeneity in the distribution of entanglements (going towards the thermodynamically stable melt; approaching equilibrium M_e), whereas the shift in the onset of the peak to higher strain, see Figure 3.4, Figure 3.7, Figure 3.9a, Figure 3.9b, Figure 3.11a and Figure 3.11b.
- The Intensity of the G" peak in LAOS increases at higher frequency. The G" peak in LAOS can be observed at a frequency close to the G' plateau and the G" minima (in the frequency sweep). See Figures 3.5 and 3.12.
- The linear viscoelastic (LVE) regime increases with the decreasing heterogeneity in distribution of entanglements. See Figures 3.4, 3.7, 3.9a, 3.9b, 3.11c and 3.11d. The increase in the LVE regime in a disentangled melt can be slowed on the continuous application of a large shear deformation in the regime R1 of entanglement formation. See Figures 3.10c, 3.10d and 3.10e. These findings will have implications in melt processing of disentangled UHMw-PE, as the melt viscosity can be altered considerably while the melt is in the R1 region of the modulus build-up time.
- In a thermodynamically stable melt, heterogeneity can induce "on the fly" under high shear flow due to removal of constraints (CCR) which increase the dissipation (G" peak) in the melt. A thermodynamically stable melt (no micro-structure or association with constant M_e) having narrow MWD with substantial

large number of entanglements, does not show the G" peak in LAOS, and G" decreases without any overshoot at higher strains. These findings combined with studies on low molecular weight samples suggest that the increasing number of entanglements per chain suppresses their effective removal by CCR. See Figures 3.7, 3.8, 3.9 and 3.11.

- Large deformation (shear) causes disengagement of chains and the effectiveness of the disengagement depends upon region (R1 or R2) where it is applied. See Figures 3.8a, 3.8d, 3.8e, 3.9e and 3.10e. The disentangled melt obtained by disengagement of chains due to large shear deformation is different than the disentangled melt from a nascent disentangled polymer at time t_0. Entanglement formation is faster in a disengaged chain (after large deformation), probably due to a memory effect, compared to a disentangled chain from a nascent disentangled (at time t_0) polymer. See Figure 3.8a.
- Entanglement formation in a disentangled UHMw-PE melt can be hindered by the continuous application of a large shear deformation in the region R1 and can facilitate the ease of processing of the polymer. See Figure 3.10e.
- Under the available experimental conditions, governed by the available rheometers, the G" peak in the low molecular weight polymer sample was not observed, because of the required high frequency. However, due to very slow relaxation times in UHMw-PE, this frequency regime is easily accessible and the G" peak can be observed. See Figures 3.5, 3.12 and 3.13.
- Intensity of G" peak decreases with increasing MWD and decreasing molecular weights. See Figure 3.2b and Figure 3.13b.

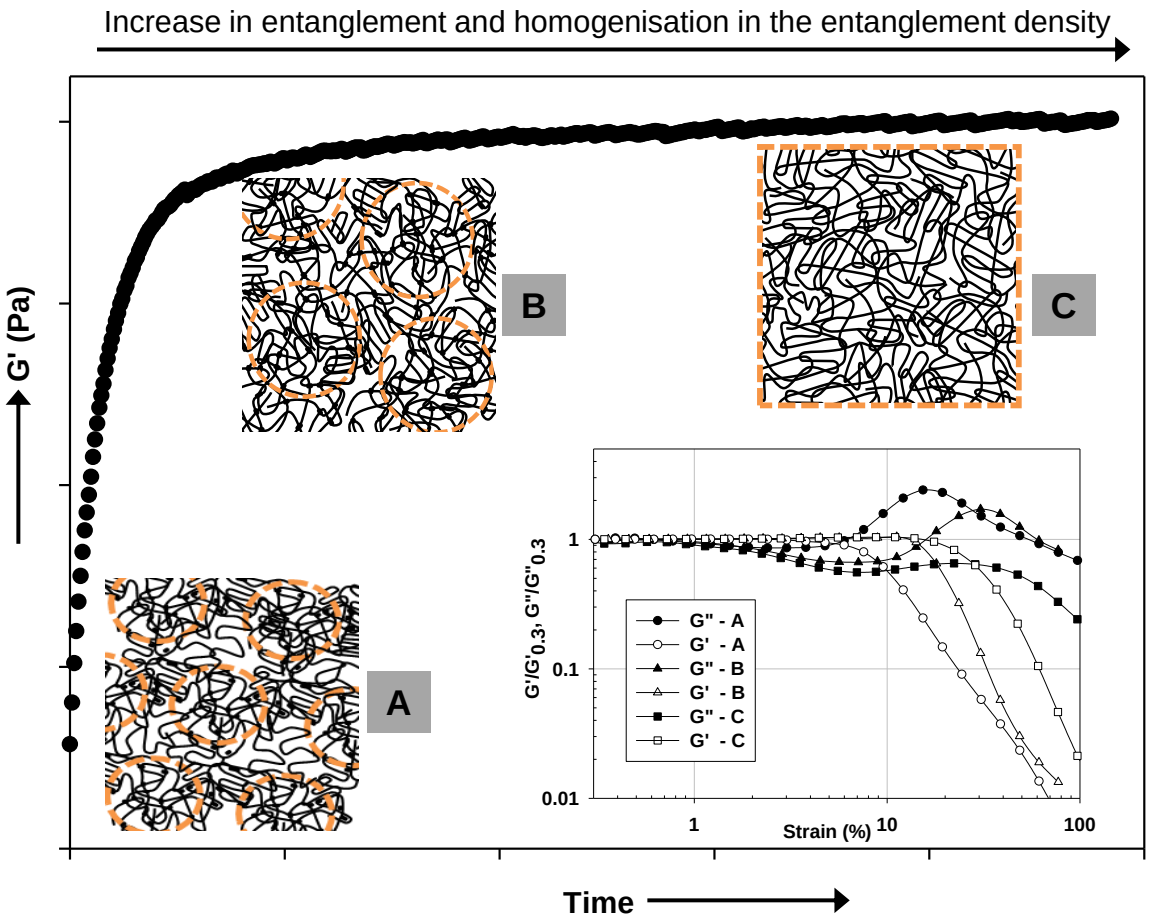

Figure 3.14. Schematic representation of different stages during entanglement formation in a synthesised disentangled UHMw-PE after melting (time t_0) and its effect on LAOS behaviour. (A) Disentangled crystal after melting start mixing through chain explosion. However, there is a difference between the entanglement densities between the domains. Domains encircled in orange colour represent entangled zone (higher modulus) compared to continuous phase (outside the orange circles) which has relatively fewer entanglements. (B) Entanglement formation and homogenisation of entanglement density occur simultaneously causing decrease in the G" peak. (C) In this stage, primarily homogenisation of entanglement density takes place; leading to the G" peak disappearance. The G" peak is caused by the removal of entanglements due to CCR which is suppressed by the increase in entanglement and in the homogenisation of the entanglement distribution with increasing annealing time. However, if the polymer has a broad MWD, then the G" peak may not disappear due to the low molecular component in the process of CCR, in ePE_3.7_8.4. E.g., see Figure 3.4d.

Chapter 4

Influence of Amorphous Component on Melting of Semi-crystalline Polymers

Unlike inorganic and organic molecules, in semi-crystalline polymers melting gets complicated because of the requirement of conformational transformation of the chain segments, where part of the same chain resides in a crystal and also in the amorphous phase. The chain segments residing in the amorphous part can be constrained, either due to adjacent or nonadjacent re-entry leading to different natures of chain folding, and the arising differences in the local chain mobility due to differences in topological constraints. Thus, different conformational possibilities in the amorphous region of a semi-crystalline polymer have implications on the melting temperature and the processes involved in the ordered to the disordered phase transformation. In this chapter, by using carefully designed DSC experiments on ultra-high molecular weight polyethylene, having different topological constraints, melting behaviour has been studied which cannot be fully explained by the general Gibbs-Thomson equation alone. The nonlinearity in melting temperature on heating rate invokes kinetics in the melting process, where, depending on the heating rate melting can occur either via successive detachment of chain stems and their reeling into the melt, or by cluster melting [117,118,127]. Observations from the previous chapter on entanglement density in the amorphous region of the synthesised disentangled UHMw-PE have been extended to understand the effect of entanglements in the melting and crystallisation of semi-crystalline polymers. To understand the effect of topological differences on melting behaviour, nascent entangled, nascent disentangled and melt-crystallised samples have been used. The role of superheating on the melting process is also addressed. Preliminary results on characteristic melting time of a crystal using TM-DSC are also presented.

4.1 Introduction

Melting in semi-crystalline polymers is a complex process, where the melting transition covers a broad temperature range and is correlated to the distribution of the crystal lamellae thickness *[122,220]*. Thermodynamically, melting in solids is defined as a first-order transition (sharp) at the intersection of the Gibbs free energy of the solid and liquid state, which is only true if equilibrium and infinite size of the involved phases are considered. However, these conditions are not met in semi-crystalline polymers such as polyethylene, either crystallised from solution or the melt. These polymers possess lamellae crystal thickness of finite dimensions (10-30 nm) with lateral dimensions of at least an order of magnitude larger *[54-56,134-136]*. The Gibbs-Thompson equation in its simple form has been widely used to describe quantitatively the maximum melting temperature correlating the lamellae thickness.

$$T_m = T_m^{\infty}[1-\frac{2\sigma}{l.\rho.\Delta H_m}] \qquad \ldots(4.1)$$

Where T_m is the experimentally determined melting temperature, T_m^{∞} is the equilibrium melting temperature for an infinite size crystal (141.5°C for polyethylene *[126,139]*), σ is the end surface free energy of the folded planes, l is the crystal lamellae thickness, ρ is the crystal density and ΔH_m is the heat of fusion per unit mass.

Recently, key questions have been raised on the validity of the Gibbs-Thomson equation for semi-crystalline polymers. For example, recent studies by Muthukumar *[44,221]* demonstrated that extended chain crystals may not be the requisite for the thermodynamically equilibrium state. Following entropic calculations, the author showed that the thermodynamically favourable structure would be chain folded crystals where the chains are adjacently re-entrant. These findings are in accordance with the recent studies performed by Höhne *[137]* on linear polyethylene that also suggest that the melting temperature will be influenced by the number of CH_2 units involved in crystal-to-liquid transition and not just the crystal stem length only. Thus, the melting temperature will strongly depend on the topological constraints that may involve more than one stem.

Thus, the greater the number of CH_2 units involved in conformational changes from trans to gauche, the higher will be the melting temperature – independent of the crystal thickness. Considering these concepts, Höhne proposed a modified Gibbs-Thomson equation *[137]*,

$$T_m^n \approx T_m^\infty \left(1 - \frac{\Delta_m G_e}{\Delta_m H_{r.u.}^\infty} \frac{1}{n}\right) \qquad \ldots(4.2)$$

Where n is the number of repeating units in the chain stem rather the crystal thickness l, $H_{r.u.}^\infty$ is the heat of fusion for the repeating unit and G_e is total excess Gibbs free energy rather than only the surface free energy, which is only part of the total excess Gibbs free energy. The number n is related to the thickness of the crystal lamella thickness as the distance between two repeating units and the tilt angle within the crystal thickness are known.

The melting behaviour and the resulting crystallisation aspects have been also challenged in a series of publications by Strobl *[45,46]*. The author showed the presence of an equilibrium melting temperature much below the anticipated equilibrium melting temperature predicted from the Gibbs-Thomson equation. These observations combined with the earlier studies reported on polyethylene crystallisation under pressure lead to the conclusion that polymer crystallisation will always proceed via a metastable phase *[222]*.

In simple terms, crystal melting should be the reverse process of crystallisation. However, in polymers such a situation is complicated as the studies are often performed on aggregates of crystallites, such as spherulites. Since polymers are semi-crystalline, randomisation of chain during the melting process is strongly influenced by the morphology that it adopts during crystallisation. For example, whether the chain is shared between different crystals or is folded back and forth within the same crystal. Consequence to these complications and the abstract topology of the chains within crystal aggregates of spherulites, melting of spherulites as observed between cross-polars is not the shrinking process of the spherical aggregates but diffusion of the intensity suggesting random melting of the crystal aggregates *[77]*.

Recently, Toda *et al. [77]* followed crystallisation and melting behaviour of single crystal polyethylene. The authors crystallised single crystals in its own melt by annealing at temperatures close to the melting point. By the annealing process, any imperfections arising during crystallisation were removed. Melting studies performed on the single crystal showed a linear decrease in the crystal length with time. The continuous decrease in length of the crystal with time at fixed temperature invoked the concepts of melting kinetics.

In parallel to these developments, it was also observed that in spite of the chain folded crystals, nascent UHMw-PE having molecular weight greater than a million g/mol, has a melting temperature closer to the equilibrium melting point *[59,101,117,118,126,127,140,157,163,223]*. Recent studies *[117,118,127,163-165,223-226]* attribute the high melting temperature to topological restrictions that arises in the amorphous region of the nascent polyethylene. The difference in melting behaviour between commercially available nascent entangled UHMw-PE and the lab-scale synthesised nascent disentangled UHMw-PE is explained by invoking kinetics.

To perform experimental studies using conventional or temperature modulated differential scanning calorimetry (DSC), it is essential to recall studies performed by Wunderlich *[123]*, where the author showed differences in the true and measured melting temperature of a polymer. Wunderlich *et al. [123]* has shown a heating rate dependence on the peak melting temperature for different crystal morphologies. For example, in case of an extended chain crystal morphology, where the crystals cannot reorganise, the peak melting temperature decreases with decreasing heating rate *[123]*. In such cases, the increase in peak melting temperature with increasing heating rate is associated with the superheating effect *[77,220]*. The increase in melting temperature includes the effect of measurement delay from the instrument.

Danley *et al. [132]* and Toda *et al. [220]* have shown an effective calibration method to measure true heat flow and true sample temperature by using instrumental coefficients pre-determined using a standard sample, such as indium. These authors successfully removed instrumental delays during heat flow. After instrumental correction, Toda *et al.* showed that in polyethylene having folded chain crystals, where the crystal re-organisation is feasible, the melting

temperature decreases with decreasing heating rate *[59,77,101,118,127,157,163,227,228]*. The authors associated the non-linear dependence of melting temperature on heating rate to the entropic barrier *[77]*. Rastogi *et al.* have also shown involvement of different activation barriers in the melting of disentangled UHMw-PE with temperature and time scale. The authors showed that in nascent disentangled UHMw-PE, melting can occur at much lower temperature by the successive detachment of single or multiple stems from the crystal surface whereas at higher temperatures melting proceeds by the breakdown of larger parts of the lattice *[117,126,127]*. Melting in polymer crystals depends upon the chain topology present in the amorphous phase *[118,126,224,225]*.

Further, Toda *et al. [77]* have successfully shown the effective use of temperature modulated DSC (TM-DSC) in studying the melting behaviour of polymer crystals by applying a so called “periodically modulating driving force”. In TM-DSC, a periodic modulation in temperature along with a linear heating or cooling ramp is applied to examine the response of heat flow to obtain the heat capacity from the modulation components of temperature and heat flow *[229-233]*. The characteristic time (τ), which characterises the speed of melting transition of each crystallite, can be calculated from the imaginary part of the effective heat capacity by equation (4.3) *[77,228,234-237]*,

$$\widetilde{\Delta C}'' \cong \frac{\bar{\bar{F}}}{2\pi\beta\tau} \times (\text{period}) \qquad \ldots(4.3)$$

Where $\widetilde{\Delta C}''$ is the imaginary part of the effective heat capacity, $\bar{\bar{F}}$ is the peak height of the underlying heat flow, β is the heating rate. The characteristic time (τ), can be calculated from the slope of the linear fit of the imaginary part of the effective heat capacity to the modulation period *[77]*.

To have an insight into the melting process, recently advanced experimental tools such as microchip calorimeters have been developed by Schick and co-workers *[238]*. Making use of the extraordinary high heating rates such as 30,000K/min, where the reorganisation processes in polymers such as isotactic polystyrene (iPS), polyethylene terephthalate (PET) etc. can be suppressed, the authors have shown that melting occurs with the relaxation of the rigid amorphous fraction just above the glass transition temperature. By using the fast

heating calorimeter, these authors have also identified that by suppressing the reorganisation process within the crystals, the crystals formed at the isothermal conditions melt just a few degrees above the crystallisation temperature. Using TM-DSC, the influence of the rigid amorphous fraction in the melting behaviour and consequently the organisation process has been also investigated in poly(oxy-2,6-dimethyl-1,4-phenylene) by Wunderlich and co-workers *[116]*. There are several studies confirming the role of the rigid amorphous fraction in the melting process of polymers having a high characteristic ratio *[114,116,119-121,239]*. However, very limited studies exist that invoke melting kinetics arising in flexible polymers such as linear polyethylene. In this chapter, conventional DSC and TM-DSC are used to explore the effect of molecular weight and chain topology in amorphous phase on the melting behaviour of nascent disentangled, nascent entangled and melt-crystallised samples of UHMw-PE.

4.2 Materials and experimental method:

4.2.1 Materials

All the samples used in this study are disentangled ultra-high molecular weight polyethylene (UHMw-PE) and have been synthesised using the synthesis conditions described as in chapter 2 and in publication by Talebi *[157]*. A commercially available grade of UHMw-PE from DSM® has also been used in understanding the difference in melting kinetics between the synthesised disentangled and the commercially available entangled UHMw-PEs. Different molecular weights (Mw) of disentangled UHMw-PE samples were synthesised using the same catalytic system and polymerisation conditions, except for their polymerisation time. All the samples were heated at heating rates of 0.05-10°C/min to understand the melting kinetics. To unravel further the effects of the morphology difference between the disentangled and the entangled UHMw-PE polymers on the melting kinetics, annealing below the peak melting temperature (T_M) was performed for varying time.

Sample preparation for DSC and TM-DSC studies: The nascent polymers (obtained directly from the reactor) were mixed with an anti-oxidant (Irganox 1010), 0.7% by weight to prevent any oxidation during the long experiments. To

have homogeneous mixing of the antioxidant with the powder, the antioxidant was first dissolved in acetone and subsequently mixed with the nascent UHMw-PE powder covered in acetone. After mixing, the powder was dried overnight in a vacuum oven at 40°C. The dried powder was used in all the experiments described below.

Table 4.1. Molecular weight (Mw) and molecular weight distribution (MWD) of the UHMw-PE samples used. Peak melting temperatures ($T_M^{\beta=1}$) at the heating rate (β) of 1°C/min are listed for the samples. Samples with prefix 'd' before PE in the sample names are disentangled (synthesised) UHMw-PE *whereas the sample with prefix 'e' is the commercially available entangled* UHMw-PE *from DSM®. The middle term in sample name is the molecular weight of the sample in million g/mole, whereas last term is the molecular weight distribution. Mw and MWD were measured using melt rheology as described in chapter 2 [169,209]. $T_M^{\beta=1}$ and $T_M^{\beta=0.05}$ are the peak melting temperature at the heating rate of 1°C/min and 0.05°C/min, respectively.*

Sample	Mw (x10^6 g/mol)	MWD	$T_M^{\beta=1}$ (°C)	$T_M^{\beta=0.05}$ (°C)
dPE_1M_1.9	1.4	1.9	139.0	137.9
dPE_2M_2.2	2.3	2.2	139.4	138.3
dPE_4M_2.5	3.9	2.5	140.2	139.3
dPE_8M_5.2	8.1	5.2	140.8	140.4
ePE_4M_8.4	3.7	8.4	140.4	139.7

For all the thermal characterisations, a Q-2000 MDSC from TA Instruments, USA, was used. Nitrogen gas with a flow rate of 50 mL min^{-1} was purged through the cell. High precision Tzero™ aluminium pans purchased from TA Instruments were used in all the tests*. The nascent powder after the addition of the anti-oxidant and drying was directly used in the pans with the weight of the sample being between 1.0 and 1.05 mg. Temperature and enthalpy calibrations were performed using indium.

**Tzero™ pans supplied by TA Instruments ensure that the material and design of the pan are manufactured to a high quality standard so to have very low variation in batch to batch pans in terms of manufacturing defects. The heat transfer co-efficient of these pans are also known and available in the machine directly with calibration for correction to minimise instrument measurement lag etc*.

4.2.2 Experimental protocols:

4.2.2.1 Peak melting temperature dependence on heating rate

The following protocol was used to study the heating rate dependence of the peak melting temperature for nascent and melt-crystallised samples of the same polymer, and is also schematically presented in Figure 4.1.

From A to B → heating from 90°C to 160°C at the examined heating rate (Ex-HR) – nascent sample.

From B to C → heating from 160°C to 190°C at 10°C/min. Isothermal for 5 minutes at 190°C.

From C to D → cooling from 190°C to 160°C at 10°C/min.

From D to E → cooling from 160°C to 90°C at 1°C/min.

From E to F → heating from 90°C to 160°C at the examined heating rate (Ex-HR) – melt-crystallised sample.

From F to G → cooling from 160°C to 90°C at 1°C/min.

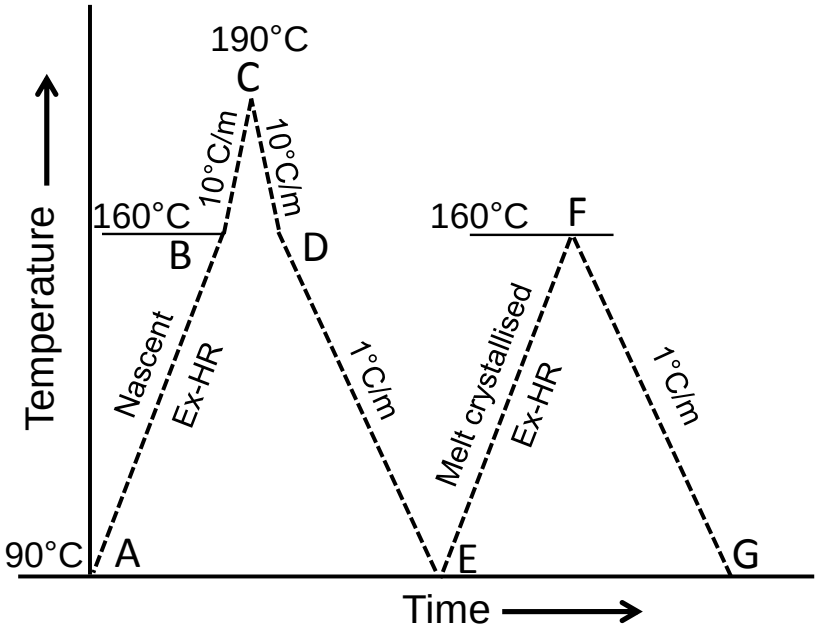

Figure 4.1. Schematic diagram showing the protocol used in the DSC runs to study the dependence of the peak melting temperature on the heating rate.

4.2.2.2 Annealing below the peak melting temperature (T_M)

The following protocol was used to study the effect of annealing in the vicinity, but below, the peak melting temperature to understand the melting of the crystals, and is also schematically presented in Figure 4.2.

From A to B → heating from 90°C to the examined annealing temperature (T_A) at 1°C/min.

From B to C → annealing at the examined annealing temperature (T_A) for varying times (melting in the vicinity, but below, the peak melting temperature), where β in superscript of T_M represents the heating rate in °C/min.

From C to D → cooling from the examined annealing temperature (T_A) to 90°C at 1°C/min.

From D to E → heating from 90°C to 160°C at 1°C/min.

From E to F → heating from 160°C to 190°C at 10°C/min, Isothermal at 190°C for 5 minutes.

From F to G → cooling from 190°C to 160°C at 10°C/min.

From G to H → cooling from 160°C to 90°C at 1°C/min.

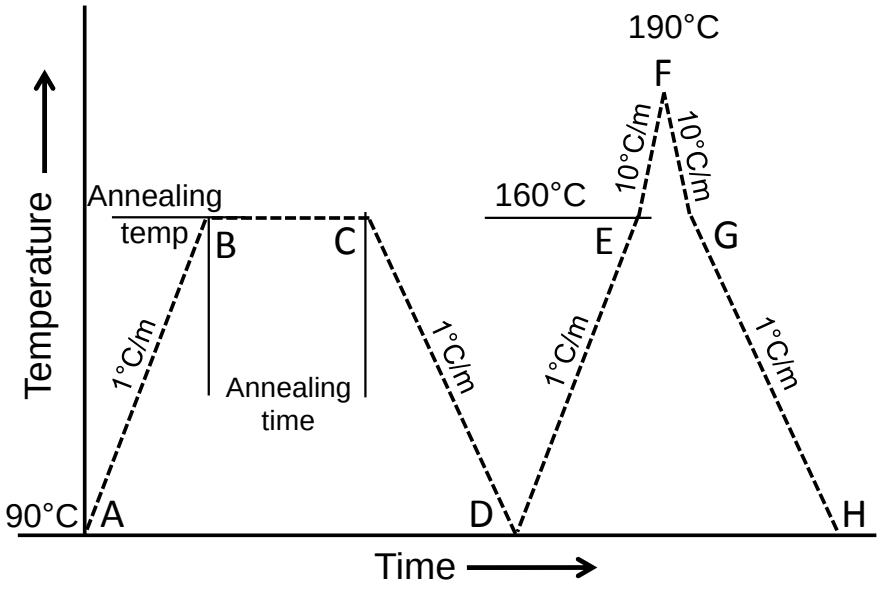

Figure 4.2. Schematic diagram showing the protocol used in the DSC runs to study the effect of annealing of the samples below their respective peak melting temperatures on the melting kinetics.

4.2.2.3 Annealing above the peak melting temperature (T_M)

The following protocol was used to study the effect of annealing time in the melt (at 160°C) on the on-set temperature of crystallisation (T_C), and is schematically presented in Figure 4.3.

From A to B → heating from 90°C to 160°C at 1°C/min.
From B to C → heating from 160°C to 190°C at 10°C/min and isothermal at 190°C for 5 minutes to erase any memory effect.
From C to D → cooling from 190°C to 160°C at 10°C/min.
From D to E → cooling from 160°C to 90°C at 1°C/min (first crystallisation step).
From E to F → heating from 90°C to 160°C at 1°C/min.
From F to G → annealing at 160°C for varying times (entanglement formation).
From G to H → heating from 160°C to 190°C at 10°C/min and isothermal at 190°C for 5 minutes to erase any memory effect.
From H to I → cooling from 190°C to 160°C at 10°C/min.
From I to J → cooling from 160°C to 90°C at 1°C/min (second crystallisation step).

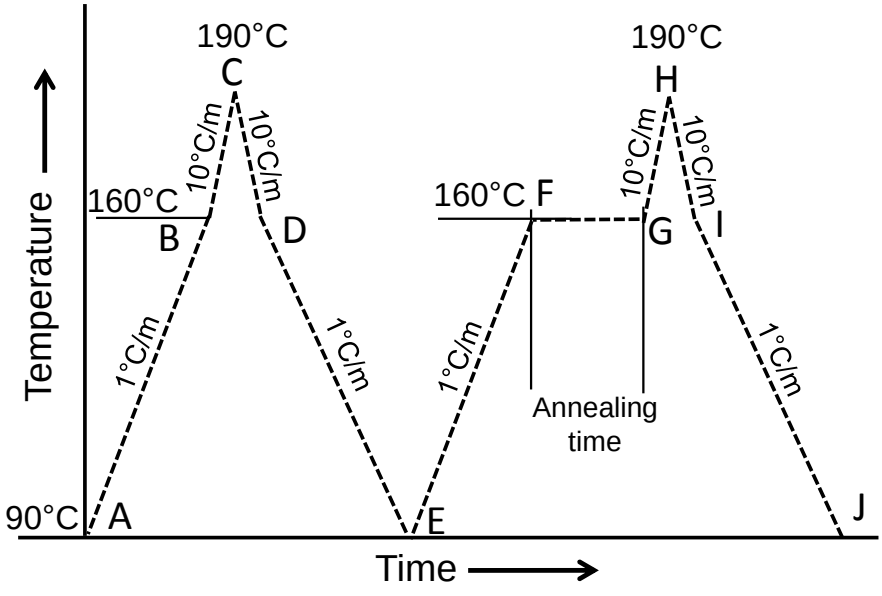

Figure 4.3. Schematic diagram showing the protocol used in the DSC runs to study the effect of annealing time in the melt on the on-set crystallisation temperature (T_C) of the synthesised disentangled polymers.

4.2.2.4 Characteristic melting time (τ) using TM-DSC

The following protocol was used to study the characteristic melting time (τ) of the crystals to understand the difference between entangled and disentangled samples, and is schematically presented in Figure 4.4.

From A to B → heating from 110°C (after isothermal for 30 minutes) to 150°C for the examined modulation period at a heating rate of 0.8°C/min. Sinusoidal temperature modulation was used with the modulation period in the range of 10-100s and the amplitude satisfying the heat only condition. The maximum amplitude was used ± 0.2°C.

From B to C → heating from 150°C to 155°C with zero modulation at 5°C/min.

From C to D → cooling from 155°C to 130°C at 5°C/min.

From D to E → cooling from 130°C to 100°C at 1°C/min.

From E to F → heating from 100°C to 150°C for the examined modulation period at a heating rate of 0.8°C/min (melting of melt-crystallised crystals).

From F to G → cooling from 150°C to 100°C at 5°C/min.

From G to H → modulating for 15 minutes with amplitude of 0.2°C and the examined modulation period at 100°C (after an isothermal hold for 30 minutes at 100°C).

From H to I → modulating for 15 minutes with an amplitude of 0.2°C and a period of 100 seconds at 100°C.

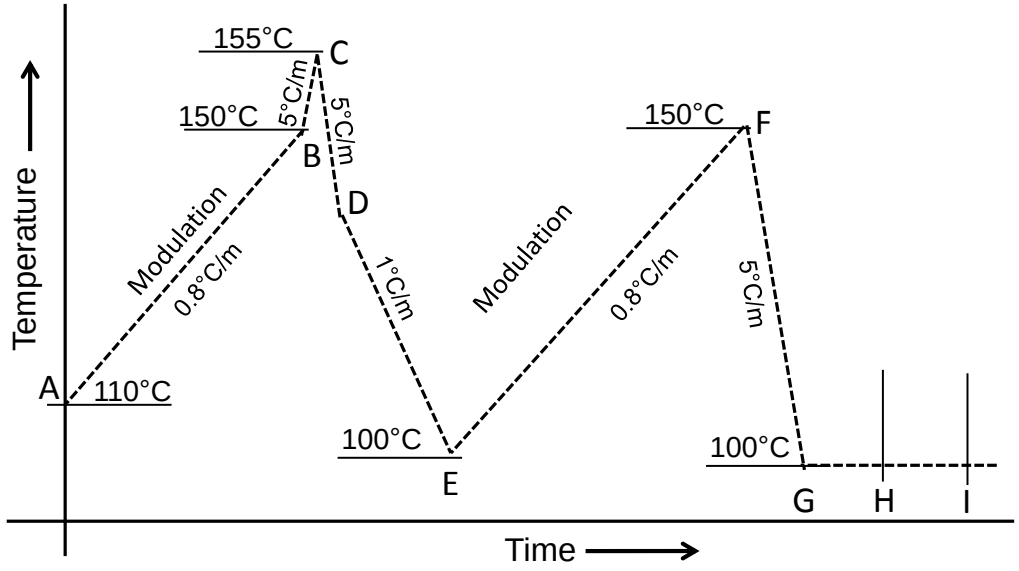

Figure 4.4. Schematic diagram showing the protocol used for the TM-DSC study of the characteristic melting time of disentangled samples.

4.3 Results and discussion:

In chapter 2, the morphology of the nascent disentangled samples synthesised at different temperatures are shown. In Figure 4.5, high-resolution SEM images showing typical morphology of the nascent, as-synthesised, disentangled polymers are shown. Randomly arranged (not stacked lamellae) single chain crystals of the order of 20 nm thickness are visible. A simple calculation suggests that 100% of the methylene units of a single chain of molecular weight in the vicinity of 2.8 million g/mol reside within the single lamellae of 20nm x 20nm x 12nm (for details please see chapter 1). All the disentangled samples studied here possess similar morphology. However, the morphology of the nascent entangled UHMw-PE (synthesised using a heterogeneous catalytic system) commercially available from DSM® used here is different where a more fibrous-like morphology is observed.

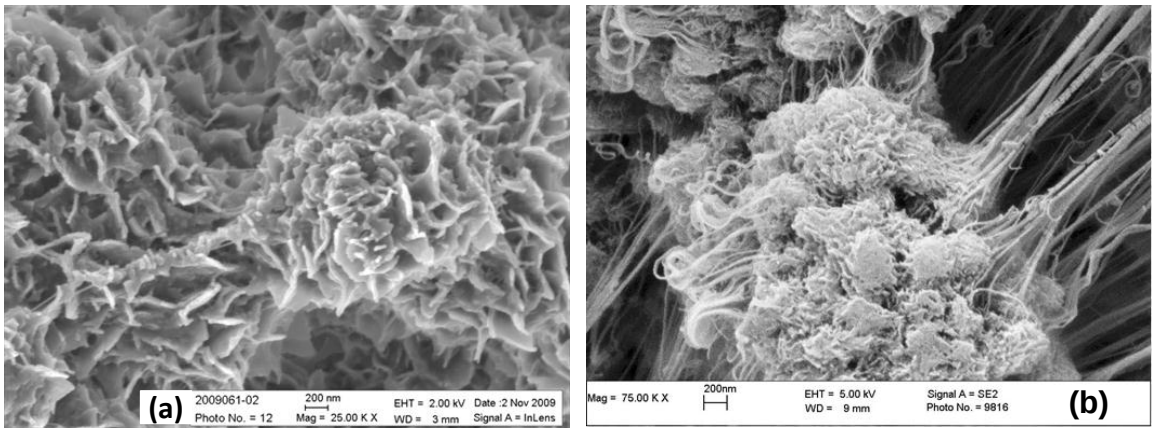

Figure 4.5. SEM micrographs of the morphology of (a) the synthesised nascent disentangled polymer (dPE_3M_2.2) and (b) the commercially available nascent entangled polymer (ePE_4M_8.4).

4.3.1 Peak melting temperature (T_M) dependence on heating rate:

4.3.1.1 Heating rate dependence of the peak melting temperature in the nascent disentangled and entangled UHMw-PE

In this chapter, observations on the morphology of the synthesised disentangled UHMw-PE from the previous chapter are extended to understand the melting in polymers and its dependence on the morphology produced during

the polymerisation by exploring the effect of molecular weight (Mw) of the disentangled UHMw-PE having a non-stacked single crystal morphology.

Figure 4.6 shows the endotherms for nascent disentangled (dPE_4M_2.5) and entangled (ePE_4M_8.4) samples of similar Mw at different heating rates of 0.05-10°C/min. Heat flow (F) in Figure 4.6 is normalised by corresponding heating rate (β). The integration of F/β over the temperature range gives the total endothermic heat i.e. the heat of fusion. The area should be independent of the heating rate if no melting kinetics effect is involved.

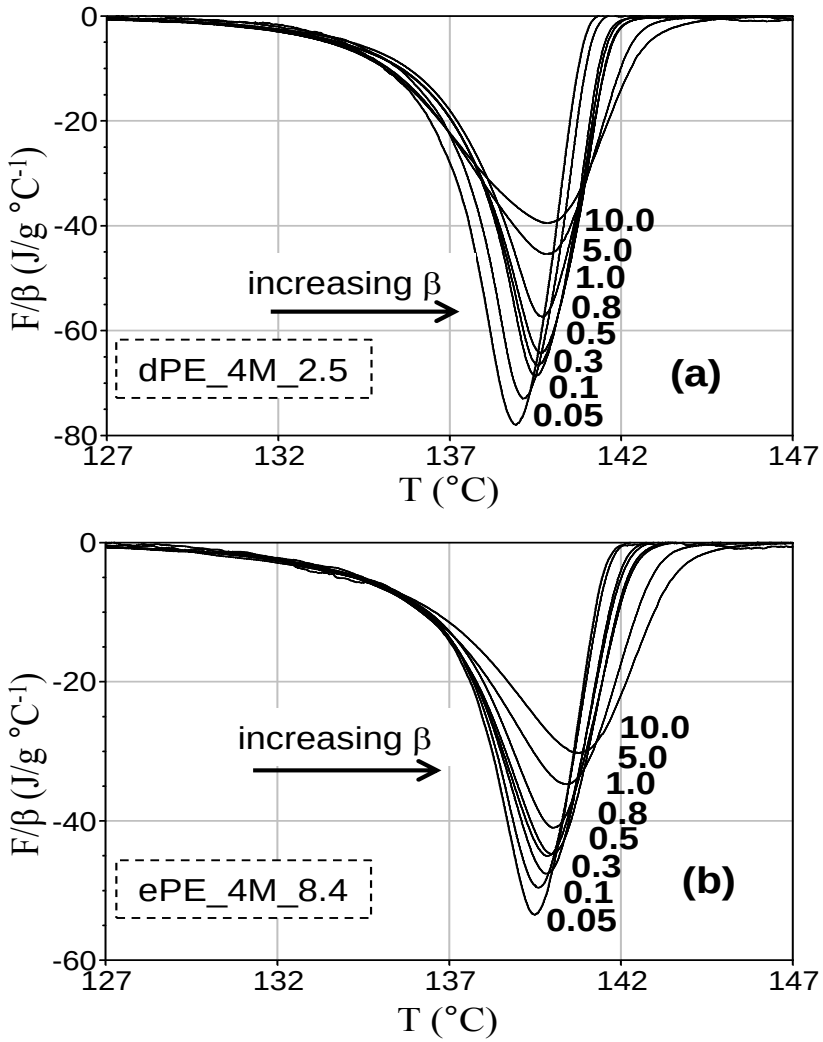

Figure 4.6. Endotherms at different heating rates of 0.05-10°C/min for (a) disentangled and (b) entangled UHMw-PE *samples of a similar Mw, 4 million g/mol. F is the heat flow rate normalised by the respective heating rate (β), F/β.*

The increase in the peak melting temperature (T_M) with increasing heating rate are in agreement with the studies performed by Toda *et al. [77]* on polyethylene having a Mw of 32,100 g/mol. Due to the melting kinetics the melting region widens with increasing heating rate, and consequently the peak height decreases to maintain the area independent of the heating rate. All the samples listed in Table 4.1, and investigated in this study show endotherms similar to Figure 4.6, where, the peak melting temperature increases with the increasing heating rates.

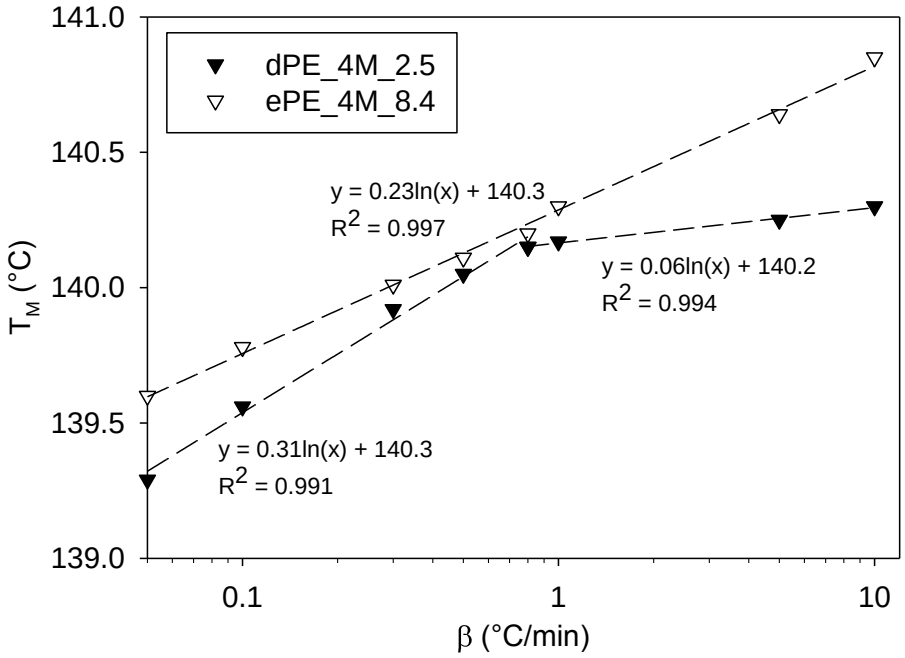

Figure 4.7. Comparison of the heating rate dependence of the peak melting temperature of the synthesised nascent disentangled (dPE_4M_2.5) and the commercially available entangled (ePE_4M_8.4) UHMw-PE of similar Mw.

In Figure 4.7, the heating rate dependence of the peak melting temperature (T_M) in the nascent disentangled and the nascent entangled UHMw-PE, having similar molecular weight, is shown. The peak melting temperature increases with increasing heating rate for both the polymers. Such an increasing trend of T_M with heating rate has been reported in polymers having an extended chain crystal morphology, where crystal thickening/perfectioning cannot occur *[123]*. Contrary to the extended chain crystals, in polymers where crystal thickening/perfection can occur by reorganisation T_M increases with decreasing heating rate. All the

synthesised disentangled UHMw-PE samples used in this study possess a folded chain morphology where crystal thickening/perfection by reorganisation should be feasible *[59,101,117]*. However, in a folded chain morphology the crystal thickening/perfectioning during heating requires larger co-operative motion of the chains within the crystals of Mw > $1x10^6$ g/mol, and will be a relatively slow process compared to melting.

The increase in T_M with heating rate has been attributed to the superheating effect, where the measured melting temperature is higher than the true melting temperature of the crystal. Wunderlich and co-workers *[123]* explained the main cause of superheating in the DSC measurement to a thermal lag between the heat source and the sample, i.e. the measurement lag between the true sample temperatures and measured melting temperature of the crystals. The apparent shift in peak melting temperature caused by instrumental delays cannot be corrected alone by temperature calibration using the on-set melting temperature of standard materials (such as indium) at the respective heating rates *[220]*. Schawe *[133]* has shown that the shift in the peak melting temperature depends upon the peak height and the slope of heat flow peak. To circumvent these artefacts, TA Instruments has introduced a new method of measuring heat flow in their selective instruments (such as the MDSC-Q2000 used in this study) with the aim to improve the measurement by including the heat storage effects of both the sensor and the pans. A new calibration procedure used to determine the instrument co-efficient is used to obtain the actual heat flow in the sample *[132]*. Toda *et al.* have used this method, described in reference *[77,220],* for examining the heating rate dependence on the peak melting temperature. To avoid any reorganisation, these authors annealed their polymer crystals for several hours prior to the experiments. In spite of the instrumental corrections, Toda *et al.* observed an increase in the melting temperature with heating rate in various polymers including PP, PE, PET and PVDF *[77,220]*. The authors found a non-linear dependence of melting on heating rates of the single crystals of linear polyethylene. Their observations were also supported by microscopy studies.

A non-linear logarithmic dependence of the increasing peak melting temperature on the heating rate for the nascent disentangled and the entangled polymers is evident from Figure 4.7. The peak melting temperature increases as

a function of the logarithm of the heating rate for both, the disentangled and the entangled polymers having a similar Mw. Contrary to the single heating rate dependence for the entangled polymer two distinct heating rate dependences of the peak melting temperature for the synthesised disentangled polymer exists, Figure 4.7. What follows is a possible explanation of the distinct difference in melting behaviour of the entangled and the disentangled crystals.

It is to be noted that in the entangled polyethylene, ePE_4M_8.4, with increasing heating rate the low-temperature sections (132-137°C) of the curves shift to a higher temperature and so is the peak melting temperature (Figure 4.6b). The shift in the melting temperature follows a logarithmic increase in the heating rate (Figure 4.7). Unlike the entangled sample, the disentangled polyethylene dPE_4M_2.5 shows a shift in the low temperature section to high temperature while increasing the heating rates from 0.05°C/min to 1.0°C/min. Above this heating rate, from 1.0°C/min to 10.0°C/min, the lower temperature section of the curve shifts to lower values. The change in the direction of the low temperature section of the curve in the region of 1.0°C/min is a phenomenon observed for all the nascent disentangled polyethylene samples that show change in the peak melting temperature slope with heating rate at 1.0°C/min, also see Figure 4.7.

In the nascent disentangled crystals, the appearance of two different slopes with heating rate strongly suggests the presence of two different mechanisms involved in the melting process. At heating rates greater than 1°C/min, melting should be a normal process where it would proceed in clusters of chain stems *[118,140]*. Above 1°C/min, the slope in Figure 4.7 suggests a stronger heating rate dependence of the nascent entangled samples compared to the nascent disentangled polymer. From the modified Gibbs-Thomson equation, see equation (4.2), at a fixed heating rate, higher melting temperature of entangled nascent crystals compared to disentangled nascent crystals means detachment of a greater number of methylene units from the entangled nascent crystals. The difference in the nonlinear melting temperature dependence on heating rate in the two samples invokes melting kinetics whereas the difference in slopes of the two samples shown in Figure 4.7 should be correlated with the topological differences that exist in the amorphous component of the two semi-crystalline

polymers. The change in slopes arising due to topological differences will be discussed in more detail in the following section.

However, at the heating rate lower than 1°C/min, in the nascent disentangled sample (Figure 4.7) a sudden increase in T_M slope with the heating rate is observed. The sudden change in slope suggests involvement of a different activation barrier in the melting process. Rastogi *et al. [117,127]* have shown differences in the enthalpic activation barrier for the detachment of chains either via cluster melting or the consecutive detachment of chain stems from the crystal surface, followed by their diffusion into the surrounding melt. Considering these concepts, an explanation for the two different mechanisms involved in the melting process of the disentangled nascent polymer may be provided. At the heating rates below 1°C/min, where the system is given sufficient time for the chain detachment process, melting in the nascent UHMw-PE polymers is likely to start from the outer surfaces by the consecutive detachment of chain stems. Melting from the outer surface compared to the core of the crystal would be preferred due to the lower surface free energy requirement i.e. a lower entropic barrier for the chain segments in contact with melt. The number of chain stems involved in melting decreases with decreasing heating rate, and so is the melting temperature. On increasing the temperature sufficiently high, i.e. increasing the heating rate above 1°C/min, the difference in surface free energy requirement for chain detachment from the crystal surface or from its centre is suppressed. Thus, a new activation barrier could be overcome that does not require consecutive melting and overcomes the entropic barrier to an extent that the nucleation process for melting can occur at different places (even from core) in the crystal.

In the case of a nascent entangled polymer, melting can only occur in clusters as chains that are shared among many crystallites and a larger co-operative motion is required to achieve the random coil state. For the same heating rate, the higher T_M of the entangled polymer compared to the disentangled polymer, also supports the requisite for a larger co-operative motion in the melting of the nascent entangled polymer. It is understood that the increase in T_M with increasing heating rate corresponds to the cluster size involved in the melting process, which increases with the increasing heating rate.

The higher heating rate dependence of the entangled polymer compared to the disentangled polymer, at heating rates >1°C/min, is due to the presence of a greater number of entanglements in the amorphous region of the nascent entangled sample. From Figure 4.7, it is evident that a distinction occurs in the melting behaviour of the entangled and the disentangled samples. Considering that the crystallinity and crystal structures of the two polymers is the same, the arising differences in the melting behaviour should be dependent on the topological differences residing in the amorphous regions, thus invoking the kinetics of the melting process of these semi-crystalline polymers.

One of the methods to probe differences in the amorphous regions is solid-state NMR spectroscopy. The ^{13}C-single pulse magic angle spin studies (SP-MAS) performed on these samples have confirmed a distinction between the amorphous chain segments. For example, the entanglement in the entangled sample hinders the chain diffusion process from amorphous to crystalline regions *[164,165,224-226]*. A consequence of this is the transfer of polarisation to the crystalline region takes a longer time in the entangled sample compared with the disentangled polymer *[1]*. A further major distinction is encountered when the segmental mobility in the amorphous region is considerably enhanced in the melt-crystallised samples compared to the nascent polymers *[224]*. The entropic differences that arise between the amorphous and the crystalline regions, due to enhanced segmental mobility of the amorphous region, restricts chain diffusion process between the two regions below the alpha relaxation temperature of the melt-crystallised sample.

To investigate the influence of topological differences in the melting process, what follows is a comparative study of the heating rate dependence of the nascent material and its melt-crystallised samples.

4.3.1.2 Heating rate dependence of the melting temperature in nascent and melt- crystallised UHMw-PE

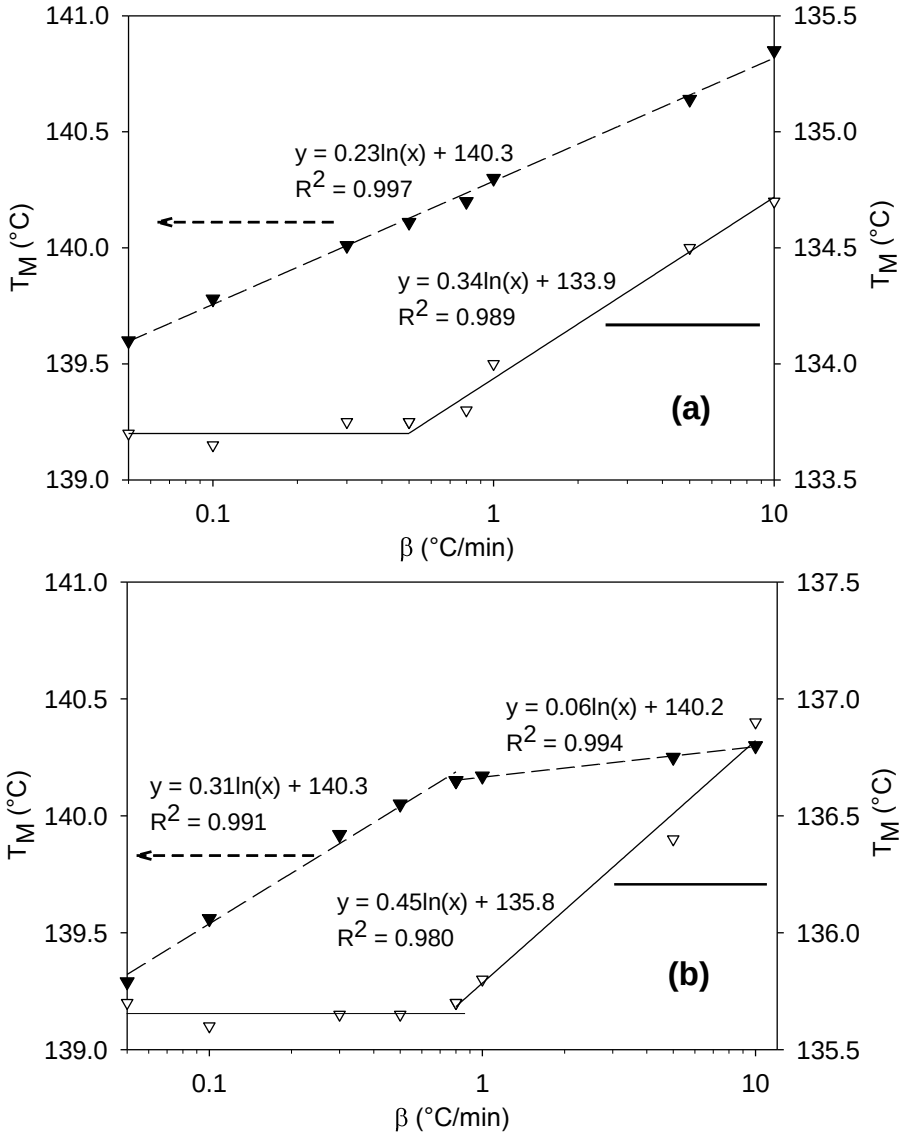

Figure 4.8. Peak melting temperature dependence on the heating rate between nascent crystal (filled symbols) and melt-crystallised (open symbols) of (a) the entangled, ePE_4M_8.4 and (b) the disentangled UHMw-PE, dPE_4M_2.5, of similar Mw.

Figure 4.8 presents the heating rate dependence of the nascent and the melt-crystallised samples of the same polymer. The melt-crystallised sample is obtained on melting of the nascent crystals to 190°C during the first heating step (step 1a, Figure 4.1) of the DSC run and re-crystallising it by cooling at 1°C/min from its melt to 100°C (step 1d, Figure 4.1). Data from the first heating step is

treated as melting of nascent crystals, whereas the second melting represents data on the same melt-crystallised sample (step E to F, Figure 4.1), thus avoiding any complication caused by a difference in the molecular characteristics of the samples. A clear difference in heating rate dependence and melting temperature between the nascent crystals and the melt-crystallised samples is apparent from Figure 4.8. The peak melting temperature of the melt-crystallised sample is lower than the nascent crystals of the same polymer at any examined heating rate. Peak melting temperature of 133.7°C and 135.7°C at a slower heating rates (<1°C/min) for melt-crystallised of entangled and disentangled polymer, respectively, is close to the peak melting temperature of 131°C predicted by the Gibbs-Thomson equation for polyethylene with a lamellar thickness of 25nm *[139]*. However, the higher peak melting temperature of ~140°C for the nascent samples having chain folded crystals, which is close to the equilibrium melting temperature of 141.5°C for polyethylene having extended chain crystals, cannot be explained by the Gibbs-Thomson equation *[126]*. Engelen *et al. [101]* have reported that nascent crystals are folded chain crystals which on cross-linking by irradiation show a low melting temperature of ~135°C. Using DSC and NMR spectroscopy, the high peak melting temperature of the nascent crystals has been attributed to its crystal topology *[117]*. The topological differences in the amorphous phase of the crystals have a profound effect on the melting of the polymer. Höhne *[137]* has shown that the number of repeating units involved in the melting dynamics governs the melting rather than the thickness of the lamella and the surface energy.

To explain the differences in the heating rate dependence on the melting temperature of the melt-crystallised sample and the nascent polymers, in Figure 4.9, schematic illustrations of the crystal structure for nascent entangled, nascent disentangled and melt-crystallised samples are presented. A nascent entangled sample that is polymerised at high temperatures using a heterogeneous catalyst system has morphology where same chain participates in formation of several other crystallites. The region between the crystals is an amorphous region having tight chains without having any specific crystallographic registration. The presence of tight chain re-entry in the amorphous region has been supported by the solid state NMR studies *[117,164,165]*.

In the case of a nascent disentangled sample, the crystals are mainly formed by re-entrant chains, ultimately monomolecular crystals, where most of the chains do not participate in the formation of other crystallites i.e. the single-site catalytic system combined with the low polymerisation temperature and low catalyst concentration promotes such a possibility. The existence of tight folds, leading to restricted chain mobility of the chain segments in the amorphous region becomes apparent in the solid state NMR studies. Single pulse NMR studies support the topological differences in the entangled and the disentangled nascent polymers *[117,164,165]*,

In melt-crystallised samples of these ultra-high molecular weight polymers, the chains are most likely to participate in the formation of several crystals with least adjacent re-entry. The presence of highly mobile chain segments in the amorphous region revealed by the NMR studies has confirmed the presence of loose chain folds or loose chain segments and higher conformational or entropic differences between the amorphous and the crystalline regions *[165]*. This entropic difference means that the detachment of chain segments from the crystal surfaces is not dependent on the neighbouring chain or the presence of the part of chain in another crystal. At low heating rates the melting will involve chain segments at the crystal surface having lengths similar to the crystal thickness, thus, peak melting temperature obeys the Gibbs-Thomson equation. Such a possibility is apparent from the plateau region observed for the melt-crystallised samples in Figure 4.8. However, at the higher heating rates, the melting temperature increases with the heating rate. The cause for the increase in the melting temperature is attributed to the simultaneous cooperative detachment of chain segments from the neighbouring crystals. The number of methylene units detached from the crystal tends to increase (due to the larger co-operativity needed) with the increasing heating rate, thus causing an increase in the melting temperature.

In the melt-crystallised sample, the independence of melting temperature on the heating rate below a critical value strengthens the argument that no correlation exists between the neighbouring chains that are connected by the mobile amorphous region within the crystals. The sudden change in the slope with the heating rate also invokes the argument of two different mechanisms

involved in melting of the melt-crystallised sample. The difference in mechanisms is encountered when the melting zones with decreasing heating rate shrink to chain segments corresponding to a crystal thickness. Since the chain segments at the crystal surface does not feel the presence of its neighbour or its connectivity to chain segments residing within the neighbouring crystal, the melting temperature shows a heating rate independence: a situation in contrast with the nascent disentangled and entangled samples.

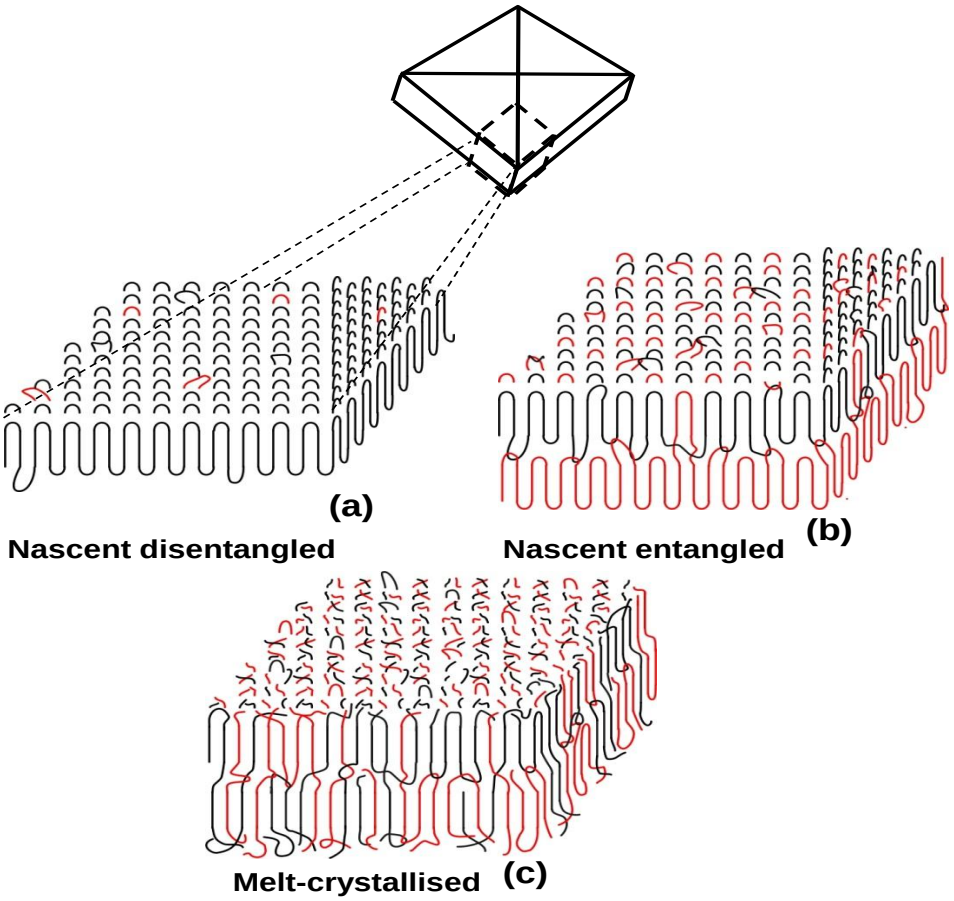

Figure 4.9. Schematic representation of the crystal structures for (a) nascent disentangled sample having re-entry chains with tight folds, (b) Nascent entangled sample having tight folds with re-entry with chains shared among several crystals and (c) melt-crystallised sample having chains having loose folds and loops with chains being shared among several crystals. A schematic of a nascent disentangled sample is made in agreement with Figure 4.5 that represents single crystal-like morphology. However, the sporadic occasions where a chain can be shared between different crystals cannot be ignored and such a possibility is shown by red folds on the crystal surface.

As seen in chapter 2, it is important to realise that because of the very nature of polymer synthesis, at least in the initial stages, the commercial polymer will have a much higher number of entanglements in its melt state compared to the melt of the synthesised disentangled polymer. The difference in the entanglement density in the melt state will have implications on the crystallisation behaviour, and is discussed in the next sections of this chapter. To recall from chapter 2, a disentangled polymer upon melting goes from the disentangled to the entangled state where the time required to attain the thermodynamically stable entangled states follows a power law of ~2.6 to the molecular weight *[59,157,209]*. Considering this power law, the total time required for the sample having a molecular weight of 4 million g/mol is nearly 30 hours as opposed to the few minutes required in the case of the entangled commercial sample. For the sake of consistency similar to the melt-crystallised entangled commercial sample, following the pathway depicted in Figure 4.1, the melt-crystallised sample of the disentangled nascent polymer reported in this section was also be left in the melt for 5 minutes prior to crystallisation. It is known that crystallisation is facilitated from the disentangled melt i.e. onset of crystallisation from the disentangled polymer melt is at a higher temperature compared to its entangled melt state *[140]*. The higher crystallisation temperature also means higher crystal thickness. Thus, the difference in melting temperatures of the melt-crystallised samples at heating rates below 1°C/min (Figure 4.8a and 4.7b) may be attributed to crystal thickness. In Figure 4.8, heating rate dependence (heating rate >1°C/min) is higher for the melt-crystallised sample as compared to the nascent crystals of the same sample. This means that by increasing the heating rate a greater number of methylene units are detached from the melt crystallised sample compared to its nascent state. Considering the morphological differences, the rate of methylene unit detachment with the heating rate is likely to be influenced by two factors: a) the number of entanglements present in the amorphous phase and b) the number of chains participating in the formation of several other crystallites. Compared to the nascent disentangled sample, chains participating in neighbouring crystals will be higher in the nascent entangled sample, thus the melting temperature dependence on the heating rate will be higher in the nascent entangled sample (or the melt-crystallised samples).

4.3.1.3 Heating rate dependence for disentangled polymers having different Mw

Figure 4.10 shows the nonlinear logarithmic heating rate dependence of the disentangled polymers having different molecular weights. It is apparent that all the polymers show a discrete change in the melting temperature above a "critical" heating rate, thus dividing melting temperature into two regimes low (heating rate <1 °C/min) and high (heating rate >1 °C/min). Secondly, it is evident that the melting temperature at a fixed heating rate increases with increasing molecular weight. The increase in melting temperature suggests a detachment of an increasing number of methylene units with increasing molecular weight. A possible explanation of this is the topological requirement that the higher molecular weight imposes, that may arise from adjacent re-entry and/or the presence of a lesser number of entanglements in the amorphous region. In chapter 2, a decrease in the entanglement density with increasing molecular weight, with the help of rheological studies on disentangled UHMw-PE synthesised at different polymerisation times, has been established *[209]*.

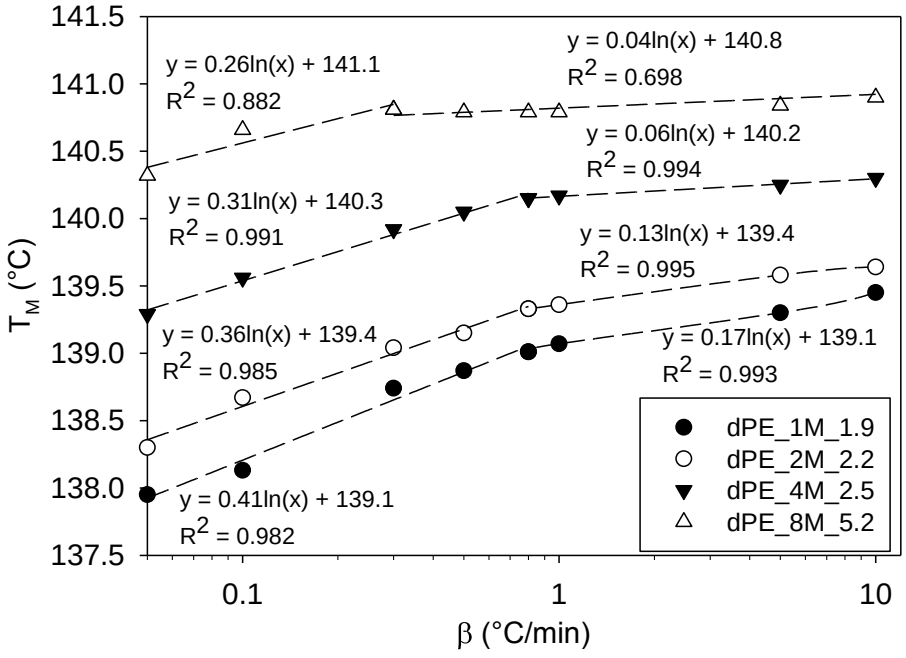

Figure 4.10. Heating rate dependence of the synthesised nascent disentangled UHMw-PE of different Mw for heating rates of 0.05, 0.1, 0.3, 0.5, 0.8, 1.0, 5.0 and 10.0°C/min.

From the Figure 4.10, it is also evident that at low heating rates the melting temperature increases faster with the heating rate in the low molecular weight polyethylene. Following the concepts described in the earlier sections, the difference in the melting temperature with the heating rate is in coherence with the differences in the entanglement density of the low and the high molecular weight nascent disentangled polyethylenes.

From the results summarised above, it can be concluded that that the heating rate has a strong influence on the melting behaviour that is associated with the topological constraints. In Figure 4.10, the experiments are performed down to the lowest accessible heating rate of 0.05°C/min. Studies were performed at a fixed temperature below the peak melting temperature to get a further insight into the melting kinetics arising due to the topological constraints present in the amorphous region of the semi-crystalline polymers. The findings are discussed in the following sections.

4.3.2 Annealing UHMw-PE samples below the peak melting temperature (T_A):

Figure 4.11 compares DSC thermograms obtained at a heating rate of 1°C/min, for a nascent disentangled sample dPE_2M_2.2, after annealing it at various temperatures (T_A) and times in the vicinity, but below, the peak melting temperature. Figure 4.11 shows the appearance of a second melting peak at lower temperature (T_{M1}) that grows with the increasing annealing time and temperature. With the increasing prominence of lower melting peak (T_{M1}) at higher annealing temperature and time, the higher melting peak (T_{M2}) decreases in magnitude, Figure 4.11. Considering the positions of the peaks, the low melting peak is associated with melting of the melt crystallised polymer obtained on annealing whereas, the high melting peak is correlated with the remainder of crystal that has not melted on annealing. The increase in magnitude of the low melting peak with annealing time suggests the involvement of chain kinetics in the melting process arising due to morphological restrictions that the nascent disentangled polymer imposes. These observations are in accordance with earlier studies reported *[59,101,118,126,127,163]* where the kinetics involved suggests successive detachment of chains from the crystal surface and its reeling into the melt. The shift in the high temperature melting peak with

annealing time also suggests an on-going reorganisation process in the remainder of the crystals.

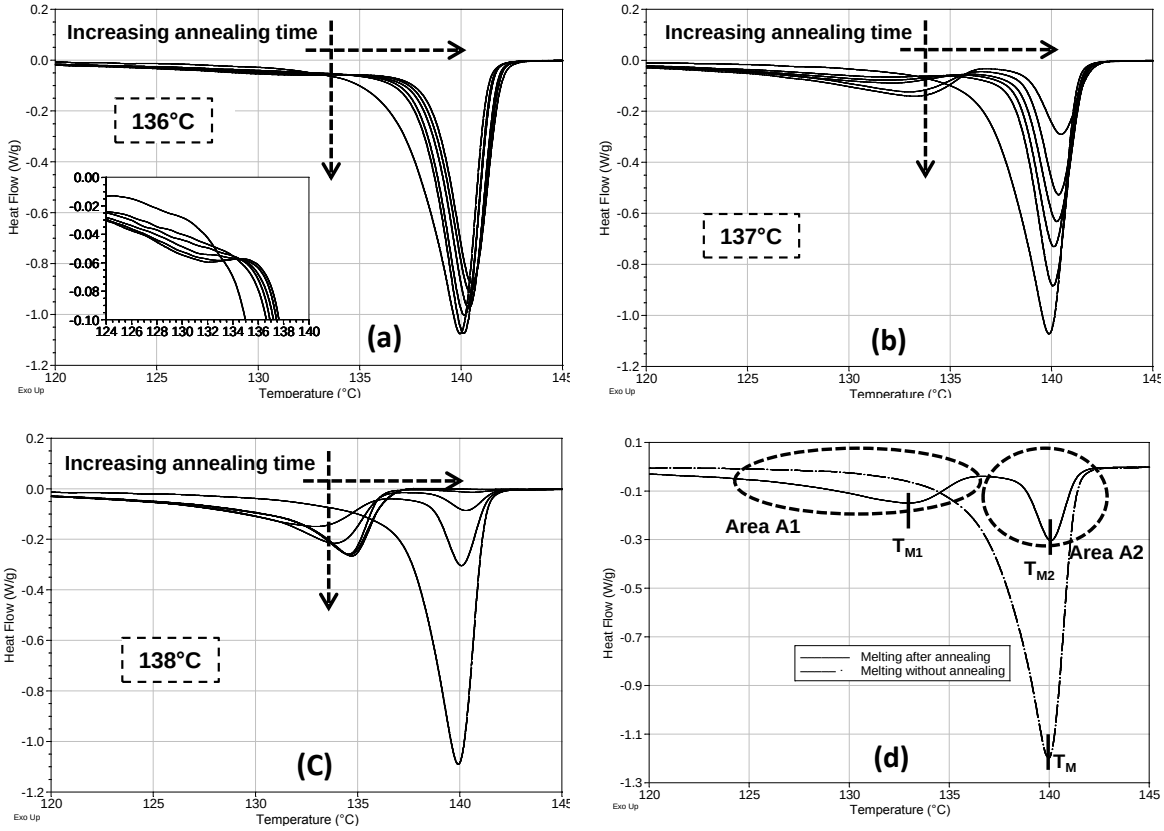

Figure 4.11. Second heating step for the nascent disentangled samples dPE_2M_2.2 after annealing at (a) 136°C, (b) 137°C and (c) 138°C for different times (0, 30, 60, 90, 120, 240 and 480 minutes). With increasing annealing times and temperatures, a lower secondary melting peak can be seen to be evolving. For annealing at 136°C, these lower peaks are small and shown in an inset. (d) Endotherms at heating rate of 1°C/min for a nascent disentangled sample dPE_2M_2.2 without any prior annealing and after annealing at 138°C for 30 minutes.

Figure 4.11d provides some quantitative estimation of the amount of crystal melted during the annealing process by the percentage ratio of the area A2 (area under the higher peak) to the total area (area A1 + area A2) and is taken as a measure at different annealing conditions. Figure 4.11d also compares the difference between melting of a nascent disentangled sample dPE_2M_2.2, before and after annealing at 138°C for 30 minutes. The decrease in total enthalpy (summation of ΔH for T_{M1} and T_{M2}) in the annealed sample compared to

the nascent sample, arises due to a loss in crystallinity in the melt crystallised component of the polymer.

As is evident from Figure 4.11, the first melting peak increases in intensity faster with the increasing annealing temperature (T_A), suggesting a faster melting process i.e. faster detachment of chains and their reeling into the surrounding polymer melt. Faster melting means a reduced annealing time for the remainder of the crystal and thus a lesser possibility for organisation, and the resultant shift in the high melting temperature (T_{M2}). On the other hand, at lower annealing temperatures (136°C) melting of the nascent crystals is not realised. An annealing temperature (T_A) too close to the peak melting temperature causes rapid melting in the nascent crystals and hence a higher melting peak (T_{M2}) may not be observed during the second melting step after annealing as all the nascent crystals might have melted during the annealing. If T_A is too low, than the T_M, the melting of the nascent crystals may not occur and hence lower melting peak at T_{M1} may not appear. A fixed reference temperature of 137°C based on the normal melting (without any prior annealing) of the sample at 1°C/min was chosen for annealing study of synthesised nascent disentangled UHMw-PE having varying Mw, Figure 4.12.

Figure 4.12 shows the percentage decrease in the enthalpic area A2 (area A2 divided by the total area A1+A2) for the nascent disentangled samples having different molecular weights (Mw), after annealing for varying times at 137°C. As discussed earlier, the area A1 is the fraction of the sample volume which possesses a melt-crystallised morphology caused by partial melting of the nascent crystals during the annealing at 137°C. It can be clearly seen that area A2 decreases rapidly for the lower Mw samples, whereas the increase is negligible for highest Mw sample. The melting in crystals proceeds from the surface for very slow heating rates (annealing below melting peak in this case) by detachment of the single stem from the surface *[117,126,140]*. However, negligible decrease in area A2 in sample dPE_8M_5.2 cannot be understand unless one considers the differences in peak melting temperature for varying Mw samples and hence, see Table 4.1.

The differences in T_M between different Mw samples cause a difference in effective degree of superheating (ΔT_A) at a fixed annealing temperature (137°C) for different Mw samples and can be represented by,

$$\Delta T_A = T_M - T_A \quad \ldots(4.4)$$

Where, ΔT_A is a "measure" of the effective degree of superheating, T_M is the peak melting temperature in second heating step (Figure 4.11d) after annealing at T_A for varying times, and T_A is the annealing temperature, 137°C, in Figure 4.12.

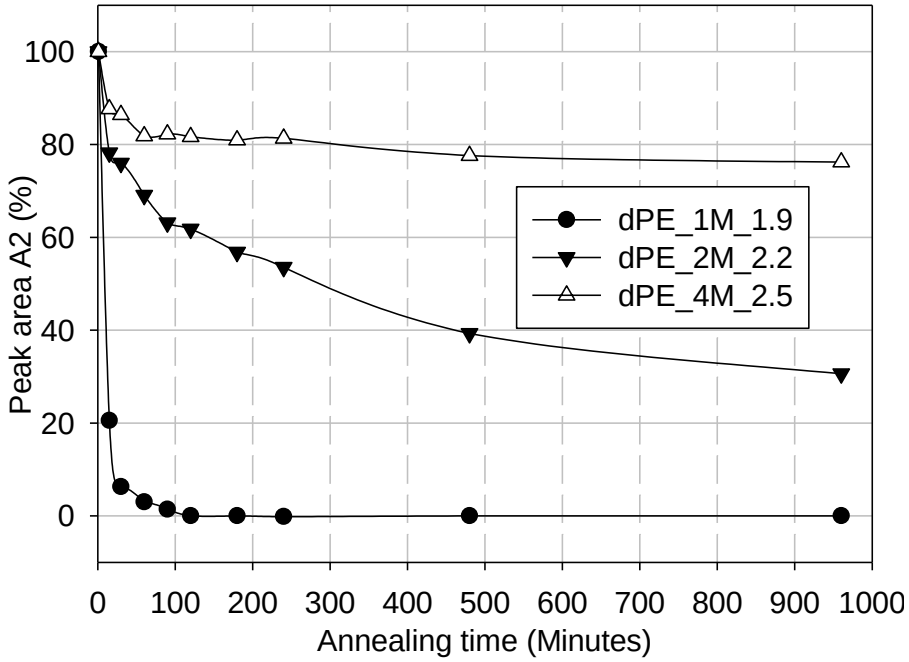

Figure 4.12. Decrease in the area A2 in the nascent synthesised disentangled polymers of varying Mw after annealing at 137°C for varying times.

Considering that the melting behaviour will be strongly dependent on the molecular weight and the resultant entangled state, for a common reference further comparisons were performed at a fixed degree of superheating ($T_M^{\beta=0.05}$- 2)°C, where $T_M^{\beta=0.05}$ is the peak melting temperature at the heating rate of 0.05°C/min intrinsic to the investigated polymer (Mw). *Note: Due to the non-linear heating rate dependence of peak melting temperature it is not feasible to find confidently the equilibrium melting temperature ($T_M^{\beta=0}$) by extrapolation. Hence, the peak melting temperature at lowest possible heating rate (0.05°C/min) was taken as the reference.*

4.3.2.1 Melting comparison between nascent entangled and disentangled UHMw-PE samples

Figure 4.13 shows the percentage decrease in the enthalpic area A2, for the nascent disentangled and the entangled samples having a similar molecular weight (Mw), with varying annealing times at respective annealing temperature defined by ($T_M^{\beta=0.05}$- 2)°C. From Figure 4.13, it is apparent that A2 decreases rapidly for the nascent disentangled polymer, whereas, the decrease is considerably less for the nascent entangled sample ePE_4M_8.4. Similar observations have been reported earlier by Rastogi *et al. [117,126,127]* on disentangled UHMw-PE polymers, concluding that the continuous melting of nascent disentangled polymer proceeds by successive detachment of chain stems and their reeling into polymer melt, where the number of chain stems detached from the crystal surface is strongly dependent on the annealing temperature. However, in the case of nascent entangled polymer no appreciable decrease (less than 30%) in the area A2 on annealing suggests that melting by chain detachment does not occur. This is also confirmed by earlier observation in section 4.3.1.1 with heating rate dependence of the nascent entangled polymer. The strong difference in melting kinetics on annealing suggests an influence of chain topology on the detachment of chains from the crystal surface. Considering melting to be the reverse process of crystallisation, in normal circumstances where the chains are adjacently re-entrant melting should occur by a simple successive detachment of chains. However, in the scenario where the chains are not adjacently re-entrant, melting will be a more complicated process where successive chain detachment will be hindered by topological constraints residing in the amorphous component of the semi-crystalline polymer. The melting behaviour summarised in Figure 4.13 suggests differences in the topological constraints of the entangled and the disentangled nascent polyethylenes. Recently, Toda *et al. [77]* followed melting behaviour of the low molecular weight single crystal polyethylene. They showed conclusively that melting in the single crystal occurs by a shrinking in crystal size, the reverse process to crystallisation. The findings were in contradiction with the observed decrease in optical intensity on melting of spherulites rather their contraction in size. The loss in intensity was

correlated with a sporadic melting process in the crystal aggregates where the chains are shared between different crystals.

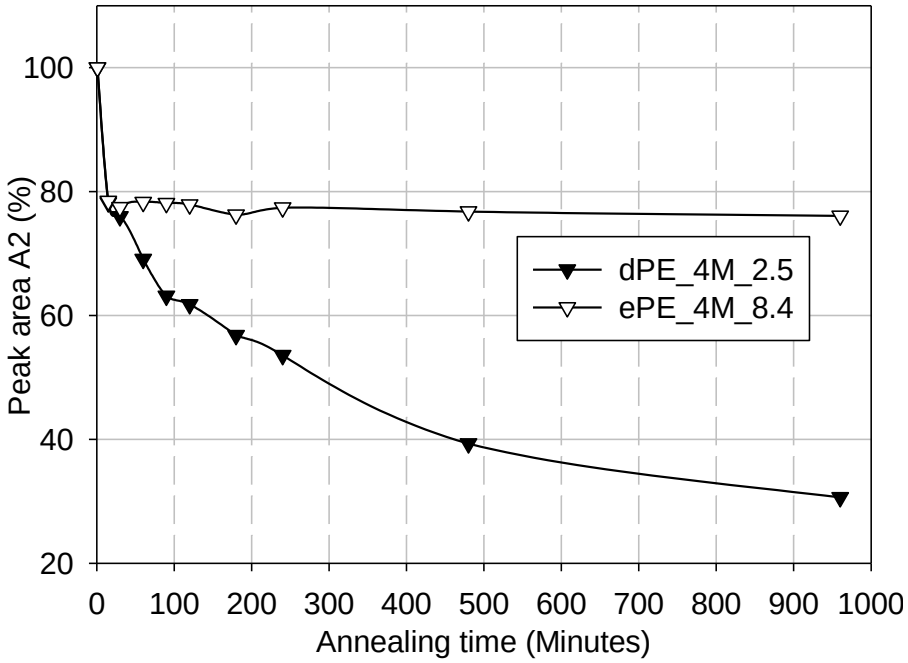

Figure 4.13. Decrease in the area A2 for the nascent synthesised disentangled (dPE_4M_2.5) and the commercially available entangled sample (ePE_4M_8.4) of similar Mw after annealing at respective temperature ($T_M^{\beta=0.05}$ - 2)°C for varying times.

In single crystals where the chains are anticipated to have adjacent re-entry, the decrease in crystal size should be linear. In the nascent disentangled samples, deviation in the linear behaviour with time arises due to the shift in the melting temperature of the remainder of the crystal due to crystal perfectioning (Figure 4.14). The shift causes an increase in the difference between the melting and annealing temperatures, thus making the chain detachment process more difficult, and consequently suppressing the melting rate. The effect of the decrease can be easily understood by replacing T_M with T_{M2} in equation (4.4). As the T_{M2} increases with increasing annealing time (Figure 4.14), the rate of the melting of the nascent crystals reduces with increasing annealing time

The non-linearity in the decrease of area A2 with the increasing annealing time is a coupled effect of simultaneous crystal melting and crystal perfection during the annealing. As T_{M2} increases with the annealing time, Figure 4.14, the measure of the effective degree of superheating (ΔT_A) increases at a fixed T_A

causing a decrease in the rate of the nascent crystal melting. Figure 4.14b shows that even though the observed changes in the degree of superheating with annealing time are lower in the nascent entangled sample, no decrease in the area A2 is observed, (Figure 4.13), as melting by chain detachment does not occur.

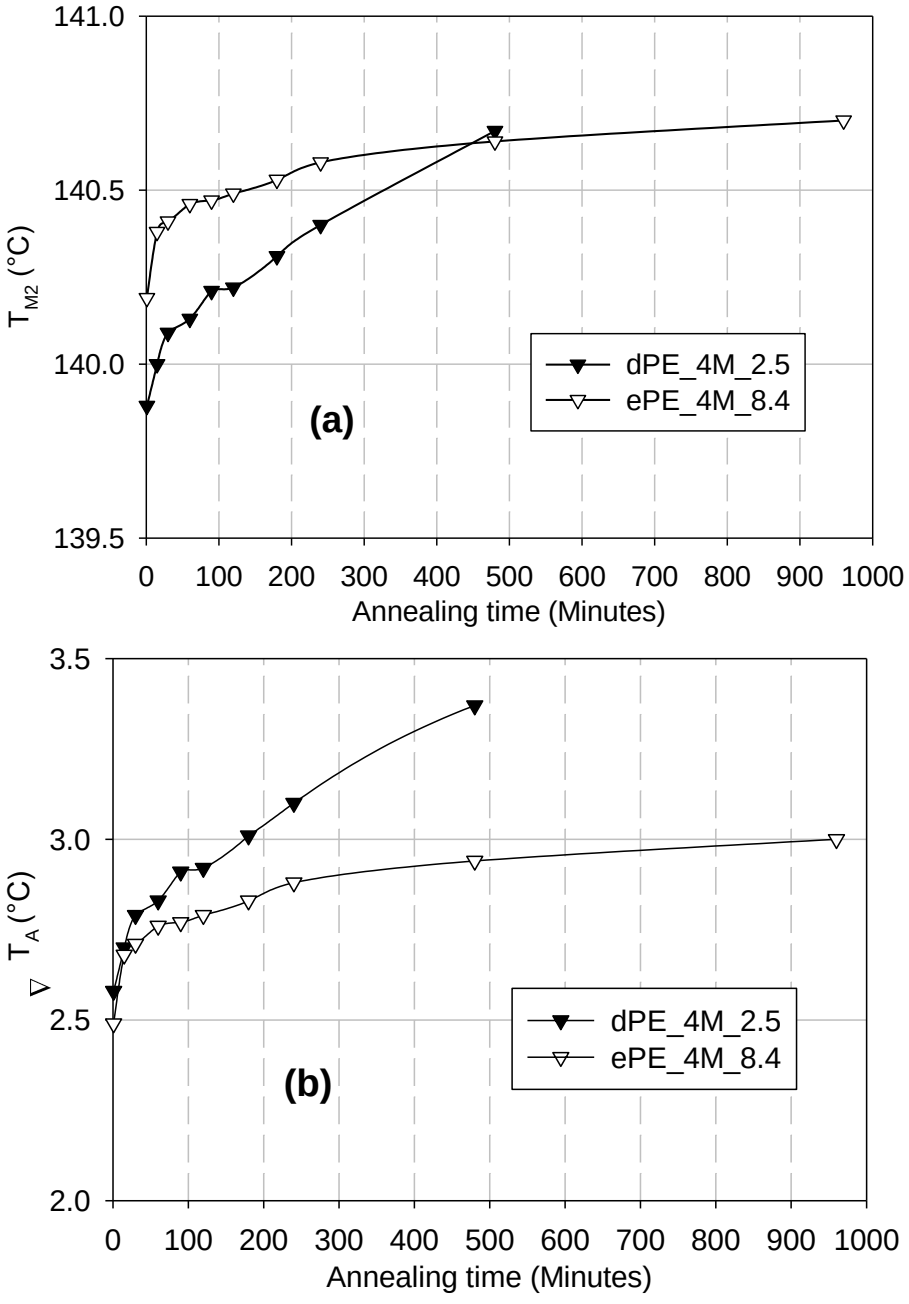

Figure 4.14. Increase in (a) the peak melting temperature of the remainder of nascent sample, T_{M2} and (b) the difference between T_{M2} and respective ($T_M^{\beta=0.05}$- 2)°C, ΔT_A, for the synthesised nascent disentangled (closed symbols) and the commercially available entangled UHMw-PE (open symbols) samples at different annealing times.

4.3.2.2 Effect of Mw on annealing of nascent disentangled UHMw-PE, below peak melting temperature ($T_M^{\beta=0.05} - 2$)

From the data comprised in Figure 4.14, it is apparent that the melting rate in the disentangled polyethylene is strongly influenced by the difference in melting temperature and annealing temperatures, ΔT_A i.e. the lower the difference the faster will be the melting rate, Figure 4.11. The possible cause of nonlinearity in the peak area A2, with increasing annealing time, is correlated with the shift in the melting temperature to higher values with annealing time, Figure 4.14. Consequence to the shift, the difference between the new melting and the annealing temperature increases, ΔT_A, resulting into a continuous decrease in the rate of melting and thus the nonlinearity. What follows is a study of the influence of molecular weight on the melting process in disentangled polyethylene.

Figure 4.15 shows the melting of nascent disentangled crystals at ($T_M^{\beta=0.05}$- 2)°C for different molecular weight samples, where $T_M^{\beta=0.05}$ is the intrinsic peak melting temperature of the chosen polymers at heating rate 0.05°C/min, as shown in Table 4.1. The Figure 4.15 shows that not only melting proceeds non-linearly with annealing time, but also the melting rate of the low Mw sample is slowest and a substantial amount of the polymer does not melt. The slowest melting rate of the lowest Mw sample appears to be counter-intuitive. However, the cause becomes apparent from Figure 4.16b which shows the highest increase in the measure of effective degree of superheating, ΔT_A. Contrary to the low molecular weight polymer, the high Mw sample melts fastest and shows the lowest increase in the degree of superheating, Figure 4.15. It becomes apparent that re-organisation during melting (annealing) has an important role which governs the melting rate of the nascent disentangled crystals. Though all Mw samples have been annealed at ($T_M^{\beta=0.05}$- 2)°C, the fastest increase in the degree of superheating in the lowest Mw sample suggests a fast crystal perfectioning/thickening by re-organisation. The faster re-organisation in the low Mw sample is associated with easier and faster co-operative motions in the smaller crystallites. Also, as the melting proceeds from side surface, causing shrinkage of the crystal size, the crystal becomes thicker towards the centre (increasing T_{M2}).

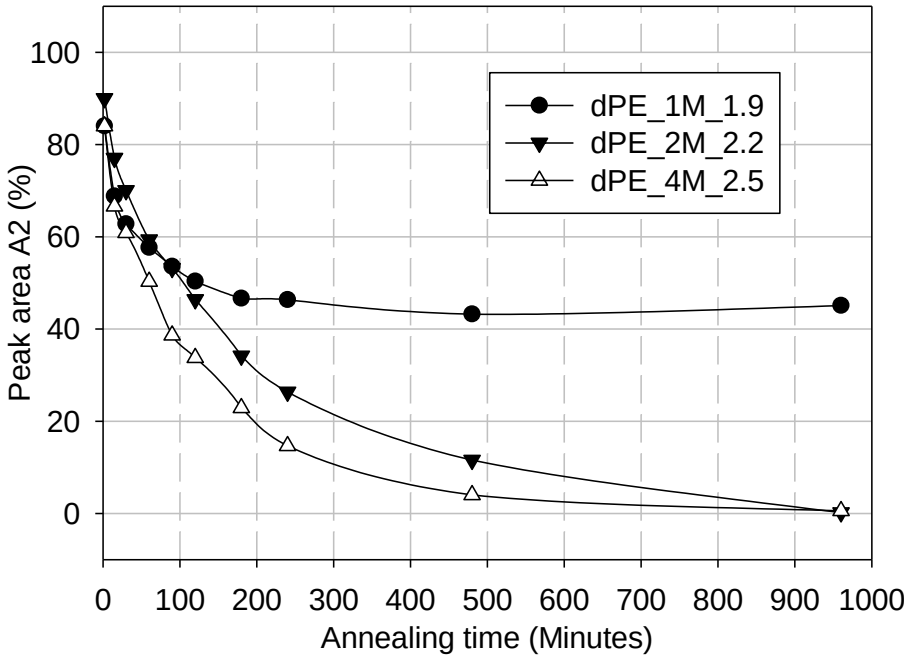

Figure 4.15. Decrease in the area A2 of nascent disentangled polyethylenes having different molecular weights. The samples were annealed at their respective ($T_M^{\beta=0.05}$ - 2)°C temperatures for different times.

To avoid the effect of crystal perfectioning/thickening on melting, Toda *et al. [77]* annealed the single crystals for a considerable time. These authors conclusively showed a linear decrease in the crystal length with increasing annealing time. In the nascent disentangled polyethylene investigated in this work, crystal perfectioning/thickening could not be decoupled from the simultaneous melting process. However, a linear decrease in the melting temperature at shorter annealing times (<60 minutes), Figure 4.17, is in accordance with the observations reported on single crystals by Toda *et al. [77]*. The parallel in melting between single crystal and a nascent disentangled polymer reinforces the concept of successive chain detachment and their reeling into the polymer melt. The non-linearity in melting can be corrected by considering the dynamics involved in the shift of ΔT_A with annealing time. However, such a correction is experimentally not feasible in nascent disentangled polyethylene as the melting process is coupled with the crystal perfectioning at the chosen annealing temperature.

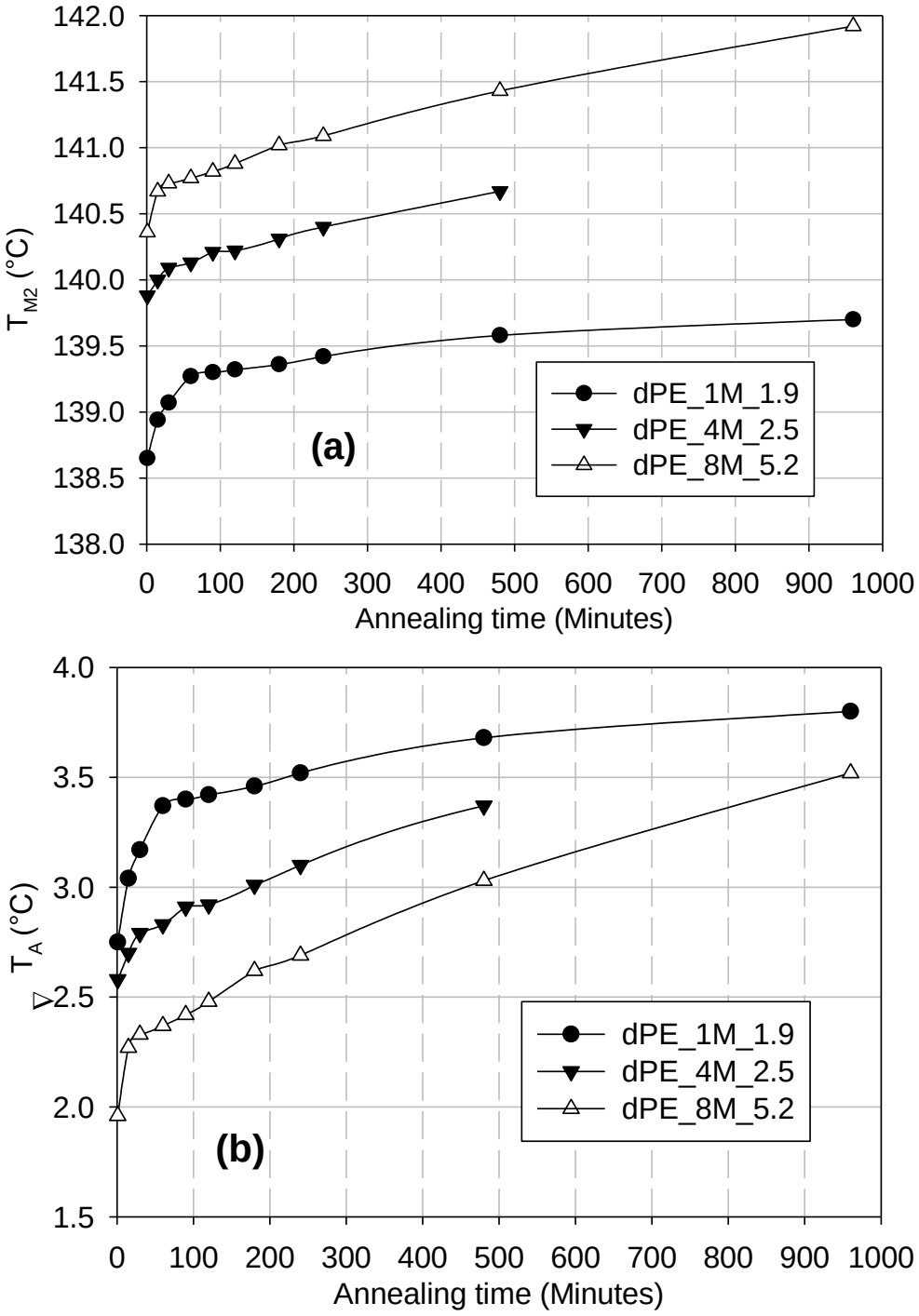

Figure 4.16. Increase in (a) the peak melting temperature of the remainder of nascent sample, T_{M2} and (b) the difference between T_{M2} and the respective ($T_M^{\beta=0.05}$- 2)°C, ΔT_A, with annealing time of the nascent disentangled UHMw-PEs having different molecular weights.

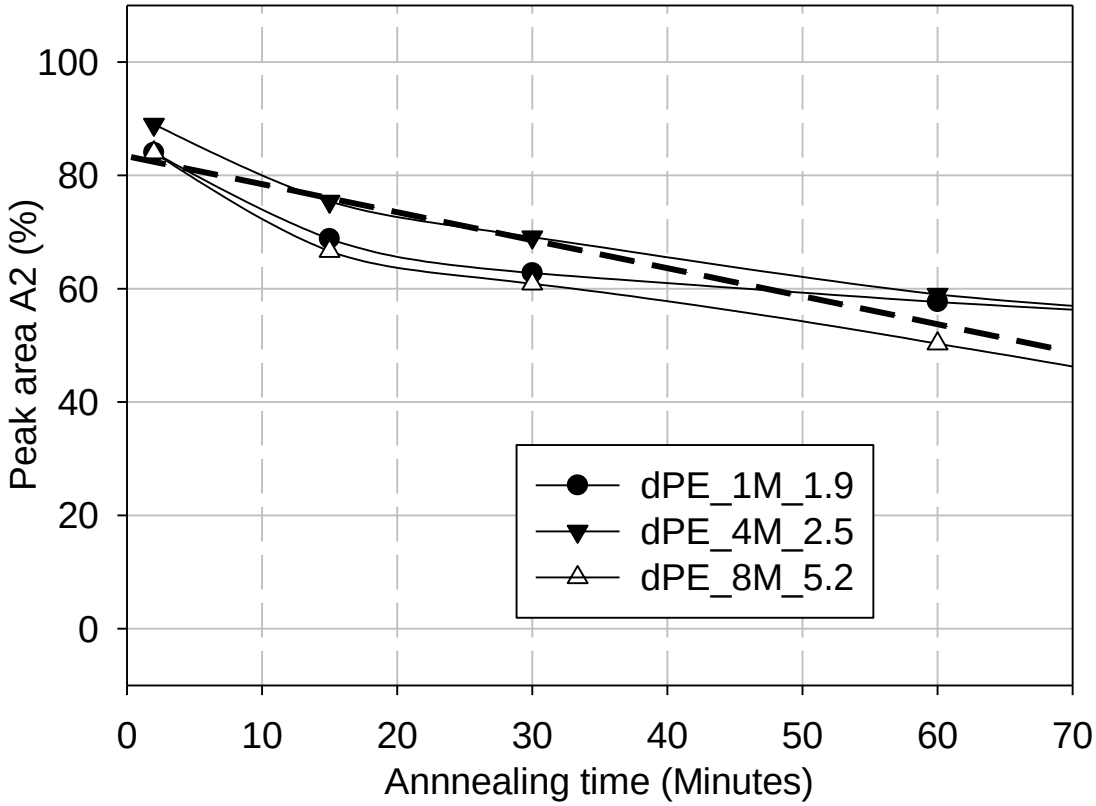

Figure 4.17. Decrease in the area A2 of the different nascent disentangled polyethylenes having different molecular weights for the lower annealing times (<60 minutes) at ($T_M^{\beta=0.05}$ - 2)°C.

4.3.3 Annealing disentangled UHMw-PE above the peak melting temperature:

4.3.3.1 Effect of annealing time in melt on on-set crystallisation temperature

Figure 4.18 shows the thermograms for the melting and cooling at a heating rate of 1°C/min for a disentangled sample dPE_1M_1.9. In Figure 4.18a, the peak melting temperature (T_M) in the first heating step is higher than in the second heating step. This is normally the case for the nascent samples (reactor powder). The differences in melting temperature of the first (nascent) and second (melt-crystallised) steps for the same polymer are caused by the topological difference in the amorphous region, as discussed in previous sections.

In Figure 4.18a, the sample was annealed at 160°C for 2 hours (step F to G section 3.2.2.3) before re-crystallising for the second melting. It can be seen that the on-set crystallisation temperature (T_C) in the second cooling step is lower than the first cooling step, and is associated with the increase in the number of

entanglements during the annealing after the first melting. Remember, similar observations have been made by studying the on-set crystallisation temperature, in chapter 2, using rheology. The on-set crystallisation temperature during the second cooling further decreases with the increasing annealing times (18 hours) in the melt, Figure 4.18b. The further decrease in T_C in Figure 4.18b is associated with further entanglement formation due to the longer annealing time of 18 hours in the melt. It is important to note that the samples were heated to 190°C (isothermal 5 minutes) after each melting to avoid any crystal memory effect.

Figure 4.18c shows the effect of annealing on a melt crystallised sample obtained after annealing the sample in the rheometer at 160°C for 18 hours, giving a fully entangled sample of dPE_1M_1.9. Even though the melt reaches the thermodynamically stable state in 5-6 hours at 160°C, the sample was annealed in the rheometer for 18 hours at 160°C to ensure a fully entangled melt. This fully entangled sample was removed from rheometer after cooling to obtain a melt crystallised sample of dPE_1M_1.9. For this fully entangled melt-crystallised sample, the first melting peak temperature can be seen to be much lower than the nascent sample. In Figure 4.18c, T_C is the same in the first and second cooling step for a fully entangled sample even after annealing for 2 hours at 160°C. T_C is also the same in the second cooling step in Figure 4.18b and Figure 4.18c where crystallisation proceeds from a fully entangled melt. Annealing for 2 hours in an already fully entangled sample does not bring any further increase in number of entanglements and hence T_C remains the same in both the cooling steps, Figure 4.18c. Decreasing on-set crystallisation temperature with the increasing annealing time (increasing entanglement) also supports the observations from the rheological data in chapter 2 on the increase of entanglements in the modulus build-up tests at 160°C and it follows a similar time scale.

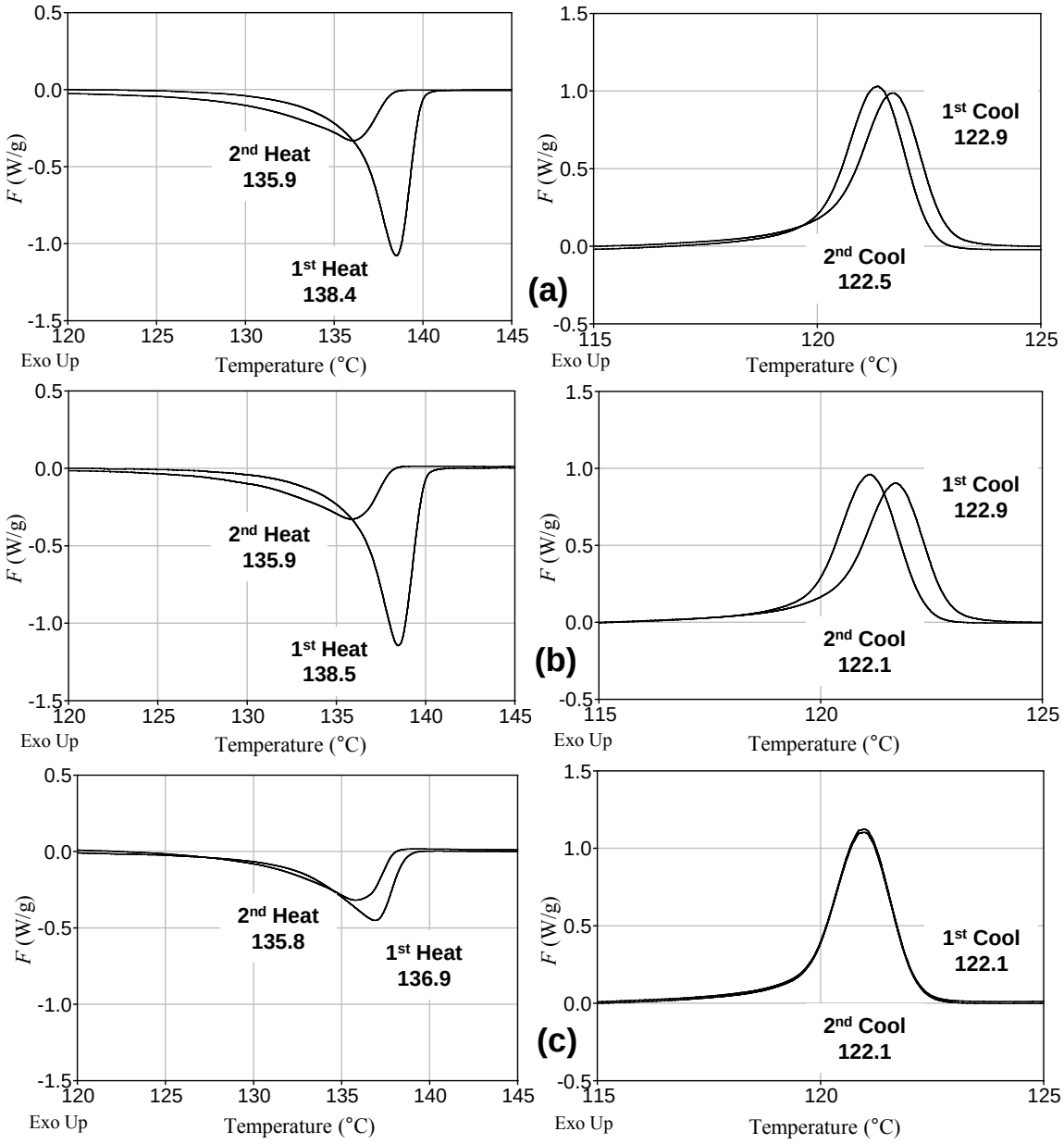

Figure 4.18. Heating and cooling steps for a nascent disentangled sample dPE_1M_1.9 at a heating rate of 1°C/min for varying annealing times at 160°C (step F to G section 3.2.2.3); (a) annealing time = 120 minutes, (b) annealing time = 18 hours and (c) annealing time = 120 minutes for a fully entangled sample obtained after a modulus build-up test of 18 hours at 160°C in the rheometer. Samples have been heated to 190°C to avoid any crystal memory effect.

A further effect of molecular weight and annealing temperature on the on-set crystallisation temperature is explored in next section.

4.3.3.2 Effect of Mw on on-set of crystallisation after annealing at different temperature for various annealing times in melt

Figure 4.19 shows a decrease in the on-set crystallisation temperature (Tc) of synthesised disentangled UHMw-PEs, after annealing at different temperature (in the melt) for varying times, having different Mw. The on-set crystallisation temperature is the lower for lower molecular weight samples and decreases with increasing annealing temperature and time. In chapter 2, similar observations were made where disentangled samples were annealed (entanglement formation) for a fixed time at different temperatures in melt. It was concluded that the entanglement formation rate is dependent on the temperature of annealing upto 160°C. Similarly, the difference in the on-set crystallisation temperature for samples annealed at different annealing temperature (145°C and 160°C) can also be seen in DSC experiments, Figure 4.19a and Figure 4.19b. The difference in Tc is associated with the number of entanglements present in the melt. A melt having a lower number of entanglements (for same Mw and MWD) will have an on-set of crystallisation at a higher temperature. A similar observation of decreasing on-set crystallisation with increasing annealing time in disentangled UHMw-PE has been made by Lippits *et al.* [*17*].

The decrease in Tc is lower for higher Mw samples for the same annealing temperature and time, Figure 4.19a and Figure 4.19b. However, for the same sample, the decrease in Tc annealed at 160°C is larger than that annealed at 145°C, for the same annealing time. The larger decrease in Tc during the same annealing time is due to faster entanglement formation at higher annealing temperatures. This is also independently confirmed with the rheological data presented in chapter 2 (difference in entanglement formation at different temperatures can be seen from rheology data in appendix 2). The rate of decrease of Tc with annealing time at a fixed temperature is slower for high Mw samples compared to low Mw ones due to slower entanglement formation and lower entanglement density in high Mw samples. These observations on the on-set crystallisation temperature with annealing temperature (in melt) and time using DSC, strengthen the similar observations made using rheological methods in chapter 2.

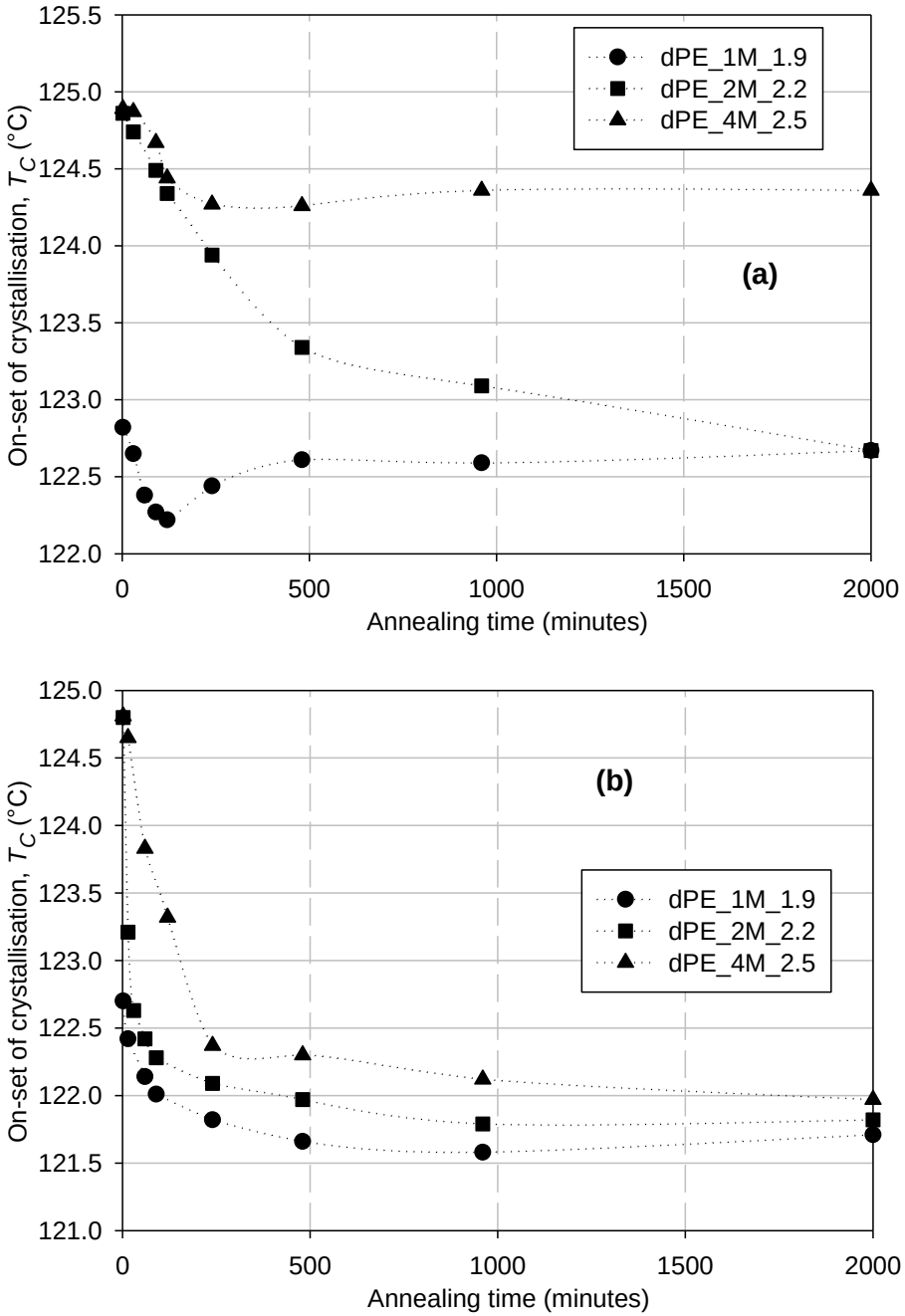

Figure 4.19. Decrease in the on-set of crystallisation (Tc) with increasing annealing time in the melt at (a) 140°C and (b) 160°C for the synthesised disentangled samples of various Mw.

The findings reported above by conventional DSC are further strengthened by modulated DSC. TM-DSC studies were performed to observe the effect of molecular weight on the melting rate of the nascent disentangled UHMw-PE. Further, the differences in the melting behaviour between the nascent and melt-crystallised morphologies of the disentangled UHMw-PE samples have been also studied.

4.3.4 Characteristic melting time of crystals by TM-DSC:

4.3.4.1 Characteristic melting time of nascent disentangled crystals

Characteristic melting time, τ, as defined in equation (4.3), has been calculated for nascent disentangled samples at the heating rate of 0.8°C/min. Figure 4.20 and Table 4.2 show the characteristic melting times for nascent disentangled polymers with different Mw. The characteristic melting time decreases with increasing molecular weight. The lower characteristic time for the higher Mw sample is associated with the faster solid to liquid transition of the crystals. Thus, the results summarised in Figure 4.20 suggest that the high molecular weight polymer, having the lowest characteristic time, will melt faster than the low molecular weight polyethylene.

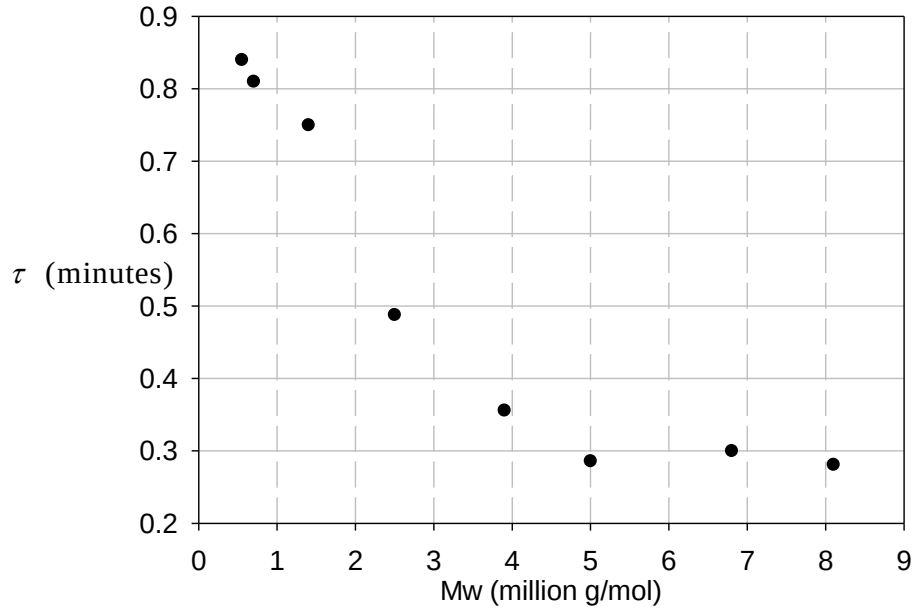

Figure 4.20. Characteristic melting time, τ, for the nascent disentangled UHMw-PEs of different molecular weights. The higher the characteristic times, slower will be the melting rate. The difference in the characteristic time is attributed to entanglement residing in the amorphous regions of the polymer.

Considering that the melting in TM-DSC is followed from the peak melting temperature, the difference in melting rates for the low and the high molecular weights may be correlated with the entangled state of the polymer i.e. the higher entanglement density in the low molecular weight polyethylene suppresses the melting rate. These observations are also in accordance with the experimental

data shown in Figure 4.10, where the higher slope of the melting temperature with heating rate, in the low molecular weight polyethylenes, was attributed to the greater number of entanglements residing in the amorphous regions of the semi-crystalline polymer. Remember, similar results of decreasing entanglement density with increasing Mw have been also observed in chapter 2 through the rheological studies of these materials.

Table 4.2. Mw, MWD and characteristic times for nascent disentangled UHMw-PEs of different molecular weights.

Sample	Mw (million g/mol)	MWD	τ (minutes) (first melting)
1	0.6	1.6	0.84
2	0.7	1.7	0.81
3	1.4	1.9	0.75
4	2.5	2.2	0.49
5	3.9	2.5	0.36
6	5.0	2.4	0.29
7	6.8	2.4	0.30
8	8.1	5.2	0.28

Further, the study of characteristic melting time was judiciously extended to the annealing of the disentangled nascent samples, to follow the effect of increasing entanglement in a melt-crystallised sample on the characteristic melting time.

4.3.4.2 Characteristic melting time with increasing annealing time in melt

Figure 4.21 shows two characteristic melting times calculated for nascent disentangled samples dPE_2M_2.2 at the heating rate of 0.8°C/min. Also see table Table 4.3. τ_n and τ_m are the characteristic melting times during the first and second melting of the same sample, respectively. In the first melting step, τ_n, characterises the melting of the nascent disentangled crystals whereas during the second melting step, τ_m, representing the melting of melt-crystallised material in the same sample (recrystallising from the melt at 155°C for various annealing times). From Table 4.3, it can be seen that τ_n (melting of the nascent crystals) is the same in all the DSC runs for the sample dPE_2M_2.2, and also confirms the

reproducibility over different runs. It can also be seen at the lower annealing time, that τ_m is higher than τ_n, which suggests that an increase in the number of entanglement increases the characteristic melting time, Table 4.3. However, τ_m (melting of the melt-crystallised samples) reduces with increasing annealing time to reach finally a constant value at higher annealing time. As the morphology (entanglement in the amorphous region) of the melt-crystallised sample increases with increasing annealing time due to the formation of entanglements, τ_m decreases. This is counter to an earlier observation of increase in the characteristic melting time from nascent to melt-crystallised morphology at lower annealing time (increased entanglements in amorphous region). Due to topological differences in the amorphous regions between the nascent and melt-crystallised morphologies of the sample, characteristic times cannot be directly compared.

Table 4.3. Characteristic times of the nascent (τ_n) and the melt-crystallised (τ_m) for the disentangled sample dPE_2M_2.2 at various annealing times at 155°C.

Time (minutes)	τ_n (minutes) (first melting)	τ_m (minutes) (second melting)
2	0.49	0.57
30	0.50	0.50
60	0.48	0.45
120	0.49	0.44
240	0.48	0.39
480	0.48	0.37
960	0.50	0.38
2000	0.49	0.37

In melt-crystallised samples annealed for the longest time, as the number of entanglements increases in the melt with increasing annealing time, upon re-crystallisation at a constant cooling rate will have higher number of entanglements present in amorphous region. Melt-crystallised samples annealed for longer times will have a morphology where a larger number of chains participate in formation of many crystallites. The decrease in the characteristic melting time is associated with the increasing number of entanglement in the

amorphous region (or the decrease in bulk crystallinity) in the melt-crystallised morphology. The similar time scale of decrease in τ_m with annealing time compared to entanglement formation observed using rheology is intriguing. See Figures 4.21 and 4.22. Although, here some preliminary relationships between the characteristic melting time and the morphology are highlighted, a more detailed study will be required to gain a clear insight.

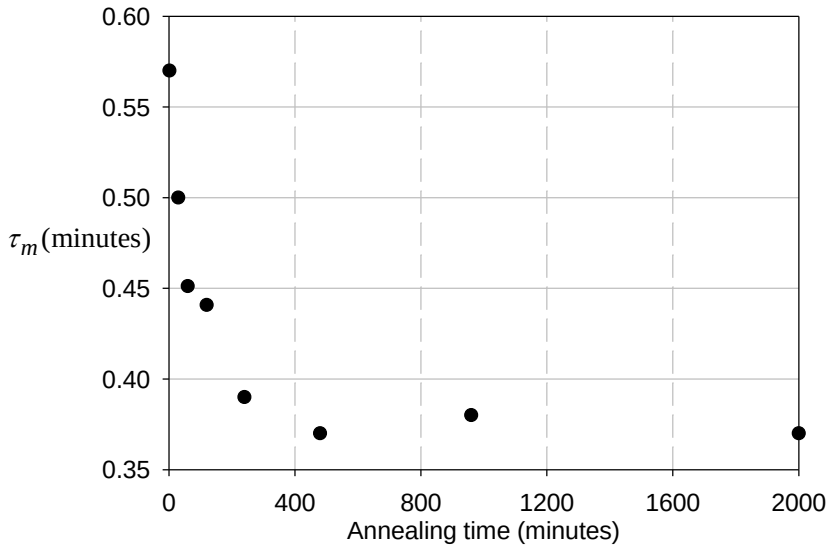

Figure 4.21. Characteristic melting time for the melt-crystallised sample (τ_m) of dPE_2M_2.2 recrystallised after annealing for various times at 155°C.

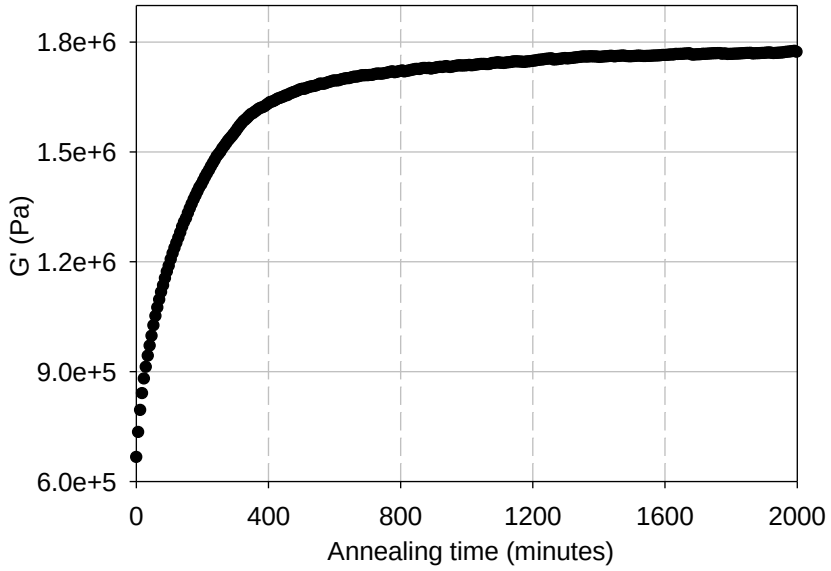

Figure 4.22. Entanglement formation (modulus build-up) in the disentangled sample dPE_2M_2.2 at the frequency of 10 rad/s, a strain of 0.5% and at 160°C. The modulus build-up with increasing time results from the increasing entanglement of the system.

4.4 Summary

One of the salient conclusions from this chapter is that the melting of the crystalline component in these semi-crystalline polymers is not only dependent on the crystal thickness, but also on the topological constraints residing in the amorphous region of the polymer. This finding, having implications for the melting of polymers in general, has been strengthened by making a judicious choice of a series of disentangled polyethylenes with varying molecular weight, where except for the polymerisation time, other polymerisation conditions such as the catalyst, the catalyst concentration, the solvent used, the temperature and the pressure are the same.

Experimental findings as a function of heating rate and topological constraints are summarised in a schematic drawing shown in Figure 4.23. The observations from the chapter are as follows.

- The mechanism involved in the melting behaviour of disentangled and entangled polymers changes with the heating rate, Figures 4.7, 4.8 and 4.9. For example, the two discrete non-linear dependences in nascent disentangled polymer are associated with a) melting by the successive detachment of chain stems from the crystal surface at low heating rates (<1°C/min), and b) cluster melting at the higher heating rates (>1°C/min), where the melting can proceed not only from the surface but also from the crystalline core.
- The discrete change in slope with heating rate (below and above 1°C/min) suggests a difference in the mechanism involved in crystal melting, where the number of chain segments involved in the melting process also increases with increasing heating rate (see Figures 4.7, 4.8 and 4.10).
- The melting process in the semi-crystalline crystals is driven kinetically and can be easily observed by annealing the samples below their peak melting temperatures, Figures 4.11, 4.12, 4.13 and 4.15.
- In the nascent disentangled polymer, two different nonlinear logarithmic heating rate dependences of the peak melting temperature was observed, whereas the nascent entangled sample showed only one nonlinear logarithmic heating rate dependence (see Figures 4.7, 4.8 and 4.10).
- In the nascent entangled polymer at low heating rates (<1°C/min), melting by successive detachment of the chain stems is not feasible as the same chain is

shared among many crystallites and demands co-operative conformational transformation at larger length scales. Thus, the requisite of simultaneous surface and cluster melting requires higher melting temperatures compared to the nascent disentangled polymer, Figure 4.7. The concept is shown schematically in Figure 4.23b.

- The melt-crystallised sample of the nascent polymers melts at a lower temperature closer to that predicted by the conventional Gibbs-Thomson equation. The lower melting temperature is due to the absence of re-entrant chains that do not require cooperative conformational transformation between the neighbouring chains. Hence, no heating rate dependence on the melting temperature is observed below 1°C/min. However, at higher heating rates (>1°C/min) where melting can occur in clusters, the heating rate dependence in arises because of cluster melting at different length scales (Figure 4.8, and schematically shown in Figure 4.23c). These findings at low heating rates are in contradiction to the melting behaviour observed in the nascent disentangled and entangled polyethylenes.
- The slope for the heating rate dependence of peak melting temperature increases with a) increasing entanglement density in the amorphous region, and b) with the increasing number of shared chains among many crystallites, Figures 4.7, 4.8, 4.9 and 4.10.
- The annealing of the nascent disentangled samples below the peak melting temperature confirms that the synthesised UHMw-PE have close to mono-molecular single crystals, which upon annealing melt from the side surfaces by the successive detachment of chain stems. These findings are in agreement with the studies performed by Toda *et al. [77]* on single polyethylene crystals and are in accordance with the studies at low heating rate, <1°C/min.
- However, the melting of chain folded nascent crystals in the vicinity and below their peak melting temperature is complicated by the simultaneous process of crystal perfectioning through re-organisation. The reorganisation process shifts the peak melting temperature to higher values and increases the measure of the degree of superheating, which is characterised by ΔT_A (= melting temperature – annealing temperature). The increase suppresses the melting process via the

successive detachment of chain stems from the crystal surface, and their reeling into the melt.

- Melting temperature of disentangled UHMw-PE polymer increases with increasing molecular weight.
- The characteristic melting time, τ, in the nascent disentangled samples, decreases with increasing molecular weights due to the lower entanglement density in the amorphous region of higher Mw samples, Figure 4.20.
- However, in the melt-crystallised samples, the characteristic melting time decreases with increasing entanglement in the amorphous region, Figure 4.21.

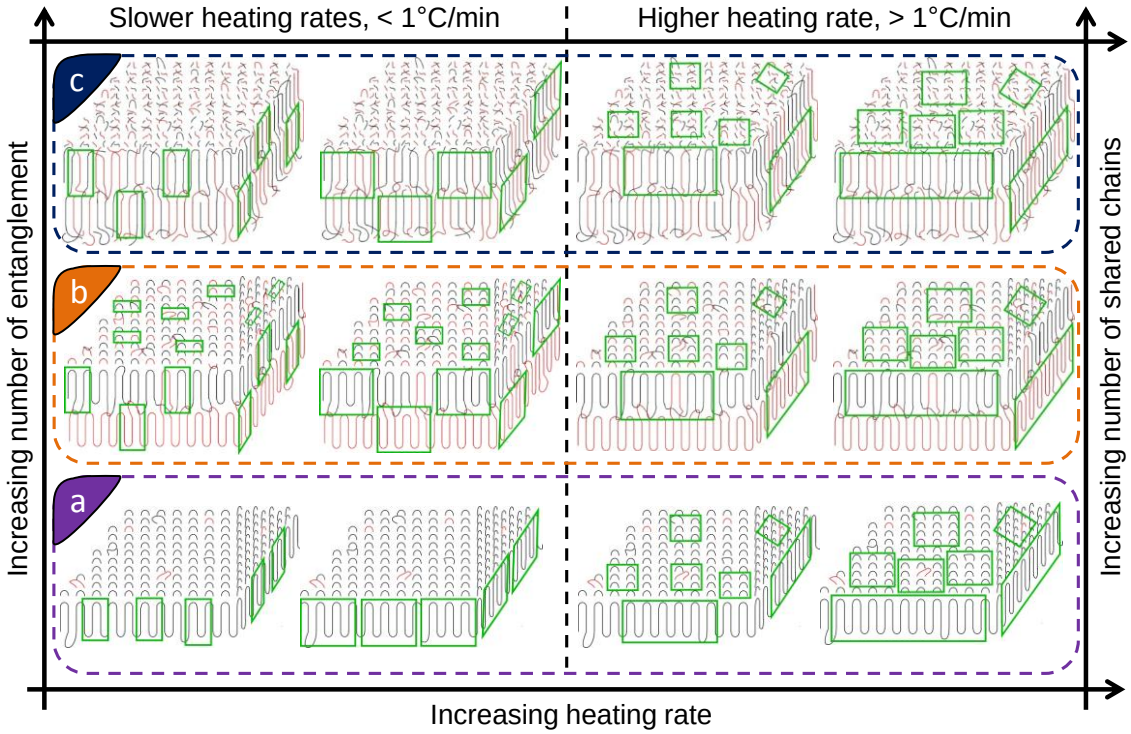

Figure 4.23. Schematic representation of melting at different heating rates for (a) nascent disentangled, (b) nascent entangled and (c) melt-crystallised morphology of UHMw-PE. Figure also shows the increasing number of entanglements in the amorphous phase of the crystals and the number of chains shared in the formation of several crystallites, which affects the peak melting temperature and the heating rate dependence. Note: crystallites are shown in stacked for the ease of representation (amorphous topology and sharing of chains). However, they may be randomly distributed and may not be stacked as seen in Figure 4.5. Green boxes represent increasing length scale during melting (number of methylene units involved) with increasing heating rate, which controls the peak melting temperature and its dependence on heating rate.

Conclusions

The effect of entanglements on polymer melt dynamics and melting kinetics have been studied by judiciously selecting disentangled ultra-high molecular weight polyethylene (UHMw-PE) samples synthesised using a homogeneous catalytic system. The number of entanglements and their distribution varies with polymerisation time (molecular weight) and temperature, and serves well as a model system to understand the effect of entanglement on melt-dynamics, melting and crystallisation. UHMw-PE also provides an opportunity to follow entanglement formation comfortably within the time scale of the experimental techniques used due to large number of entanglements involved (> 400-500) and the relatively slow dynamics of this system. Although, most of the studies performed in this thesis are on UHMw-PE samples; many of the results and the understanding developed from the work can be extended and applied to polymers in general. Some of the salient conclusions from this work on many aspects of entanglement effect in polymers physics are as follow.

1. Entanglement formation and its heterogeneous distribution during the synthesis of disentangled polymer

The effective use of melt rheology as a tool to qualitatively assess entangled state in nascent polymers is well established. Entanglement formation takes place by mixing of chains on the transformation of crystal into random coil state referred as region R1. Whereas in region R2 entanglement formation proceeds via chain reptation. The entanglement formation rate in regions R1 and R2 is dependent on the temperature at which experiments are performed. For example, at a temperature 15°C higher than the equilibrium melting temperature for linear polyethylene, the entanglement formation rate shows a strong dependence on the experimental temperature, whereas the temperature dependence of entanglement formation decreases when the experiments are performed above 160°C. These findings are depicted in chapter 2 and in the appendix of this thesis. The entanglement formation rate shows a molecular weight dependence

and is faster for disentangled polymers synthesised at lower polymerisation times (lower molecular weights). Total entanglement build-up time scales as $Mw^{\sim 2.6}$.

One of the important findings is that entanglement formation and its distribution along the chain length, which in turn controls the morphology of the sample, continues after the initiation of the chain growth and depends on the polymerisation conditions. Entanglement distribution along the entire chain length in a synthesised disentangled UHMw-PE sample is heterogeneous where the maximum density resides along the part of the chain produced during the initial stages of polymerisation. For the same polymerisation conditions, with time the crystallisation rate is anticipated to gain upper hand over the polymerisation rate because of (a) the suppression in the nucleation barrier due to crystallisation of chains synthesised at the earlier stages, (b) the decrease in the catalyst activity due to growing difficulty in diffusion of ethylene to the active centre, and (c) the decrease in the temperature difference at the catalyst and its surroundings due to exothermic polymerisation.

Experimental findings on entanglement formation and distribution as function of polymerisation conditions are summarised in Figure 2.21.

2. Non-linear rheology behaviour of UHMw-PE and the effect of entanglement

One of the prominent findings from the study of the non-linear melt rheology is that the polymer melt shows a G" peak in a Large Amplitude Oscillatory Shear (LAOS) experiment, which is a signature of glassy (metastable) systems. The G" peak in LAOS is also confirmed in polystyrene samples having narrow and broad polydispersities (see Appendix 5). This finding suggests that the G" peak in a LAOS experiment is universal and in case of polymer melts can arise due to convective constraint release (CCR) under high deformation. In CCR, constraints on chains due to entanglement are removed because of the high shears, which can create chains with different Rouse chain lengths having different relaxation times. Removal of entanglements "on the fly" due to high flow involved may be associated to the G" peak in LAOS experiments. In case of disentangled UHMw-PE, the G" peak diffuses (finally disappearing) with increasing number of entanglements (with increasing annealing time) and can be associated with

increasing difficulty in the removal of entanglements (disengagement) under similar high flow.

The G" peak is only observed in the frequency range of the G' plateau and the G" minima in a frequency sweep experiment. The Intensity of the G" peak also depends upon the experimental frequency and it decreases with decreasing or increasing frequency away from the G' plateau and the G" minima. The linear viscoelastic regime also increases with increasing entanglement. Large shear deformation causes disengagement of the chains in a disentangled UHMw-PE melt, and the continuous application of shear in region R1 can hinder entanglement formation. The drop in viscosity, arising from the disengagement of chains and their existence in a non-equilibrium state for longer time, may facilitate the processing of the disentangled UHMw-PE polymer. Experimental observations on LAOS behaviour as a function of entanglement in a polymer melt is summarised in a schematic drawing shown in Figure 3.14.

Although, the G" peak in the non-linear behaviour in polymer melts, similar to the glassy systems are very exciting results. However, for a precise understanding of molecular characteristics responsible for such a non-linear behaviour in polymer melts, using molecular theories are highly desirable.

3. Effect of entanglements residing in the amorphous region on the melting behaviour of semi-crystalline polymers

One of the main conclusions from the melting study of nascent disentangled, nascent entangled and melt-crystallised samples of UHMw-PE is that the melting of crystalline component is not only dependent on the crystal thickness, but also on topological constraints residing in the amorphous region of the polymer. The conventional Gibbs-Thomson equation cannot describe different melting temperatures for crystals of similar thickness. The non-linear heating rate dependence on melting temperature is due to the number of chain segments involved in melting process which increases with the increasing heating rate. Nascent disentangled polymers show two discrete non-linear dependences of melting temperature on the heating rate; associated with (a) the melting by successive detachment of chain stems from the crystal surface at low heating rates and (b) cluster melting at higher heating rates. In the latter, melting

can proceed not only from the surface, but also from the crystalline core. Nascent entangled samples shows only one non-linear heating rate dependence because melting by successive detachment of the chain stems is not feasible as the same chain is shared among many crystallites which demands co-operative conformational transformation at larger length scales by the simultaneous surface and cluster melting requiring a higher melting temperature compared to the nascent disentangled polymers.

The melt-crystallised sample of the nascent polymers melts at lower temperature closer to the predicted values by the conventional Gibbs-Thomson equation. The low melting temperature is due to the absence of re-entrant chains that does not require co-operative conformational transformation between the neighbouring chains. Melt-crystallised samples also do not show any heating rate dependence on the melting temperature for low heating rates. However, at higher heating rates where melting can occur in clusters, the heating rate dependence in melting arises because of cluster melting at different length scales. The slope for the heating rate dependence of the peak melting temperature increases with (a) increasing entanglement density in the amorphous region, and (b) with the increasing number of shared chains among many crystallites.

Annealing of the nascent disentangled samples below the peak melting temperature confirms that the synthesised UHMw-PEs are close to mono-molecular single crystals, which upon annealing (very slow heating rates) melt from side surfaces by the successive detachment of chain stems. However, the melting of chain folded nascent crystals gets complicated by the simultaneous process of crystal perfectioning through re-organisation. The increase in crystal thickness (by perfectioning), while annealing under isothermal conditions, suppresses the melting process via successive detachment of chain stems from the crystal surface and the melting rate of the crystals show a non-linearity. Experimental findings from the melting study as a function of heating rate and topological constraints are summarised in a schematic drawing shown in Figure 4.23.

Future work recommendations

In this thesis, disentangled ultra-high molecular weight polyethylene (UHMw-PE) synthesised using a single-site catalytic system using controlled polymerisation conditions of low catalyst concentration and temperature was studied. The key conclusions drawn from the study on polymer dynamics, melting and crystallisation on these polymers present important insights into formation of entanglements and these effects on several aspects of polymer physics. However, there are still many aspects and areas where the study of disentangled polymers promises a great opportunity in terms of the fundamental understanding having some industrial relevance.

1. Relation between polymerisation conditions and entanglement formation

One of the important outcomes of this study is that entanglement formation and its distribution along the chain length, which in turn controls the morphology of the sample, continues after the initiation of the chain growth and depends on polymerisation conditions. By judiciously selecting samples synthesised for different polymerisation times and temperatures, it is established that entanglement formation and its distribution along the chain length is a balance between the crystallisation and polymerisation rates. However, there are also many other important parameters in polymerisation which controls the balance between the crystallisation and polymerisation rates and need to be studied further. Some of the important parameters are polymerisation pressure (monomer feed), catalyst-co-catalyst activity, the polymerisation medium (for example use of a solvent), catalyst concentration etc. The effects of these parameters on entanglement formation and distribution can be studied in the similar way using melt rheology as described in chapter 2. Extending the understanding of the polymerisation conditions on entanglement formation during polymerisation can provide ability to fine tune the optimum conditions to achieve the maximum yield

of the polymer produced while maintaining the maximum disentangled state important for processing. These studies would also help to establish the link between polymer chemistry and the physical characteristics of the synthesised polymer.

2. Effect of entanglement on non-linear rheology behaviour

Observation of the G" peak in the non-linear viscoelastic region of the polymer melt is one of the exciting features in this work. However, finding this behaviour, which is signature of colloidal-glassy systems, in a homo-polymer melt is intriguing and opens the possibility to integrate two areas of complex fluids. G" peak in polymer melts specifically appears in the frequency regime where the G' plateau and the G" minima are realised in a frequency sweep. However, a molecular explanation for the importance of this frequency regime to observe the G" peak is required. It is also important to verify, if recently developed molecular theories for polymer melt accounting for fast flows such as the Rolie Poly model can predict the G" peak in large amplitude oscillatory shear (LAOS) experiments. If current molecular theories cannot predict G" peak, then the need arises for further modifications in the theoretical models.

Recently, researchers have used non-linear rheology to characterise complex fluids by using waveform analysis and Fourier transform (FT) and stress decomposition techniques successfully. Disentangled UHMw-PE samples can serve as a model system to understand the effect of entanglement and particularly the distribution of entanglements on the non-linear behaviour can be very exciting. The effect of entanglement on stress relaxation behaviour can also be studied. Easy processability of the disentangled UHMw-PE during early annealing times after melting through a simple capillary rheometer has presented a great promise of melt-processing these otherwise intractable materials from the commercial point of view. However, by using high-shear extruders (industrial processing equipment) and process designed to take the advantage of less entanglement in disentangled melt during initial annealing time can be commercially attractive. A multi pass rheometer (MPR) can be used to study the effect of entanglement in-situ on chain orientation and relaxation under high flow.

3. Many other possibilities

One of the subtle features of disentangled polymer to be used as a model system for studying the effect of entanglement is due to change in number of entanglements or its distribution without any change in the basic molecular characteristics such as molecular weight and molecular weight distribution.

- One of the important properties of polymer materials is extensional viscosity (melt-strength), a requirement in forming, blow moulding etc. Disentangled UHMw-PE provides a unique opportunity to investigate the influence of entanglement, while avoiding a variation in molecular weight.
- An unperturbed single chain of polyethylene of molar mass 300,000 g/mole has a density of ~8.8×10^{-3} g/cm^3, whereas, bulk density of the linear polyethylene is approximately 0.96 g/cm^3. This difference in density arises due to the difference in the free volume around the chain and will decrease with increase in overlap of chains (entanglement). The increase in entanglement density with annealing time in a melt (using PVT apparatus) will not only validate the relationship, but will also provide a further insight into regions R1 and R2 of the entanglement formation.
- To gain further insight on polymer dynamics, simultaneous wide and small angle X-ray and neutron scattering (SAXS and/or SANS) studies can be performed to follow local density fluctuations with entanglement formation at different molecular length scales.
- Further, by synthesising deuterated-protonated disentangled polyethylene and following the exchange process from the crystal to the amorphous regions or vice-versa, solid-state nuclear magnetic resonance spectroscopy (NMR) can give further insights into the entangled state.

Appendices

1. Modulus build-up in the same disc of disentangled UHMw-PE after undergoing different annealing times

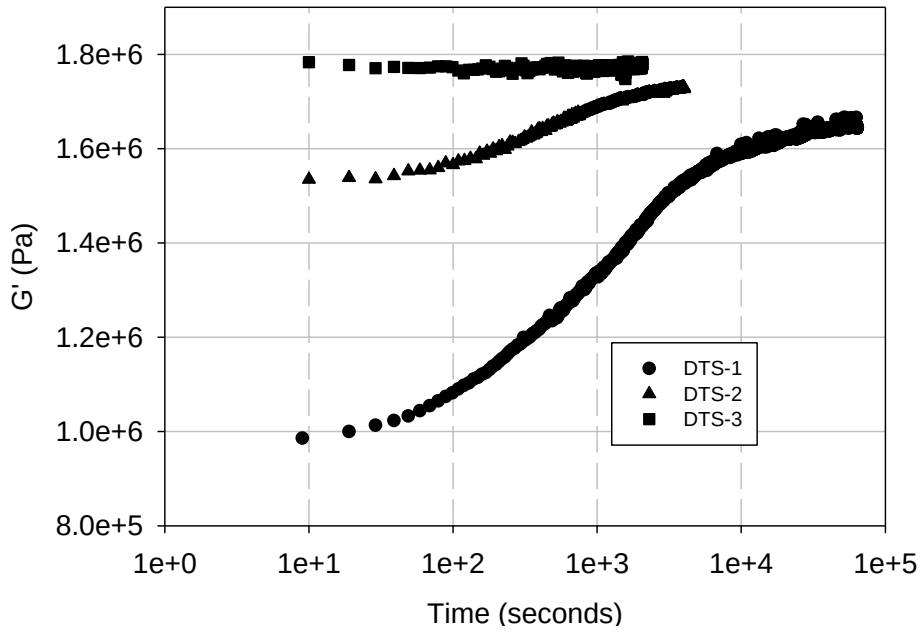

Figure A.1. Modulus build-up in synthesised disentangled UHMw-PE sample having a Mw of 2.5 million g/mol and a MWD of 2.4 at 160°C, frequency of 10 rad/s and strain 0.5% (within LVE). DTS-1, DTS-2 and DTS-3 represents repeats of modulus build up on the same sample disc after cooling and removing the sample from the rheometer and reusing to follow the modulus build up in a consecutive experiment.

Figure A.1 shows entanglement formation in the same sample disc of a nascent disentangled polymer having Mw of 1.8 million g/mol and MWD of 2.1 after keeping it for different annealing time in melt (160°C). DTS-1 experiment was performed on an initially disentangled sample to follow the entanglement formation. Entanglement formation was followed (DTS-1) for 16 hours reaching to a fully entangled (thermodynamically stable) state. At this point, the sample was

cooled (at a slow rate of 0.1°C/min) to 110°C and was removed from the rheometer after solidification. Now, this melt-crystallised sample (after undergoing fully entangled state) disc was again used to follow the entanglement formation during DTS-2. It can be seen that in DTS-2 the modulus started from a higher value compared to the previous DTS-1 test. However, the starting modulus value (1.55 MPa) in DTS-2 is lower than the final value (1.65 MPa) of modulus in DTS-1 experiment. The lowering of modulus is associated with the crystallisation (during cooling from melt at 160°C after DTS-1), bringing back some disentanglement (crystallisation is the opposite of entanglement formation) into the system, hence, lowering the starting value of modulus in DTS-2. Modulus build-up can again be seen in second DTS-2, but R1 (mixing zone) is not prominent compared to the DTS-1.

After the DTS-2 test, the sample was again cooled, but this time at the higher cooling rate of about ~30°C/min from 160°C to 110°C, after solidification sample was removed from rheometer. This solidified sample was placed again in the rheometer to follow entanglement formation in DTS-3. It can be seen that in DTS-3, the modulus (1.8 MPa) starts around the final modulus value (1.75 MPa) of DTS-2. After entanglement formation in DTS-2, cooling at a very high rate (quenching) gave a very small time for the chains to disengage (disentangle) themselves from melt; hence, nearly freezing the entangled state at the final time of DTS-2 in solid state. During DTS-3 test on the sample which possesses fully entangled state of sample from DTS-2, no modulus build up could be seen. This clearly proves the idea that the modulus build-up seen in the DTS experiments are not an artefact caused by a contact problem in the rheology experiments of UHMw-PE, and are essentially modulus build-up due to entanglement formation in the system with annealing time.

2. Modulus build-up at different annealing temperatures in melt

Figure A.2 shows entanglement formation in a synthesised disentangled sample UHMw-PE at different annealing temperatures (in the melt). The entanglement formation rate increases with increasing annealing temperature, but is more or less independent after 160°C. The increase in the entanglement

formation rate from 145°C to 160°C can be associated with increasing free volume in melt; promoting increase in diffusion of chains. To further strengthen the effect of increasing temperature on entanglement formation; samples were cooled after a fixed annealing time (~50,000 seconds) at different observation temperatures (145-200°C) and the on-set crystallisation temperatures were compared. The on-set crystallisation temperature decreases with increasing annealing temperature below 160°C and is independent of temperature above 160°C, see chapter 2.

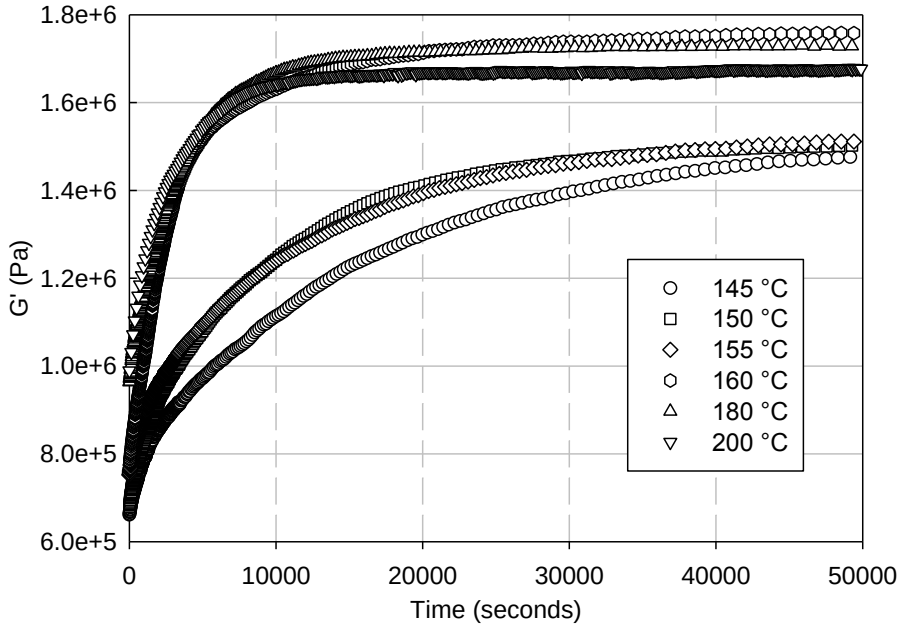

Figure A.2. Modulus build-up in the synthesised disentangled UHMw-PE sample having Mw of 2.5 million g/mol and MWD of 2.4 at different temperature (in melt), frequency of 10 rad/s and strain 0.5% (within LVE). Modulus build-up rate is slower at lower temperatures (145-155°C), but becomes independent after 160°C (the temperature chosen for all the rheological measurements in this thesis).

3. Modulus build-up during heating to the experimental temperature

Figure A.3 shows the entanglement formation during heating from 130°C to 160°C at a heating rate of 10°C/min for different Mw of synthesised disentangled UHMw-PE. The modulus decreases before the peak melting temperatures above which modulus increases with increasing temperature (time). The starting temperature of modulus build-up increases with increasing Mw as the peak

melting temperature also increases with increasing Mw. The modulus build-up rate is faster for lower Mw samples.

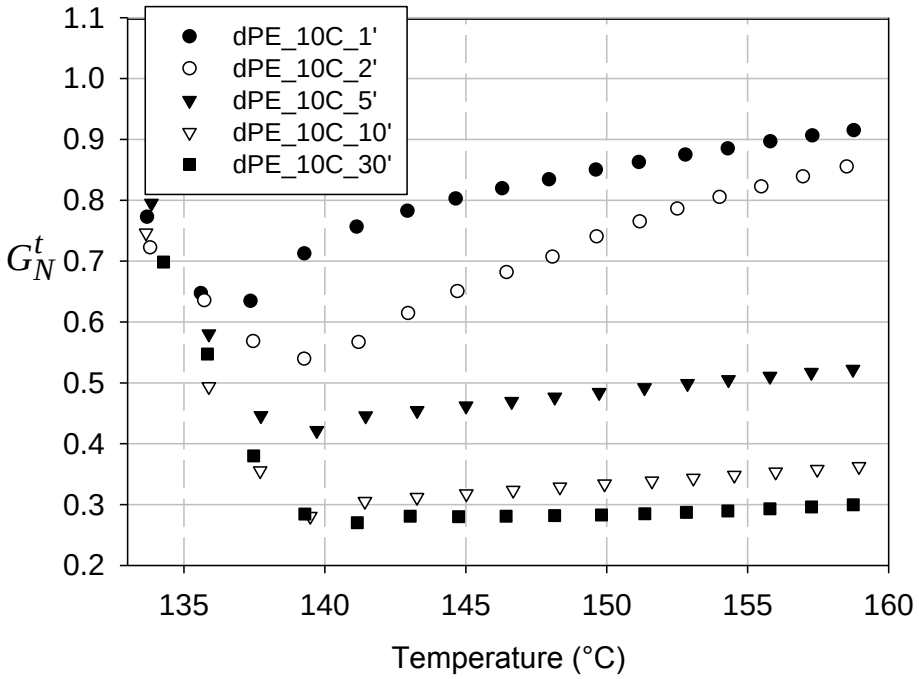

Figure A.3. Modulus build-up in synthesised disentangled UHMw-PE samples of different Mw, during heating from 130°C to 160°C at a heating rate of 10°C/min, a frequency of 10 rad/s and a strain of 0.5%. Initially the modulus decreases (below the peak melting temperature of the sample) as the sample goes from solid to melt, after melting entanglement formation starts and modulus increases gradually, where the rate of modulus increase is dependent on molar mass.

It is acknowledged that modulus build-up during heating to the observation temperature (160°C) can affect the comparison with the initial starting modulus value ($G_N^{t=0}$) at 160°C. However, in comparison to the increase in modulus build-up during annealing at the observation temperature (160°C), the differences due to modulus build-up during heating can be neglected. Modulus (G_N^t) during heating (at different temperatures) in Figure A.3 is normalised by G'_{max} , the value measured once the sample has reached 160°C. The G'_{max} should be used with precaution because the modulus will be different at different temperatures in the metastable melt. However, the normalisation is required because of a fixed chosen frequency would give different G' values for different molecular weights.

4. Intensity of higher harmonic moduli in LAOS

Figure A.4 shows the intensity of the higher harmonics and the loss modulus in a large amplitude oscillatory shear (LAOS) experiment performed at 100 rad/s on the disentangled UHMw-PE sample of Mw ~ 1.1 million g/mol and MWD ~ 1.8. The G" peak at large strains can be seen in experiments performed on two different rheometers (old ARES and new ARES-G2, TA Instruments). A large value of I_3/I_1 at smaller strain in Figure A.4a compared to Figure A.4b is due to poor signal to noise ratio in the older ARES rheometer. However, at larger strains the I_3/I_1 values are similar in both the rheometers as the signals from higher harmonic moduli overcome the contribution due to noise (mechanical and electronic noise) during the experiment. It can be also seen that the on-set of increase in I_3/I_1 shifts to higher strains with increasing annealing time (entanglement formation), similar to the shift in the G" peak. The values of I_3/I_1 were less than 0.15 in the region of G" peak, hence, the contribution from higher harmonics could be neglected *[185,210]*. All the results discussed in chapter 3 were performed on an older ARES rheometer. Experiments on a new ARES-G2 rheometer were performed in Prof. Wilhelm's laboratory at the Karlsruher Institut für Technologie (KIT), Germany for verification of the data. As the higher harmonic moduli contributions are less than 10-15% of the first harmonic and do not affect the LAOS behaviour (G" peak), dynamic moduli data directly available from the rheometer were used without any further analysis.

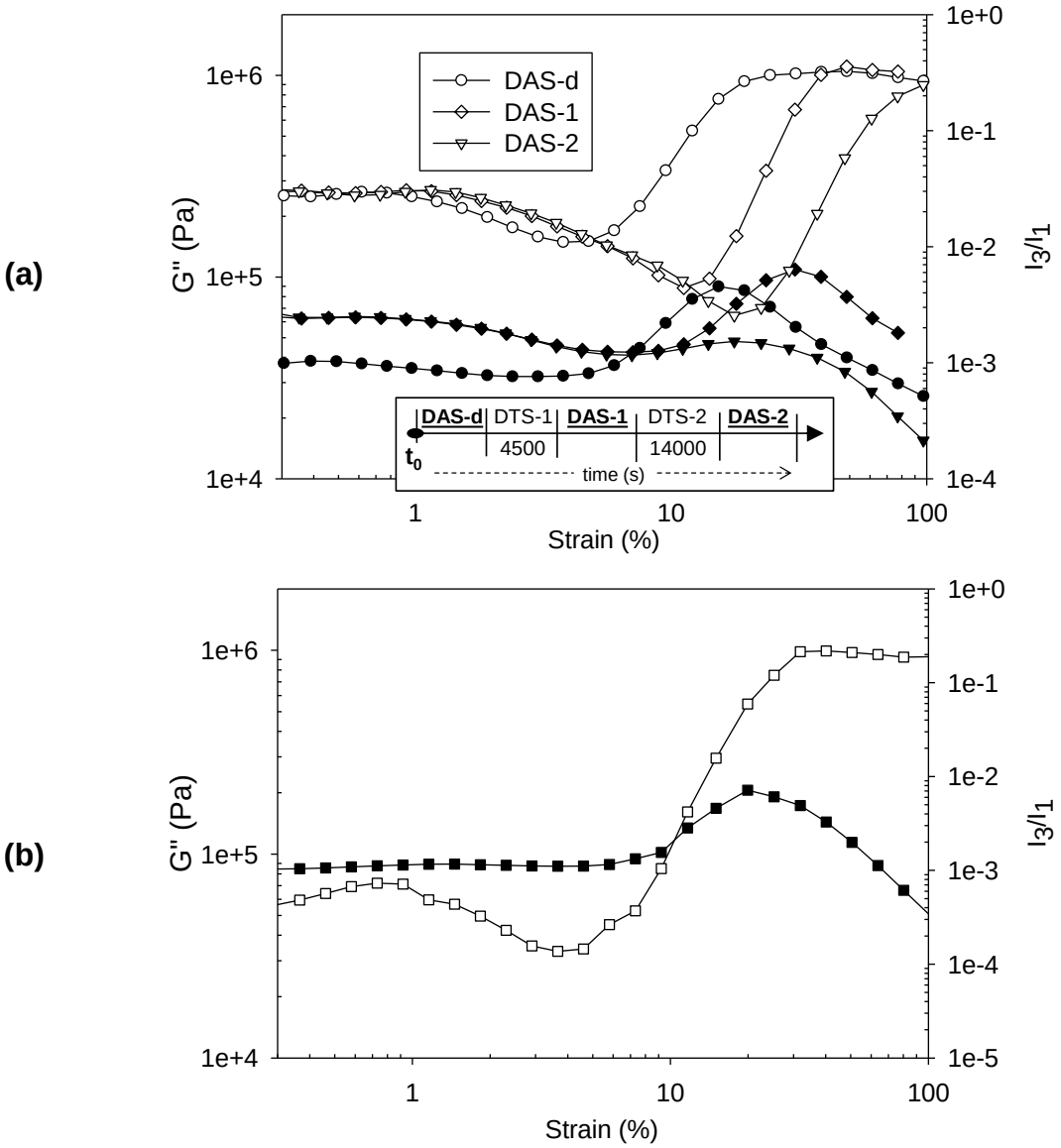

Figure A.4. Ratio of the third harmonic to the first harmonic moduli (I_3/I_1) and loss modulus (G") as a function of strain at 100 rad/s for the disentangled UHMw-PE sample of Mw ~ 1.1 million g/mol and MWD ~ 1.8. Experiments carried out on (a) ARES rheometer, older machine where the signal-to-noise ratio is high (b) ARES-G2 rheometer, newer machine with built-in FT-rheology features having a low signal-to-noise ratio. Open symbols (I_3/I_1) and closed symbols (G").

5. G" peak LAOS behaviour in high Mw polystyrene melt

Figure A. 5 and Figure A. 6 show LAOS studies on high molecular weight (Mw) polystyrene (PS) samples having Mw ~ 310,000 g/mol and MWD of ~ 1.05 and 2.1, respectively. Both PS melts show G" peak behaviour (Type-3 like) in the

LAOS similar to UHMw-PE samples studied in chapter 3. G" peak intensity is maximum (Figure A. 5a) at a frequency close to the frequency where G" minima and G' plateau appear in the frequency sweep experiments (Figure A. 5d) and decreases with frequencies away from the frequency of G" minima and G' plateau. This is strengthened by the data at higher temperature (160°C), where the G" peak intensity is lower than the G" peak at the lower temperature of 150°C for the same frequency of 5 rad/s (Figure A. 5c). The frequency range where G" peak is observed lies between the inverse of the Rouse time of the chain (τ_R) and the Rouse time for the entangled strand (τ_e). Figure A. 5b shows normalised G' in DAS at different frequencies and the onset of decrease in G' is nearly the same for all the frequencies.

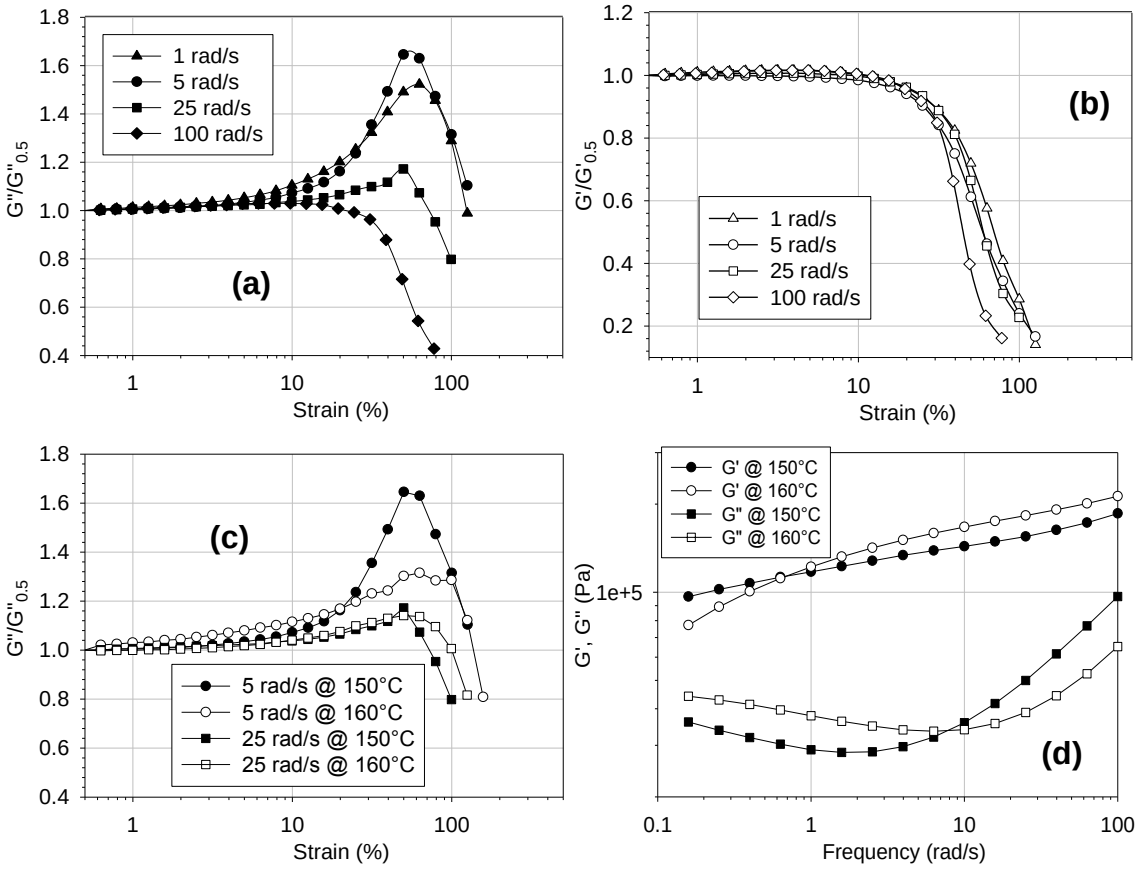

Figure A. 5. Dynamic amplitude sweep (DAS) and dynamic frequency sweep (DFS) on the polystyrene melt having Mw ~ 310,000 g/mol and MWD ~1.05. (a) Normalised G" (by G" at 0.5% strain) in DAS at 150°C for different frequencies, (b) normalised G' (by G' at 0.5% strain) in DAS at 150°C for different frequencies, (c) comparison of normalised G" in DAS between 150 and 160°C for different frequencies, and (d) frequency sweep at 150 and 160°C performed with 5% strain (within the LVE regime).

Figure A. 6 shows the G" peak behaviour in LAOS for the PS melt having the broader MWD (~ 2.1) compared to the nearly monodisperse sample shown in Figure A. 5. The broad polydisperse melt also shows similar G" peak behaviour and frequency dependence as the mono-disperse sample. However, a maximum G" peak intensity is lower than the mono-disperse sample. The G" peak in DAS experiment is associated with convective constrain release (CCR) at high strains which causes disengagement (removal of entanglements) and could be lower due to the smaller chain components (less entanglement) in a broad polydisperse sample. It should be noted that involvement of CCR in the G" peak behaviour needs to be validated by molecular theories for fast flow such as Rolie-Poly model *[215,216]*.

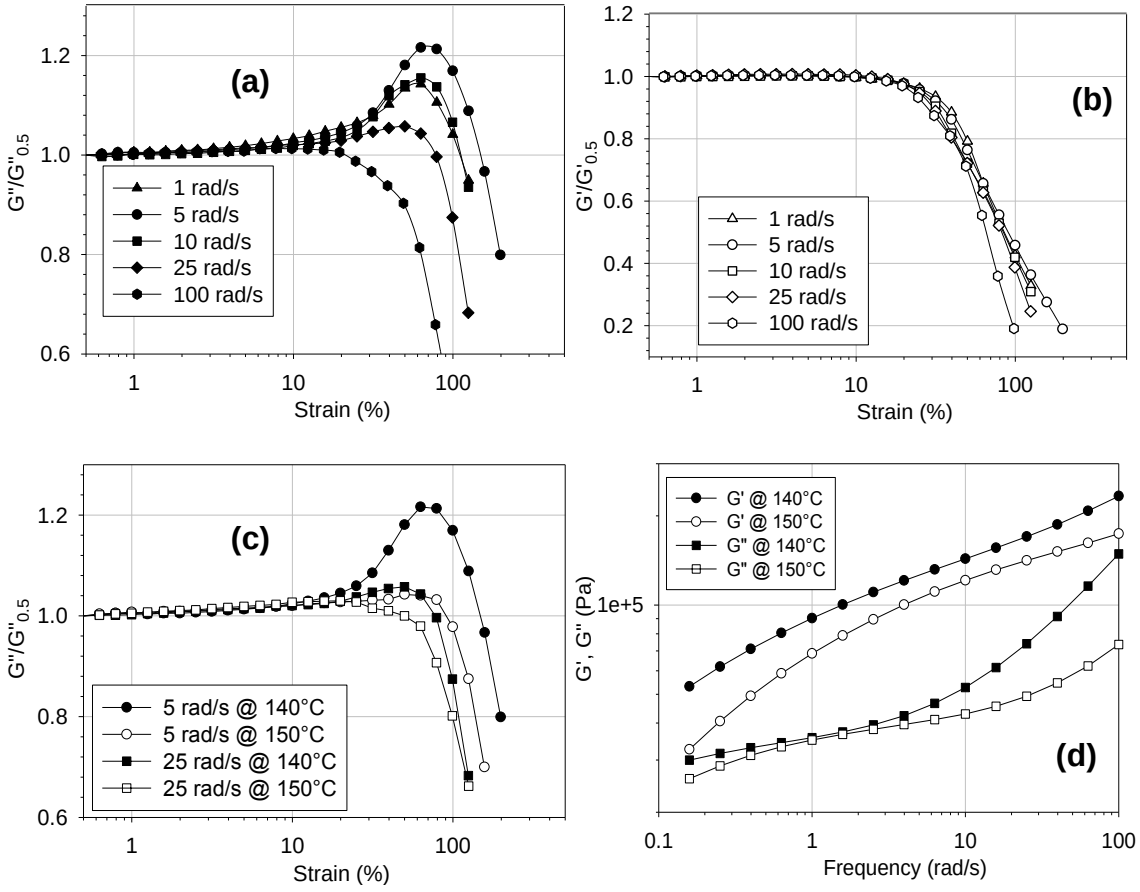

Figure A. 6. Dynamic amplitude sweep (DAS) and dynamic frequency sweep (DFS) on the polystyrene melt having Mw ~ 310,000 g/mol and MWD ~2.1. (a) Normalised G" (by G" at 0.5% strain) in DAS at 140°C for different frequencies, (b) normalised G' (by G' at 0.5% strain) in DAS at 140°C for different frequencies, (c) comparison of normalised G" in DAS between 140 and 150°C for different frequencies, and (d) frequency sweep at 140 and 150°C performed with 5% strain (within LVE regime).

6. Flow-ability of disentangled UHMw-PE (Slit MultiPass rheometer)

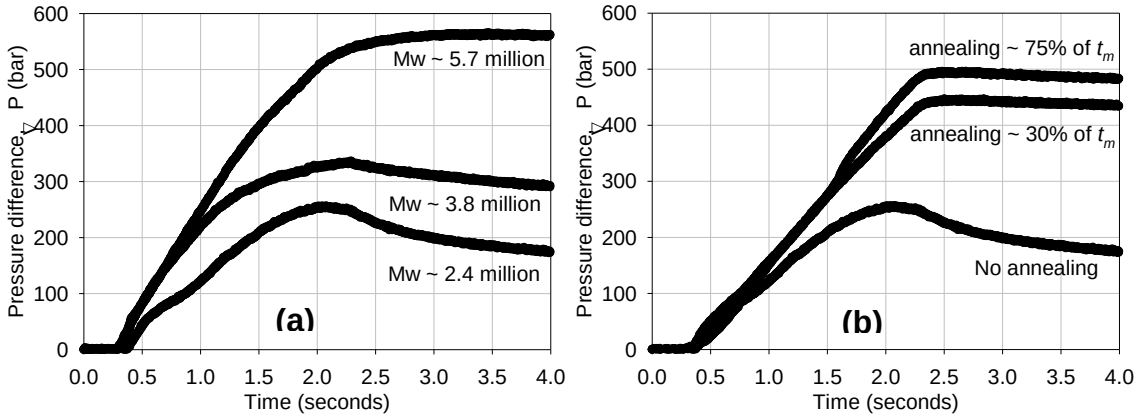

Figure A. 7. Pressure difference data from the the Slit Multi Pass rheometer (MPR) at 160°C for piston speed of 2 mm/s. (a) Pressure build up data on different molecular weight of synthesised disentangled UHMw-PE, and (b) pressure data compared for same molecular weight (2.4 million g/mol) with increasing entanglement.

Figure A. 7 shows the flow behaviour of the disentangled UHMw-PE samples in a slit MultiPass rheometer (MPR) *[240]* in collaboration with the SKT group at Eindhoven University of Technology. Figure A. 7a shows the increase in required pressure for flow of the material with increasing molecular weight. All samples were synthesised using the homogeneous catalytic system and the same polymerisation conditions, except for their polymerisation times to vary the Mw. Increase in pressure is due to the increase in viscosity (resistance in flow) of high Mw samples. The sample having a Mw ~ 2.4 million g/mol, Figure A. 7b, shows an increase in pressure with increasing entanglement density (with annealing time). The increase in pressure from the disentangled melt (without annealing) to a melt annealed for 30% of t_m (30% of total modulus build-up time) is around 1.8 times, while the increase for the melt annealed for 30% of t_m to melt annealed for 75% of t_m is small (1.1 times). The large difference in the increase from the disentangled melt to the melt at 30% of t_m, and the small difference of increase from melt at 30% of t_m to melt at 75% of t_m , is due to faster and slower entanglement formation (increase in viscosity) in defined regions, R1 and R2 of modulus build-up. Remember, in region R1 entanglement formation proceeds at a faster rate by the mixing process (through chain explosion *[126,167,174]*),

while, in region R2 entanglement formation proceeds slower and is governed by reptation dynamics.

7. Characteristic melting time calculation using TM-DSC

Figure A.8 shows raw data of heat capacity, heat flow phase and reverse specific heat capacity at different modulation periods for a disentangled sample. They increase with increasing modulation period (decreasing frequency) for a fixed heating rate. The characteristic time (τ), can be calculated from the inverse of slope of the linear fit to the imaginary part of the effective heat capacity to the modulation periods. Figure A.8d.

The imaginary part of the effective heat capacity, $\Delta C''$, is calculated at the peak melting temperature of the corresponding modulation period.

$$\Delta C'' \cong \frac{\Delta C.\sin(\alpha)}{\overline{F}}.\beta$$

$\overline{F}$ is the underlying heat flow, β is the heating rate, α is the heat flow phase and ΔC is the effective heat capacity of complex quantity. The magnitude and the phase angle of the heat capacity were adjusted for the data outside the transition region (in melt at 155°C). No reference pan was used during the experiment, as the theoretical basis used in these experiments, avoids any introduction of uncontrollable parameter of thermal contact between the reference pan and the base plate. For details on the above equation and its derivation, please refer to a publication by Toda *et al. [237]*.

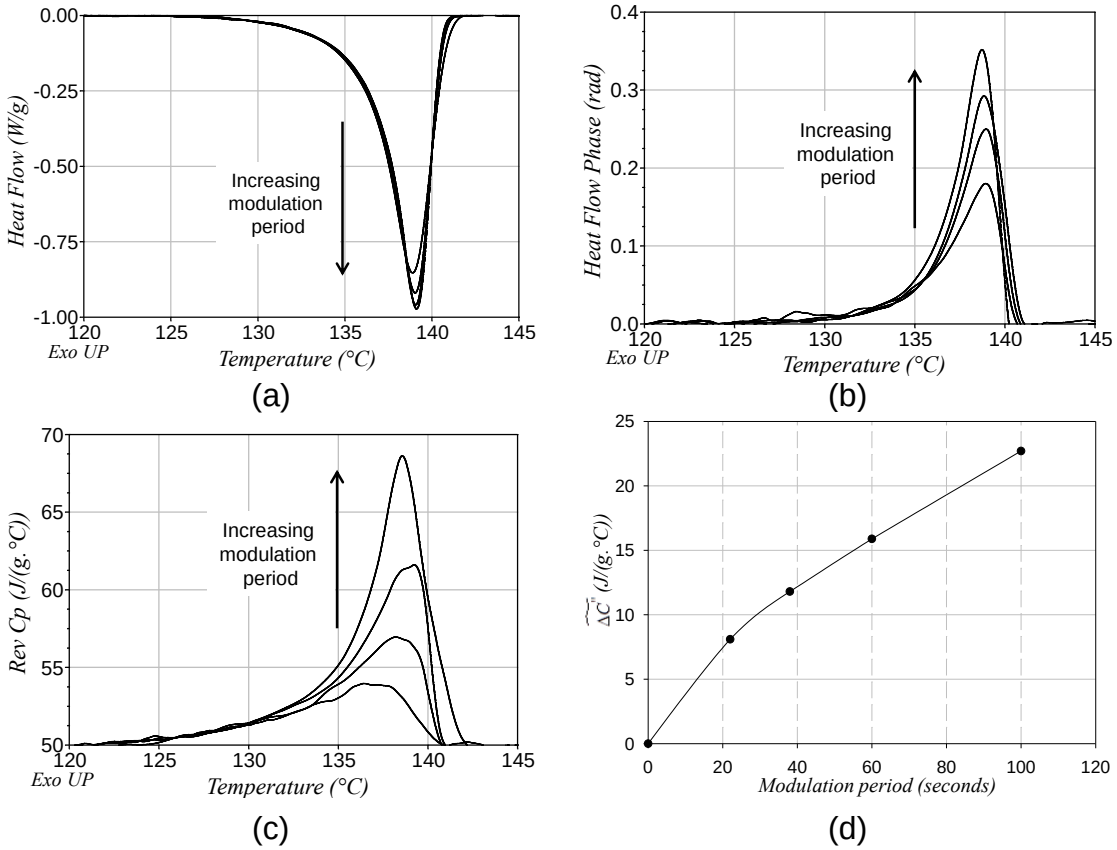

Figure A.8. (a) Heat flow, $\overline{F}$, (b) heat flow phase, α, (c) reverse specific heat capacity, ΔC, at different modulation periods (22, 38, 60 and 100s) and a heating rate of 0.8°C/min for the synthesised disentangled sample having Mw ~ 2.5 million g/mol and MWD ~ 2.2. (d) Imaginary part of the effective heat capacity, $\Delta C''$, with respect to the modulation period. Note: High value of Rev Cp (~50 J/g.°C) in Figure A.8C for liquid polyethylene (at 145°C) is higher than the reported value of 2.6 J/g,°C due to measurement without reference pan. Experiments (not shown here) carried out with reference pan have heat capacity of liquid polyethylene close to 2-3 J/g°C at 145°C for all the modulation periods.

Bibliography

[1] Rastogi, S.; Yao, Y.; Ronca, S.; Bos, J., and Eem, J. van der. 'Unprecedented High-Modulus High-Strength Tapes and Films of Ultrahigh Molecular Weight Polyethylene via Solvent-Free Route' *Macromolecules* **2011** *44*, 5558-5568.

[2] Rubinstein, M.; and Colby, R.H. 'Polymer physics' Oxford University Press, USA **2003**.

[3] Dealy, J.; and Larson, R. 'Structure and Rheology of Molten Polymers' Carl Hanser Verlag, Munich **2006**.

[4] Ferry, J.D. 'Viscoelastic properties of polymers' John Wiley & Sons Inc, New York **1980**.

[5] Graessley, W. 'The entanglement concept in polymer rheology' *Advances in Polymer Science* **1974** *16*, 1-179.

[6] Graessley, W. 'Entangled linear, branched and network polymer systems-molecular theories' *Advances in Polymer Science* **1982** *47*, 67-117.

[7] Doi, M.; and Edwards, S. 'The theory of polymer dynamics' Oxford University Press, USA **1988**.

[8] Guillou, J.L., and Zinn-Justin, J. 'Critical exponents from field theory' *Physical Review B* **1980** *21*, 3976–3998.

[9] Muthukumar, M., and Nickel, B.G. 'Expansion of a polymer chain with excluded volume interaction' *The Journal of Chemical Physics* **1987** *86*, 460-476.

[10] Cotton, J.P.; Decker, D.; Benoit, H.; Farnoux, B.; Higgins, J.; Jannink, G.; Ober, R.; Picot, C., and Cloizeaux, J. des. 'Conformation of Polymer Chain in the Bulk' *Macromolecules* **1974** *7*, 863-872.

[11] Wittmer, J.; Beckrich, P.; Johner, A.; Semenov, A.; Obukhov, S.; Meyer, H., and Baschnagel, J. 'Why polymer chains in a melt are not random walks' *Europhysics Letters* **2007** *77*, 56003.

[12] Jones, R. 'Soft condensed matter' Oxford University Press, USA **2002**.

[13] Erman, B., and Mark, J. 'Rubber-like elasticity' *Annual Review of Physical Chemistry* Annual Reviews **1989** *40*, 351–374.

[14] Kuhn, W.; and Grün, F. 'Beziehungen zwischen elastischen Konstanten und Dehnungsdoppelbrechung hochelastischer Stoffe' *Colloid & Polymer Science* **1942** *101*, 248-271.

[15] Watanabe, H. 'Viscoelasticity and dynamics of entangled polymers' *Progress in Polymer Science* **1999** *24*, 1253-1403.

[16] McLeish, T. 'Tube theory of entangled polymer dynamics' *Advances in Physics* **2002** *51*, 1379–1527.

[17] Rouse Jr, P.E. 'A theory of the linear viscoelastic properties of dilute solutions of coiling polymers' *The Journal of Chemical Physics* **1953** *21*, 1272-1280.

[18] Zimm, B.H. 'Dynamics of Polymer Molecules in Dilute Solution: Viscoelasticity, Flow Birefringence and Dielectric Loss' *The Journal of Chemical Physics* **1956** *24*, 269-278.

[19] Colby, R.H.; Fetters, L.J., and Graessley, W.W. 'Melt viscosity-molecular weight relationship for linear polymers' *Macromolecules* **1987** *20*, 2226-2237.

[20] Doi, M.; and Edwards, S. 'Dynamics of concentrated polymer systems. Part 2.-Molecular motion under flow' *Journal of the Chemical Society, Faraday Transactions 2: Molecular and Chemical Physics* **1978** *74*, 1802–1817.

[21] Gennes, P.G. de. 'Reptation of a Polymer Chain in the Presence of Fixed Obstacles' *The Journal of Chemical Physics* **1971** *55*, 572-579.

[22] Doi, M. 'Explanation for the 3.4-power law for viscosity of polymeric liquids on the basis of the tube model' *Journal of Polymer Science: Polymer Physics Edition* **1983** *21*, 667-684.

[23] Doi, M. 'Explanation for the 3.4 power law of viscosity of polymeric liquids on the basis of the tube model' *Journal of Polymer Science: Polymer Letters Edition* **1981** *19*, 265-273.

[24] Doi, M.; and Edwards, S. 'Dynamics of concentrated polymer systems. part 4.-Rheological properties' *Journal of the Chemical Society, Faraday Transactions 2: Molecular and Chemical Physics* **1979** *75*, 38–54.

[25] Doi, M.; and Edwards, S. 'Dynamics of concentrated polymer systems. Part 3.-The constitutive equation' *Journal of the Chemical Society, Faraday Transactions 2: Molecular and Chemical Physics* **1978** *74*, 1818–1832.

[26] Doi, M.; and Edwards, S. 'Dynamics of concentrated polymer systems. Part 1.-Brownian motion in the equilibrium state' *Journal of the Chemical Society, Faraday Transactions 2: Molecular and Chemical Physics* **1978** *74*, 1789–1801.

[27] Milner, S.; and McLeish, T. 'Reptation and Contour-Length Fluctuations in Melts of Linear Polymers' *Physical Review Letters* **1998** *81*, 725-728.

[28] Klein, J. 'The onset of entangled behavior in semidilute and concentrated polymer solutions' *Macromolecules* **1978** *11*, 852–858.

[29] Daoud, M.; and Gennes, P.G. De. 'Some remarks on the dynamics of polymer melts' *Journal of Polymer Science: Polymer Physics Edition* **1979** *17*, 1971-1981.

[30] Klein, J. 'Evidence for reptation in an entangled polymer melt' *Nature* **1978** *271*, 143-145.

[31] Klein, J. 'Dynamics of entangled linear, branched, and cyclic polymers' *Macromolecules* **1986** *19*, 105-118.

[32] Bent, J.; Hutchings, L.R.; Richards, R.W.; Gough, T.; Spares, R.; Coates, P.D.; Grillo, I.; Harlen, O.G.; Read, D.J.; Graham, R.S.; Likhtman, a E.; Groves, D.J.; Nicholson, T.M., and McLeish, T.C.B. 'Neutron-mapping polymer flow: scattering, flow visualization, and molecular theory.' *Science* **2003** *301*, 1691-1695.

[33] Richardson, M.J. 'The Direct Observation of Polymer Molecules and Determination of Their Molecular Weight' *Proceedings of the Royal Society A: Mathematical, Physical and Engineering Sciences* **1964** *279*, 50-61.

[34] Cloizeaux, J.D. 'Double Reptation vs. Simple Reptation in Polymer Melts' *Europhysics Letters* **1988** *5*, 437-442.

[35] Ianniruberto, G.; and Marrucci, G. 'A simple constitutive equation for entangled polymers with chain stretch' *Journal of Rheology* **2001** *45*, 1305-1318.

[36] Pearson, D.; Herbolzheimer, E.; Grizzuti, N., and Marrucci, G. 'Transient behavior of entangled polymers at high shear rates' *Journal of Polymer Science Part B: Polymer Physics* **1991** *29*, 1589–1597.

[37] Marrucci, G.; and Grizzuti, N. 'Fast flows of concentrated polymers: Predictions of the tube model on chain stretching' *Gazzetta Chimica Italiana* **1988** *118*, 179-185.

[38] Ianniruberto, G.; and Marrucci, G. 'On compatibility of the Cox-Merz rule with the model of Doi and Edwards' *Journal of Non-Newtonian Fluid Mechanics* **1996** *65*, 241–246.

[39] Marrucci, G. 'Dynamics of entanglements: A nonlinear model consistent with the Cox-Merz rule' *Journal of Non-Newtonian Fluid Mechanics* **1996** *62*, 279-289.

[40] Mead, D.W.; Larson, R.G., and Doi, M. 'A Molecular Theory for Fast Flows of Entangled Polymers' *Macromolecules* **1998** *31*, 7895-7914.

[41] Ianniruberto, G.; and Marrucci, G. 'A multi-mode CCR model for entangled polymers with chain stretch' *Journal of Non-Newtonian Fluid Mechanics* **2002** *102*, 383–395.

[42] Reiter, G.; and Sommer, J.U. 'Polymer crystallization: observations, concepts, and interpretations' Springer, Berlin Heidelberg **2003**.

[43] Reiter, G.; and Strobl, G.R. 'Progress in understanding of polymer crystallization' Springer, Verlag **2007**.

[44] Muthukumar, M. 'Shifting paradigms in polymer crystallization' . In *Progress in Understanding of Polymer Crystallization* (Reiter, G., and Strobl, G. R., Eds.), pp 1–18 Springer, Berlin, Heidelberg **2007**.

[45] Strobl, G. 'From the melt via mesomorphic and granular crystalline layers to lamellar crystallites: A major route followed in polymer crystallization?' *The European Physical Journal E* **2000** *3*, 165-183.

[46] Strobl, G. 'Crystallization and melting of bulk polymers: New observations, conclusions and a thermodynamic scheme' *Progress in Polymer Science* **2006** *31*, 398-442.

[47] Cheng, S.Z.D.; Li, C.Y., and Zhu, L. 'Commentary on polymer crystallization: Selection rules in different length scales of a nucleation process' *The European Physical Journal E* **2000** *3*, 195-197.

[48] Cheng, S.Z.D.; and Lotz, B. 'Nucleation control in polymer crystallization: structural and morphological probes in different length- and time-scales for selection processes.' *Philosophical transactions. Series A, Mathematical, Physical, and Engineering Sciences* **2003** *361*, 517-537.

[49] Lotz, B. 'What can polymer crystal structure tell about polymer crystallization processes?' *The European Physical Journal E: Soft Matter and Biological Physics* **2000** *3*, 185–194.

[50] Muthukumar, M. 'Commentary on theories of polymer crystallization' *The European Physical Journal E: Soft Matter and Biological Physics* **2000** *3*, 199–202.

[51] Doye, J. 'Computer simulations of the mechanism of thickness selection in polymer crystals' *Polymer* **2000** *41*, 8857-8867.

[52] Doye, J.P.K.; and Frenkel, D. 'The effect of temperature jumps during polymer crystallization' *Polymer* **2000** *41*, 1519–1528.

[53] Herman, K.; Gerngross, O., and Abitz, W. 'A fringed micelle model for polymer crystals' *Zeitschrift für Physikalische Chemie* **1930** *B130*, 371-394.

[54] Keller, A. 'A note on single crystals in polymers: evidence for a folded chain configuration' *Philosophical Magazine* **1957** *2*, 1171–1175.

[55] Fischer, E. 'Step and spiral growth of high polymers' *Z. Naturforsch* **1957** *12a*, 753-754.

[56] Till Jr, P. 'The growth of single crystals of linear polyethylene' *Journal of Polymer Science* **1957** *24*, 301–306.

[57] Jaccodine, R. 'Observations of Spiral Growth Steps in Ethylene Polymer' *Nature* **1955** *176*, 305-306.

[58] Flory, P. 'On the morphology of the crystalline state in polymers' *Journal of the American Chemical Society* **1962** *84*, 2857–2867.

[59] Lippits, D.R. 'Controlling the melting kinetics of polymers; a route to a new melt state' *Dissertation* Eindhoven University of Technology **2007**.

[60] Blundell, D.; and Keller, A. 'Nature of self-seeding polyethylene crystal nuclei' *Journal of Macromolecular Science, Part B* **1968** *2*, 301-336.

[61] Blundell, D.; and Keller, A. 'Controlled crystal-growing procedures in polyethylene involving self-seeding: Some novel twinning habits' *Journal of Macromolecular Science, Part B* **1968** *2*, 337-359.

[62] Blundell, D.; Keller, A., and Kovacs, A. 'A new self-nucleation phenomenon and its application to the growing of polymer crystals from solution' *Journal of Polymer Science Part B: Polymer Letters* **1966** *4*, 481–486.

[63] Toda, A.; Miyaji, H., and Kiho, H. 'Regime II growth of polyethylene single crystals from dilute solution in n-octane' *Polymer* **1986** *27*, 1505-1508.

[64] Toda, A. 'Growth kinetics of polyethylene single crystals from dilute solution at low supercoolings' *Polymer* **1987** *28*, 1645-1651.

[65] Toda, A. 'Polyethylene crystallization from dilute solutions: adsorption isotherm on the growth face' *Journal of the Chemical Society, Faraday Transactions* **1995** *91*, 2581-2586.

[66] Toda, A.; Okamura, M.; Hikosaka, M., and Nakagawa, Y. 'AFM observation of polyethylene single crystals: selective handedness of screw dislocations in a chair type' *Polymer* **2003** *44*, 6135-6138.

[67] Keller, A. 'A study of growth rates of polyethylene single crystals' *Journal of Crystal Growth* **1973** *18*, 111-123.

[68] Tian, M. 'Understanding the organization and reorganization of polymer crystals' Technical University of Eindhoven **2004**.

[69] Bunn, C.W.; and Alcock, T.C. 'The texture of polythene' *Transactions of the Faraday Society* **1945** *41*, 317-325.

[70] Keller, A. 'The spherulitic structure of crystalline polymers. Part I. Investigations with the polarizing microscope' *Journal of Polymer Science* **1955** *17*, 291–308.

[71] Wunderlich, B. 'Macromolecular Physics. Vol. 1, Crystal Structure, Morphology' Academic Press, New York **1973**.

[72] Bassett, D.C.; Frank, F.C., and Keller, a. 'Lamellae and their Organization in Melt-Crystallized Polymers [and Discussion]' *Philosophical Transactions of the Royal Society A: Mathematical, Physical and Engineering Sciences* **1994** *348*, 29-43.

[73] Maxfield, J.; and Mandelkern, L. 'Crystallinity, Supermolecular Structure, and Thermodynamic Properties of Linear Polyethylene Fractions' *Macromolecules* **1977** *10*, 1141-1153.

[74] Lopez, J.; and Gedde, U. 'Morphology of binary linear polyethylene blends' *Polymer* **1988** *29*, 1037-1044.

[75] Hoffman, J.; Frolen, L.; Ross, G., and Lauritzen Jr, J. 'On the growth rate of spherulites and axialites from the melt in polyethylene fractions: regime I and regime II crystallization' Journal of Research of the National Bureau of Standards **1975** *79A*, 671–699.

[76] Hoffman, J.D.; and Miller, R.L. 'Kinetic of crystallization from the melt and chain folding in polyethylene fractions revisited: theory and experiment' *Polymer* **1997** *38*, 3151-3212.

[77] Toda, A.; Kojima, I., and Hikosaka, M. 'Melting kinetics of polymer crystals with an entropic barrier' *Macromolecules* **2008** *41*, 120-127.

[78] Mackley, M.R.; Frank, F.C., and Keller, a. 'Flow-induced crystallization of polyethylene melts' *Journal of Materials Science* **1975** *10*, 1501-1509.

[79] Pennings, A.; and Kiel, A. 'Fractionation of polymers by crystallization from solution, III. On the morphology of fibrillar polyethylene crystals grown in solution' *Colloid & Polymer Science* **1965** *205*, 160–162.

[80] Pennings, A.; and Pijpers, M. 'On the Kinetics of Crystallization of Polymers from Stirred Solutions' *Macromolecules* **1970** *3*, 261–262.

[81] Keller, A. 'Crystalline polymers; an introduction' *Faraday Discussions of the Chemical Society* **1979** *68*, 145-166.

[82] Andrews, E.H. 'Spherulite Morphology in Thin Films of Natural Rubber' *Proceedings of the Royal Society A: Mathematical, Physical and Engineering Sciences* **1962** *270*, 232-241.

[83] Buthenuth, G. 'Zur Struktur von Polytetrafluroathylen' *Verhandl. Kolloid. Ges* **1958** *18*, 168.

[84] Kantor, S.W.; and Osthoff, R.C. 'High molecular weight polymethylene' *Journal of the American Chemical Society* **1953** *75*, 931–932.

[85] Melillo, L.; and Wunderlich, B. 'Extended-chain crystals VIII. Morphology of polytetrafluroethylene' *Kolloid-Zeitschrift & Zeitschrift für Polymere* **1972** *250*, 417-425.

[86] Toyota, N.; and Machi, S.U.E. 'Morphology of Polyethylene Crystals as Polymerized by 7-Radiation Morphology of Polyethylene Formed in Methanol' *Polymer* **1969** *7*, 153-161.

[87] Emirova, I.; Ermakov, Y.; Nevyantsev, I., and Ratner, I. 'Morphological structures of medium pressure polyethylene arising directly during polymerization' *Vysokomol. Soedin* **1970** *B12*, 23.

[88] Wunderlich, B. 'Macromolecular Physics, Vol. 2: Crystal Nucleation' Academic Press, New York **1976**.

[89] Blais, P.; and Manley, R. 'Morphology of Nascent Ziegler-Natta Polymers' *Science* **1966** *153*, 539-541.

[90] Blais, P.; and Manley, R.S.J. 'Morphology of nascent polyolefins prepared by Ziegler-Natta catalysis' *Journal of Polymer Science Part A-1: Polymer Chemistry* **1968** *6*, 291-334.

[91] Keller, A. 'Solution grown polymer crystals' *Colloid & Polymer Science* Springer Berlin / Heidelberg **1969** *231*, 386-421.

[92] Chanzy, H.; Day, A., and Marchessault, R. 'Polymerization on glass-supported vanadium trichloride: Morphology of nascent polyethylene' *Polymer* **1967** *8*, 567–588.

[93] Loos, J.; Arndt-Rosenau, M.; Weingarten, U.; Kaminsky, W., and Lemstra, P. 'Melting behavior of nascent polyolefins synthesized at various polymerization conditions' *Polymer Bulletin* **2002** *48*, 191-198.

[94] Keller, A.; and Willmouth, F. 'On the morphology and orgin of the fibres observed in Nascent Ziegler polyethylene' *Die Makromolekulare Chemie* **1969** *121*, 42–50.

[95] Graff, R.J.L.; Kortleve, G., and Vonk, C.G. 'On the size of the primary particles in ziegler catalysts' *Journal of Polymer Science Part B: Polymer Letters* **1970** *8*, 735-739.

[96] Chanzy, H.D.; Revol, J.F.; Marchessault, R.H., and Lamandé, a. 'Nascent structures during the polymerization of ethylene' *Kolloid-Zeitschrift & Zeitschrift für Polymere* **1973** *251*, 563-576.

[97] Muñoz-Escalona, A.; and Parada, A. 'Factors affecting the nascent structure and morphology of polyethylene obtained by heterogeneous Ziegler—Natta catalysts: 2. Crystallinity and melting behaviour' *Polymer* **1979** *20*, 859-866.

[98] Muñoz-Escalona, A.; and Parada, A. 'Factors affecting the nascent structure and morphology of polyethylene obtained by heterogeneous ziegler-natta catalyst : III. Crystal morphology and growth mechanism' *Journal of Crystal Growth* **1980** *48*, 250-258.

[99] Kakugo, M.; Sadatoshi, H.; Sakai, J., and Yokoyama, M. 'Growth of polypropylene particles in heterogeneous Ziegler-Natta polymerization' *Macromolecules* **1989** *22*, 3172–3177.

[100] Kakugo, M.; Sadatoshi, H.; Yokoyama, M., and Kojima, K. 'Transmission electron microscopic observation of nascent polypropylene particles using a new staining method' *Macromolecules* **1989** *22*, 547–551.

[101] Tervoort-Engelen, Y.; and Lemstra, P. 'Morphology of nascent ultra-high molecular weight polyethylene reactor powder: chain-extended versus chain-folded crystals' *Journal of Polymer Communications* **1991** *32*, 343–345.

[102] Nooijen, G. 'On the importance of diffusion of cocatalyst molecules through heterogeneous Ziegler/Natta catalysts' *European Polymer Journal* **1994** *30*, 11-15.

[103] Uehara, H.; Nakae, M.; Kanamoto, T.; Ohtsu, O.; Sano, A., and Matsuura, K. 'Structural characterization of ultrahigh-molecular-weight polyethylene reactor powders based on fuming nitric acid etching' *Polymer* **1998** *39*, 6127-6135.

[104] Ivan'kova, E.; Myasnikova, L.; Marikhin, V.; Baulin, A., and Volchek, B. 'On the memory effect in UHMWPE nascent powders' *Journal of Macromolecular Science, Part B* **2001** *40*, 813–832.

[105] Uehara, H.; Aoike, T.; Yamanobe, T., and Komoto, T. 'Solid-State 1 H NMR Relaxation Analysis of Ultrahigh Molecular Weight Polyethylene Reactor Powder' *Macromolecules* **2002** *35*, 2640-2647.

[106] Tsobkallo, K.; Vasilieva, V.; Khizhnyak, S.; Pakhomov, P.; Galitsyn, V.; Ruhl, E.; Egorov, V., and Tshmel, A. 'Effect of the morphology of reactor powders on the structure and mechanical behavior of drawn ultra-high molecular weight polyethylenes' *Polymer* **2003** *44*, 1613–1618.

[107] Tsobkallo, K.; Vasilieva, V.; Kakiage, M.; Uehara, H., and Tshmel, A. 'Remnant Features in Melt Crystallized Samples of Polyethylenes Originated from Reactor Powders' *Journal of Macromolecular Science, Part B* **2006** *45*, 407-415.

[108] Geil, P. 'Polymer single crystals' Interscience (Wiley), New York **1963**.

[109] Georgiadis, T.; and St John Manley, R. 'Morphology of nascent polyethylene prepared with the catalyst VOCl3(C2H5)2AlCl' *Polymer* **1972** *13*, 567-574.

[110] Georgiadis, T.; and Manley, R.J. 'The morphology of nascent polyethylene prepared with the soluble catalyst (C5H5)2 TiCl2-R2AlCl' *Colloid & Polymer Science* **1972** *250*, 557-572.

[111] Smith, P.; Chanzy, H.D., and Rotzinger, B.P. 'Drawing of virgin ultrahigh molecular weight polyethylene: an alternative route to high strength fibres' *Polymer Communication* **1985** *26*, 258-260.

[112] Smith, P.; Chanzy, H.D., and Rotzinger, B.P. 'Drawing of virgin ultrahigh molecular weight polyethylene: An alternative route to high strength/high modulus materials Part 2 Influence of polymerization temperature' *Journal of Materials Science* **1987** *22*, 523–531.

[113] Rotzinger, B.; Chanzy, H., and Smith, P. 'High strength/high modulus polyethylene: synthesis and processing of ultra-high molecular weight virgin powders' *Polymer* **1989** *30*, 1814-1819.

[114] Lu, S.X.; and Cebe, P. 'Effects of annealing on the disappearance and creation of constrained amorphous phase' *Polymer* **1996** *37*, 4857–4863.

[115] Baker, A.M.E.; and Windle, A.H. 'Evidence for a partially ordered component in polyethylene from wide-angle X-ray diffraction' *Polymer* **2001** *42*, 667-680.

[116] Pak, J.; Pyda, M., and Wunderlich, B. 'Rigid Amorphous Fractions and Glass Transitions in Poly(oxy-2,6-dimethyl-1,4-phenylene)' *Macromolecules* **2003** *36*, 495-499.

[117] Rastogi, S.; Lippits, D.R.; Höhne, G.W.H.; Mezari, B., and Magusin, P.C.M.M. 'The role of the amorphous phase in melting of linear UHMW-PE; implications for chain dynamics' *Journal of Physics: Condensed Matter* **2007** *19*, 205122.

[118] Rastogi, S.; Lippits, D.; Terry, A., and Lemstra, P. 'The Role of the Interphase on the Chain Mobility and Melting of Semi-crystalline Polymers; A Study on Polyethylenes' *Progress in Understanding of Polymer Crystallization* (Reiter, G., and Strobl, G. R., Eds.) Springer, Berlin, Heidelberg **2007** *714*, 285–327.

[119] Righetti, M.C.; Lorenzo, M.L.D.; Tombari, E., and Angiuli, M. 'The low-temperature endotherm in poly(ethylene terephthalate): partial melting and rigid amorphous fraction mobilization.' *The Journal of Physical Chemistry. B* **2008** *112*, 4233-4241.

[120] Lorenzo, M.L. Di. 'The melting process and the rigid amorphous fraction of cis-1, 4-polybutadiene' *Polymer* **2009** *50*, 578–584.

[121] Lorenzo, M.L. Di;; Righetti, M.C.; Cocca, M., and Wunderlich, B. 'Coupling between Crystal Melting and Rigid Amorphous Fraction Mobilization in Poly(ethylene terephthalate)' *Macromolecules* **2010** *43*, 7689-7694.

[122] Wunderlich, B. 'Macromolecular Physics, Vol. 3: Crystal Melting' Academic Press, New York **1976**.

[123] Hellmuth, E.; and Wunderlich, B. 'Superheating of Linear High-Polymer Polyethylene Crystals' *Journal of Applied Physics* **1965** *36*, 3039–3044.

[124] Prime, R.B.; Wunderlich, B., and Melillo, L. 'Extended-chain crystals. V. Thermal analysis and electron microscopy of the melting process in polyethylene' *Journal of Polymer Science Part A-2: Polymer Physics* **1969** *7*, 2091-2097.

[125] Kovacs, A.; Gonthier, A., and Straupe, C. 'Isothermal growth, thickening, and melting of poly(ethylene oxide) single crystals in the bulk' *Journal of Polymer Science* **1975** *325*, 283-325.

[126] Rastogi, S.; Lippits, D.R.; Peters, G.W.M.; Graf, R.; Yao, Y., and Spiess, H.W. 'Heterogeneity in polymer melts from melting of polymer crystals.' *Nature Materials* **2005** *4*, 635-41.

[127] Lippits, D.; Rastogi, S., and Höhne, G. 'Melting Kinetics in Polymers' *Physical Review Letters* **2006** *96*, 1-4.

[128] Wunderlich, B.; and Kashdan, W. 'Thermodynamics of crystalline linear high polymers. I. Comparison of the melting transitions of solution and melt-crystallized polyethylene' *Journal of Polymer Science* **1961** *50*, 71–78.

[129] Wunderlich, B.; and Poland, D. 'Thermodynamics of crystalline linear high polymers. II. The influence of copolymer units on the thermodynamic properties of polyethylene' *Journal of Polymer Science: Part A* **1963** *1*, 357–372.

[130] Liberti, F.N.; and Wunderlich, B. 'Melting of polycaprolactam' *Journal of Polymer Science Part A-2: Polymer Physics* **1968** *6*, 833-848.

[131] Hohne, G. 'On de-smearing of heat-flow curves in calorimetry' *Thermochimica Acta* **1978** *22*, 347–362.

[132] Danley, R.L.; and Caulfield, P.A. 'DSC resolution and dynamic response improvements obtained by a new heat flow measurement technique' . In *Proceedings of the 29th Conference of the North American Thermal Analysis Society*, pp 673–678 **2001**.

[133] Schawe, J. 'A new method to estimate transition temperatures and heats by peak form analysis' *Thermochimica Acta* **1993** *229*, 69–84.

[134] Rånby, B.; Morehead, F., and Walter, N. 'Morphology of n-alkanes, linear polyethylene, and isotactic polypropylene crystallized from solution' *Journal of Polymer Science* **1960** *44*, 349–367.

[135] Reneker, D.; and Geil, P. 'Morphology of polymer single crystals' *Journal of Applied Physics* **1960** *31*, 1916–1925.

[136] Bassett, D.C. 'The growth of polymer crystals' *Journal of Crystal Growth* **1968** *3-4*, 92-96.

[137] Höhne, G. 'Another approach to the Gibbs-Thomson equation and the melting point of polymers and oligomers' *Polymer* **2002** *43*, 4689–4698.

[138] Strobl, G.R. 'The physics of polymers' Springer, Berlin **1997**.

[139] Wunderlich, B.; and Czornyj, G. 'A study of equilibrium melting of polyethylene' *Macromolecules* **1977** *10*, 906–913.

[140] Lippits, D.R. 'Controlling the melting kinetics of polymers; a route to a new melt state' *Dissertation* Eindhoven University of Technology **2007**.

[141] Lippits, D.R.; Rastogi, S.; Höhne, G.W.H.; Mezari, B., and Magusin, P.C.M.M. 'Heterogeneous Distribution of Entanglements in the Polymer Melt and Its Influence on Crystallization' *Macromolecules* **2007** *40*, 1004-1010.

[142] Carothers, W.H.; and Hill, J.W. 'Studies of polymerization and ring formation. XV. Artificial fibers from synthetic linear condensation superpolymers' *Journal of the American Chemical Society* **1932** *54*, 1579–1587.

[143] Treloar, L. 'Calculations of elastic moduli of polymer crystals: I. Polyethylene and nylon 66' *Polymer* **1960** *1*, 95-103.

[144] Frank, F. 'The strength and stiffness of polymers' *Proceeding of Royal Society London* **1970** *319A*, 127-136.

[145] Capaccio, G.; and Ward, I. 'Ultra-high-modulus linear polyethylene through controlled molecular weight and drawing' *Polymer Engineering & Science* **1975** *15*, 219–224.

[146] Capaccio, G.; Crompton, T., and Ward, I. 'The drawing behavior of linear polyethylene. I. Rate of drawing as a function of polymer molecular weight and initial thermal treatment' *Jornal of Polymer Science: Polymer Physics Edition* **1976** *14*, 1641-1658.

[147] Capaccio, G.; Crompton, T., and Ward, I. 'Drawing behavior of linear polyethylene. II. Effect of draw temperature and molecular weight on draw ratio and modulus' *Journal of Polymer Science: Polymer Physics Edition* **1980** *18*, 301-309.

[148] Pennings, A.; Zwijnenburg, A., and Lageveen, R. 'Longitudinal growth of polymer crystals from solutions subjected to single shear flow' *Colloid & Polymer Science* **1973** *251*, 500-501.

[149] Pennings, A. 'Bundle-like nucleation and longitudinal growth of fibrillar polymer crystals from flowing solutions' *Journal of Polymer Science: Polymer Symposia* **1977** *59*, 55-86.

[150] Zwijnenburg, A.; and Pennings, A. 'Longitudinal growth of polymer crystals from flowing solutions III. Polyethylene crystals in Couette flow' *Colloid & Polymer Science* **1976** *254*, 868-881.

[151] Pennings, A.; Smook, J.; Boer, J.D.; Gogolewski, S., and Hutten, P. van. 'Process of preparation and properties of ultra-high strength polyethylene fibers' *Pure & Applied Chemistry* **1983** *55*, 777-798.

[152] Smith, P.; and Lemstra, P. 'Ultrahigh-strength polyethylene filaments by solution spinning/drawing, 2. Influence of solvent on the drawability' *Die Makromolekulare Chemie* **1979** *180*, 2983-2986.

[153] Smith, P.; and Lemstra, P.J. 'Ultra-high-strength polyethylene filaments by solution spinning/drawing' *Journal of Materials Science* **1980** *15*, 505-514.

[154] Smith, P.; Lemstra, P.J., and Pijpers, J.P.L. 'Tensile strength of highly oriented polyethylene. II. Effect of molecular weight distribution' *Journal of Polymer Science: Polymer Physics Edition* **1982** *20*, 2229-2241.

[155] Lemstra, P.; Bastiaansen, C., and Rastogi, S. 'Salem DR (ed) Structure formation in polymeric fibers', Hanser p 185 **2000**.

[156] Gruter, G.; and Wang, B. 'Process for the homopolymerisation of ethylene' EP Patent 1,057,837 **2000**.

[157] Sharma, K.G. 'Easily processable ultra high molecular weight polyethylene with narrow molecular weight distribution' Technische Universiteit Eindhoven **2005**.

[158] Talebi, S. 'Disentangled Polyethylene with Sharp Molar Mass Distribution; Implications for Sintering' Technische Universiteit Eindhoven **2008**.

[159] Rastogi, S.; Garkhail, K.; Duchateau, R.; Gruter, G., and Lippits, D.R. 'Process for the preparation of a shaped part of an ultra high molecular weight polyethylene' *WO Patent WO/2004/* **2010**.

[160] Rastogi, S.; Kurelec, L.; Lippits, D.; Cuijpers, J.; Wimmer, M., and Lemstra, P.J. 'Novel route to fatigue-resistant fully sintered ultrahigh molecular weight polyethylene for knee prosthesis.' *Biomacromolecules* **2005** *6*, 942-7.

[161] Weijer, A. De;; De Hee, H. Van;; Peters, M.; Rastogi, S., and Wang, B. 'Polyethylene film with high tensile strength and high tensile energy to break' *WO Patent WO/2010/* **2010**.

[162] Rastogi, S.; Spoelstra, a B.; Goossens, J.G.P., and Lemstra, P.J. 'Chain Mobility in Polymer Systems: on the Borderline between Solid and Melt. 1. Lamellar Doubling during Annealing of Polyethylene' *Macromolecules* **1997** *30*, 7880-7889.

[163] Bastiaansen, C.; Meyer, H., and Lemstra, P. 'Memory effects in polyethylenes: influence of processing and crystallization history' *Polymer* Elsevier **1990** *31*, 1435–1440.

[164] Lada, C.-K. 'Chain Mobility in Polymer Systems; on the Border Line between Solid and Melt' *Macromolecules* Technische Universiteit Eindhoven **2001**.

[165] Yao, Y.-F.; Graf, R.; Spiess, H.; Lippits, D., and Rastogi, S. 'Morphological differences in semicrystalline polymers: Implications for local dynamics and chain diffusion' *Physical Review E* **2007** *76*, 1-4.

[166] Yao, Y.; Graf, R.; Spiess, H., and Rastogi, S. 'Influence of Crystal Thickness and Topological Constraints on Chain Diffusion in Linear Polyethylene' *Macromolecular Rapid Communications* **2009** *30*, 1123–1127.

[167] Uehara, H.; Uehara, A.; Kakiage, M.; Takahashi, H.; Murakami, S.; Yamanobe, T., and Komoto, T. 'Solid-state characterization of polyethylene reactor powders and their structural changes upon annealing' *Polymer* **2007** *48*, 4547-4557.

[168] Lippits, D.R.; Rastogi, S.; Talebi, S., and Bailly, C. 'Formation of entanglements in initially disentangled polymer melts' *Macromolecules* **2006** *39*, 8882–8885.

[169] Mitani, M.; Furuyama, R.; Mohri, J.-ichi;; Saito, J.; Ishii, S.; Terao, H.; Kashiwa, N., and Fujita, T. 'Fluorine- and trimethylsilyl-containing phenoxy--imine Ti complex for highly syndiotactic living polypropylenes with extremely high melting temperatures.' *Journal of the American Chemical Society* **2002** *124*, 7888-9.

[170] Talebi, S.; Duchateau, R.; Rastogi, S.; Kaschta, J.; Peters, G.W.M., and Lemstra, P.J. 'Molar Mass and Molecular Weight Distribution Determination Of UHMWPE Synthesized Using a Living Homogeneous Catalyst' *Macromolecules* **2010** *43*, 2780–2788.

[171] Mitani, M.; Mohri, J.-ichi;; Yoshida, Y.; Saito, J.; Ishii, S.; Tsuru, K.; Matsui, S.; Furuyama, R.; Nakano, T.; Tanaka, H.; Kojoh, S.-ichi;; Matsugi, T.; Kashiwa, N., and Fujita, T. 'Living polymerization of ethylene catalyzed by titanium complexes having fluorine-containing phenoxy-imine chelate ligands.' *Journal of the American Chemical Society* **2002** *124*, 3327-36.

[172] Yang, H.; Wang, Q.; Fan, Z., and Xu, H. 'Improved high-temperature performance of iron (II) complexes for ethylene polymerization by variation of aluminoxanes' *Polymer international* **2004** *53*, 37–40.

[173] Tritto, I.; Marestin, C.; Boggioni, L.; Sacchi, M.C.; Brintzinger, H.-H., and Ferro, D.R. 'Stereoregular and stereoirregular alternating ethylene-norbornene copolymers' *Macromolecules* **2001** *34*, 5770–5777.

[173] Hyun, K.; Wilhelm, M.; Klein, C.O.; Cho, K.S.; Nam, J.G.; Ahn, K.H.; Lee, S.J.; Ewoldt, R.H., and McKinley, G.H. 'A Review of Nonlinear Oscillatory Shear Tests: Analysis and Application of Large Amplitude Oscillatory Shear (LAOS)' *Progress in Polymer Science* **2011** *In Press.*

[174] Barham, P.; and Sadler, D. 'A neutron scattering study of the melting behaviour of polyethylene single crystals' *Polymer* **1991** *32*, 393-395.

[175] Mead, D. 'Determination of molecular weight distributions of linear flexible polymers from linear viscoelastic material functions' *Journal of Rheology* **1994** *38*, 1797-1827.

[176] Tuminello, W.H. 'Molecular weight and molecular weight distribution from dynamic measurements of polymer melts' *Polymer Engineering & Science* **1986** *26*, 1339–1347.

[177] Bersted, B. 'An empirical model relating the molecular weight distribution of high-density polyethylene to the shear dependence of the steady shear melt viscosity' *Journal of Applied Polymer Science* **1975** *19*, 2167–2177.

[178] Bersted, B.H.; and Slee, J.D. 'A relationship between steady-state shear melt viscosity and molecular weight distribution in polystyrene' *Journal of Applied Polymer Science* **1977** *21*, 2631-2644.

[179] Barnes, H.A.; Hutton, J.F., and Walters, K. 'An introduction to rheology' Elsevier, Amsterdam **1989**.

[180] Larson, R.G. 'The structure and rheology of complex fluids' Oxford University Press, New York **2001**.

[181] Macosko, C.W.; and Larson, R.G. 'Rheology: principles, measurements, and applications' Wiley-Vch, New York **1994**.

[182] Vittorias, I., and Wilhelm, M. 'Application of FT rheology to industrial linear and branched polyethylene blends' *Macromolecular Materials and Engineering* **2007** *292*, 935–948.

[183] Klein, C.O.; Spiess, H.W.; Calin, A.; Balan, C., and Wilhelm, M. 'Separation of the nonlinear oscillatory response into a superposition of linear, strain hardening, strain softening, and wall slip response' *Macromolecules* **2007** *40*, 4250–4259.

[184] Hyu, K., and Wilhelm, M. 'Non-Linear Rheology of Entangled Linear and Branched Polymer Melts under Large Amplitude Oscillatory Shear' *KGK Testing and Measuring* **2010** *63*, 123–129.

[185] Miyazaki, K.; Wyss, H.; Weitz, D., and Reichman, D. 'Nonlinear viscoelasticity of metastable complex fluids' *Europhysics Letters* **2006** *75*, 915-921.

[186] Fletcher, W.; and Gent, A. 'Nonlinearity in the Dynamic Properties of Vulcanized Rubber Compounds' *Rubber Chemistry and Technology* **1954** *27*, 209-222.

[187] Payne, A.R. 'The dynamic properties of carbon black-loaded natural rubber vulcanizates. Part I' *Journal of Applied Polymer Science* **1962** *6*, 57-63.

[188] Giacomin, A.; and Oakley, J. 'Structural network models for molten plastics evaluated in large amplitude oscillatory shear' *Journal of Rheology* **1992** *36*, 1529-1546.

[190] Jeyaseelan, R.S.; and Giacomin, A.J. 'Best fit for differential constitutive model parameters to non-linear oscillation data' *Journal of Non-Newtonian Fluid Mechanics* **1993** *47*, 267–280.

[191] Yosick, J.A.; Giacomin, A.J., and Moldenaers, P. 'A kinetic network model for nonlinear flow behavior of molten plastics in both shear and extension' *Journal of Non-Newtonian Fluid Mechanics* **1997** *70*, 103–123.

[192] Yosick, J.; and Giacomin, A. 'Can nonlinear deformation amplify subtle differences in linear viscoelasticity?' *Journal of Non-Newtonian Fluid Mechanics* **1996** *66*, 193–212.

[193] Giacomin, A.; and Jeyaseelan, R. 'A constitutive theory for polyolefins in large amplitude oscillatory shear' *Polymer Engineering & Science* **1995** *35*, 768–777.

[194] Jeyaseelan, R.S.; and Giacomin, A.J. 'Structural network theory for a filled polymer melt in large amplitude oscillatory shear' *Polymer Gels and Networks* **1995** *3*, 117–133.

[195] Jeyaseelan, R.S.; and Giacomin, A.J. 'Network theory for polymer solutions in large amplitude oscillatory shear' *Journal of Non-Newtonian Fluid Mechanics* **2008** *148*, 24–32.

[196] Harris, J. 'Response of time-dependent materials to oscillatory motion' *Nature* **1965** *207*, 744.

[197] MacDonald, I.F.; Marsh, B.D., and Ashare, E. 'Rheological behavior for large amplitude oscillatory motion' *Chemical Engineering Science* **1969** *24*, 1615–1625.

[198] Tee, T.T.; and Dealy, J. 'Nonlinear viscoelasticity of polymer melts' *Journal of Rheology* **1975** *19*, 595-615.

[199] Komatsu, H.; Mitsui, T., and Onogi, S. 'Nonlinear viscoelastic properties of semisolid emulsions' *Journal of Rheology* **1973** *17*, 351-364.

[200] Matsumoto, T.; Segawa, Y.; Warashina, Y., and Onogi, S. 'Nonlinear behavior of viscoelastic materials. II. The method of analysis and temperature dependence of nonlinear viscoelastic functions' *Journal of Rheology* **1973** *17*, 47-62.

[201] Dodge, J.S.; and Krieger, I.M. 'Oscillatory Shear of Nonlinear I. Preliminary Investigation' *Journal of Rheology* **1971** *15*, 589-601.

[202] Onogi, S.; Masuda, T., and Matsumoto, T. 'Non-linear behavior of viscoelastic materials. I. Disperse systems of polystyrene solution and carbon black' *Journal of Rheology* **1970** *14*, 275-294.

[203] Wilhelm, M.; Maring, D., and Spiess, H.W. 'Fourier-transform rheology' *Rheologica Acta* **1998** *37*, 399–405.

[204] Wilhelm, M.; Reinheimer, P., and Ortseifer, M. 'High sensitivity Fourier-transform rheology' *Rheologica Acta* **1999** *38*, 349-356.

[205] Wilhelm, M. 'Fourier-transform rheology' *Macromolecular Materials and Engineering* **2002** *287*, 83-105.

[206] Dusschoten, D. van;; and Wilhelm, M. 'Increased torque transducer sensitivity via oversampling' *Rheologica Acta* **2001** *40*, 395–399.

[207] Cho, K.S.; Hyun, K.; Ahn, K.H., and Lee, S.J. 'A geometrical interpretation of large amplitude oscillatory shear response' *Journal of Rheology* **2005** *49*, 747-758.

[208] Hyun, K.; and Wilhelm, M. 'Establishing a New Mechanical Nonlinear Coefficient Q from FT-Rheology: First Investigation of Entangled Linear and Comb Polymer Model Systems' *Macromolecules* **2009** *42*, 411-422.

[209] Hyun, K.; Kim, S.H.; Ahn, K.H., and Lee, S.J. 'Large amplitude oscillatory shear as a way to classify the complex fluids' *Journal of Non-Newtonian Fluid Mechanics* **2002** *107*, 51–65.

[210] Pandey, A.; Champouret, Y., and Rastogi, S. 'Heterogeneity in the Distribution of Entanglement Density during Polymerization in Disentangled Ultrahigh Molecular Weight Polyethylene' *Macromolecules* **2011** *44*, 4952–4960.

[210] Wyss, H.; Miyazaki, K.; Mattsson, J.; Hu, Z.; Reichman, D., and Weitz, D. 'Strain-Rate Frequency Superposition: A Rheological Probe of Structural Relaxation in Soft Materials' *Physical Review Letters* **2007** *98*, 238303.

[211] Rochefort, W.E. 'Rheology of Xanthan Gum: Salt, Temperature, and Strain Effects in Oscillatory and Steady Shear Experiments' *Journal of Rheology* **1987** *31*, 337-369.

[212] Marrucci, G.; and Ianniruberto, G. 'Effect of flow on topological interactions in polymers' . In *Macromolecular symposia*, pp 233–240 **1997**.

[213] Ianniruberto, G.; and Marrucci, G. 'Convective orientational renewal in entangled polymers' *Journal of Non-Newtonian Fluid Mechanics* **2000** *95*, 363–374.

[214] Sim, H.; Ahn, K., and Lee, S. 'Large amplitude oscillatory shear behavior of complex fluids investigated by a network model: a guideline for classification' *Journal of Non-Newtonian Fluid Mechanics* **2003** *112*, 237-250.

[215] Likhtman, A.; and Graham, R. 'Simple constitutive equation for linear polymer melts derived from molecular theory: Rolie-Poly equation' *Journal of Non-Newtonian Fluid Mechanics* **2003** *114*, 1-12.

[216] Graham, R.S.; Likhtman, A.E.; McLeish, T.C.B., and Milner, S.T. 'Microscopic theory of linear, entangled polymer chains under rapid deformation including chain stretch and convective constraint release' *Journal of Rheology* **2003** *47*, 1171.

[217] Mullins, L.; and Tobin, N. 'Stress softening in rubber vulcanizates. Part I. Use of a strain amplification factor to describe the elastic behavior of filler-reinforced vulcanized rubber' *Journal of Applied Polymer Science* **1965** *9*, 2993-3009.

[218] Babu, R.R.; Singha, N.K., and Naskar, K. 'Melt Viscoelastic Properties of Peroxide Cured Polypropylene-Ethylene Octene Copolymer Thermoplastic Vulcanizates' *Polymer Engineering and Science* **2010** *50*, 455-467.

[219] Pandey, A.; Rastogi, S.; Singh, R., and Peters, G. 'Process for the melt extrusion of ultra high molecular weight polyethylene' **2011**.

[220] Toda, A.; Hikosaka, M., and Yamada, K. 'Superheating of the melting kinetics in polymer crystals: a possible nucleation mechanism' *Polymer* **2002** *43*, 1667–1679.

[221] Muthukumar, M. 'Modeling polymer crystallization' . In *Interphases and Mesophases in Polymer Crystallization III*, pp 241–274 Springer Berlin/Heidelberg **2005**.

[222] Keller, A.; Hikosaka, M.; Rastogi, S.; Toda, A.; Barham, P., and Goldbeck-Wood, G. 'An approach to the formation and growth of new phases with application to polymer crystallization: effect of finite size, metastability, and Ostwald's rule of stages' *Journal of Materials Science* **1994** *29*, 2579–2604.

[223] Rastogi, S.; Yao, Y.; Lippits, D.; Gunther, W.; Graf, R.; Spiess, H., and Lemstra, P. 'Segmental Mobility in the Non-crystalline Regions of Semicrystalline Polymers and its Implications on Melting' *Macromolecular Rapid Communications* **2009** *30*, 826-839.

[224] Yao, Y.-F.; Graf, R.; Spiess, H.W., and Rastogi, S. 'Restricted Segmental Mobility Can Facilitate Medium-Range Chain Diffusion: A NMR Study of Morphological Influence on Chain Dynamics of Polyethylene' *Macromolecules* **2008** *41*, 2514-2519.

[225] Rastogi, S.; and Terry, A.E. 'Morphological implications of the interphase bridging crystalline and amorphous regions in semi-crystalline polymers' *Interphases and Mesophases in Polymer Crsytallization* Springer **2005** *180*, 223-234.

[226] Rastogi, S.; Kurelec, L., and Lemstra, P. 'Chain Mobility in Polymer Systems: On the Borderline between Solid and Melt. 2. Crystal Size Influence in Phase Transition and Sintering of Ultrahigh Molecular Weight Polyethylene via the Mobile Hexagonal Phase.' *Macromolecules* **1998** *31*, 5022-31.

[227] Toda, A.; Tomita, C., and Hirosaka, M. 'Temperature modulated DSC of irreversible melting of nylon 6 crystals' *Journal of Thermal Analysis and Calorimetry* **1998** *54*, 623–635.

[228] Toda, A.; Tomita, C.; Hikosaka, M., and Saruyama, Y. 'Melting of polymer crystals observed by temperature modulated dsc and its kinetic modelling' *Polymer* **1998** *39*, 5093–5104.

[229] Gill, P.; Sauerbrunn, S., and Reading, M. 'Modulated differential scanning calorimetry' *Journal of Thermal Analysis and Calorimetry* **1993** *40*, 931–939.

[230] Reading, M.; Elliott, D., and Hill, V. 'A new approach to the calorimetric investigation of physical and chemical transitions' *Journal of Thermal Analysis and Calorimetry* **1993** *40*, 949–955.

[231] Reading, M.; Luget, A., and Wilson, R. 'Modulated differential scanning calorimetry' *Thermochimica Acta* **1994** *238*, 295-307.

[232] Wunderlich, B.; Jin, Y., and Boller, A. 'Mathematical description of differential scanning calorimetry based on periodic temperature modulation' *Thermochimica Acta* **1994** *238*, 277–293.

[233] Boller, A.; Jin, Y., and Wunderlich, B. 'Heat capacity measurement by modulated DSC at constant temperature' *Journal of Thermal Analysis* **1994** *42*, 307-330.

[234] Toda, A.; Tomita, C.; Hikosaka, M., and Saruyama, Y. 'Kinetics of irreversible melting of polyethylene crystals revealed by temperature modulated DSC' *Thermochimica Acta* **1998** *324*, 95–107.

[235] Toda, A.; Arita, T.; Tomita, C., and Hikosaka, M. 'Computer simulation of the melting kinetics of polymer crystals under condition of modulated temperature' *Thermochimica Acta* **1999** *330*, 75-83.

[236] Toda, A.; Arita, T., and Hikosaka, M. 'An unusual behavior in the melting region of isotactic polypropylene crystals revealed by temperature-modulated DSC' *Journal of Materials Science* **2000** *35*, 5085 - 5090.

[237] Toda, A.; Arita, T., and Hikosaka, M. 'Transition kinetics of a Ti-Ni alloy examined by temperature-modulated DSC' *Thermochimica Acta* **2005** *431*, 98-105.

[238] Minakov, A.A.; Mordvintsev, D.A.; Tol, R., and Schick, C. 'Melting and reorganization of the crystalline fraction and relaxation of the rigid amorphous fraction of isotactic polystyrene on fast heating (30,000 K/min)' *Thermochimica Acta* **2006** *442*, 25–30.

[239] Schick, C.; Wurm, a, and Mohamed, a. 'Vitrification and devitrification of the rigid amorphous fraction of semicrystalline polymers revealed from frequency-dependent heat capacity' *Colloid & Polymer Science* **2001** *279*, 800-806.

[240] Housmans, J.; Balzano, L.; Santoro, D.; Peters, G., and Meijer, H. 'A design to study flow induced crystallization in a multipass rheometer' *International Polymer Processing XXIV* **2009** *2*, 185-197.